Università degli Studi di Napoli Federico II

Department of Structures for Engineering and Architecture

Mauro Iacuaniello

A new prototype of window and panel for pyroclastic flow mitigation

PhD dissertation
XXXIII cycle

The Coordinator
Prof.Eng. Luciano Rosati

Tutor
Prof.Arch. Giulio Zuccaro

Co-Tutors
Eng. Daniela De Gregorio
Eng. Andrea Montanino

Mattia
I see this spark in you.
It's amazing.
Whatever you choose to do with it you'll be great.
You're on your way. Just keep going.

When do I know I'm Spider-Man?
You won't. That's all it is, Miles... a leap of faith.

[Phil Lord, SPIDER-MAN: INTO THE SPIDER-VERSE (2018)]

Abstract

Over the centuries, volcanic eruptions have brought death and destruction. The number of victims caused by documented events from1997 to 2017 is about 2400. Today, almost 800 million people, mainly concentrated in the tropics, are at risk from volcanic activity. Large conurbations, such as Tokyo, Mexico City, Seattle and Naples, are located within a few dozen kilometres of volcanoes with a high probability of an eruption. Also, high rates of urban population growth in developing countries cause great concern, as many cities are located right on top of tectonic belts, which host most of the world's most explosive volcanoes. The safety of these populations requires the planning of mitigation strategies that, in order to be implemented, need a careful volcanic risk assessment. In perspective, the object of this PhD thesis is the development of methodologies for the modelling and evaluation of technical solutions, guidelines for the design and implementation of new industrial products for the building envelope aimed at volcanic risk mitigation and energy saving. The areas studied are the urban settlements in the Neapolitan volcanoes Vesuvius and Campi Flegrei (Campania Region, Italy). The phenomena analysed within the Neapolitan explosive eruptions because they are considered most destructive are pyroclastic flows and ashfall. In the case of pyroclastic flows, a gas-solid mixture that can flow downstream and reach considerable distances from the point of emission, with speeds that can easily exceed 100km/h (30m/s) (Neri et al., 2008)[26], the damage caused to buildings depends on several factors, including the duration of the phenomenon, the temperature of the flow and the impact pressure . At the same time, ash falls, which are formed by the accretion of clasts falling by gravity from an eruptive column, affect (albeit with different levels of intensity) a large area, the definition of which is closely linked to the direction and intensity of the wind and the type of eruption. Thus, the Emergency Plans, developed by the Civil Protection for both volcanoes, identify the "red zone', as an area potentially affected by both pyroclastic flows and the risk of roofs collapse in a short time due to ashfall. For this zone, the only solution is a preventive evacuation of the population. The research project tries to identify potentially resilient sectors within the red zone, where the structures, whose vulnerable elements such as windows and roofs have been strengthened, can resist the actions foreseen by the scenarios of the eruption to obtain economic benefits and facilitate reconstruction (Zuccaro and Leone, 2013) [48]. In order

to define these resilient sectors, it is necessary to define the vulnerability of the elements exposed to risk, following a different approach from the one taken in the literature, which was based on the analysis of technical data sheets of products on the market and carrying out qualitative assessments (Zuccaro and Leone, 2010) [46]. The elements' vulnerability analysis was carried out in the present thesis through different numerical analyses in the mechanical and thermal fields. The study and research activities carried out are described below. They are divided into 8 chapters, although they can be grouped into four parts.

- The first part (Chapters 1, 2, 3) concerns examining eruptive phenomena, potentially generated by an eruption and expected in the Campania region (ashfall, pyroclastic flows), the risk associated with them and their schematisation in terms of actions on the structures involved. The different emergency plans were also studied.

- The second part of the thesis (Chapter 5) concerns the analysis of the exposure of the areas at risk. About the phenomena studied, three groups have been considered: frames/shutters, vertical structure, and horizontal structure among the elements collected in different in situ survey campaigns.

- The third part concerns (Chapter 6 and 7) analysing the elements' volcanic vulnerability through non-linear static and thermal FEM analysis. This thesis points out that the most vulnerable building elements to the pyroclastic flows are the windows that fail to resist both the flow pressures and temperatures; their failure would allow the flow to enter the building, causing extensive damage and fire. So the first step carried out was the evaluation of the windows and doors present on both territories, which turned out to be unsuitable because, for example, the aluminium thermal break windows lost the continuity solution between the internal and external frame since the thermal break which is a plastic element that cannot resist high temperatures, or the uPVC windows which also turned out to be unsuitable since they are made of plastic material whose critical temperature is very low. Another critical issue with the windows analysed is the type of glass used, which does not resist both pressure and thermal shock.

- The final part (Chapter 8) of the research project consists of exporting the final prototype developed to some international volcanic areas, such as Mount Pinatubo and Kanlaon (Philippines), Mount Pelée (Martinique), La Soufrière (Guadeloupe), Furnas (Azores) and Teide (Tenerife). The first step was the analysis of the exposure of some specific areas, in particular, Azores and Tenerife, the building realities similar to the Italian ones so, once the eruption scenarios are known, it is possible to intervene with the same prototypes and use them as a starting point for new configurations. On the other hand, in the French and Philippine islands, construction

reality is different in architectural and building materials. Since Tropical cyclones are a risk to buildings in these areas and buildings are designed taking them into account, the idea is to carry out incremental innovations, such as to make the relative mitigation strategies suitable to meet the safety requirements of volcanic phenomena.

Table of contents

List of figures

List of tables

Chapter 1

Volcanic activity

To forecast the consequences of a volcanic event, it is essential to know the various ways in which the phenomenon can occur on the surface. When magma is in conditions that reach the planet's outer surface, there is a volcanic eruption. This can occur through the expulsion of magma as a continuous liquid with variable viscosity that flows along the surface, possibly fragmenting during the flow, or through the violent expulsion of mixtures of gas and solid or partially molten material, fragmented due to the explosive expansion of the volatiles contained in the magma or due to the instantaneous vaporization of water outside the system, which can come into contact with the magmatic body. In the first case, the eruption is effusive, and its product is a lava flow (Figure1.1);

in the second case, the eruption is explosive and will cause a wide range of pyroclastic products. A first fundamental requirement, necessary for an effusive eruption to occur, is a sufficiently low content of volatiles exuded in the magma to prevent their pressure from causing explosive fragmentation. Since, except for some basic and ultrabasic magmas, most magmas' volatiles content would be sufficient to determine their explosive fragmentation, the magma must degas before it comes into daylight. This may occur either by gradual removal of the volatiles through fumaroles or hydrothermal sources or rapidly through episodic phreatic explosions. Similarly, one or more explosive eruptive phases can cause the removal of most gases from a magma chamber, allowing the magma's quiet outpouring still present, in the form of lava flows, in the final phases of an eruptive cycle.

1.1 Measuring Explosive Eruptions

Measuring a volcanic eruption's strength is more challenging than collecting wind speed data or measuring ground motion with an instrument. Volcanic eruptions produce different types of products, have different durations and develop in different ways. A first study describing and classifying explosive volcanic eruptions concerning ashfall deposits was

Fig. 1.1 Example of effusive eruptions: Etna volcano, Italy.

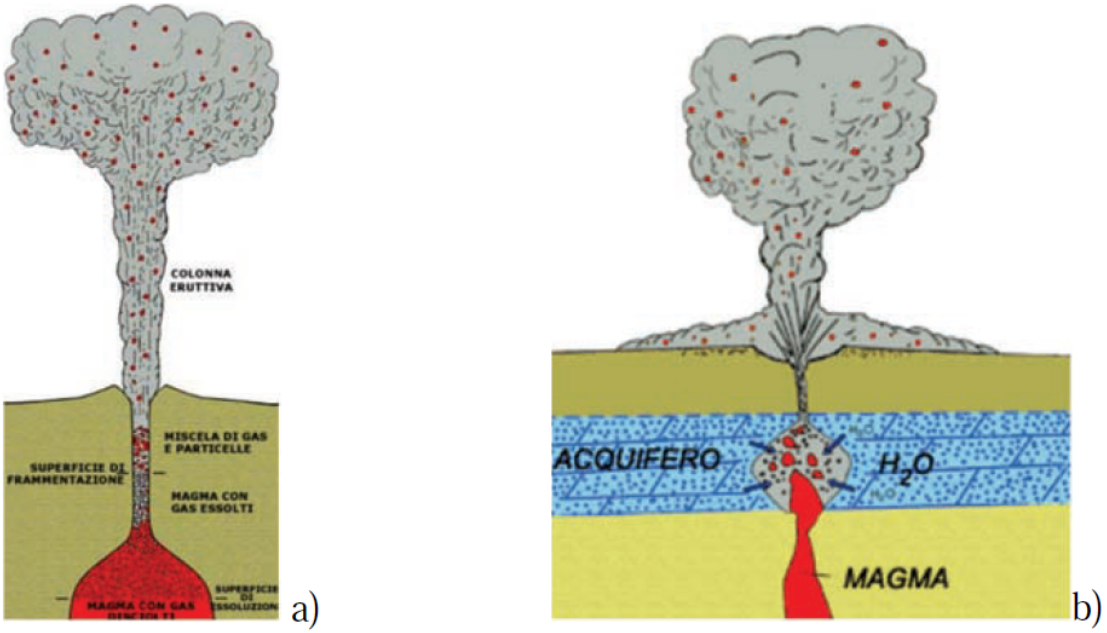

Fig. 1.2 Explosive eruptions: a) magmatic; b) phreatomagmatic.

carried out by Walker in 1973 (Figure1.3). He constructed a quantitative scheme that relies on careful measurement of the thickness of the fallout deposits and particle size analysis to determine two parameters: the dispersion (D) and the fragmentation index (F) of the deposit. The dispersion of a falling deposit (D) is defined as the area enclosed in the isopach (a curve of equal thickness) connecting the points where the deposit's thickness is equal to 1 % of the maximum thickness. Fragmentation (F), on the other hand, is defined as the percentage of particles finer than 1mm, at the point where the dispersion axis of the deposit intersects the isopach connecting the points where the deposit is 10 % of the maximum thickness

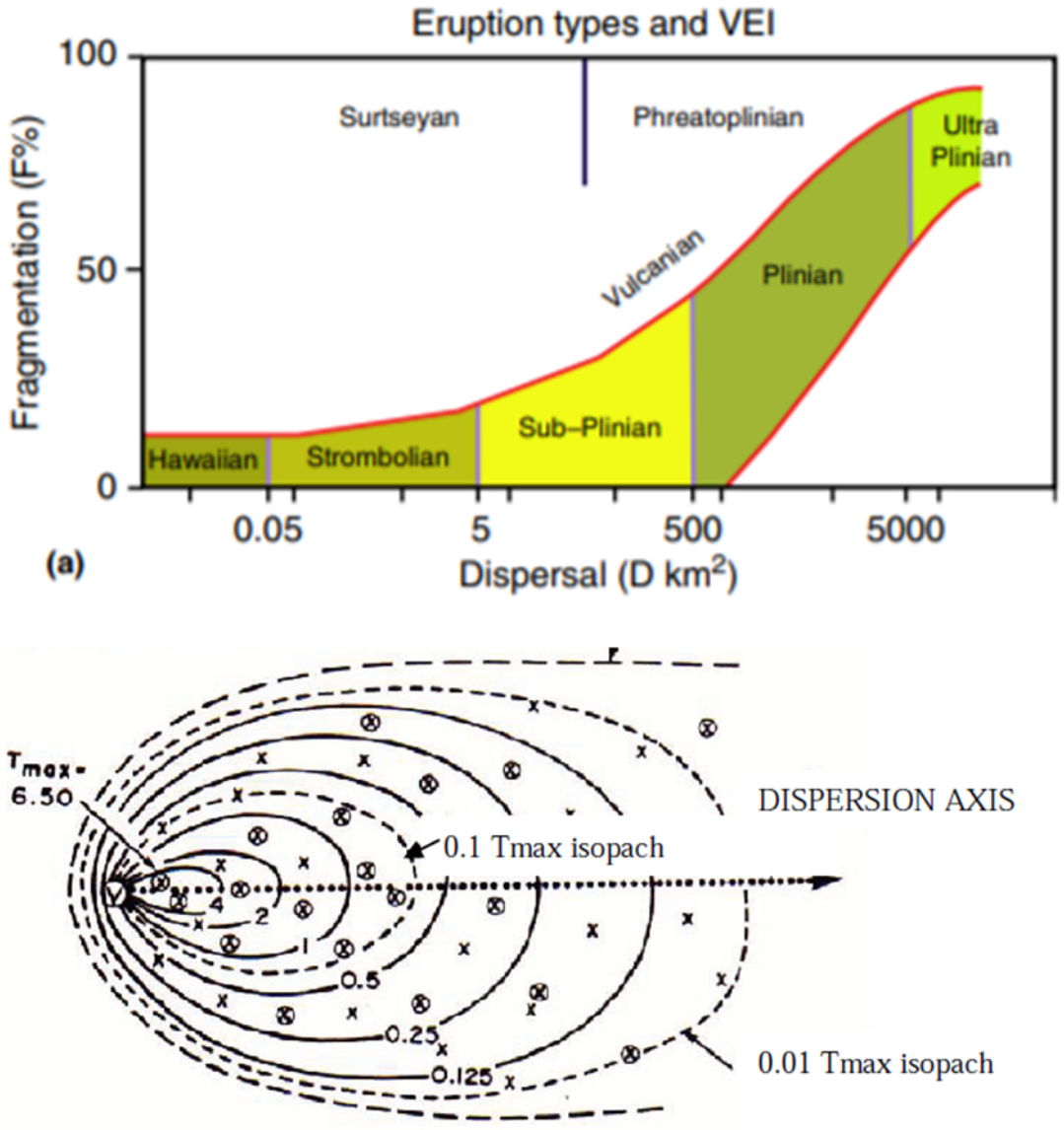

Fig. 1.3 Scheme for classifying eruptions according to the dispersion index (D) and fragmentation index (F) according to Walker. (Waker, 1973) [41]

Walker's classification scheme is genetic and provides for an initial distinction into two groups of explosive eruptions. The first group includes magmatic eruptions which, in increasing order of dispersion and fragmentation, can be schematised as follows: Hawaiian, Strombolian, Sub-Plinian, Plinian and Ultra-Plinian eruptions. The second group includes phreatomagmatic eruptions and comprises only two categories: Surtseyan and Phreatoplinian eruptions. These two types of eruption occupy the sector of the Walker diagram with the highest degree of fragmentation. In contrast, an intermediate type of eruption in which the interaction between water and magma plays a more or less important role, including Vulcan eruptions, is located in a central portion of the diagram. The different heights of the Plinian columns for the eruptions described by Walker have illustrated in Figure 1.4:

- 2 km for Hawaiian eruptions
- 10km for Strombolian eruptions
- 30km for Sub-Plinian eruptions and 55km for Plinian and Ultra-Plinian eruptions

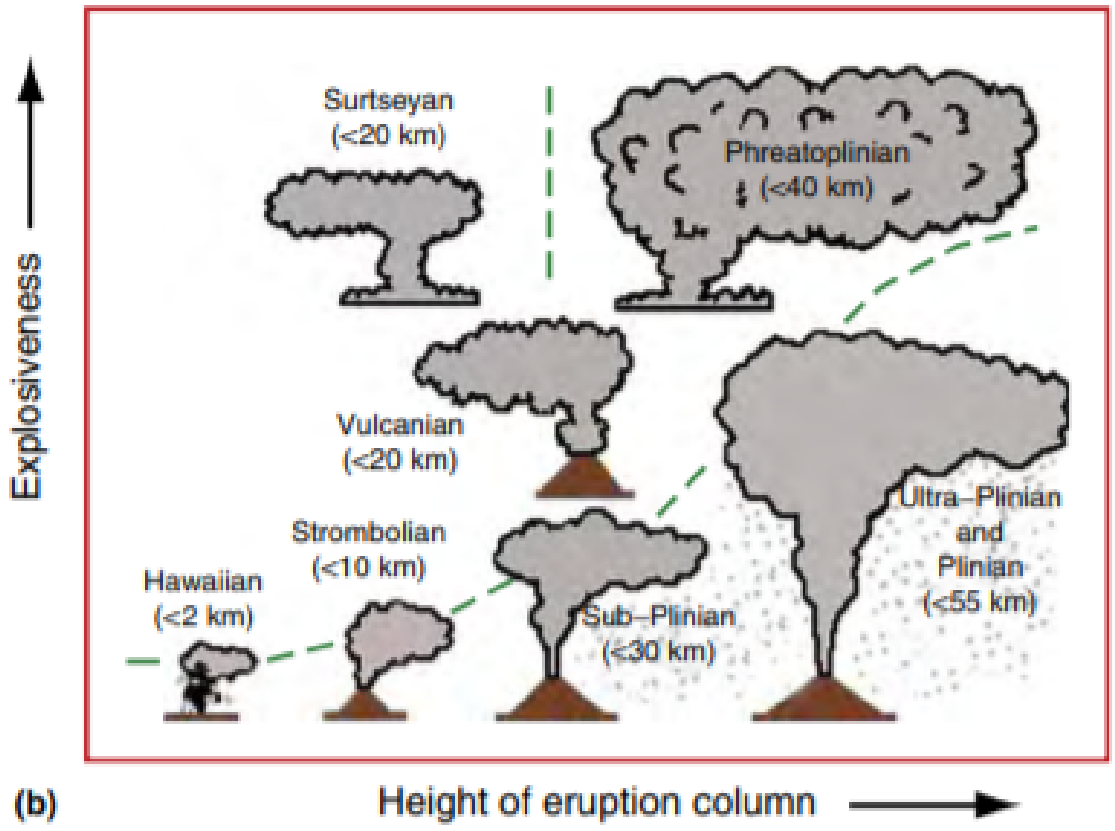

Fig. 1.4 Diagram of eruptive column height as a function of explosivity/ degree of fragmentation as a function of explosivity/degree of fragmentation. (Wright and Cas, 1988) [42]

Chris Newhall of the United States Geological Survey and Stephen Self of the University of Hawaii developed the Volcanic Explosivity Index (VEI) in 1982 [28]. It is based on a series of parameters observable during an eruption, combined in such a way as to provide a scale of relative magnitude between the various events. The scheme has been particularly designed to formulate a classification of an eruption's explosiveness and therefore does not allow an adequate classification of purely effusive events. Table 1.1 shows the scheme by which the index is assessed. The volume of extruded materials, the height of eruptive clouds and qualitative observations (using terms ranging from "light" to "mega-colossal") are used to assess the explosive capacity of an eruption. It is an indefinite scale from 0, for a non-explosive eruption (less than $10^4 m3$ of pyroclastic material emitted), to 8, for mega-colossal eruptions can emit 1012m3 of clasts, with an ash column more than 25km high. Each scale interval represents an increase by a factor of 10 in observation.

Since the VEI was introduced, it has become widely used despite some admitted limitations. The following are three notable limitations.

1. The VEI scale combines the concepts of magnitude and intensity as initially defined and distinguished by Walker (1980) and later adopted by Pyle (1995). Prolonged dome-building eruptions can be practically non-explosive yet produce large volumes of dome-collapse pyroclastic flows, thereby earning a misleadingly high VEI.

2. Below VEI 3, several orders of magnitude are combined, making the scale ordinal rather than cardinal. Generalizations about power-law behaviour apply only to eruptions of VEI ≥ 3.

3. Only bulk volumes are considered. This has the advantage of not requiring bulk density data, but the disadvantage of not being strictly comparable from one eruption to another. Dense rock equivalency (DRE) is a useful, normalizing concept, but users should be aware of considerable uncertainty in its calculation.

Ideally, any explosive eruption description should define both magnitude (expressed in mass) and intensity (expressed in mass ejection rate per unit time). The most popular alternative to VEI is the mass-based magnitude (M) scale of Pyle (1995, 2000, 2015 [36]). As originally proposed (Pyle, 1995 [35]), the M scale referred only to tephra (sensu latu, all pyroclastic material) (Newhall et al., 2018 [27]). With the above mentioned exception of dome-collapse materials, it can be expected to correlate well with VEI with the added advantage of higher accuracy and precision if the deposit volumes and bulk densities are well known. The LaMEVE database of Crosweller et al. (2012) also refers only to tephra, excluding lava. However, Pyle (2000, 2015) and Oppenheimer (2011) [31]; using the abbreviation Me) combined masses of tephra and lavas. Ultimately, a way forward to a more consistent and quantitative description of eruptions might be to use both intensity

Table 1.1 Classification scheme of eruptions based on the VEI explosive index. (Newhall and Self, 1982).

VEI	**0**	**1**	**2**	**3**	**4**	**5**	**6**	**7**	**8**
Description	non explosive	little	moderate	large-moderate	large	very large			
Log10 Volume [m]	4	4¸6	6¸7	7¸8	8¸9	9¸10	10¸11	11¸12	>12
Column height [km]	from vent			from sea level					
	<0,1	0,1 ¸ 1	1 ¸ 5	3 ¸ 15	10 ¸ 25	>25			
Qualitative description	non explosive	moderate	explosive	violent	cataclysmic	paraxysmal	colossal	super colossal	mega colossal
Classification	Strombolian			Plinian					
	Hawaiian		Vulcan			Ultra - Plinian			
Duration [hours of continuous emission]	<1				>12				
			1: 6						
				6 : 12					
Tropospheric injection	irrelevant	minor	moderate	substantial					
Stratospheric injection	nothing			possible	sure	considerable			

and magnitude but add subscripts to indicate the material measured, e.g., Mt for magnitude based on tephra, or M_l for magnitude based on lava, and the same for intensities It and Il. Estimates based on a combination of tephra and lava could be indicated as Mtl or Itl. This suggestion follows convention in seismology to indicate the basis on which the magnitude of an earthquake was estimated, e.g., M_w for moment magnitude.

Chapter 2

Volcanic Risk in Neapolitan Area

2.1 Vesuvius

Due to the high urbanization developed in recent decades at its slope, where more than 550,000 people live, Vesuvius is now one of the highest risk volcanoes in the world. It is currently in a inactive state. Throughout its history, Vesuvius has been characterized by the alternation between periods of eruptive activity, with the volcano's conduit open, and periods of rest, with the conduit obstructed. The periods with an obstructed conduit are characterized by the absence of eruptive activity and the accumulation of magma in a magmatic chamber located deep inside. These periods were always interrupted by very energetic eruptions, followed by periods of open conduit activity with frequent effusive or explosive low energy eruptions. The 1631 eruption (Figure 2.1) interrupted a rest period that had lasted for almost five centuries.

Tela raffigurante l'eruzione del 1631 (Lorraine)

Fig. 2.1 Vesuvius in eruption: 1631

From 1631 to 1944, the eruptions were followed by rest periods of a few years. Scholars believe that the 1944 eruption (Figure 2.2) marked the end of a period of open conduit activity and the beginning of an obstructed conduit rest period. In fact, from 1944 to the present day, Vesuvius has given only fumarolic activity and seismic swarms of moderate energy, without soil deformations or significant variations in the physical and chemical parameters of the system. In the light of past behaviour, it is expected that, should activity resume within a few decades, the next eruption would be of the sub-Plinian type, like that of 1631 or 472.

Fig. 2.2 Vesuvius in eruption: 1944

2.1.1 Reference scenario

One of the objectives of volcanological research is to be able to estimate the probability of an eruption occurring in a determined time interval and to assess its magnitude and/or intensity. To this aim, some authors hypothesize a Poissonian distribution of the events, which implies the hypothesis that the intensity is independent of the rest time, and by the intensity of the eruption that preceded it. However, it is still impossible to define maximum size limits of the energy of the next eruption, as highlighted in many scientific works. Recent statistical studies suggest that the Maximum Expected Eruption of Vesuvius (or EMA), considered in the previous Emergency Plan (1995, DPC 2001), is not the maximum event that can be expected in case of reactivation of Vesuvius and does not exclude the possibility of 3 that there may be a significantly higher eruption than EMA, although with a

lower probability. The results of studies by Marzocchi et al. (2004) also show that the size of the most likely event has a VEI=3, i.e. less than that of the eruption taken as reference in the previous Emergency Plan, of VEI=4. These studies are based on the analysis of the eruption catalogues of all the volcanoes in the world, of 17 volcanoes "similar" to Vesuvius, and of Vesuvius itself. The authors distinguish two different cases:

- eruptions preceded by a resting time between 60 and 200 years;
- eruptions preceded by a rest time greater than 60 years, but without

Both models, in fact, refer to "closed conduit" rest periods (greater than 60 years) but, while the first model is more suitable for short to medium term forecasts, the second is preferable for long-term assessments. The choice of the reference eruptive event for the definition of the scenario to be used as a basis for planning emergency, is of course the most delicate and difficult choice, and is the one that most strongly affects the entire Emergency plan. In the previous Plan, a sub-Plinian eruption similar, but not identical, to the eruption was chosen as EMA of Vesuvius in 1631. In the current Plan, the concept of EMA has been surpassed, preferring an approach based on the evaluation of the probability of occurrence of the different scenarios, corresponding to the main types of eruption listed in Table 2.1.

Table 2.1 Styles of Vesuvius eruptive activity (Marzocchi et al., 2009) [24]

	Violent Strombolian	**Sub-Plinian I**	**Plinian**
	VEI = 3	**VEI = 4**	**VEI = 5**
Vesuvius: resting time between 60 and 200 years	72%	27%	1%
Vesuvius: resting time greater than 60 years	65%	24%	11%

A probabilistic model, based on Bayesian statistics, has made it possible to develop a so-called "tree event" which, applied to Vesuvius, provided the results shown in Table 2.2, which indicate, in case of eruption, the likelihood of that specific eruptive type occurring.

Table 2.2 Styles of Vesuvius eruptive activity

Eruptive Style	**Rest (years)**	**Volume (km3)**	**MDR peak**	**Column height (km)**	**Pyroclastic flow**
Plinian	10^2-10^3	1-10	107-108	>20	yes
Sub-Plianian I	10^2	10^{-1}- 1	10^7	15 - 20	yes
Sub-Plianian II	10^2	10^{-2}- 10^{-2}	10^6- 10^7	10 - 15	minor
Violent Strombolian	10 - 10^2	10^{-3} - 10^{-2}	10^5 - 10^6	5 - 10	no
Continuous ash emission	10 - 10^2	Up to 10^{-2} cumulative			no
Medium Strombolian	1-10	10^{-3}			no

These results, the absolute validity of which is affected by the scarce information and data available to process an objective probabilistic model, however, have led to believe that there may be a probability not negligible (around 10%) to have a scenario corresponding to

the maximum event recorded in the eruptive history of the Vesuvius (Pliniana with VEI=5). It should be noted, however, that this result is provided by events with a period of rest of more than 60 years, which obviously includes also very long ones, of several centuries up to the millennium, that seem characteristic of some Plinian eruptions of Vesuvius. The probability of a Plinian eruption with VEI=5 goes down to 1% if rest periods between 60 and 200 years are considered (Table 2.2), a rest period that better corresponds to a mid-term evaluation of the possible event. The lowest energy event (VEI=3) would be the most likely from Table 2.2. These are events (Strombolian violent) preceded by short rest periods, mostly of the order of tens of years, the dangerousness of which is substantially associated with the fallout of pyroclastic materials and the formation of lahar and without pyroclastic castings. So it is considered reasonable that the reference scenario to be used in the Emergency Plan may be like that already assumed in the previous plan and must, therefore, be a sub-Plinian event for the following justifications:

- has a rather high conditional probability of occurrence, just under 30%;
- corresponds to a reasonable choice of "acceptable risk" considering that the probability that this event is exceeded by a Plinian eruption with VEI=5 is, in the next 140 years or so, only 1%;
- the geophysical data do not reveal the presence of a superficial magma chamber with enough volume to generate a Plinian type eruption ().

It should also be noted that the most probable events (VEI=3), while not producing pyroclastic flows, may give rise to mudflows that could invade a large part of the area exposed to the danger of pyroclastic flows in the reference event (VEI=4). Therefore, the definition of the high danger zone based on the reference event (VEI=4) also covers the highly hazardous area for eruption-induced events with VEI=3.

2.2 Campi Flegrei

The Campi Flegrei are a volcanic caldera of more than ten kilometres in diameter centred on the town of Pozzuoli. The northern and western part of the caldera is above sea level and is characterized by the presence of numerous volcanic cones and craters. The southern part extends mainly in the Gulf of Pozzuoli. Compared to central volcanoes often characterized by frequent eruptions that occur from a single crater, and by the deposition of volcanic materials (lava flows and pyroclastic products) that lead to the construction of cones, the calderas show significantly different structure and behaviour. Most calderas produce eruptions that are difficult to trace back to regular patterns, originating from scattered vents. In general, explosive eruptions of variable scale prevail in the calderas, some or

many of which can also be of very strong intensity and violence. The calderas are also marked by underground thermal anomalies and the presence of abundant hydrothermal manifestations. The difficulty in recognizing simple behavioural patterns makes it difficult to predict; the thermal anomaly of the subsoil and the abundant hydrothermal circulation complicate the ability to predict eruptions in the short term, significantly increasing the risk of false alarms. The knowledge acquired over the last thirty years has highlighted a series of structural and behavioural elements that contribute significantly to the definition of the system volcanic and how it works. The essential elements that have emerged are:

- the presence of a large collapsing caldera produced by two large explosive eruptions (Ignimbrite Campana and Yellow Tuff), characterized by an intense hydrothermal activity;
- the occurrence of periods of volcanic activity lasting centuries (eruptive periods) alternating with rest periods lasting thousands of years;
- the occurrence of predominantly explosive eruptions;
- the occurrence over the last 15,000 years of eruptions from scattered eruptive vent inside the caldera;
- the occurrence of phenomena related to the interaction of magma with groundwater; and/or superficial, of variable significance for different eruptions and eruptive phases.

Moreover, two main areas are identified within the caldera most likely to open future eruptive vent. The area at maximum probability is located roughly in the Astroni-Agnano area, while the second area for values of probability is located at Averno - Monte Nuovo. It can therefore be concluded that the body of knowledge available today agrees in identifying these two areas as those characterised by the highest probability of future eruptive vents opening, with the area to the east (Astroni-Agnano) characterized by higher probability values. However, in this picture there are other areas characterized by a high probability of eruptive vents opening, thus leaving a high overall uncertainty. In the definition of the expected eruptive scale in case of next eruption at the Campi Flegrei, in the Dossier are considered the basic assumptions and choices made in the work of Orsi et al.(2001) [32] and the statistical analysis is extended to consider both the last 15 k of post-eruption activity of the Neapolitan Yellow Tuff, and the events of very large eruptive scale, i.e. the eruptions of the Yellow Tuff and Ignimbrite Campana, dated respectively to about 15 and 39 ka BP. Using this average time frequency together with those related to the other eruptive scales reported in Table (2.3) and considering that the normalized frequencies do not differ substantially from the average value of the conditioned probability we obtain an estimate of the conditioned probabilities for a future eruption in the Campi Flegrei

including the eruptions of "very large" scale (the Table 2.3 shows the average values). Consequently, it is possible to assume a next eruption at the Campi Flegrei is (average value) at 95%. approximately on a scale of probability less than or equal to the average.

Table 2.3 Conditional probability (assumed to coincide with observed frequency) for 'Effusive' to 'Very Large' eruption scales (Orsi et al., 2009) [33]

Eruptive scale	Conditional probability [%]
	11,9
Small	59,6
Medium	23,8
Large	4
Very large	0,7
Medium Strombolian	1-10

2.2.1 Reference scenario

The phenomena expected in case of resumption of eruptive activity at the Campi Flegrei are of intensity and impact different depending on the type and scale of the event. In order to provide the civil protection operator with a picture of the possibilities, it is worth analysing on four different types of scenarios.

- Scenario n.1: explosive eruption (magmatic eruptive event of scale: small, medium, large and very large);
- Scenario n.2: multiple eruption (simultaneous eruptive activity from different mouths);
- Scenario n.3: phreatic explosion in hydrothermal areas;
- Scenario n.4: effusive eruption.

The four scenarios configure different phenomena and impacts, and it was appropriate to analyse and comment separately in order to better prepare the intervention plans for the protection of people and for the organizational design of the evacuation plans. Scenario n.1 envisages impacts on the territory of different scales in relation to the scale of the eruption considered, but also according to the local conditions where the vent opens (presence or absence of water) and the topographical conditions around the vent itself. It remains implicit that the description of the expected phenomena results in affected by considerable margins of uncertainty. The expected phenomena and their sequential development as follow presented, derive in part from the study of volcanic deposits in the Campi Flegrei, and in part from the overall of knowledge and observations related to recent crises in other

volcanic districts. Finally, the expected phenomena consist of a series of phases (eruptive phases) that occur typically according to the following idealized sequence:

1. opening phase;
2. sustained explosive emission phase, with development of a convective eruptive column;
3. pulsating phase with formation of pyroclastic density currents (surge and pyroclastic flows);
4. Prolonged emission phase of ash and water vapour (sludge deposition and possible lahar formation);
5. possible outgassed lava emission.

During phase 1 there may be explosions that launch blocks and bombs, even large dimensions (decimeters/meters), up to distances of 1.5-2 km, accumulations of significant thicknesses (decimeters) of ash and lapilli within 1 km from the mouth, and relevant (meters) within 500 m from the mouth. The explosions can be accompanied by the formation of shock waves. Limited flow phenomena pyroclastic / surges can occur within 2 km of the eruptive vent. The 1 generally has a short duration (from tens of minutes to a few hours) and the convective eruptive column is kept for kilometres far away. The existence throughout the Phlegrean area of underground aquifers makes possibility/probable at this stage the vaporization of external water and the deposition of limited amount of wet ashes. During phase 2 there is the full development of a sustained convective column that can reach heights from a few kilometres up to over 30 km depending on the intensity of the eruption, i.e. of the event scale (with the maximum values associated with "Plinian" type eruptions). The development of the eruptive column and the overlying cloud in the shape of an "umbrella", which normally widens into all the directions expanding predominantly along the direction of the dominant winds at high altitude, produce darkening. When the darkening is accompanied by the fall of ash from the column, conditions become highly stressful for the population within a radius of several dozen miles from the mouth. From the edges of the column and the umbrella-shaped cloud a continuous rain (fall) of mostly cold lapilli. The rate of accumulation on the ground varies according to the scale of the eruption. For large scale events the rate can be relatively high (from centimetres to decimetres per hour) depending on the distance, wind direction and intensity of the eruption. The accumulation of ash and lapilli on the ground significantly limits the usability of roads and overloading on roofs can cause roofs to collapse. The fall of hot bombs (incandescent inside) can cause fires to start within the first few kilometres of the mouth. The ashes falling to the ground are typically dry and hit very large areas downwind (even hundreds

of kilometres from the mouth). The convective column remains active on average for 5-10 hours and can be replicated several times. During the sustained eruptive phases there is a continuous tremor of the soil whose amplitude decreases rapidly moving away from the mouth (Costa et al., 2009) [9]. During phase 3 the activity tends to become pulsating, with repeated collapses of the eruptive column and generation of pyroclastic density currents (pyroclastic flows) that can radiate 360° around the eruptive mouth or preferentially along specific sectors. The distance that the flows can travel depends on the intensity of the eruption, the collapse regime of the column (incipient, partial or total) which in turn controls the mass flow that feeds the currents, and the position of the mouth with respect to the topographic context. The reliefs limit and/or deviate the flow travel, the topographic lows favour its flow. In the propagation area of the flows the possibility of survival is very poor, the structures are severely damaged to the point of destruction, high temperatures can cause fires even of vast proportions. The entry into the sea of the flows can produce water vaporisations on a large scale with successive rains of lapilli (wet balls of aggregate fine ash) and muddy downwind rains. Phase 3 can last from several hours to days. It should be noted that in the case of "large" scale eruptions, during this phase there may be collapses of the structure surrounding the eruptive mouth, up to diameters of the structure sinking several kilometres, and final differences in height of the order of hundreds of metres. During phase 4 the eruptive intensity decreases substantially. The main phenomenon consists in the emission of gas and ash with the formation of an eruptive column a few kilometres high. Downwind of the mouth, the atmosphere can be charged with fine ash and dust, with reduced visibility; staying outside the structures can be made difficult due to breathing difficulties and eye irritation (need to wear dust masks and closed glasses). Over the course of the hours, layers of wet ash containing accretion stones can be deposited. The accumulation of wet ashes on the ground hinders the use of roads; the use of windscreen wipers for window cleaning causes abrasion, hindering or preventing visibility. The weight of the wet ashes, possibly added to that of the tombstones, can cause further overload and possible collapse of the roofs. The deposition of layers of wet ash may cause power failure due to short circuit produced on the overhead line insulators; finally, wet ash may contain significant amounts of acidic substances capable of attacking metals (corrosion).

Chapter 3

Eruption Hazards

Eruption hazards are diverse (Figure 3.1) and they depend on the type of eruption may extend more than thousands of kilometres from an active volcano. In the case of effusive eruptions, the main product is lava. Lava flows are streams of molten rock that pour or leak from an erupting vent. The speed at which lava moves across the ground depends on several factors, including

- type of lava erupted and its viscosity;
- the steepness of the ground over which it travels;
- whether the lava flows as a broadsheet, through a confined channel, or down a lava tube; and
- rate of lava production at the vent.

While in the case of explosive eruptions, the main products are pyroclasts expelled through the eruptive column. A part of them enter solid-gas dispersions called pyroclastic and surges flows, characterised respectively by high or low concentration; the rest, instead, falls by gravity (ash fall) or can be exploded into the air from the crater (bombs or volcanic missiles). Pyroclastic flows and ashfall, which are expected for both analysed areas, are examined in detail in the following paragraphs. In particular, the effects on the constructions of both phenomena have been studied. (Zuccaro and De Gregorio, 2013) [44] In addition to these phenomena, it is necessary to consider the effects of the volcanic phenomenon. The eruptions are generally accompanied by telluric movements (volcanic earthquakes) produced by the breaking of rocks due to magma's rise and by lahars. The Indonesian term stands for a hot or cold mixture of water and rock fragments that flows down the slopes of a volcano and typically enters a river valley, set in motion by the rains that could occur during volcanic events. Besides, large lahars can crush, abrade, bury, or carry away almost anything in their paths, including buildings and valuable land may be

partially or entirely buried. By destroying bridges and roads, lahars can also trap people in areas vulnerable to other hazardous volcanic activity. Finally, do not underestimate the possibility of volcano-induced tsunamis, generated by underwater earthquakes or falling into the sea of lava or pyroclastic material (Blong, 2013)[3].

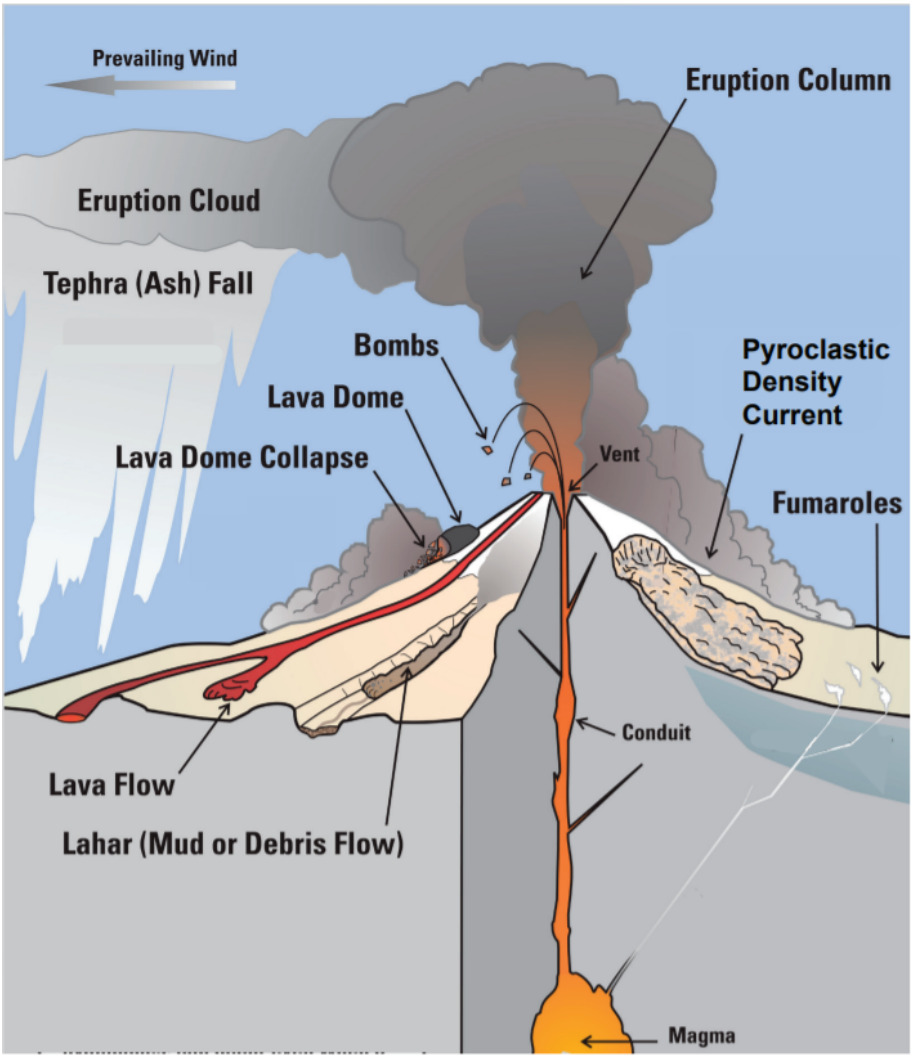

Fig. 3.1 Schematic representation of volcanic hazards

3.1 Pyroclastic Flows (PF)

Pyroclastic flows are defined as mixtures of gases and solid particles, contained in variable percentages, flowing on the ground by gravity, following a first impulse due to a directional explosion or the collapse of the eruptive column. Although it is possible to identify two types of flows such as: pyroclastic flows (Pyroclastic Density Current, PDC), characterized by a high concentration of particles, little expanded and characterized by laminar motion

and the surges that are more diluted and characterized by a turbulent motion, their mobility is always very high and their destructive power is devastating (Figure 3.2). In fact these clouds of particles and gases are able to flow down the slopes like a snow avalanche and reach considerable distances from the point of emission, with speeds that can easily reach 100 kmh (30 ms) with temperatures even higher than 500 °[26]. Damage due to pyroclastic

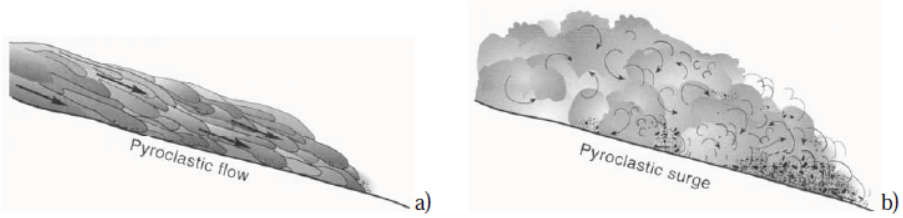

Fig. 3.2 Schematisation of the laminar motion of a pyroclastic flow (a) and the turbulent motion of a surge (b).(Texas Bureau of Economic Geology, 2009)

and surges flows, second only to fall deposits, are associated with high temperatures, dynamic pressure (density function) and speed. Pyroclastic currents can break down and incinerate any type of obstacle up to several kilometres from the centre of emission. The deposits connected to them can have considerable thickness and therefore cause damage by burial. The part of the current with dynamic pressure and reduced speed is able to penetrate inside a building, through the breaking of the openings, and the consequent ash ingress can cause combustion of flammable elements such as furniture. The portion of the current with faster and higher dynamic pressure, may be able to put in flight "missiles" of all kinds (particles, fragments, stones, bins, etc. ...) increasing the destructive impact. In addition, due to the finer ashes, which tend to be removed from the current during its progress and when it stops, pyroclastic flows can cause rapid loss of life by inhalation and/or burns. In order to analyse the evolution of Vesuvian pyroclastic flows, Todesco et al. (2002) [40] have adopted a model based on the solution of Navier-Stokes generalized equations for a multi-phase mixture. Magma was assumed as a two-phase mixture, consisting of a homogeneous portion in the molten state (magma and crystals) and a gaseous portion (water vapour). The model solves three equations of conservation of mass for the gas, liquid and solid states and two equations of conservation of momentum for the liquid magma system plus mixture of crystals and gas. This model was applied to the Vesuvius (Esposti Ongaro et al., 2002 [14]), which was schematically symmetrical to the vertical axis of the volcanic conduit. The simulations refer to two different sections of the volcano, identified through the topographic profiles of the southern slope (Sector A) and the northern slope (Sector B) of the volcano (Figure 3.3). The latter is characterised by the presence of the Monte Somma elevation.

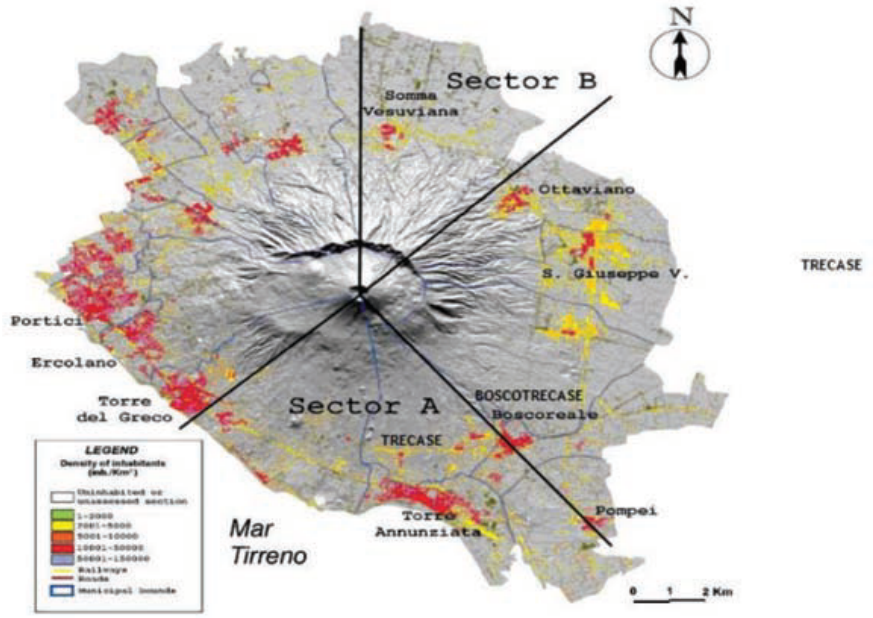

Fig. 3.3 The Vesuvian area and its urban settlements. Sectors A and B indicate the slopes represented by the two topographic profiles considered in the simulations (Todesco et al., 2002).

Among the simulations carried out, the most unfavourable one refers to a Vesuvian event of sub Plinian type, characterised by an eruptive mass of $5x10^7 kgs^{-1}$. In order to exclude the turbulence generated by the flows in contact with the urban settlements, the pressure values are evaluated in an undisturbed atmosphere, 5 and 15m from the ground floor. In Figure 3.4, regarding sector A of Vesuvius, the peaks of the dynamic pressures exerted by a flow with a total water content (w) equal to 2% and a magma temperature (T) at the exit from the crater equal to 950°C are shown. The pressure is a function of the radial distance from the crater. The flow propagation angle α strongly influences peak values. For the simulation with α equal to 90° (Figure 3.4a), the maximum dynamic pressure values are 10kPa at 2km from the crater, 2kPa at 3.5km and about 1-2kPa for longer distances. In cases where the diffusion angle is 180° and 360 ° (Figure 3.5 b-c), the maximum pressure values, at 2 km from the crater, are about 3 and 1.5kPa, respectively, with values less than 1kPa for longer distances. The simulations relative to sector A, with an angle α equal to 90°, water content w equal to 2% and magma temperature T at the exit from the crater equal to 950°C (A90-W2-t950), have returned the temporal variations (starting from the beginning of the eruption) of density, radial velocity and flow temperature indicated in Figure 3.5, at distances of 2, 4, 7.5km from the crater and 5m in height from the ground plane. For the same simulation, the values of dynamic and isotropic pressures, compared with atmospheric pressure, are shown in Figure 3.6.

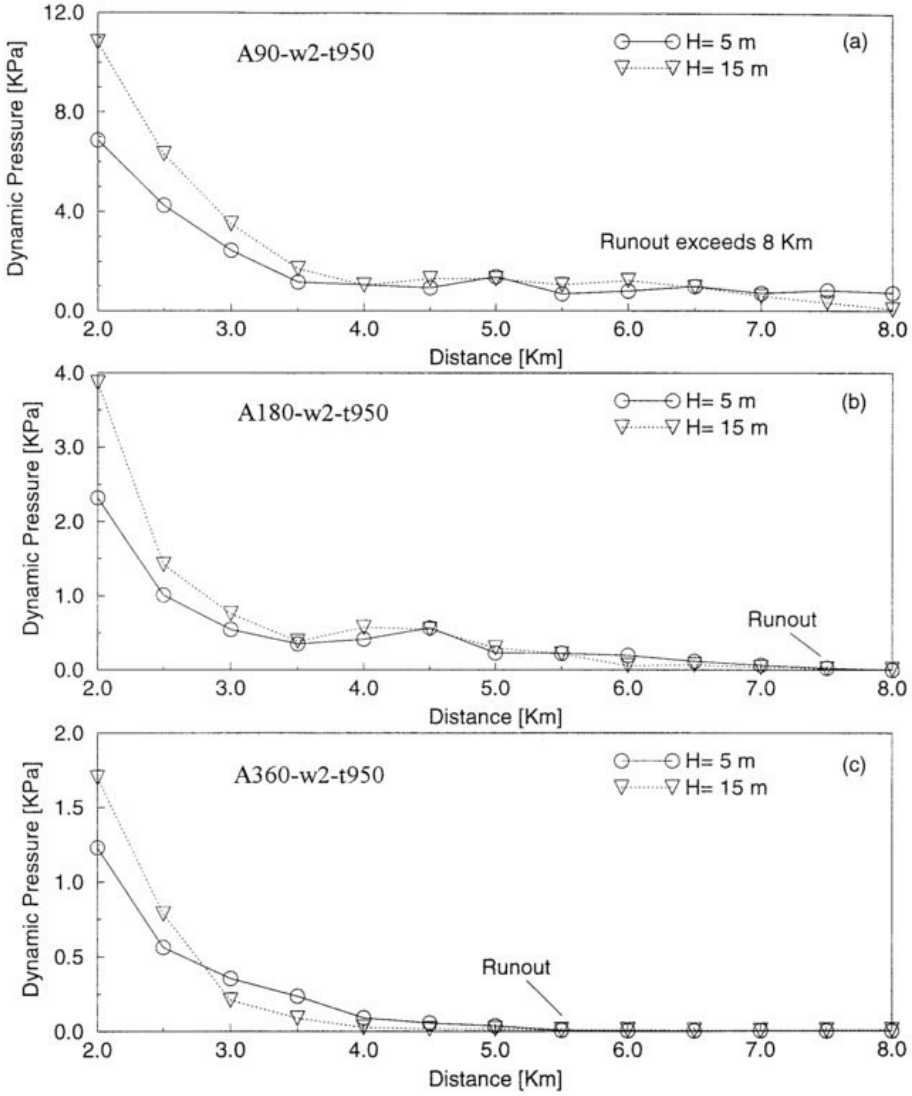

Fig. 3.4 Peaks of dynamic pressures as a function of distance from the crater, varying the angle α of flow propagation: a) α=90°; b) α=180°; c) α=360°(Esposti Ongaro et al., 2002).

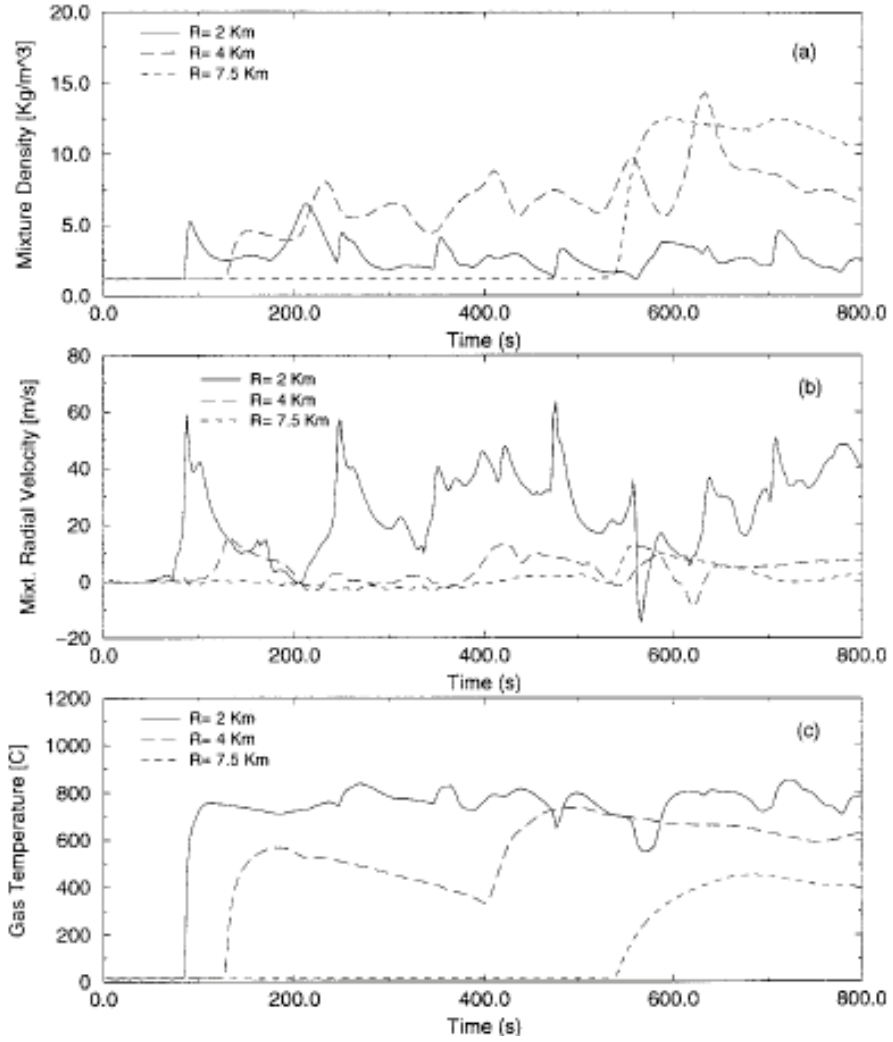

Fig. 3.5 Simulation A90-W2-t950, relative to the southern sector A. Evaluation made at different distances from the crater, at 5m from the ground. a) Density distribution of the mixture. b) Radial velocity of the mixture. c) Gas temperature (Esposti Ongaro et al., 2002).

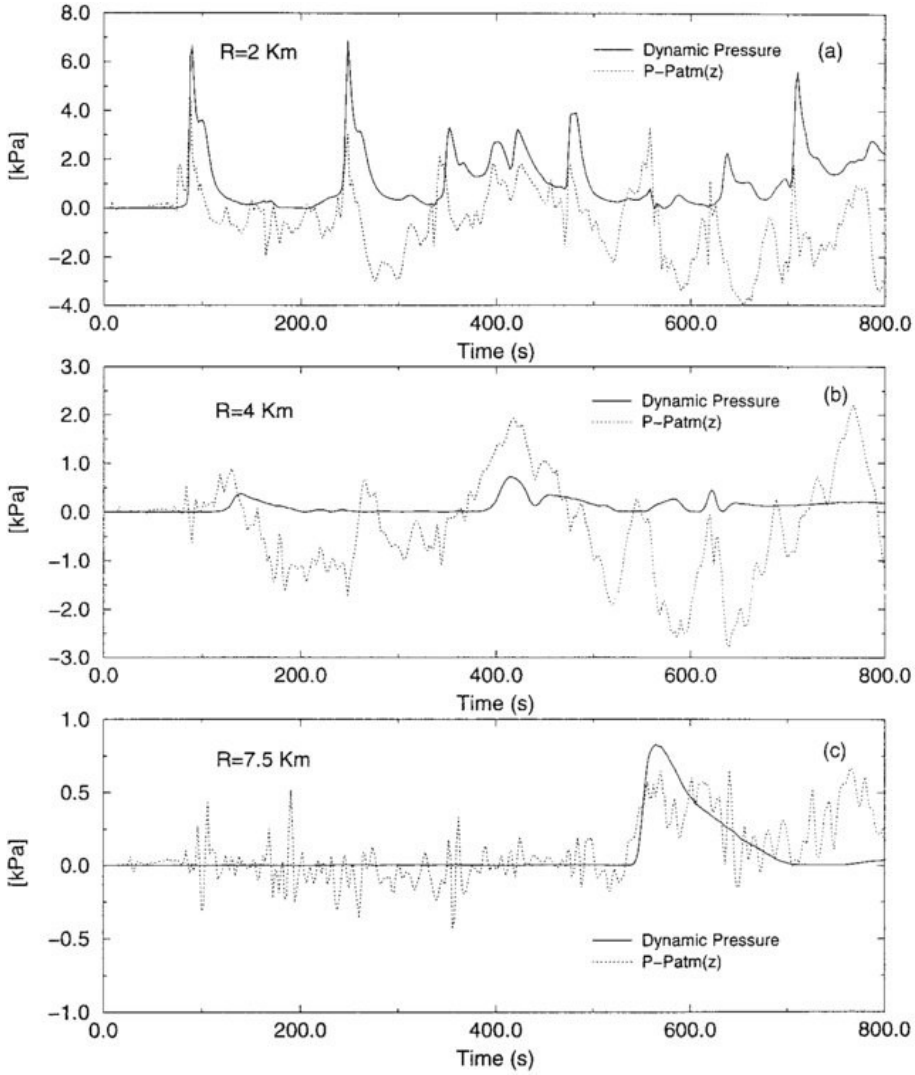

Fig. 3.6 Simulation A90-W2-t950, relative to the southern sector A. Evaluation made at different distances R from the crater, at 5m from the ground: a) R=2km; b) R=4km; c) R=7.5km (Esposti Ongaro et al., 2002).

The simulations relative to sector B, with an angle α equal to 90°, water content w equal to 2% and magma temperature T at the exit from the crater equal to 950°C (B90-W2-t950), have returned the temporal variations (starting from the beginning of the eruption) of density, radial velocity and flow temperature indicated in Figure 3.7, at distances of 2, 4, 7.5km from the crater and 5m in height from the ground plane. For the same simulation, the values of dynamic and isotropic pressures, compared with atmospheric pressure, are shown in Figure 3.8.

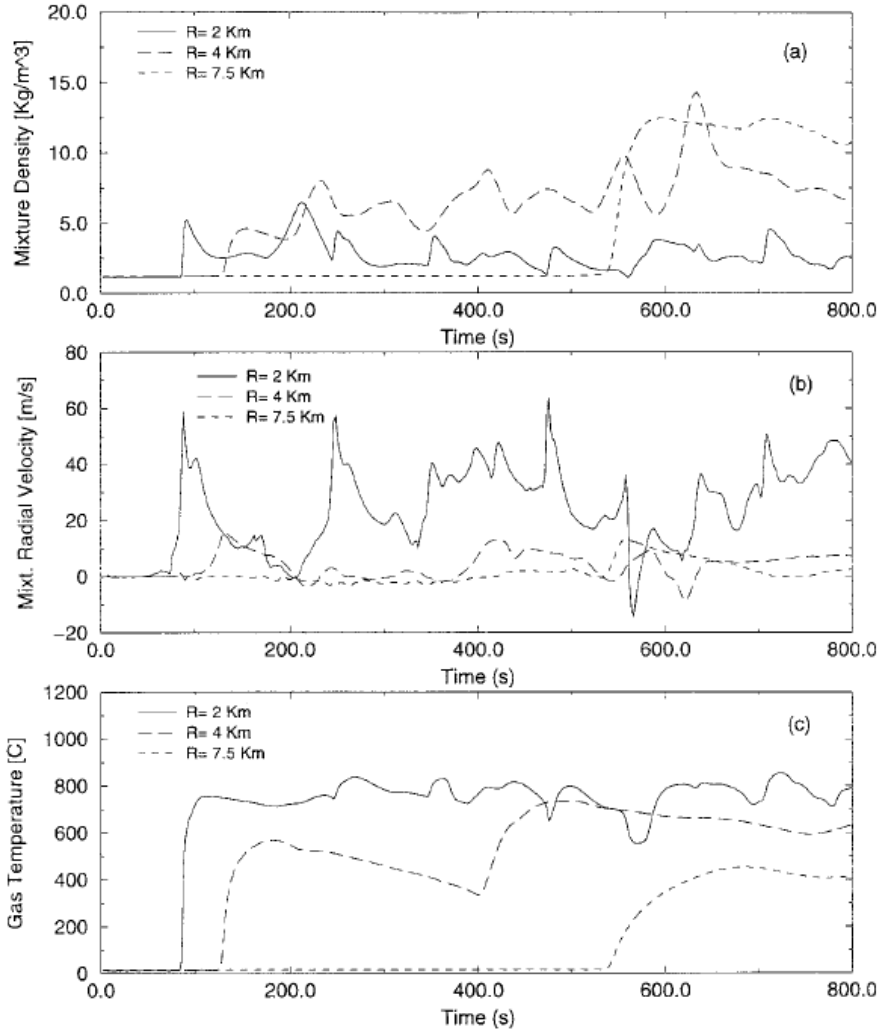

Fig. 3.7 Simulation B90-W2-t950, relative to the northern sector B. Evaluation made at different distances from the crater, 5m above ground. a) Density distribution of the mixture. b) Radial velocity of the mixture. c) Gas temperature. (Esposti Ongaro et al., 2002).

The analysis of the results shows that the current temperatures are lethal for people in the open air. For example, in southern sector A, at a distance of 7.5km from the crater, flow temperatures can be around 400°C; while in northern sector B, at a distance of 7.5km, temperatures can reach 600°C and not fall below 200°C at a distance of 10km. Within the

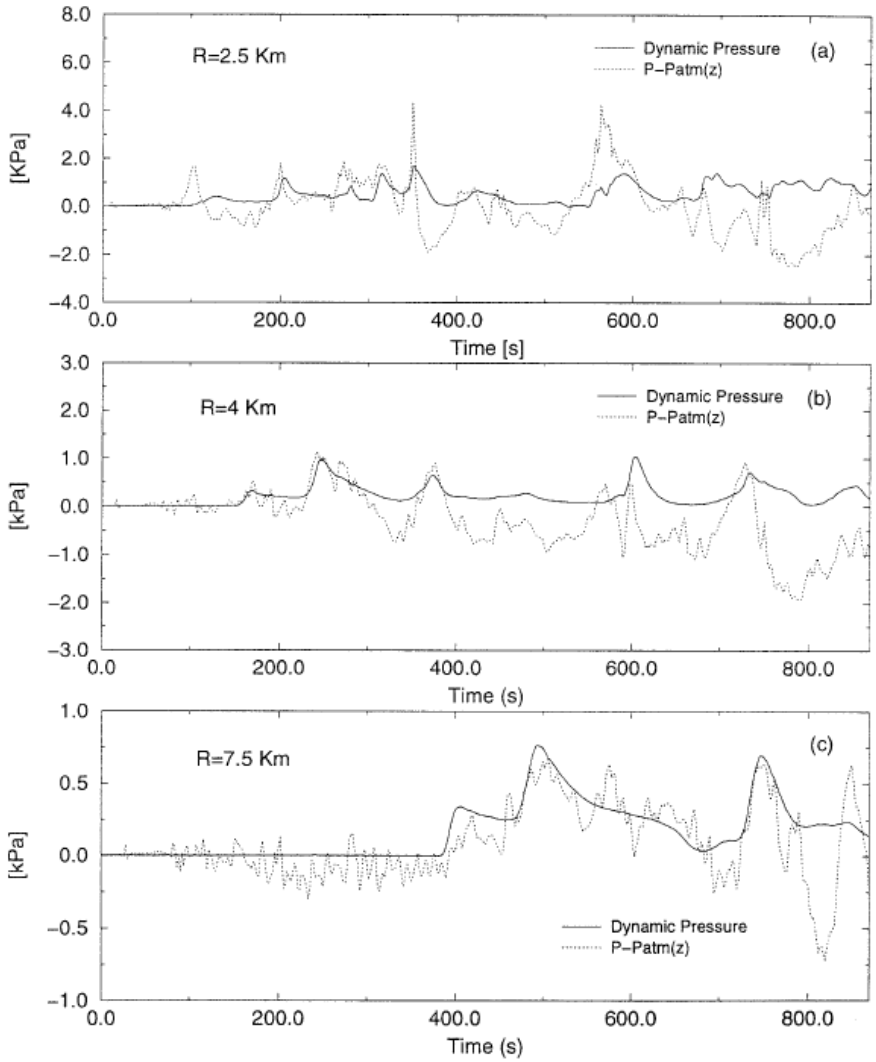

Fig. 3.8 Simulation B90-W2-t950, relative to northern sector B. Evaluation made at different distances R from the crater, at 5m from the ground: a) R=2km; b) R=4km; c) R=7.5km (Esposti Ongaro et al., 2002).

European project EXPLORIS (EVR1-CT-2002-40026) the illustrated PDCs simulation model has been integrated, including the 3D effects of the volcano topography and flow propagation (Esposti Ongaro et al., 2008). Five simulations were conducted:

- SIM1: convective column, with eruptive mass m' equals to $5x10^7 kgs^{-1}$
- SIM2: incipient column collapse, with m'= $5x10^7 kgs^{-1}$
- SIM3: the partial collapse of the column, with m'= $5x10^7 kgs^{-1}$
- SIM4: total column collapse, with m'= $5x10^7 kgs^{-1}$
- SIM5: the partial collapse of the column, with m'= $8x10^7 kgs^{-1}$

Figure 3.9 shows a map of the maximum dynamic pressure reached by the pyroclastic flow, in case of the total collapse of the Plinian column (SIM4), in an undisturbed atmosphere 10m from the ground, in the time interval 0-900s. The dynamic pressure values indicated so far neglect the effect of the turbulence generated by the interaction of the pyroclastic flow with an urban settlement. Zuccaro and Ianniello (2004) [45] examine the problem through the study of a sector of the municipality of Torre del Greco, south-east side of Vesuvius, affected by pyroclastic flow with a velocity of 20ms-1, density of $10 kgm^{-3}$ and viscosity of $10^{-3} Pa * s$. The results obtained highlight the barrier effect of the first buildings hit by the flow on those behind it. The barrier effect has even been shown to produce depressions (Figure 3.10), with a multiplicative pressure coefficient in the range [-3; +2].

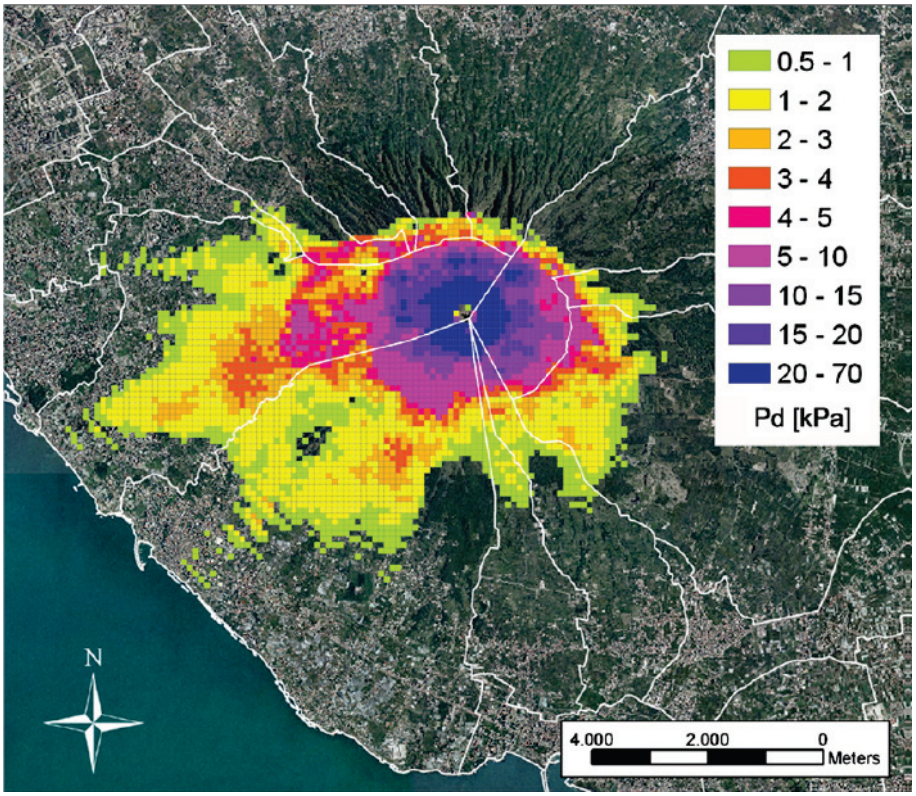

Fig. 3.9 Map of the maximum dynamic pressure reached by the pyroclastic flow, in the case of total collapse of the Plinian column (SIM4), in an undisturbed atmosphere at 10m above ground, in the time interval 0-900s (Esposti Ongaro et al., 2008). [30]

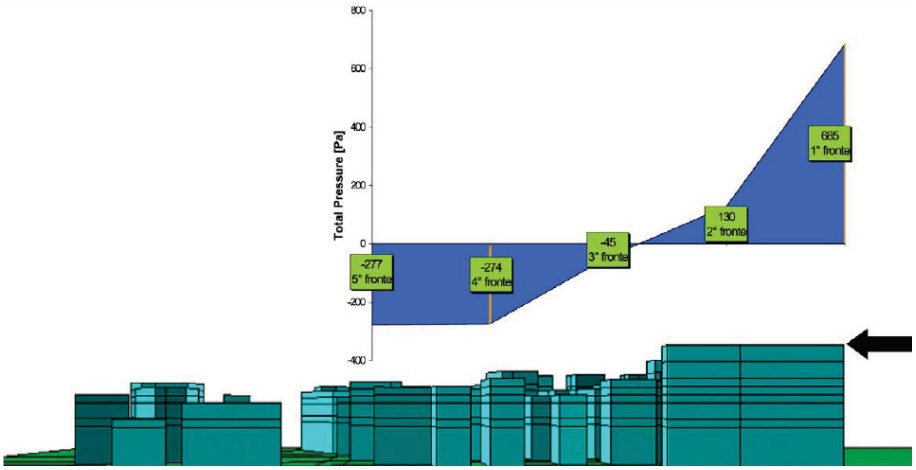

Fig. 3.10 Reduction of pressures in the main direction of pyroclastic flow (Zuccaro and Ianniello, 2004) [45]

3.1.1 Action and effects on the buildings

Based on the model by Todesco et al. (2002) [40] and simulations by Esposti Ongaro et al. (2002), Spence et al. (2004) [38] evaluated the impact of a pyroclastic flow produced by a sub-Plinian eruption of Vesuvius on the buildings of four cities in the red area, Torre del Greco, Trecase, Boscotrecase and Boscoreale. In particular, the pressures produced by the pyroclastic flow generated by the partial collapse of the Plinian column during a sub-Plinian eruption were estimated. In Table 3.1, the peaks of the pressures acting on the four faces of a building, at 5 and 15m from the ground floor, are reported as the distance from the vent varies.

The resulting dynamic pressures in Table 3.1 are apparently very low, but modelling is unable to incorporate many local topography factors and the shape of the building, which would significantly influence peak pressures. In summary, the action of a pyroclastic flow on an invested building can be schematically characterised as a uniformly distributed horizontal overpressure qH along the facades exposed to the crater and a downwind depression along the facades equal to qH/3 (Figure 3.11), accompanied by temperatures between 150 and 400°C. The value assumed by qH is a function of distance from the crater and scale of the eruption (Plinian, Sub-Plinian, Strombolian, etc.). For example, in the case of a sub-Plinian Vesuvian eruption, to distances of more than 4-5km from the crater, qH can be assigned a value of 2- 4 kPa, adopting a multiplicative coefficient of the pressures due to the turbulences equal to 2.

Table 3.1 Dynamic pressure on different building facades at 5 and 15m above ground, exerted by a pyroclastic flow (Spence et al., 2004)[38]

	Walls of a building 5m above the ground				**Walls of a building 15m above the ground**			
Distance from the vent [km]	**Dynamic flow pressure [kPa]**	**Windward front wall [kPa]**	**Side Wall [kPa]**	**Back wall downwind [kPa]**	**Dynamic flow pressure [kPa]**	**Windward front wall [kPa]**	**Side Wall [kPa]**	**Back wall downwind [kPa]**
4-5	0,9	0,77	-0,63	-0,27	1,25	1,06	-0,88	-0,38
5-6	0,7	0,6	-0,49	-0,21	1,05	0,89	-0,74	-0,32
6-7	0,95	0,81	-0,67	-0,29	0,95	0,81	-0,67	-0,29
>7	0,8	0,68	-0,56	-0,24	0,35	0,3	-0,25	-0,11

The resulting dynamic pressures in Table 3.1 are apparently very low, but modelling is unable to incorporate many local topography factors and the shape of the building, which would significantly influence peak pressures. In summary, the action of a pyroclastic flow on an invested building can be schematically characterised as a uniformly distributed horizontal overpressure qH along the facade3.11), accompanied by temperatures between 150 and 400°C. The value assumed by qH is a function of distance from the crater and scale of the eruption (Plinian, Sub-Plinian, Strombolian, etc.). For example, in the case of a sub-Plinian Vesuvian eruption, to distances of more than 4-5km from the crater, qH can be assigned a value of 2- 4 kPa, adopting a multiplicative coefficient of the pressures due to the turbulences equal to 2.

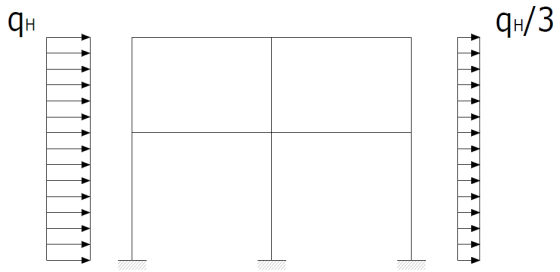

Fig. 3.11 Schematisation of the load due to a pyroclastic flow (De Gregorio et al., 2010) [11]

Pyroclastic flows and surges can swallow up human settlements with a short warning and may cause many human losses, thus such as the destruction of goods and infrastructure. Recently, the observations direct relating to Mt St Helens in the USA (1980), Unzen in Japan (1991), and Montserrat, the Lesser Antilles in the Caribbean Sea (1997) made it possible to study some characteristics of pyroclastic flows. For each type of building, there is a degree of correlation between the flow characteristics and the degree of damage, which can be used for to obtain more direct measurements of the flow variables, as is done for the earthquakes with the intensity scale. Baxter et al. (2005) [2], based on the observations made in Montserrat proposed a descriptive classification damage levels. The severity of the observed damage increases in the distance of 2-3 km from the periphery to the main axis of diffusion of flows, showing a crescendo from more or less light damage (window breakage, partial roof collapse, etc.) until destruction in the central flow area (Figures 3.12 and 3.13). The relationship between flow characteristics and damage to structures is important. It allows, in fact, to deduce the level of impact of any future pyroclastic flow and, consequently, to estimate human losses and damage to buildings in any inhabited area. This type of information is of fundamental importance for the preparation of security plans for areas at risk. The test area shows that light damages (Damage Level 1) are in all peripheral and intermediate areas to the flow to the central area's edges (Figure 3.12 a). While in the intermediate area of the flow in Figure 3.12 b, the damage levels vary between 1 and 3 for buildings located within a short distance of each other. Furthermore, the relationship between flow characteristics and damage to structures is important. It allows to deduce the impact level of any future pyroclastic flow and, consequently, estimate human losses and damage to buildings in any inhabited area. This type of information is of fundamental importance for the preparation of safety plans for areas at risk.

Besides Spence et al. (2004) [39] have assessed that the main critical points concern the impact on openings, which are particularly vulnerable. In these cases, although the static nature of the building is not compromised, the risk connected with the passage of the flow in the internal environments following the breakthrough of the openings is significant. It is therefore necessary to distinguish the risk of partial collapse due to damage

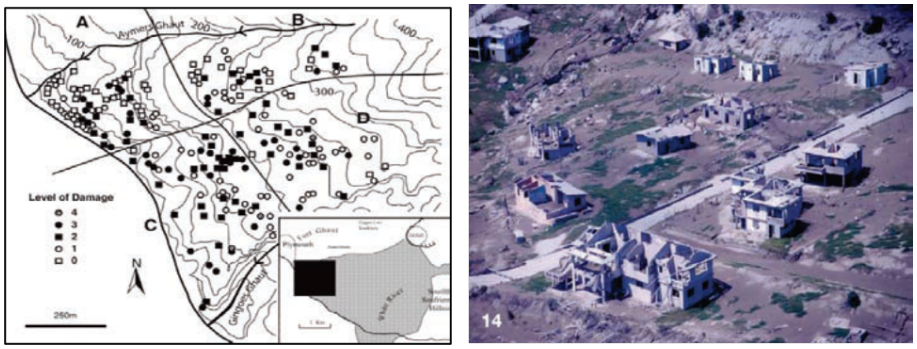

Fig. 3.12 Soufrière Hills volcano eruption, Montserrat, December 1997. St. Patrick area. a) Location of dwellings and their damage levels. b) Damage produced by a pyroclastic flow in an intermediate flow zone. (Baxter et al., 2005) [2]

to structural and non-structural elements in combination with other types of phenomena (such as seismic action), from the risk of fire caused by the passage of the flow inside the building following the breakthrough of existing windows and openings. The damage caused by the impact of pyroclastic flows on buildings depends on the combination of multiple factors such as: the duration of the phenomenon, the temperature of the flow and the pressure produced by the impact. The prevailing typological characteristics capable of influencing the structural response of buildings are linked to their mass and height, and also to the ability of specific technical elements, such as curtain walls and openings, to resist lateral pressure; for this reason, masonry buildings have an intrinsic ability to resist such phenomena, thanks to the generally low height and high stiffness of the structural elements. In reinforced concrete buildings, on the other hand, the presence of weak or large-sized curtain walls can be a factor of weakness. Existing openings are hardly able to withstand the impact of pyroclastic flows, due to the vulnerability of the glazed parts to the combined action of pressure and temperature.

Fig. 3.13 Soufrière Hills volcano eruption, Montserrat, December 1997. Damage produced by a pyroclastic flow: a) in a peripheral zone of the flow; b)in an intermediate zone of the flow; c) in the central zone of the flow. (Baxter et al., 2005) [2]

3.2 Ash Fall (AF)

Deposits due to ashfall are formed by the increase of clasts falling by gravity from an eruptive column. The distance at which they fall depends on the initial ejection speed and angle. The larger clasts fall near the point of emission, the more fragmented ones are deposited at a greater distance, while the finer ones, due to the stratospheric winds, are transported at an even greater distance; therefore, as the distance from the vent increases, the deposits are finer. Usually, the topography is covered by a uniform layer (Figure 3.14), but as they are materials with a very reduced consistency, they can easily accumulate in the most depressed areas of the territory. During violent explosive eruptions, such as the Plinian and Sub-Plinian eruptions, large pumice deposits cover an elliptical area around the crater elongated in the direction of the wind (Figure 3.15 a-d). On the other hand, moderate explosive eruptions produce clast deposits whose distribution is symmetrical around the crater (Figure 3.15 e-f), since the material is not thrown high enough to be carried by the wind. The dangerousness of the ash fall depends on its thickness and density, which is a function of its composition (ratio between solid and vesicular particles), the degree of compactness and humidity of the deposit, and the occurrence of subsequent atmospheric disturbances. In fact, depending on the different atmospheric conditions, the density can vary from 400/1600 kg/m3 in dry conditions to 800/2000 kg/m^3 in wet conditions. Also, Cioni et al. defined the characteristics of the main 24 Vesuvian eruptions (Table 3.2); indicating not only the VEI and the column height (H), but also the extent (A) of the area included in the 10 cm isopach, the volume (V) of the ejected pyroclasts and their density (ρ).

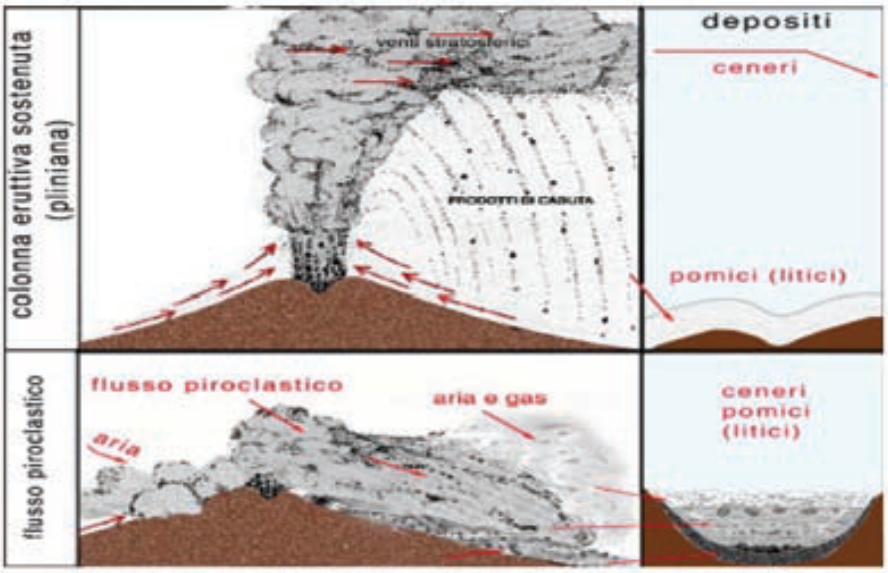

Fig. 3.14 Ash-fall (INGV, 2010)

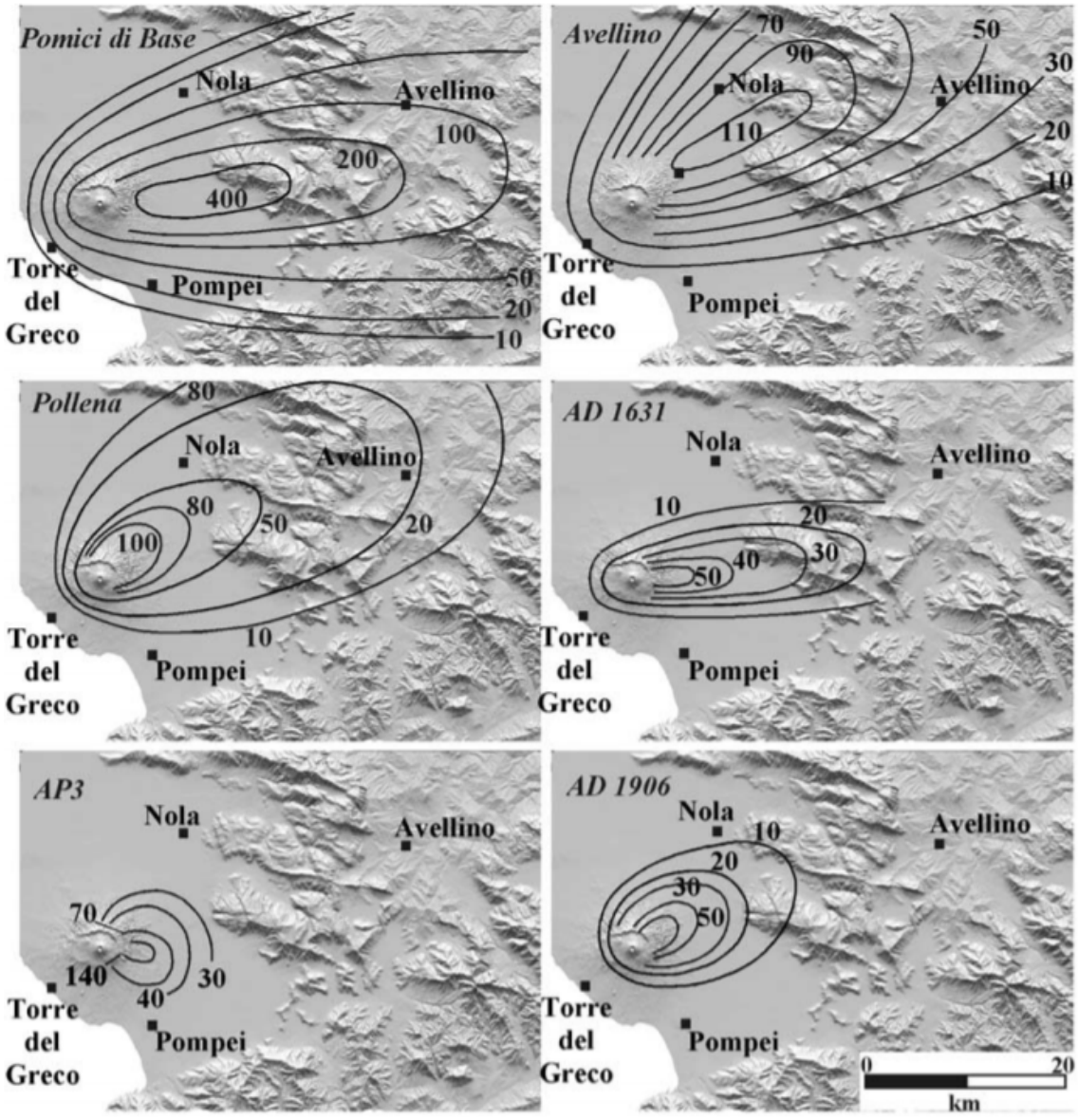

Fig. 3.15 Isopache maps (in cm) of some Vesuvian eruptions: a) Pomici di Base, 18300 ± 180 BP; b) Avellino, 3960 ± 60 BP; c) Pollena, 472 dC; d) 1631dC; e) AP3, 2710 ± 60 BP; f) 1906 dC. (Raffaele Cioni et al., 2003 [8]).

Table 3.2 Main characteristics of some events at Vesuvius. (Cioni et al., 2003).

Eruptions	**VEI**	**H [m]**	**A [km^2]**	**V [$x10^6 m^3$]**	**ρ[kg/m^3]**
A.D. 1944	3	4	270	110	1200
A.D. 1906	3	13	210	80	1100
A.D. 1631	5	19	300	210	1000
PM6	3	-	35	10	900
PM5	3	-			
PM4	3	-	60	100	900
PM3	3	-			
PM2	3	10	65	40	900
PM1	4	14	210	90	900
Pollena	5	-	1000	420	900
A.D. 79-472	3	-	150	150	900
Pompeii W	6	26	1540	1100	500
Pompeii G	6	32	3430	1800	1000
AP5	4	-	180	80	1500
AP4	4	-	280	120	1300
AP3	4	15	350	150	1500
AP2	4-5	20	400	170	1500
AP1	4-5	-	300	150	1500
Avellino W	5	23	585	320	400
Avellino G	6	31	2420	1250	800
Mercato	6	22	2150	1400	600
Verdoline	5	20	885	430	1000
Pomici di Base	6	-	2920	4400	900

3.2.1 Action and effects on the buildings

As described above, the ash fall can accumulate and reach the necessary thickness to cause the roofs' collapse. Columns, walls or foundations can also collapse due to ash deposits (Figure 3.17), because of the increase in vertical loads. To establish the tephra effect on

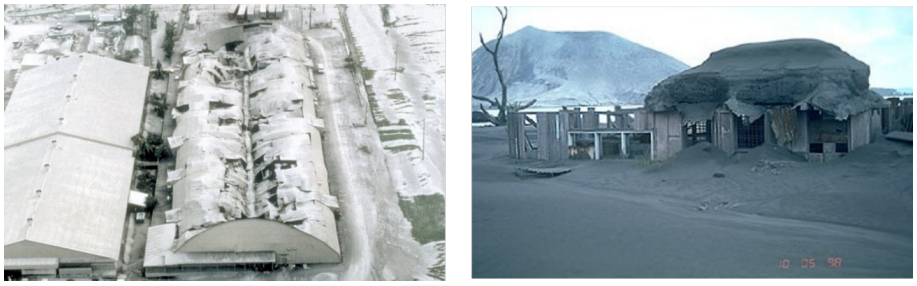

Fig. 3.16 Collapse of roofs following the ashfall. On the right, the thickness of the deposit is visible on the portion of the roof that did not collapse.

the building, it is necessary to determine the load per unit of surface. Therefore the action due to the ash fall can be schematized as a uniform vertical static pressure (Figure 3.17) defined through the following product:

$$q_v = \rho h g \tag{3.1}$$

where:

- g represents the acceleration of gravity (9.81 m / s2),
- h is the thickness (m) of the deposit,
- ρ is the density (kg /m3) of the deposit.

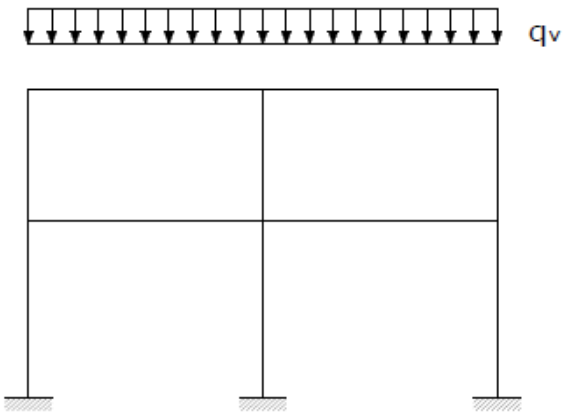

Fig. 3.17 Schematisation of the load due to falling deposits.(De Gregorio et al., 2010)

It must be underlined that, however, although the maximum ash-fall load can be deduced from an isopach map, the maximum load produced on a roof can be different for various reasons. In fact, the deposit could slip from a roof or be more or less humid or be transported away by rain or wind. In some aspects, such as falling load from very sloping roofs or accumulation in excavations, the action due to the accumulation of tephra is the same as that of the snow; therefore it is possible to consider the load from tephra as a distributed gravitational load, similar to the snow one. According to current Italian legislation, the snow action can reach 3/4 kPa, in the case of the northern regions, while for the Neapolitan area it does not exceed 1kPa. In order to define the action exercised by a pyroclastic deposit De Gregorio et al. (2010) proposed a completely similar approach to that used in the 2008 NTC; that is, the load in qS coverage can be assessed through the following expression:

$$q_s = \mu_1 \cdot q_v \cdot C_E \tag{3.2}$$

where:

- μ_1 represents the form coefficient of the roof,
- q_v is the characteristic reference value of the ash fall load on the ground [kN / m2] provided by the relation 3.2 with reference to the isopaches of the previous eruptions,
- C_E is the exposure coefficient.

The values of the μ_1 coefficient are shown in Table 3.4, referring to one or two pitch roofs; the angle formed by the pitch with the horizontal is indicated with α.

Table 3.3 Values of the shape coefficient μ (NTC 2008)

Coefficient of form	$0° \leq \alpha \leq 30°$	$30° < \alpha < 60°$	$\alpha > 60°$
μ_1	$0.8 \cdot \frac{60-\alpha}{30}$	0.8	0

Furthermore, two different load arrangements must be considered:

- ash fall load deposited in the absence of wind;
- ash fall load deposited in the presence of wind.

In the case of single-pitch roofing, it is assumed that the deposit is not prevented from slipping. If the end of the pitch ends in a parapet or other obstruction type, then the form factor cannot be assumed to be less than 0.8, regardless of the angle α. The load condition considered must be considered both in the presence of wind and in absence. Concerning

the two-pitch roof De Gregorio et al. assume that the deposit is not prevented from sliding and that if at the end of the pitch there is a parapet or other type of obstruction then the shape coefficient cannot be considered less than 0.8, regardless of α. Furthermore, for the case of load in the absence of wind, they propose to consider the condition Case I (Figure 3.18), while, for the case of load in the presence of wind, they indicate as load condition to be considered the one called Case II (Figure 3.18). Finally, the CE coefficient, which modifies the load's value, depends on the specific characteristics in which the buildings rise (Table 3.5). It is important to underline that the load from ash deposit causes an overload q_S and exerts a further burden on the structures affected, due to the high temperatures, between 150° and 350°, which cause a degradation of the mechanical characteristics of the materials.

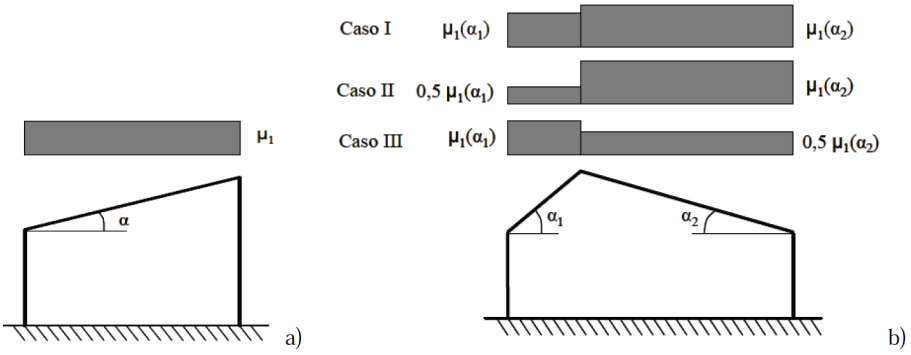

Fig. 3.18 Schematisation of the load due to falling deposits.(De Gregorio et al., 2010)

Table 3.4 C_E exposure coefficient values (NTC, 2018).

Topography	Description	CE
Windswept	Flat, unobstructed areas exposed on all sides, without buildings or taller trees.	0,9
Normal	Areas where there is no significant removal of load on the construction	1
Sheltered	Areas where the construction in question is significantly lower than the surrounding terrain or surrounded by taller buildings or trees.	1,1

Chapter 4

Emergency Plans

Emergency plans are an indispensable tool for risk mitigation and are also the only tool available to local authorities today as a solution to safeguard the population. For volcanic risk are elaborated according to the eruptive scenario and alert levels defined for a specific volcano and for a specific time, population, distribution over the territory, infrastructure and vulnerability, and people's most likely behaviour. Each of these parameters can vary over time due to the advancement of scientific knowledge, volcano behaviour changes, administrative measures that can change the urban planning of the territory, and education and information programmes. Therefore, an emergency plan should not be considered a static instrument valid for an indefinite period. On the contrary, it should be understood as a dynamic instrument to be periodically updated to changes in parameters on which it has been drawn up. Based on the expected maximum eruption scenario, a national emergency plan for the Vesuvius and Campi area was drawn up by a commission set up by the Minister of Civil Protection. The plan is currently being updated by the "Commission responsible for updating the emergency plans for the Campi Flegrei and Vesuvian areas". It is essential to point out that the maximum expected event is not necessarily the most likely: the actual eruption could be more modest than the event considered a reference for elaborating the emergency plan. The only defence for people against the explosive eruption of the type described above is to move away from the area at most significant risk, i.e. the area likely to be invaded by PDCs, before the eruption begins. In past years, timely evacuations have saved hundreds of thousands of lives, including the recent eruptions of the Pinatubo volcano in the Philippines, Usu in Japan, Tavurvur and Vulcan in New Guinea and Popocatepetl in Mexico. On the contrary, tens of thousands of deaths had occurred when the volcano's precursor phenomena were not followed by civil protection interventions, as at Nevado del Ruiz in Colombia in 1986. The decision to remove the area's population at the most significant risk will be based on analysing the Vesuvius Observatory surveillance system's precursor phenomena. Historical information relating to the last centuries of

Emergency Plans

Vesuvius activity and the phenomena recorded before the last eruptions indicate that, as for most volcanoes, Vesuvius eruptions have had precursor phenomena, such as intense seismic activity, noticeable soil deformations and intensification of fumarolic activity. The historical evidence of precursor phenomena and the knowledge acquired today on the volcano structure and history have made it possible to define alert levels, according to which the emergency plan is divided into various phases. These levels characterise the volcano's evolution until the eruption and are defined by variations in seismicity, gravimetric and magnetic field, chemical composition and temperature of fumaroles, progressive soil deformations, etc. The levels have also been defined by analogy with the trend of variations in physical and chemical parameters recorded on volcanoes similar in structure to Vesuvius. The data collected on the activity of Vesuvius in recent decades have made it possible to define the base level characteristic of the volcano in recent decades. This level is represented by the absence of soil deformation, low seismicity, absence of significant variations in the gravimetric field, constant composition values, and decreasing fumarolic gas temperature values. Alert levels following the primary level are linked to progressive changes in measured parameters (Table 4.1).

Table 4.1 Operational module of the Vesuvius emergency plan (Protezione Civile, 2010).

Alert levels	Volcano status	Probability of eruption	Expected eruption time	Operational phases of the plan
Base	No significant changes in controlled parameters	Very low	Indefinite, however not less than several months	Ordinary activity
Attention	Significant change in controlled parameters	Low	Indefinite, but not less than several months	I Phase Attention
Pre-alarm	Further variation of controlled parameters	Medium	Indefinite, but not less than a few weeks	Phase II Pre-alarm
Alarm	Occurrence of phenomena and/or trend in controlled parameters indicating pre-testing dynamics	High	Weeks to months	Phase III Alarm

The plan identifies the actions to be carried out according to the alert level and three specific areas of intervention, called Red Zone, Yellow Zone and Blue Zone, based on the type and extent of the hazards from which they could be affected (Figure 4.1).

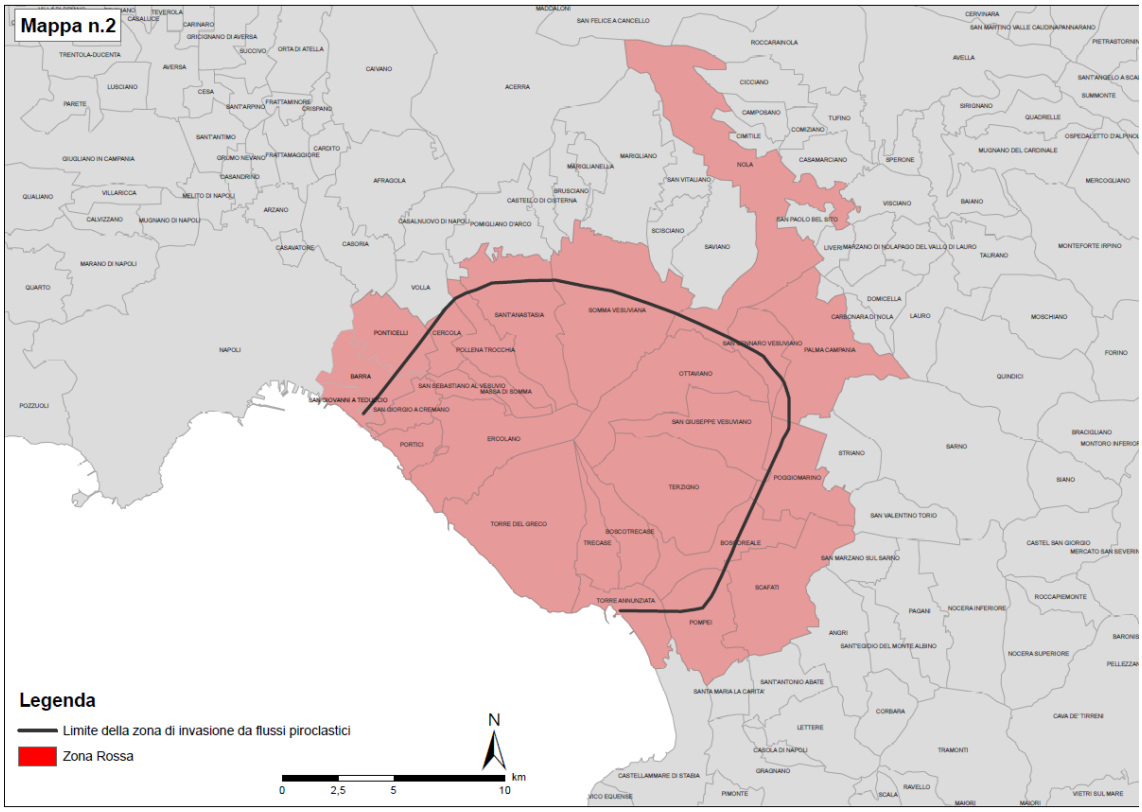

Fig. 4.1 Volcanic risk map from the Vesuvius emergency plan (Protezione Civile, 2010).

The Red Zone has been identified by using the data related to the distribution of products of the Plinian and Sub-Plinian eruptions and simulating different phases of the maximum expected eruption on the computer. Large portions of this zone could be invaded by pyroclastic flows and mudflows and covered by fall products' thick accumulations. It has an extension of 200 km^2, including 18 municipalities, all in the province of Naples, where a population of 600,000 inhabitants live. During the eruption of 1631, almost 20% of this area was destroyed by pyroclastic flows. The wall of Monte Somma, which in recent centuries has protected the towns located to the north from lava flows, may not be high enough to prevent it from being bypassed by pyroclastic flows. For this reason, the Red Zone has a circular geometry. Owing to the pyroclastic flows' speed and high destructive power, the populations will have to move away from this area before the beginning of the eruption. The Yellow Zone is the area that could be affected by falling particles with a load greater than 300 kg/m2, which could cause roofs to collapse. It has an extension of 1,100 km2 and includes several dozen municipalities in the provinces of Naples, Salerno, Avellino, Caserta, and Benevento. Only one sector of this area will be affected by the fall

of large quantities of ashes, pumices and fragments of rock, which could cause roofs to collapse, darkness, breathing disturbances, engine blockage, difficulties in the circulation of vehicles and interruption of the regular operation of service networks. The area of the yellow zone that will be affected by the fall of particles cannot be identified in advance because the height that the eruptive column will reach, the direction and speed of the high winds at the time of the eruption will define it. Therefore, only a part of the yellow zone inhabitants will have to move away during the eruption. In 1631 about 10% of this area was seriously damaged. The Blue Zone is that area which, in addition to being exposed to falling particles with a load more than 300 kg/m2, could be invaded by mudflows and flooding. It has an extension of about 100 km2 and corresponds to the Nola basin. Today, more than 300,000 people live within the now active part of the entire structure of the Campi Flegrei, the caldera, while those living in its immediate vicinity are more than a million. Due to the caldera's high danger and the intense urbanisation both inside and in the surrounding areas, the volcanic risk is exceptionally high. To reduce this high risk, the Civil Protection has established a National Commission in charge of updating the existing emergency plan to be implemented in case of resumption of eruptive activity. The Commission's work is still ongoing. Since it is not possible, as for Vesuvius, to identify a reference eruption, the scenario has been constructed based on the most frequently occurring eruptive phenomenologies (the type of eruption, volume of magma emitted). Alternating magmatic and phreatic-magmatic explosions characterise these. Magmatic explosions will result in the formation of a sustained column, with behaviour like that described for the eruptive scenario of the emergency plan "Vesuvius", and consequent fall of particles to the ground. Phreatic-magmatic explosions will generate pyroclastic currents (mainly surges), which will flow to the ground at high speed. The scientific community hypothesised the eruptive scenario, and the maps of The Civil Protection has defined the area of highest risk for the eruptive phenomena produced by this one. The latter includes the area exposed to the danger of pyroclastic currents and identified as the Red Zone, currently inhabited by about 350,000 people (Figure 4.2). It includes the municipalities of Monte di Procida and Bacoli and part of those of Pozzuoli and Naples.

In view of the foreseeable variations in the physical and chemical parameters of the volcanic system that will be recorded by the surveillance system of the Vesuvian Observatory, four alert levels have been defined (Table 4.2). These range from the basic level, which characterizes the current state of the caldera, to the alert level, characterized by a high probability of eruption. In the latter case, the Civil Protection has provided for the removal of the population from the red zone, and its transfer to other Italian regions. In view of the brady seismic events that have occurred several times in the last thirty years, for the portion of the red zone that could be affected, a plan is being drawn up for the bradyseismic emergency, with interventions that also provide for the relocation

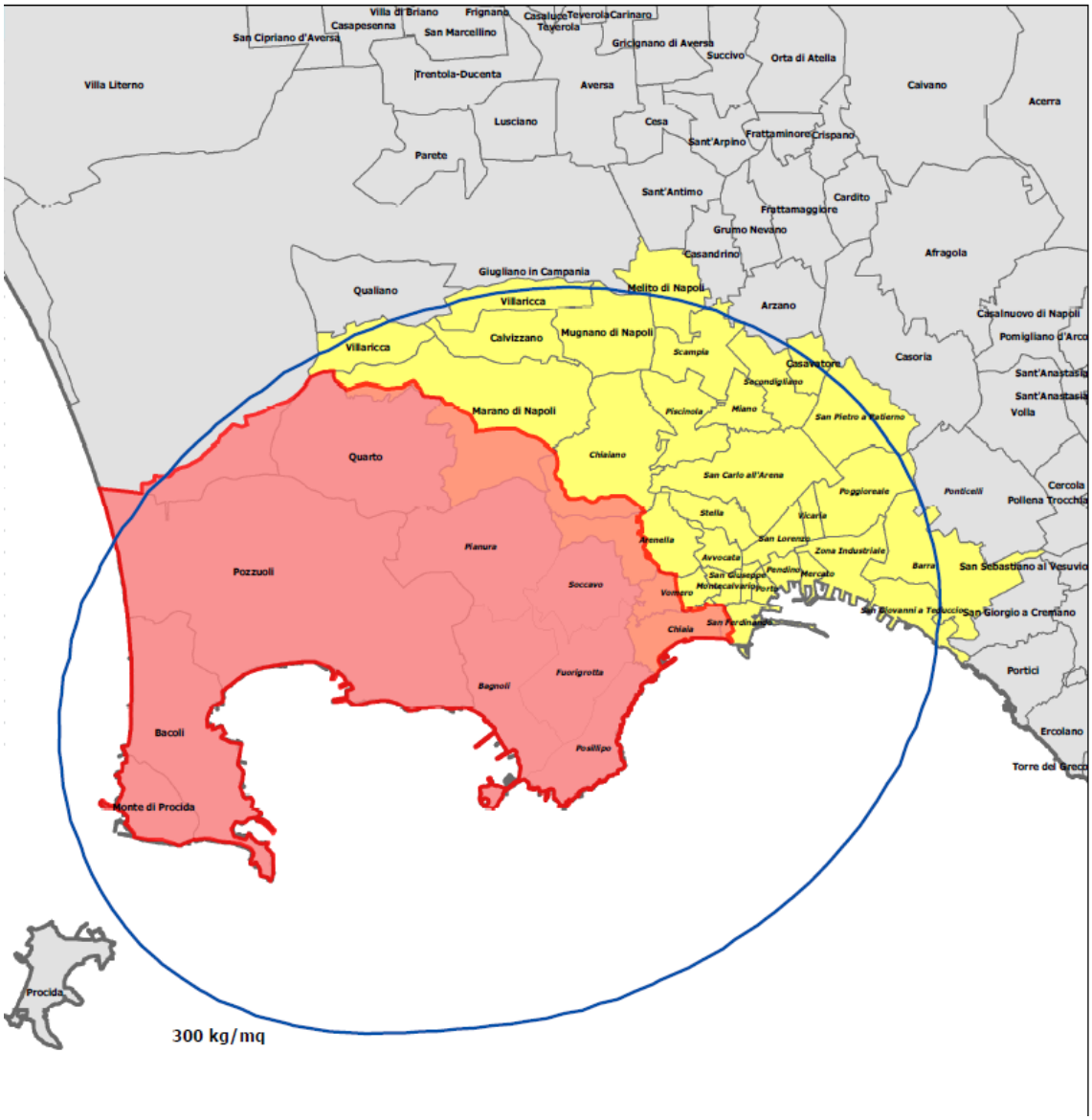

Fig. 4.2 Volcanic risk map from the Vesuvius emergency plan (Protezione Civile, 2010).

of the population involved in structures in Campania. Currently in elaboration is also a detailed zoning of the Neapolitan-Flegrean area exposed to the danger of falling pyroclastic material, and the definition of the intervention strategy in this area, called the Yellow Zone.

Table 4.2 Alert levels and related actions by the scientific community for the Campi Flegrei caldera (Protezione Civile, 2010).

Alert levels	Volcano status	Probability of eruption	Expected eruption time	Action	Comunication
Base	No significant changes in controlled parameters	Significant change in controlled parameters	Further variation of controlled parameters	Surveillance activities as planned	Occurrence of phenomena and/or trend in controlled parameters indicating pre-testing dynamics
Attention	Very low	Low	Medium	Scientific and technical alert status and increase in surveillance systems	High
Pre-alarm	Indefinite, however not less than several months	Indefinite, but not less than several months	Indefinite, but not less than a few weeks	Surveillance activities continue; simulation of possible eruptive phenomena.	Weeks to months
Alarm	The Vesuvius Observatory produces six-monthly bulletins on the activity of the volcano.	The Vesuvius Observatory produces a daily bulletin and communicates information on the volcano's status to the Department of Civil Protection.	The Vesuvius Observatory continuously communicates information about the status of the volcano to the Civil Protection Department.	Surveillance with remote system	The Vesuvius Observatory continuously communicates information about the status of the volcano to the Civil Protection Department.

Chapter 5

Identification of typological structural characteristics of elements at risk under effects of pyroclastic flows and ash fall

To define a proper mitigation strategy concerning the mechanical and thermal stresses, which characterise pyroclastic flows and ashfalls, the Campania buildings' structural characteristics, which most influence the building's volcanic vulnerability, were analysed concerning roofs, facades and openings. The data were collected by the PLINIVIS centre (Centre for Hydrological, Volcanic and Seismic Engineering, Scientific Director Prof. G. Zuccaro) during the European project EXPLORIS (2002-2005) [43], through a specific form which is divided into the following eight sections:

1. The **IDENTIFICATION** section locates the building regarding the geographical parameters provided by the Campania region;

2. The **GENERAL INFORMATION** section refers to the type (ordinary building, warehouse, power station, etc.), destination (hospital, school, etc.), use (fully used, partially used, unused and abandoned) and exposure (ordinary, strategic, exposed to particular risks) of the building.

3. The **CONDITIONING** section refers to the age, the state of conservation of the structure (low, mediocre, good and excellent) and the type of finishing (economical, ordinary, luxury).

4. The **DESCRIPTIVE FEATURES** section refers to the total number of floors starting from the ground floor, the number of floors above ground, including the penthouse; the number of residential apartments; the presence of basement occupied or not; the height of the first floor; the minimum and maximum heights of all floors

up to the roof; the presence of obstacles higher than 2m; the orientation (angle between the longest facade or the main facade and the North); and the position in the unit within the aggregate (Figure).

5. The **STRUCTURAL FEATURES** section refers to the primary type (reinforced concrete, masonry, wood, steel and mixed); to vertical structures (bag masonry with or without reinforcements, the masonry of hewn stones, masonry in tuff blocks, reinforced concrete frame. with weak or resistant plugging, etc.); to horizontal structures (wooden floor, floor with steel beams, concrete floor, vaults, etc.); to wall thickness; and the type of curtain walls (tuff blocks or squared stones, concrete blocks, etc.).

6. The **OPENINGS** section refers to the percentage of openings on the facade, the number of small, medium and large windows dimensions, material (wood, PVC, aluminium or wood-aluminium, light steel, anti-intrusion steel), their protection and condition.

7. The **INTERVENTION** section refers to the age and type of intervention (extraordinary maintenance, upgrading and adaptation).

8. The **REGULARITY** section refers: to the distribution of masses and rigidity in plan and elevation; to the type of structure (with a single or double one-way frame, with single or double directional walls, or walls with frames); to the presence of soft floor (pilotis on the part of the ground floor, ground floor completely open, or soft intermediate floors); and the eventual presence of soft elements.

5.1 Roofs

The data on the roofs were grouped by vertical structure, geometry and roofing material. From a careful examination of the available information, it is possible to define the following macro-groups for the Campi Flegrei:

- Flat Reinforced concrete floors or slabs
- Flat Main frame made of metal beams
- Multi-pitched Reinforced concrete floors or slabs

While the following two classes were identified for the Vesuvius area:

- Flat Reinforced concrete floors or slabs
- Flat Main frame made of metal beams

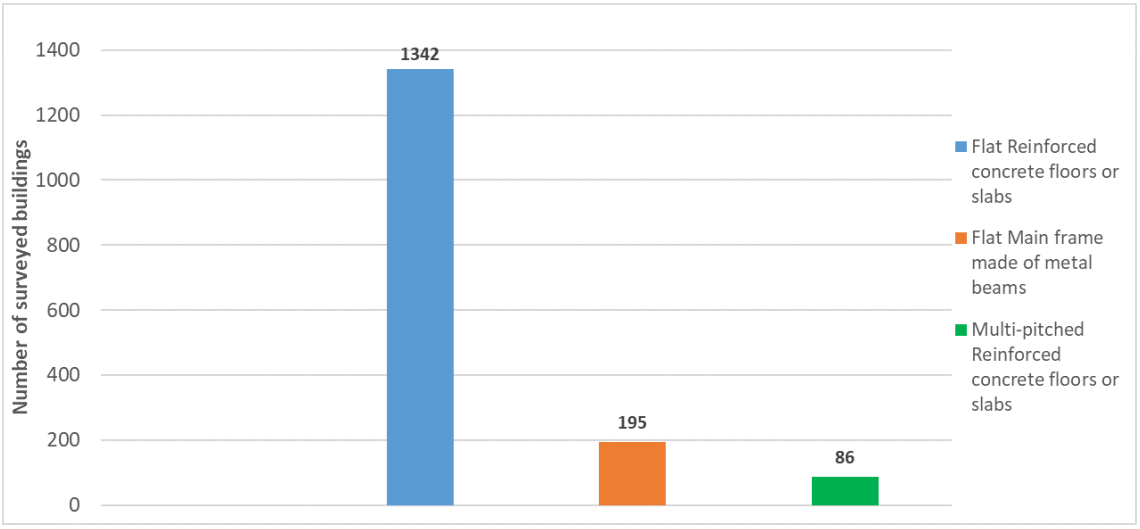

Fig. 5.1 Breakdown of surveyed buildings in the Campi Flegrei area by roof type

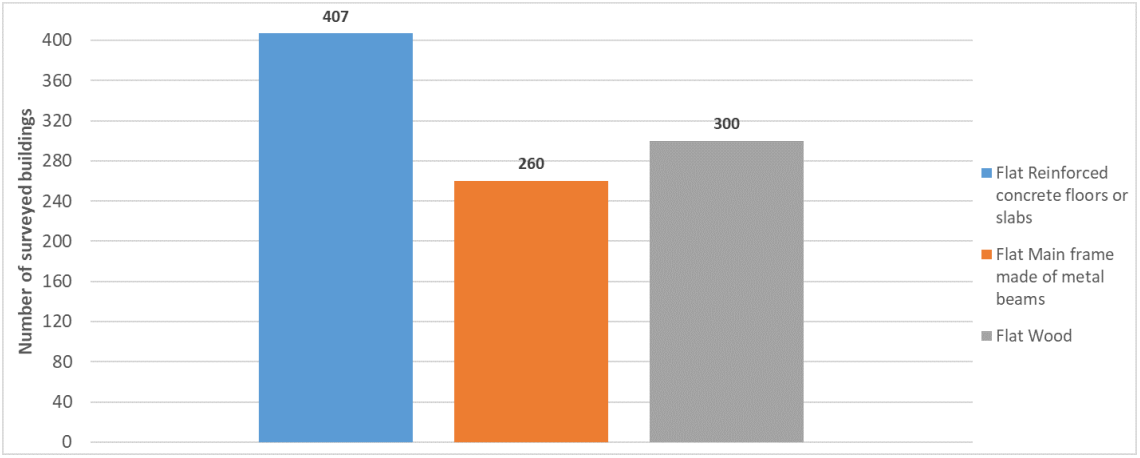

Fig. 5.2 Breakdown of surveyed buildings in the Vesuvio area by roof type

5.1.1 Wood Floor

Wooden floors consist of a main load-bearing structure made of rough or squared beams and a secondary structure made of slabs resting on the beams; the simplest and most common types consist of a single row of load-bearing beams. The main beams are generally made of rough chestnut, round beams, without squaring, with a diameter varying between 20 and 30 cm, which was laid in special recesses in the bearing walls, for a length greater than or equal to 1/20 of the load-bearing capacity of the floor; they were arranged at a distance between centres of 80-90 cm, with the largest diameter alternating from one side to the other. In the beam warping's normal direction, the rough secondary beams were placed, of a semi-cylindrical shape, whose length varied between 92 and 106 cm. The first layer of mortar with pozzolan and ordinary sand and slaked lime 3 cm thick was placed on the secondary beams. Finally, a layer of a conglomerate of the quarry or volcanic lapillus and lime was placed on top (Figure 5.3).

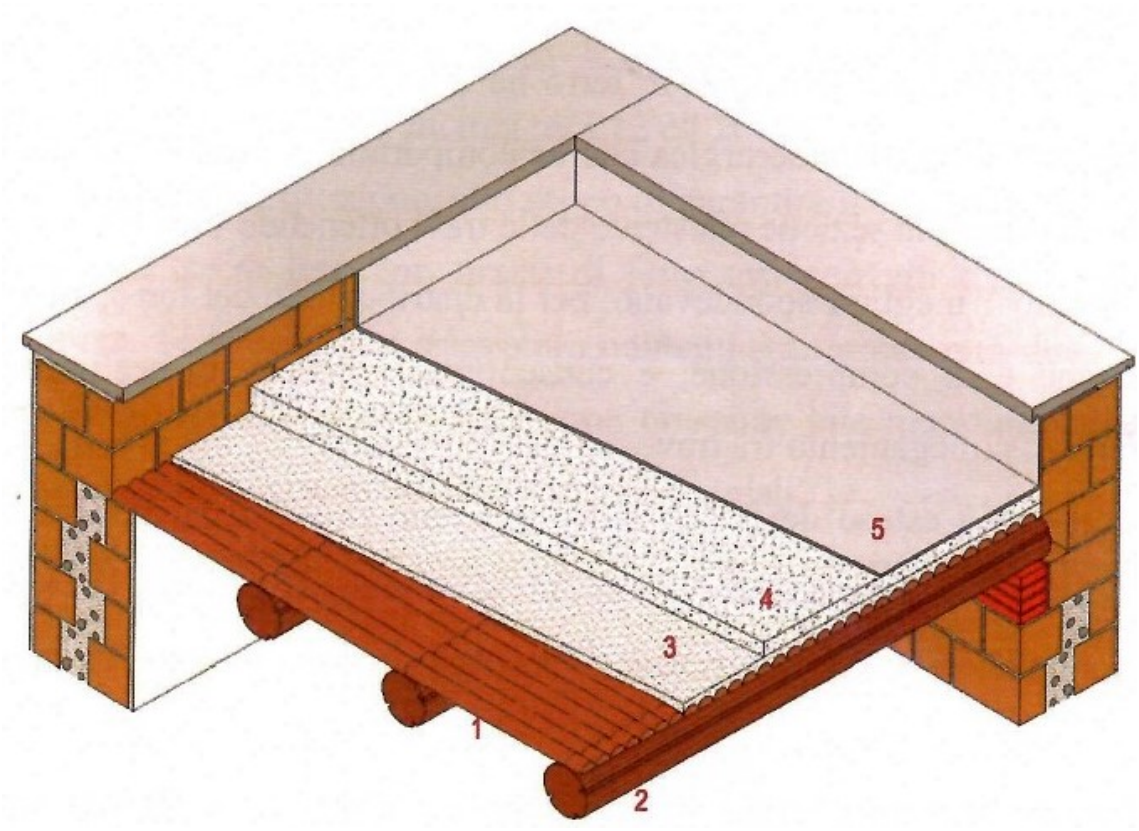

Fig. 5.3 Wooden floor: 1) Main beam, 2) Secondary beams, 3) Mortar layer, 4) Slope screed, 5) Waterproofing layer.

5.1.2 Floor slab with steel beams

The use of this typology was considerably increased with the development of the iron and steel industry, which involved the production of double-T profiles, thus succeeding in reducing the resistant section of the beams obtaining a reduction in costs. The increasingly widespread use of the iron floor has been favoured by a series of factors: resistance to fire and deterioration due to humidity, ease of execution and long life. The beams' ends were placed on "bearings formed by some rows of brick masonry or hard stone elements. The secondary structure could be made with wooden planks and boulder, masonry vaults, or brick vaults (drilled or solid) or with particular elements of terracotta and slabs or reinforced concrete. In the first iron slabs, the beams' connection elements were the masonry vaults, whose thickness depended on the beams' spacing and varied between 12 and 20 cm (Figure 5.4). While the most typical floor involves bricks of elongated rectangular shape, varying in height between 4 and 10 cm, between 70 and 150 cm long, and 25 cm wide, they are generally laid on the lower wings of the IPE beams. A surface of variable thickness is created on this plane, made light by aggregates with low specific weight, such as lapilli or expanded clay, and reinforced by an iron mesh. (Figure 5.5).

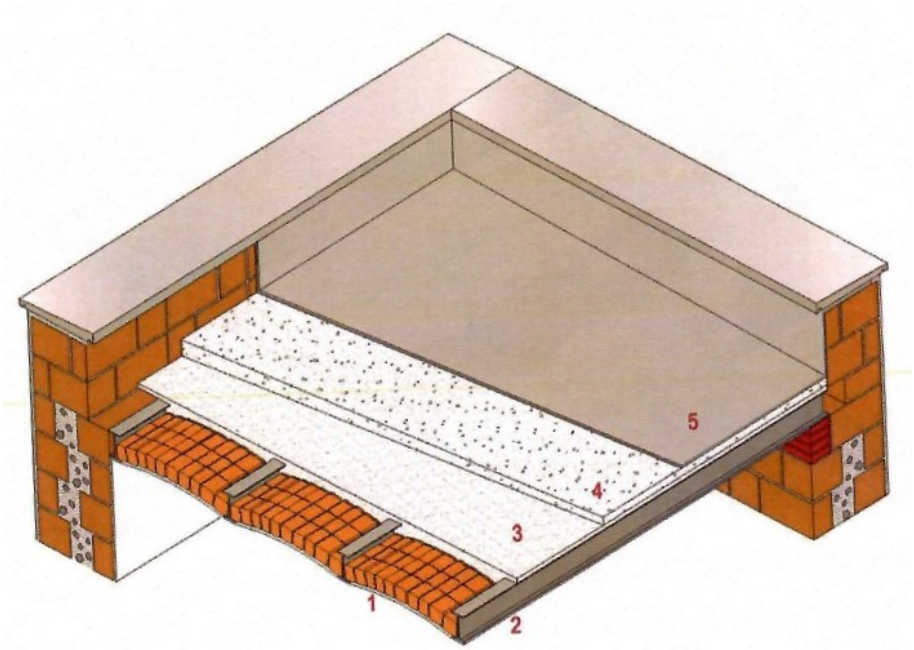

Fig. 5.4 Ceiling with iron beams: 1) Tuff arches, 2) Steel beams, 3) Mortar layer, 4) Slope screed, 5) Waterproofing layer.

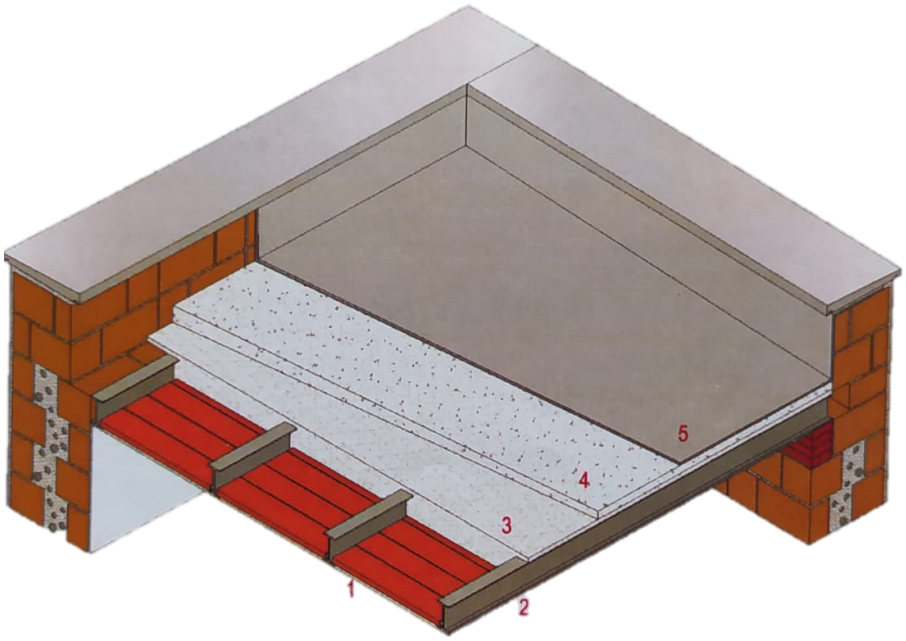

Fig. 5.5 Iron slab: 1) brick tiles, 2) steel beams, 3) concrete screed, 4) slope screed, 5) waterproofing layer

5.1.3 Reinforced Concrete roof

In the past, the concrete slabs cast on-site were the only type of mixed brick and reinforced concrete slab, while at present, due to the cost of their installation, they are used only when the building plan has irregularities that prevent the use of prefabricated elements. The brickwork blocks, fitted with side fins or accompanied by brick buttresses, are placed on a temporary support deck dismantled as soon as the conglomerate has reached enough mechanical strength. After placing all the blocks and casting the rafters and the concrete slab, the reinforcing irons are positioned using spacers or equivalent systems to ensure that the irons maintain a correct arrangement during the casting phase (Figure 5.1).

5.1.4 SAP floor

It has been defined as a slab consisting of reinforced brick beams packed at the foot of the building, joined and connected with cement mortar, characterized by a large subdivision of the metal reinforcement into small diameter rounds placed at a distance not exceeding 7 cm. The width of the beams is 20 cm.(Figure 5.7).

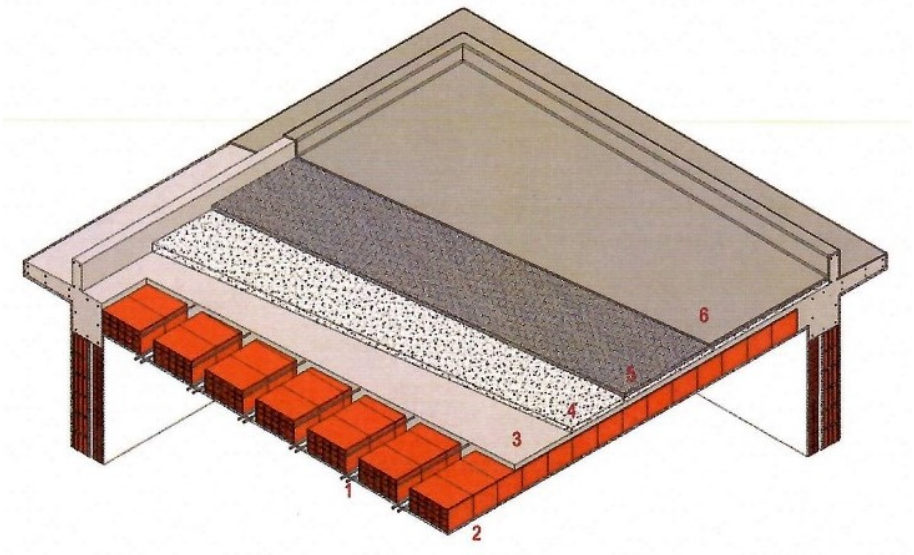

Fig. 5.6 Reinforced concrete slab: 1) Steel reinforcement, 2) Brick infill, 3) Concrete slab, 4) Slope layer, 5) Insulation layer, 6) Waterproofing membrane.

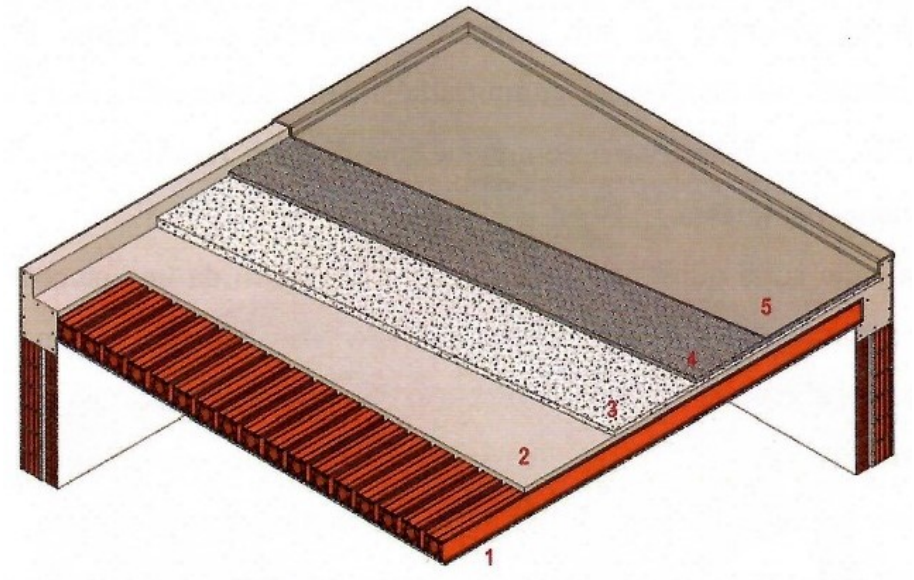

Fig. 5.7 SAP floor: 1) Reinforced brick beams, 2) Mortar layer, 3) Slope screed, 4) Insulation layer, 5) Waterproof sheathing

5.2 Roofs' vulnerability assessment

Some analyses concerning the coverings to the stresses exerted by the fall deposits were carried out by De Gregorio (2010), concerning the most widespread types in the Vesuvian area. The effect of pyroclastic deposits was assessed by defining the vertical failure overload that the structure can sustain. In particular, the study was carried out by considering different geometric configurations and different design accidental loads (0.6 and 2.0 kNm2). Finally, a thermal analysis was also carried out, considering the thermal degradation of the materials. The types of roofs analysed are ventilated and non-ventilated wooden roofs, roofs with metal girders and hollow core slabs and concrete roofs. The static scheme assumed is that of a beam on two supports subjected to its own and permanent loads g and an accidental load qR produced by the ashfall. Furthermore, the thermal degradation was assumed to be uniformly distributed in the cross-section, according to the indications of Eurocodes 2, 3 and 5, parts 1.2, about four temperatures (20, 200, 300 and 400°C).

5.2.1 Last remaining vertical load

The ultimate residual load q was determined for each type analysed as a function of different angles α of pitch inclination (0 - 45°) and temperatures (20 - 400 °C). For timber roofs, a maximum temperature of 100 °C was considered, above which the material offers negligible resistance. Table 5.1 shows the load ranges q, particularly for reinforced concrete (RC), for which different construction codes were considered, determined by varying the geometry.

Besides, for steel roofs, the q load has been determined as a function of the section's geometry and the span (L). Furthermore, the curves refer to two specific cases: temperature between 20 and 100°C and variable angle of inclination α (Figure5.8 a); and flat roofs (α = 0°) and variable temperature (Figure 5.8 b). The results show that the ultimate residual load q exhibits an increase of approximately 30-40% as the pitch angle α varies from 0 to 45°. On the other hand, high temperatures produce a decrease in the vertical collapse load due to the materials' thermal degradation, equal to 30% at 200°C and 50% at 300°C. Finally, when the temperature of the clasts is 400°C, the sustainable overload is negligible for most of the sections considered, and, in some cases, collapse already occurs in the presence of the permanent load only.

Further analysis to improve the analysis of roof strength was proposed by Spence et al. (2005) [37]. The method analyses spectral vibrations and seeks a correlation with structural characteristics that define roof strength. To apply this method to Vesuvian roofs, a series of experiments were conducted on real roof structures. The degradation of structural materials over time and the effects of non-structural materials such as mortar, plaster, and tiles were

Table 5.1 Ranges of the residual ultimate loads q (kNm^{-2}) for each type of roofing analysed, varying the angle of inclination of the pitch of the temperatures T (De Gregorio, 2010)

		$\alpha = 0°$	$\alpha = 20°$	$\alpha = 30°$	$\alpha = 45°$
T = 20-100 °C					
Wood (ventilated)	Circular	0,6-3,4	0,7-3,7	0,8-4,0	0,9-4,9
	Rectangular	0,7-5,2	0,8-5,6	0,9-6,0	1,1-7,4
Wood (no ventilated)	Circular	0,6-2,8	0,7-3,0	0,8-3,2	0,9-4,0
	Rectangular	0,6-7,6	0,7-8,1	0,8-8,8	0,9-10,8
Steel	IPE	1,2-5,1	1,3-5,5	1,4-5,9	1,8-7,3
R.C	RD 1939	0,8-2,6	0,8-2,7	0,9 - 3,0	1,1 - 3,6
	DM 1972	0,9 - 2,2	0,9 - 2,3	1,0 - 2,5	1,2 - 3,1
	DM 1996	0,9 - 2,4	1,1 - 2,6	1,1 - 2,8	1,3 - 3,4
	NTC 2008	1,1 - 3,1	1,1 - 3,3	1,2 - 3,6	1,5 - 4,4
T = 200 °C					
Steel	IPE	0,8 - 4,4	0,9 - 4,7	0,9 - 5,1	1,2 - 6,3
R.C	RD 1939	0,1 - 1,6	0,1 - 1,7	0,1 - 1,9	0,2 - 2,3
	DM 1972	0,2 - 1,3	0,2 - 1,4	0,2 - 1,5	0,2 - 1,9
	DM 1996	0,3 - 1,6	0,3 - 1,7	0,4 - 1,8	0,5 - 2,2
	NTC 2008	0,4 - 2,5	0,4 - 2,5	0,5 - 2,8	0,6 - 3,3
T = 300 °C					
Steel	IPE	0,4 - 3,8	0,4 - 4,0	0,5 - 4,3	0,6 -5,3
R.C	RD 1939	0,0 - 1,2	0,0 - 0,9	0,0 - 1,0	0,0 - 1,2
	DM 1972	0,0 - 0,6	0,0 - 0,7	0,0 - 0,7	0,0 - 0,9
	DM 1996	0,0 - 0,8	0,0 - 0,9	0,0 - 0,9	0,0 - 1,2
	NTC 2008	0,0 - 1,5	0,0 - 1,6	0,0 - 1,8	0,0 - 2,2
T = 400 °C					
Steel	IPE	0,0 - 3,1	0,0 - 3,3	0,0 - 3,6	0,1 -4,4
R.C	RD 1939	0,0 - 0,1	0,0 - 0,1	0,0 - 0,1	0,0 - 0,2
	DM 1972	0,0 - 0,0	0,0 - 0,0	0,0 - 0,0	0,0 - 0,0
	DM 1996	0,0 - 0,1	0,0 - 0,1	0,0 - 0,1	0,0 - 0,2
	NTC 2008	0,0 - 0,7	0,0 - 0,8	0,0 - 0,8	0,0 - 1,0

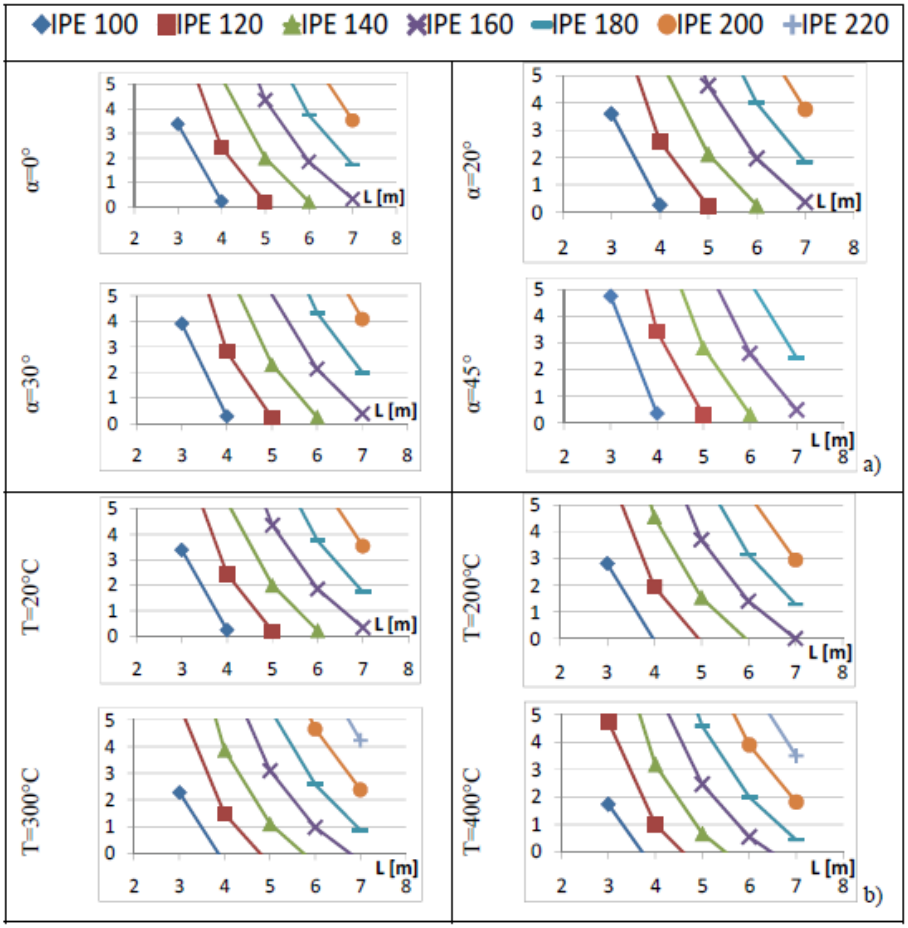

Fig. 5.8 Ultimate residual load q vs. span L, for steel roofs with distance between centres i equal to 1.00 m: a) for T=20°C as the angle of inclination of the pitch varies alpha; b) for alpha = 0° as the angle of inclination of the pitch varies alpha; c) for alpha = 0° as the angle of inclination of the pitch varies alpha. (De Gregorio et al., 2010)

taken into account in the analysis. Eighteen flat roofs of different construction forms were used. The natural frequency of a roof was calculated using the following equation:

$$f = \frac{\alpha}{2\pi L^2}\sqrt{\frac{EI}{\gamma}} \tag{5.1}$$

where:

- E Young's modulus (Pa),
- I moment of inertia (m4),
- L spam (m),
- α coefficient relating to the end joint restraints (dimensionless),
- γ mass per unit length (kg/m).

The frequency was calculated through experimental studies, while to calculate the 'end joint restraint parameter α, static tests were performed, but it was not possible to determine the stiffness because of the transverse spread of the load. For each roof, a full-scale static test with multiple displacement sensors was carried out. The deformed shape of the slab was used to determine the end joint restraint parameter α. Subsequently, each roof was subjected to a dynamic test, using ambient vibrations, with accelerometers determining the response. From the responses' peak values, the first vibration mode's natural frequency, f, was determined. Using the value of α determined by the static test, the equation was then used to determine the stiffness of the slab assembly, which was defined as EI_a; while the original stiffness (EI_0) was calculated using data about materials and the dimensions of the different components and the moment of inertia considering the characteristic section. Finally, the current stiffness (EI_S), which also was estimated by calculation, using the cross-section of the structural part, a value of the elastic modulus for the concrete taken from laboratory tests on concrete samples taken from the structure, and the well-defined value of elastic modulus for the steel. Thus the EI_a/EI_0 ratio describing the decay of stiffness is expected to be lower than 1 (Figure 5.9a), while the EI_a/EI_S ratio is a measure of the stiffness increment produced by the non-structural materials and is expected to be greater than 1 (Figure 5.9 b).

Once these values were defined, the limit value of the load per unit area (Q_lim) was calculated

$$Q_lim = \frac{\delta\beta M}{L^2} - w \tag{5.2}$$

where:

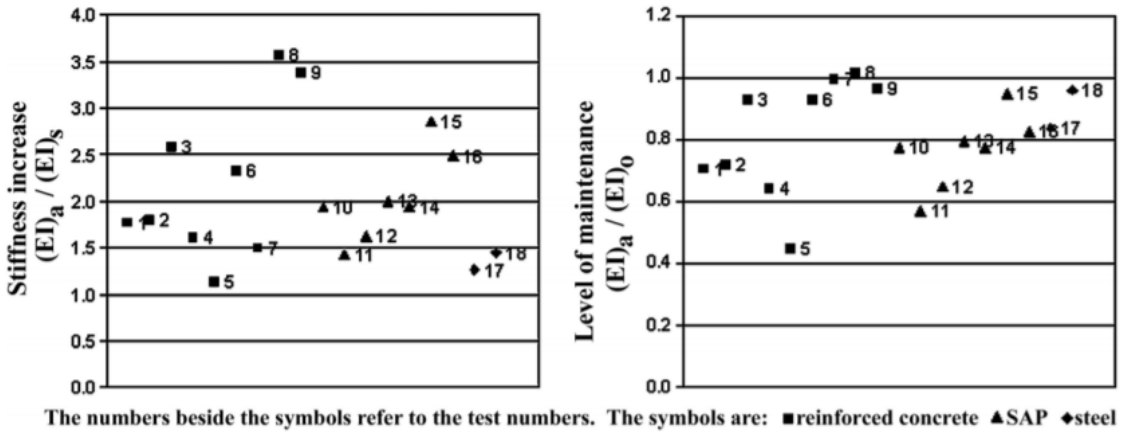

Fig. 5.9 Experimental results from individual tests of deviations from the theoretical stiffness due to non-structural material ((a) left) and material degradation ((b) right). Each point represents a separate tested roof. (Spence et al., 2005)

- β Increase of strength induced by non-structural layers (dimensionless),
- M Per unit slab width, the limit bending moment in the span's centre (Nm/m),
- L spam (m),
- w Slab's weight per unit area (Pa (N/m^2)),
- δ Coefficient relating to the extreme joint restraints and reinforcements, dependent on values of the limit bending moment at the joints and the span's centre (dimensionless).

Table 5.2 Parameters used to evaluate the lower and the upper limit of roof resistance for each typology (Spence et al., 2005) [37]

		Lower Limit					Upper Limit					
Type	**w(kPa)**	**M (kNm/m)**	δ	β	**L (m)**	Q_{lim} **(kPa)**	**M (kNm/m)**	δ	β	**L (m)**	Q_{lim} **(kPa)**	Q_{mean} **(kPa)**
Wooden pitched roof and flat iron	5	1	8	1	1	2	1.5	8	1	1	7	4.5
Reinforced concrete SAP.	5	9	12	1.2	6	0	12	16	1.5	4	10	5
Reinforced concrete older than 20 years.	5	17.5	12	1.2	6	2	22.5	16	1.5	4	25	13.5
Reinforced concrete younger than 20 years or steel beam with reinforced concrete slab.	5	22.5	12	1.2	6	4	27.5	16	1.5	4	35	20
Reinforced concrete pitched roof	5	30	12	1.2	6	7	40	16	1.5	4	50	28.5

For all slab types, a value of self-weight, w = 5 kPa (kN/m2) has been used (Table 5.2). Based on this analysis, the probability of collapse is calculated from:

$$p(collapse) = \Phi(Q_{mean}, Q_{dev}) \tag{5.3}$$

Proposed values for Q_{mean} and Q_{dev} for each of 5 classes of roof are provided in Table 5.3. Thus, from the results of the tests carried out, Spence et al.(2005) [37] point out that the weakest roofs are wooden pitched roofs, steel joists, and reinforced concrete SAPs, and state that their replacement would be a necessary first mitigation strategy.

Table 5.3 Parameters to estimate roof collapse probabilities for Vesuvian roof types (Spence et al.,2005)

Type	**Qmean (kPa)**	**Qdev (kPa)**
Wooden pitched roof and flat iron	4.5	0.9
Reinforced concrete SAP	2.5	0.5
Reinforced concrete older than 20 years	9.5	1.9
Reinforced concrete younger than 20 years or steel beam with reinforced concrete slab	13.5	2.7
Reinforced concrete pitched roof	20	4

A final consideration for the analysis of the mechanical vulnerability of roofs to the action of ash fall is the analysis of the vulnerability of non-structural elements. Hampton et al.(2015) [15] showed that ash overload on the roof also depends on ash migration and accumulation on the gutters. The performance of PVC gutters was evaluated through a testing ring. The testing ring is an adjustable frame that can be tilted with variable inclination (inclination 15°, 25°, 30°, 35° and 45°), and an overlying sieve distributes the ash. Besides, the roof was constructed following the New Zealand Building Code. For the tests, a galvanized corrugated iron roof (sheet) cladding and plastic gutter Marley "Stormcloud" polyvinyl chloride (PVC) with maximum bracket spacing of 500 mm is used. The roofing is 3 m wide, consisting of four corrugated 0.5 mm thick, 840 mm light × 1800 mm long galvanized iron sheets (corrugation ridges at 76.20 mm, with a depression depth of 19 mm), with a minimum projection of 50 mm cover over eaves. This roof cladding and gutter configuration style is typical of New Zealand and is classified as light to the medium-strong roof. The tests performed followed the scenarios defined in Table 5.4, and the observations were carried out for thicknesses less than 5 mm, greater than 5 mm and greater than 10 mm.

In the first scenario (Dry -Dry), the tests indicated settling and accumulation with a roof pitch $\leq 30°$, in particular, the ash formed small asymmetrical piles under the roof undulations. In contrast, with a pitch $\geq 35°$, ash was limited to depositing on the roof

Table 5.4 Volcanic ash roof and guttering testing regimes and procedures. (Hampton et al., 2015)[15]

Testing regime	Roof pitch(es)	Observation ash thickness	Procedures
Dry–Dry Dry ash on a dry roof	15°, 25°, 30°, 35°, and 45°	5 mm, 5 mm, and 10 mm	Ash dispensed over the roof surface until failure (ash, roof, or guttering) or no changes observed.
Wet–Dry Dry ash on a wet roof	45°	5 mm, 5 mm, and 10 mm	Initial wetting of roof surface using a fine mist/spray (1.2 L over 5.4 m^2 (equiv. 0.11 mm/min)), resulting in a roof surface that was visibly wet with small areas of runoff. Ash was then dispensed over the roof surface until ash slides off the roof, gutters fail, or no changes observed.
Wet–Dry–Wet Dry ash on a wet roof withrepeated wetting	45°	5 mm, 5 mm, and 10 mm	Initial fine mist/spray until visibly wet roof surface with small areas of runoff. Ash dispensed until even coverage (could not see previous surface), the roof area then wetted (1.2 L for 2 min per cycle—which was sufficient to saturate ash), followed by the re-application of ash and so on. The process was repeated until all ash was dispensed (typically 14 cycles). Roof area was then sprayed (at rate of 0.6 L per minute) until all ash was removed from the roof or failure of guttering.

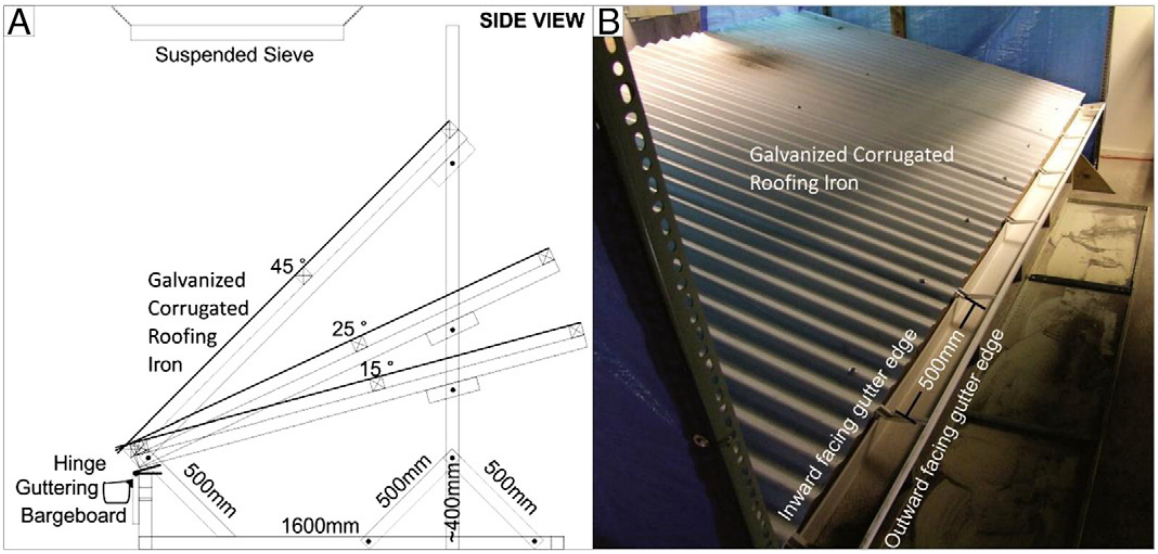

Fig. 5.10 VAT Lab testing setup (Hampton et al.,2015)[15]

surface (Table 5.4) (Table 5.4) with the rapid filling of the gutters, remaining mobilized and quickly transported downward, remaining buoyant/suspended, and directed by airflow (drawn downward) during ash migration along the roof.

In addition, in the second scenario (Wet - Dry), tests show that at a roof pitch of 45°, dry ash covered the roof's wet surface (Figures 5.11) (Figure 5.12). Also, the greatest roof ash failure occurred at a depth of 30 mm (ash in the ripple trough); the initial failure occurred in a 1 m^2 area with multiple tensional cracks (Figure 5.12 c). With further water application, parallel roof failures developed along or at the interface of the initially dry ash on the wet roof; with further application of ash, multiple failures developed, filling and then bypassing the gutters (Figure 5.12 c - e).

Finally, tests of the last scenario (Wet-Dry-Wet) emphasize that the interaction of ash with the wet roof surface at 45° is similar to that observed for dry ash on a wet roof; nevertheless, with water application, ash within corrugation troughs remained stable, with deposited on the front edge of the roof metal (above the gutter) remained in situ and did not slide into the gutter. In experiments, ash covered the roof, with the lower 30-40 cm of the roof accumulating greater thicknesses. The gutters' filling was asymmetrical, with the outer portion (furthest from the roof) being mostly filled (Figure 5.13 a), with the ash forming a thicker deposit that decreased toward the roof. Once the ash completely filled the gutter, the ash then further filled up to the roof. Ash then backfilled up the roof with further ashfall, which formed talus-like aprons, enabling ash to bypass the guttering. After 14 cycles of wetting and application of ash to a thickness of >30 mm on the roof, a slight curvature of the guttering occurred in the middle section along with the top lip profile. The plastic gutters did not fail in the Dry-Dry test series, flexural deformation within the

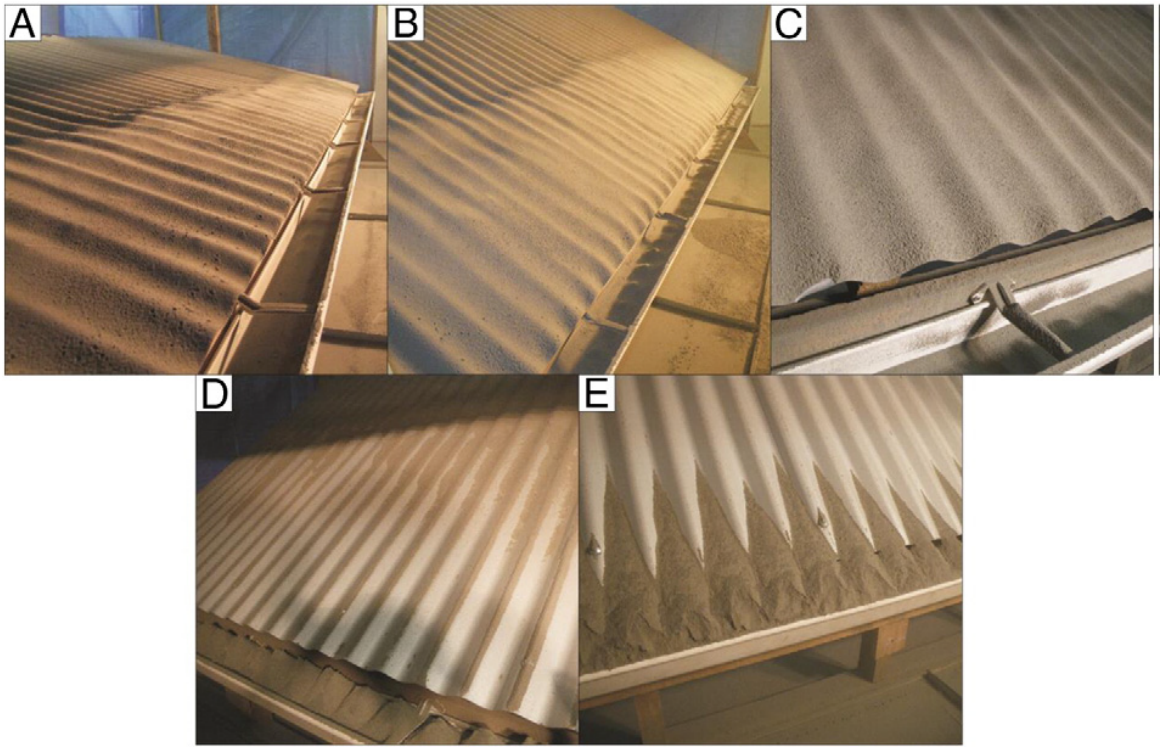

Fig. 5.11 Accumulation of ash in guttering in dry ash on dry roof testing regimes, relative thickness of ash indicated in Table 5.4 (Hampton et al., 2015)

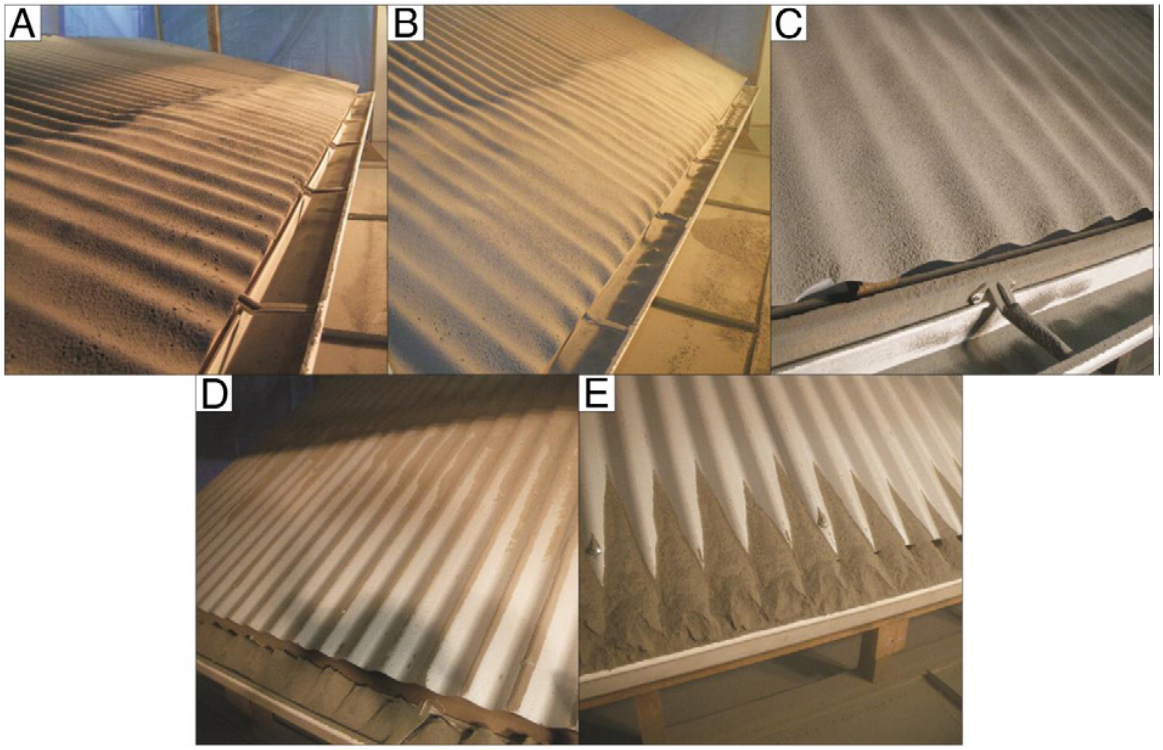

Fig. 5.12 Dry ash applied onto a wet roof surface at 45° roof pitch, relative thickness of ash indicated in Table 5.4 (Hampton et al., 2015)

system occurred with 10-15 mm of failure (downward) in the centre section of the 3 m span, increasing the gap between the gutter and barge edge between brackets from 8 mm to 15 mm in both the 35° and 45° tests when the gutter was fully loaded with ash. The gutter failure occurred in the Wet-Dry-Wet tests, which were increased with sustained saturation of the ash in the gutter and remobilized from the roof, causing overloading of the bracket clip (primarily due to plastic deformation). The deformation and subsequent detachment were due to the rotation and unclipping of the front bracket into the gutter, and the back (bargeboard side) of the gutter remains attached (Figure 5.13 h).

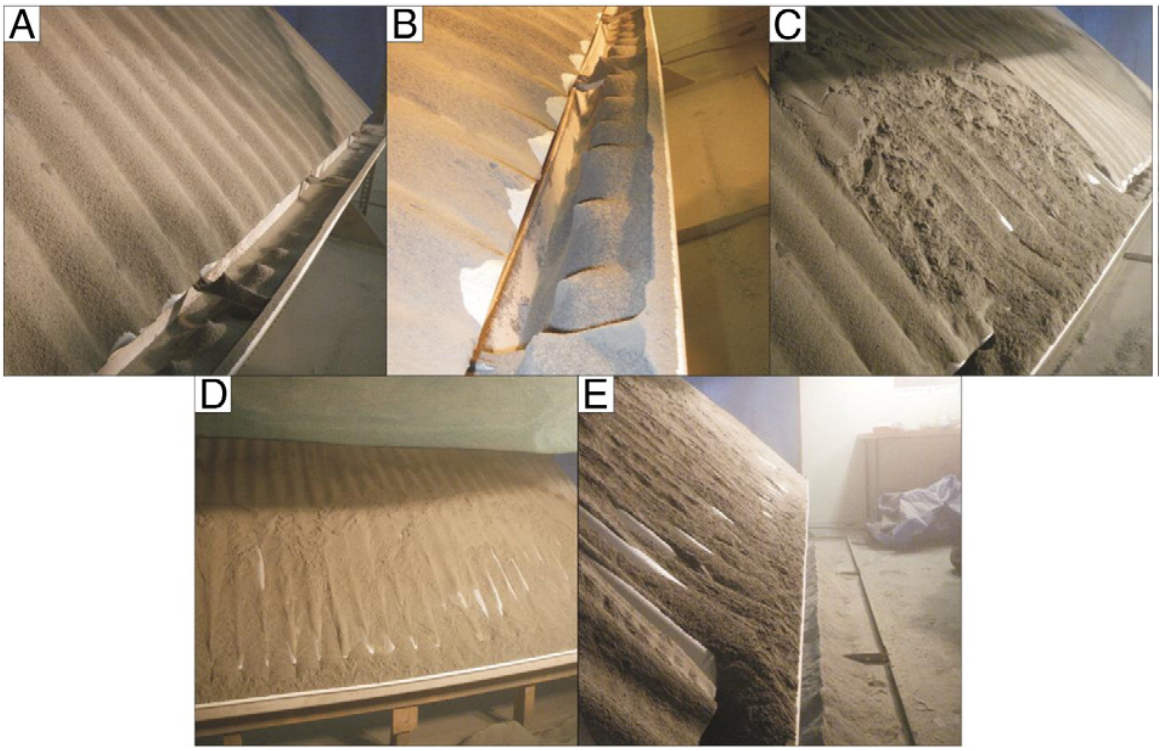

Fig. 5.13 Dry ash with wetting and drying cycles on a 45° roof pitch (Hampton et al., 2015)

5.2.2 Thermal Analysis

For the thermal analyses, De Gregorio et al. (2010) [11] evaluated the time needed to reach the critical temperature TCR at the roof's intrados, assuming a temperature applied to the different roof models equal to 400°C. Furthermore, the times were studied for the same types of floors with the interposition at the extrados of rock wool thermal insulation with a thickness of 3cm and a thermal conductivity $\lambda = 0.004\ \frac{W}{mK}$. The times of reaching the critical temperature T_CR are indicated in Table 5.5, while the relative temperature-time (T-t) curves (Figure 5.14) show the time trend of the temperatures for the different types of

roofing, regarding two different control points: the extrados (A) and the intrados (B) of the beam.

Table 5.5 Time required to reach critical temperature T_{CR} with 400°C clast deposit at the extrados (De Gregorio, 2010) [11]

Type of roofing	**TCR**	**Without insulation**		**With insulation**	
	°C	**min**		**min**	
		A	**B**	**A**	**B**
Wood	**100**	90	180	190	430
Ventilated Wood	**100**	50	120	120	300
Steel	**400**	2000		6200	
Reinforced Concrete	**400**	2900		12950	

The results show, in addition to the benefits of the insulating layer, especially for reinforced concrete roofs, that in the case of steel and reinforced concrete roofs, the curves for control points A and B are almost superimposed; therefore, the times for reaching the critical temperature (Figure 5.14) are valid for any height of the beam. On the other hand, on a wooden floor, the extrados and intrados' temperatures are different due to the material's thermal inertia. Referring to a wooden beam of 16 cm (ϕ 16), when the temperature reached in B is 100°C, in A, a temperature of 50°C is recorded.

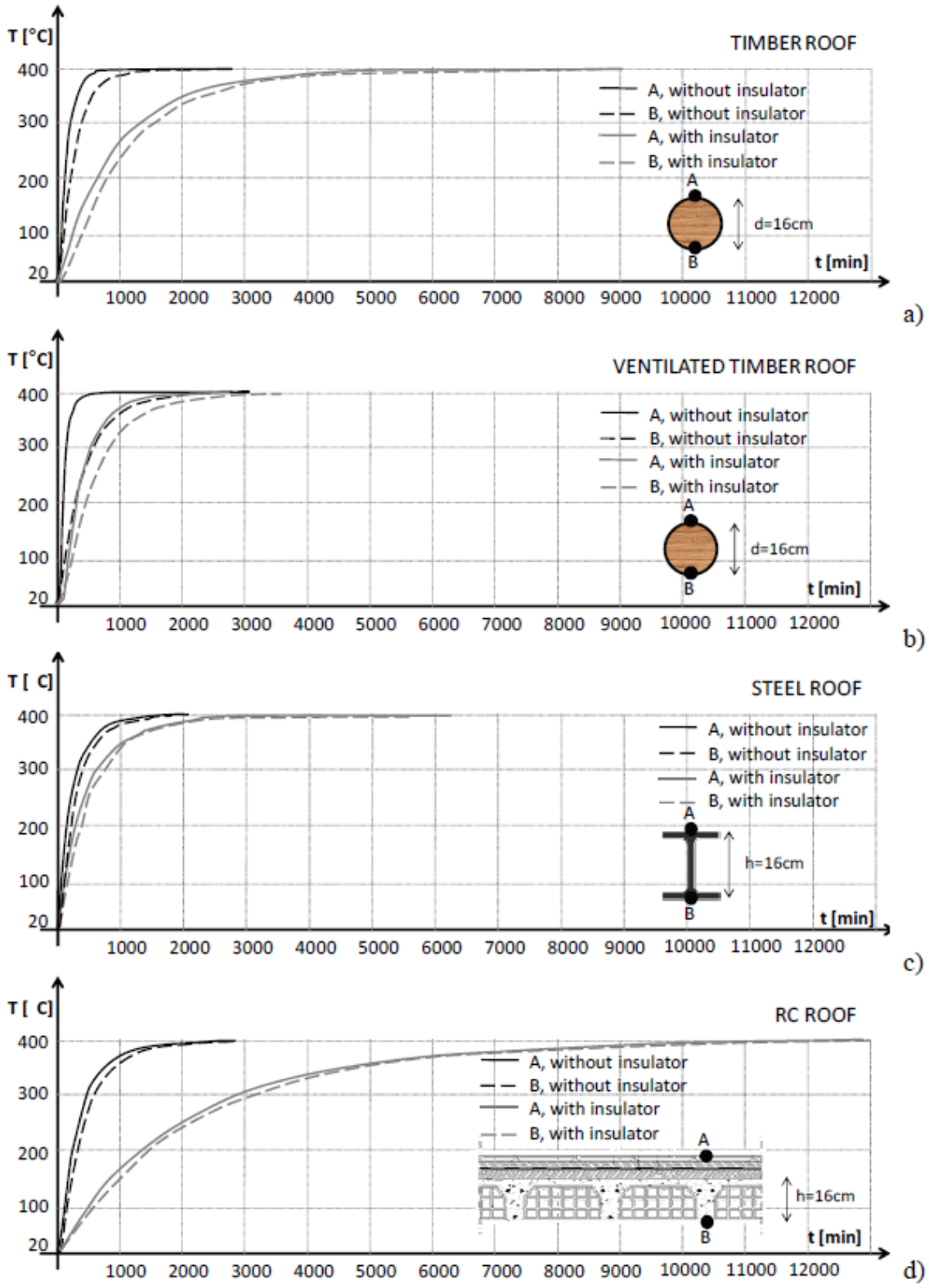

Fig. 5.14 Temperature-time curves (T-t) for roofs: a) in wood; b) in ventilated wood; c) in steel; d) in reinforced concrete. (De Gregorio, 2010)

5.3 Façade

The reorganisation of the data concerning the vertical structures for both areas (Figure 5.15, Figure 5.16) shows that the predominant ones are tuff or rough-hewn masonry, followed by reinforced concrete structures with weak infill.

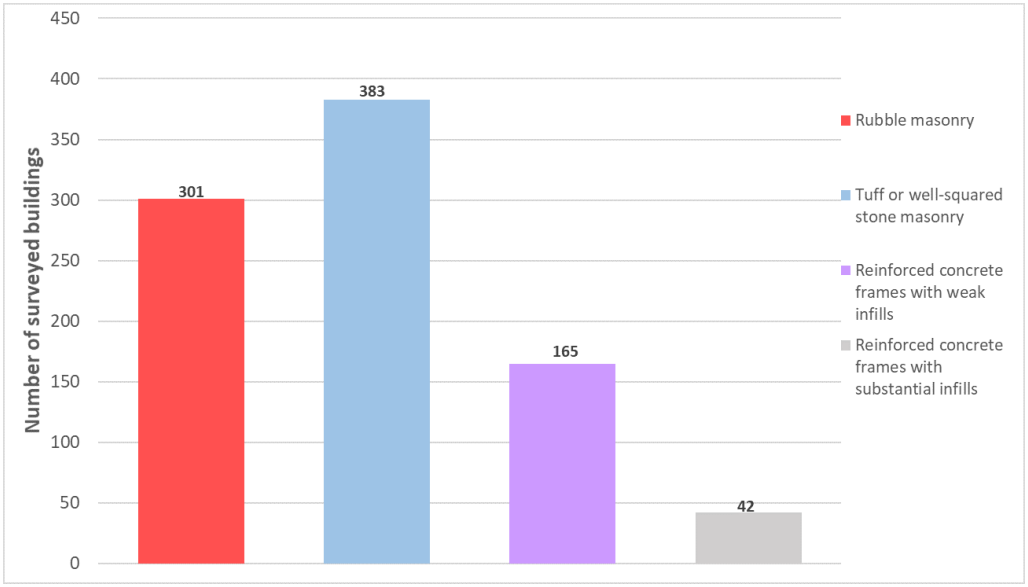

Fig. 5.15 Breakdown of surveyed buildings in the Vesuvio area by vertical structure

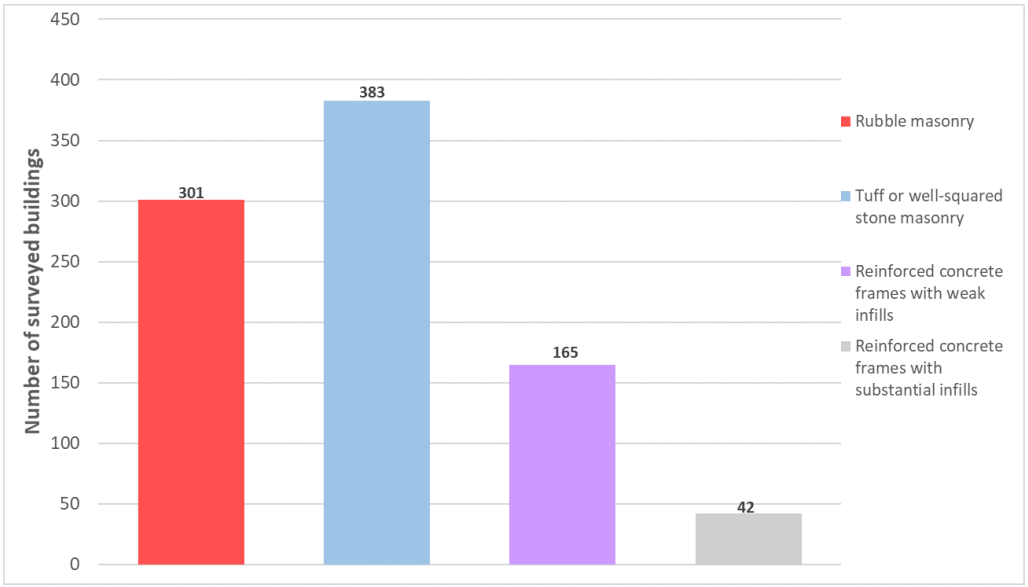

Fig. 5.16 Breakdown of surveyed buildings in the Campi Flegrei area by vertical structure

5.3.1 Rubble masonry

It is an irregular masonry and is usually made of mortar and square or polygonal natural stones (rounded or pointed river pebbles, lava stone, etc.). The strength of the rubble masonry depends on the mortar's quality, the use of through stones and the correct mortar filling between the stone spaces. Further classifications of this type of masonry are (Figure 5.17) (Dato,2017) [10]:

a) Coursed rubble masonry. In coursed rubble masonry, there are course stones of equal height.

b) Un-coursed rubble masonry. In un-coursed random rubble masonry, the courses are not regularly maintained. The larger stones are laid first, and the spaces between them are then filled with small stones.

c) Dry rubble masonry. In dry rubble masonry, a wall's strength is not dependent on the bond between the stones and the mortar; the friction between the interlocking the masonry blocks and the force of gravity are often strong enough to provide an excellent connection between the elements.

d) "Composite" stone masonry.

5.3.2 Squared rubble masonry

Squared masonry represents a high level of quality in the construction of structures. The ashlars are flat and regular on all faces to ensure large contact surfaces. The cut stone structure can be distinguished into regular and irregular. The first consists of a series of parallelepiped stones, placed horizontally one on top of the other, all of the same height or different heights; provided, however, that the ashlars of the same order are of equal height (courses or rows). An irregular structure is one in which the parallelepipeds are not arranged in regular courses but have widely varying heights along the row. Further classifications of this kind of masonry are (Figure 5.18) (Dato,2017 [10]):

e) Ashlar fine masonry. In this kind of masonry, each stone is cut to a uniform size and shape with all sides rectangular, so that the stone gives perfectly horizontal and vertical joints with adjoining stone.

f) Ashlar rough masonry. In this type of masonry, stone's exposed faces generally have a finely dressed chisel drafting all around the edges. The portion of the face stone enclosed by the chisel draft is rough tooled. The stones thickness should never exceed 6mm.

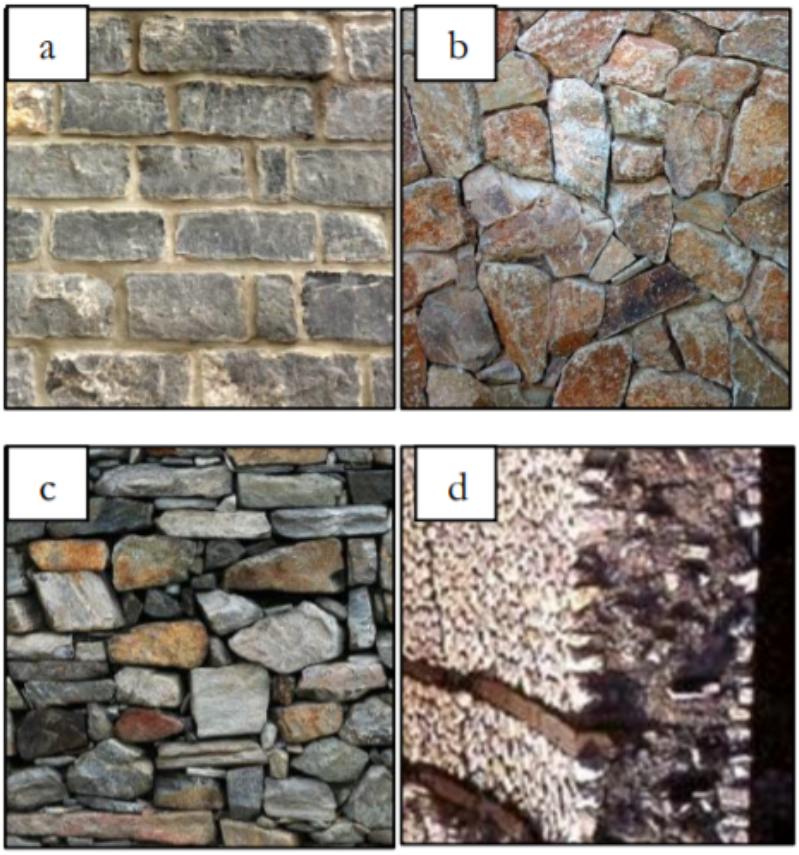

Fig. 5.17 General classification of rubble masonry: (a) coursed masonry, (b) uncoursed masonry, (c) dry masonry, (d) “composite” masonry. (Dato,2017 [10]

g) Ashlar chamfered masonry. This type masonry is similar to the one described above with the only difference that the edges around the exposed faces of stone are bevelled off at an angle of 45° for a depth of 25mm or more

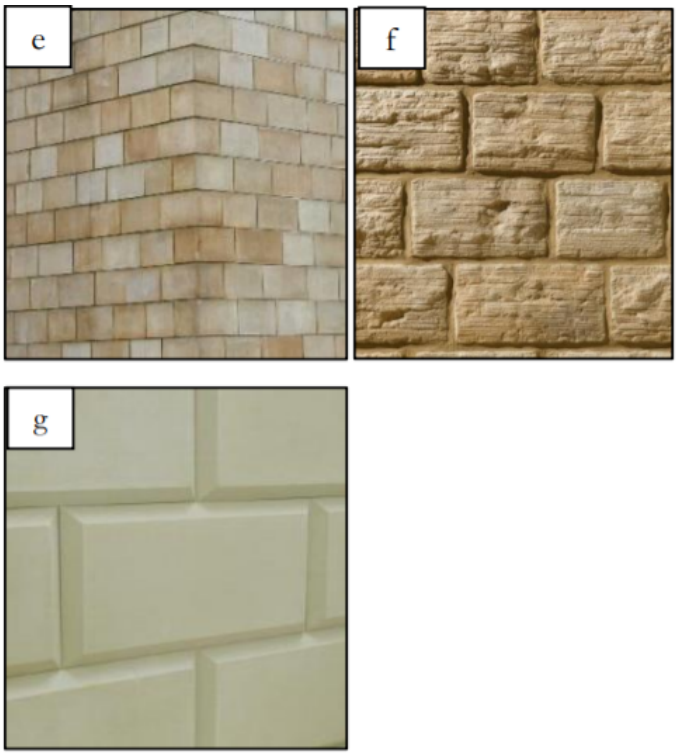

Fig. 5.18 General classification of ashlar masonry: (e) Fine masonry, (f) Rought masonry, (g) Chamfered masonry. (Dato,2017 [10]

5.3.3 Infill Panels

Infill panel is masonry that performs the function of closing the perimeter of the realised building. They are mainly made of brick or concrete blocks. The brick elements usually used are of the hollow-core type (also called perforated, or hollow) to guarantee the necessary lightness to the masonry as a whole and increase its thermal insulation capacity. About the weight, brick infill walls usually weigh around 1200 kg/m3 and have a compressive strength of approximately 25 kg/cm2. Concrete elements are mainly made of lightweight concrete, again to meet the requirements of lightness and insulation. Also, there are two types of infill:

- Single-layer walls, which use the same type of full-thickness resistant element capable, without the support of further specialised layers other than the cladding layer, of fulfilling the performance requirements of thermal and acoustic insulation, water tightness and, of course, self-supporting;

- Multilayer walls, in which specialised layers' strategic presence offers better control over the regulations' performance for external perimeter walls. The most common are the thermal and acoustic insulation layer, the vapour barrier, the watertight layer, the fire barrier and the levelling layer. The most common multi-layered walls are those with a single layer of resistant element and one or more functional layers, the presence and positioning of which often give the type of wall its name.

In fact, the positioning of the thermal insulation layer about the thickness of the wall is particularly relevant, so much so that nomenclature has been created specifically for the various cases, which can be divided into three fundamental categories: the positioning the insulation on the inside of the perimeter wall, which generates the so-called "cold wall". In this case, it is less effective in providing adequate thermal insulation, both because of the difficulties in avoiding thermal bridges at horizontal closures, and because of the inability of the wall part, being on the outside, to cooperate with the insulation function. the positioning of the thermal insulation inside the perimeter wall's cavity creates the so-called "double wall", consisting of two vertical layers of bricks or blocks, one external and the other internal, with a cavity or air chamber in between to provide insulation. In the case of framed structures, the insulation needs to wrap around all the structural elements present, be they pillars, beams or partitions, to avoid thermal bridges. A particular case is the "continuous curtain wall", in which the outer layer is anchored and supported with brackets by the backbone of the building. The insulation's positioning on the external part of the perimeter wall, a case more commonly known as "external insulation"

5.4 Façade's vulnerability assessment

As analytical methods for determining the resistances of masonry wall were unreliable, Spence et al (2004) [39] decided to conduct tests on three panels considered to be typical of local construction:

- Infill panel of hollow terra-cotta brick, with dimensions 2.9 m high by 3.1 m wide without openings,
- Infill panel of hollow terra-cotta brick of 2.9 m high by 3.05 m wide, with openings whose dimensions were 1.3 m high by 1.4 m wide.
- Tuff brick in-fill panels; whose dimensions were 2.9 m high by 1.9 m wide, besides the tuff bricks were positioned between two reinforced concrete columns.

The load was applied by a hydraulic jack acting through a system of chains pulling from inside the house on a rectangular grid of steel applied to outside of the wall. Besides the

results (Table 5.6) were confronted with theoretical estimates of the collapse load using limit analysis methods elaborated by Heyman (1969) and later by Baratta (1991). The method assumes that vertical hinges from in the masonry panels, whose openings are resisted by compressive confining forces from the strong reinforced concrete columns confining the panel, but no vertical loading is assumed. The comparison showed that the calculated collapse loads are in reasonable agreement with the observed failure loads.

Table 5.6 Collapse loads and maximum displacements of infill panel test and calculated loads (Spence, 2004) [39]

Infill panel types	Collapse pressure (kPa)	Maximum displacement (mm)	Calculated collapse pressure (kPa)
Terra cotta infill panel without window	5,5	89,5	5,5
Terra cotta infill panel with window	8,9	15	7,6 - 8,9
Tuff panel without window	>25	33,5	10 - 13

While, in order to evaluate the resistance of reinforced concrete buildings, Spence et al.(2004) [39] defined a range of resistance to lateral pressure concerning four classes: strong aseismic, weak aseismic, strong non-seismic and weak non-seismic. For each class, a collapse mechanism was calculated through an elastoplastic analysis, assuming one of two mechanisms:

- Mechanism type 1 (strong beam, weak column): plastic hinges occur at the tops and bases of the ground-floor columns;
- Type 2 mechanism (strong column, weak beam): plastic hinges are formed at each beam's ends and bases of ground-floor columns.

The following considerations were taken into account in the analyses:

- Realistic values were assumed for story heights, column and beam sizes, their variation with height, and proportions and positioning of reinforcement.
- Material strengths were assumed to vary over ranges characteristic of the period in which the frames were constructed.
- No account was taken of the strengthening effect of masonry infill walls.
- The lateral load causing collapse was assumed uniformly distributed over each building's height and converted to an equivalent lateral pressure.

In each case, the type 1 mechanism is the one that governs failure. The results (Figure 5.19) show that the worst case is an irregular building in plan. It was also pointed out that the resistance decreases as the building's height increases; in fact, for a 9-storey weak aseismic building, the limiting pressure is 3.5 kPa.

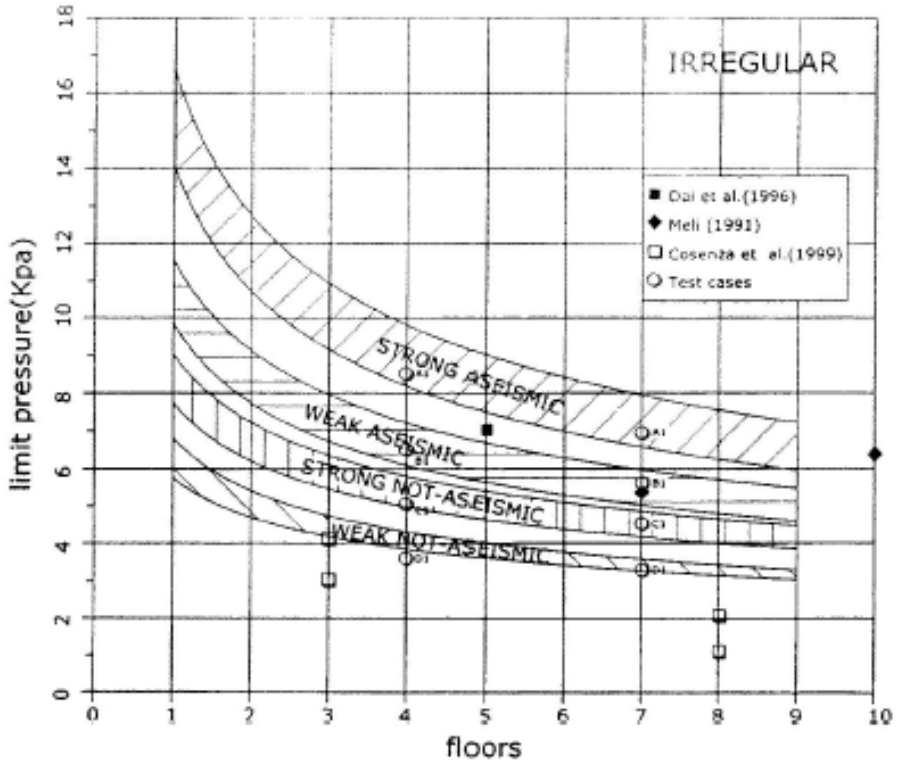

Fig. 5.19 Lateral failure pressures for reinforced concrete frame buildings of irregular plan

5.5 Openings

The openings such as windows and together with the doors represent a weak point of the building envelope during a pyroclastic flow event (Spence et al. 2004) [38] since the dynamic pressure exceeds the characteristic resistance of them, increasing the vulnerability. The data collected, through the PLINIVS sheet, have been analysed gathering them for the sizes of openings which are:

- Large windows, whose area is greater than 1,5 m^2;
- Typical windows, whose area range from 0.5 to 1.5 m^2;
- Small windows, whose area is less than 0.5 m^2.

Then each group was divided by the material of the frame and the shutters. Each of these characteristics is important in assessing the vulnerability and so in defining the adequate mitigation measures. In Campi Flegrei and Vesuvian Red Zones, examining the results of the surveys (Figure 5.20) (Figure 5.21), it is evident there are a wide spread of typical aluminium windows following by the wood windows.

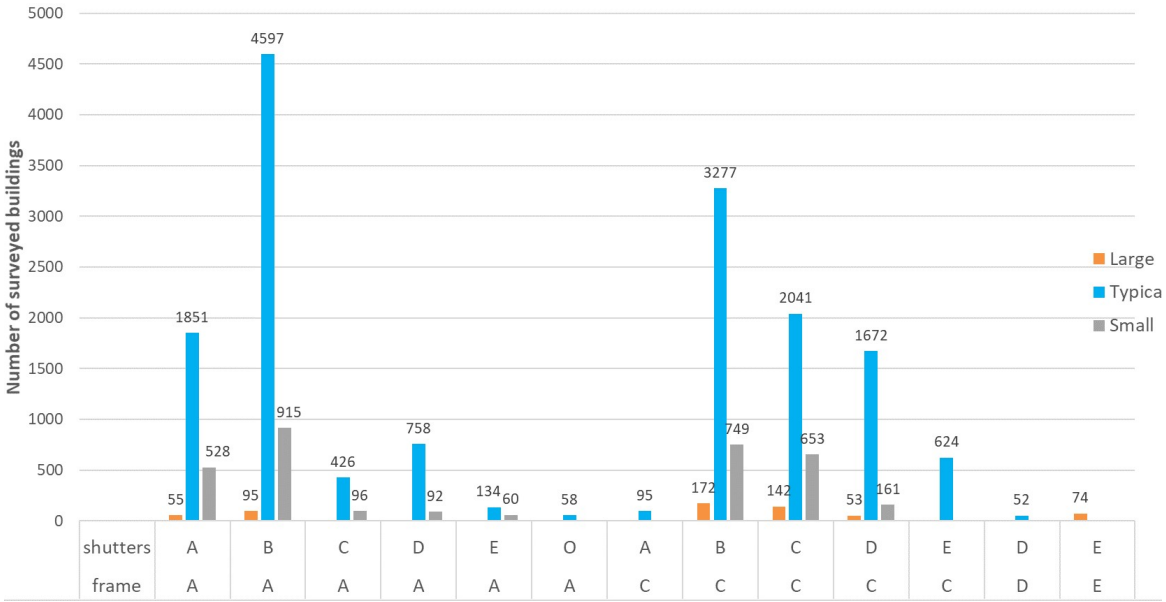

Fig. 5.20 Breakdown of surveyed buildings in the Vesuvio area by openings and shutters

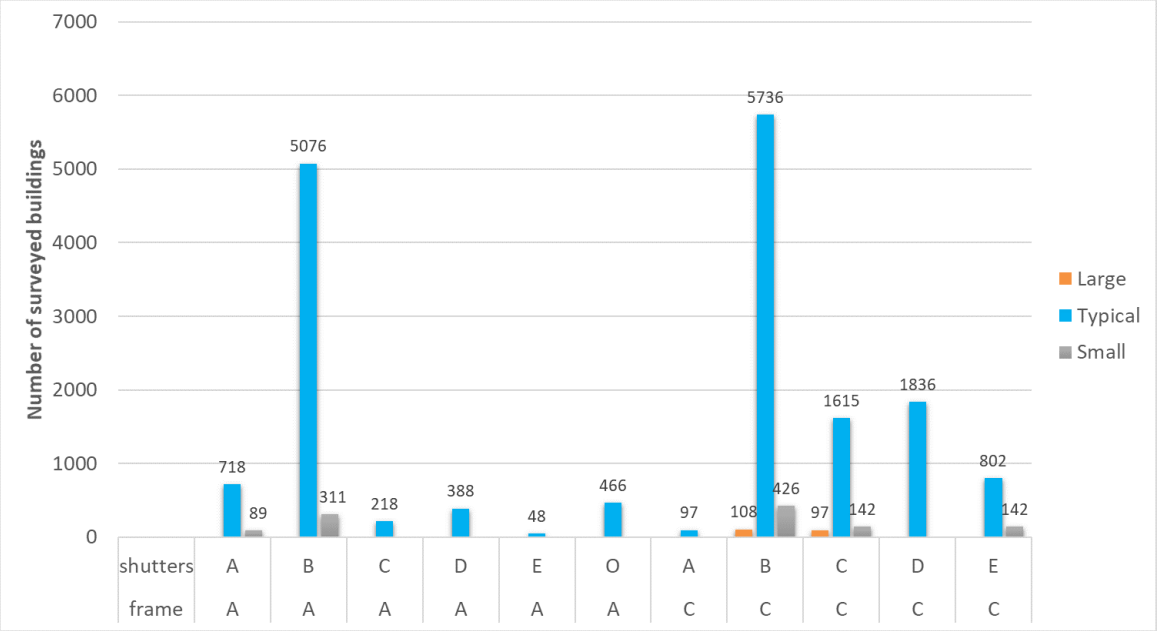

Fig. 5.21 Breakdown of surveyed buildings in the Campi Flegrei area by openings and shutters

5.5.1 Aluminium windows

The EN AW-6060 alloy is the most widespread extrusion alloy on the European market, thanks to its high hot forming speed. The alloy allows the production of profiles with even complex sections, including cavities and multiple grooves, to bring the design of the extruded part as close as possible to that of the finished product and to minimise intermediate machining. The characteristics of the alloy are (Table 5.7):

Table 5.7 Physical and mechanical properties of aluminium EN-AW 6060

Density	2700 [kg/m3]
Elastic modulus	70000 [MPa]
Ultimate Tensile Strength	160 [MPa]
Poisson Coefficient	0.33
Specific heat capacity	900 [J/kgK]
Thermal conductivity	238 [W/mK]
Thermal expansion	3,7 e-7 [1/K]

The type of glass commonly used is composed of silica oxide and lime. As defined in the Instructions for the design, execution and control of constructions with structural glass elements, the latter can be considered a homogeneous, isotropic material with linear elastic behaviour up to fracture, both tensile and compressive. The characteristics of this type of glass (Table 5.8) are:

Table 5.8 Physical and mechanical properties of soda lime glass

Density	2400 [kg/m3]
Elastic Modulus	71000 [MPa]
Ultimate Tensile Strength	41 [MPa]
Compressive strength	300 [MPa]
Poisson's ratio	0.33
Specific Heat Capacity	800 [J/kgK]
Thermal Conductivity	1 [W/mK]

Moreover, especially in the vulnerability analyses, two different technological units of vertical aluminium closures were considered, i.e. the aluminium frame with and without a thermal break (Figure 5.22) (Figure 5.23), due to the impossibility of recognising one model over the other during the investigation. The thermal break technology is used to improve the thermo-hygrometric characteristics of the frame. The cut is made by depolarising (i.e. depriving of continuity) the external part of the frames from the internal part and joining the two parts using polyurethane or polyamide elements. A possible more precise classification of the thermal bridge interruptions inside the profiles has been described by:

- Open joint system: corresponds to the most common case described above. It derives from the adoption of discontinuous frames in the sense of thickness; that is, distinct in an external part and an internal part joined by connectors in plastic/synthetic material with high thermal resistance and at the same time with mechanical resistance suitable for the structural requirements of the frames themselves.

- Thermal break system: In this case, the continuity of the aluminium profiles is interrupted, but the two parts of the frame connected are made integral by rigid insulating material. The production process involves injecting liquid polyurethane into the cavity, which expands and solidifies, assuming structural resistance. Subsequently, some parts of the aluminium frames are milled to interrupt their continuity and entrust the frames themselves' structural resistance in the milled sections to the polyurethane inserts. The thermal performance obtained for this type of frame is particularly satisfactory.

- Thermal shield system: used more rarely, it involves the use of a thermal break profile for a fixed frame, with an internal stop on the frame like the one commonly used in open joint configurations, and that the external stop of the mobile frame on the fixed frame is made of plastic and thermally insulating material, placed on the mobile frame in such a way as to cover its external face completely.

Finally, glazing technology is that of the insulating glass unit, which is a combination of two or more panes of equal or variable thickness, separated by a cavity, usually of air. For analysis, two panes of the same thickness, i.e. (4/5/6) mm.

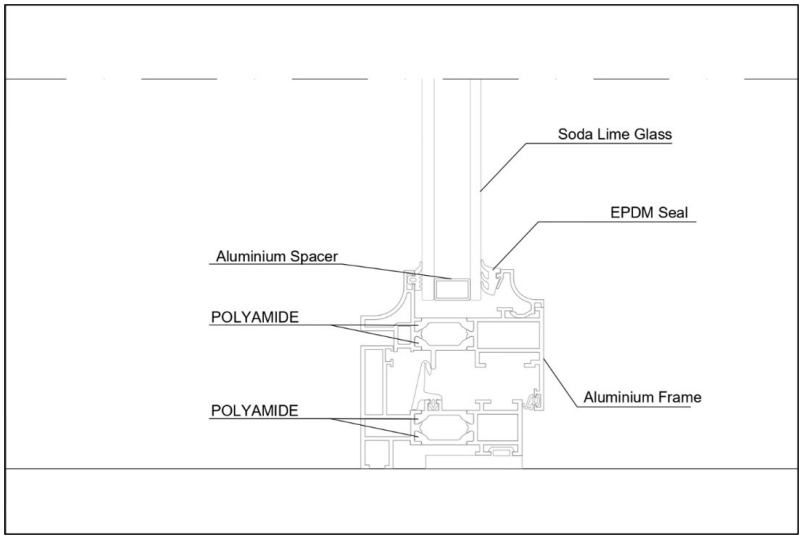

Fig. 5.22 Thermal break aluminum window section

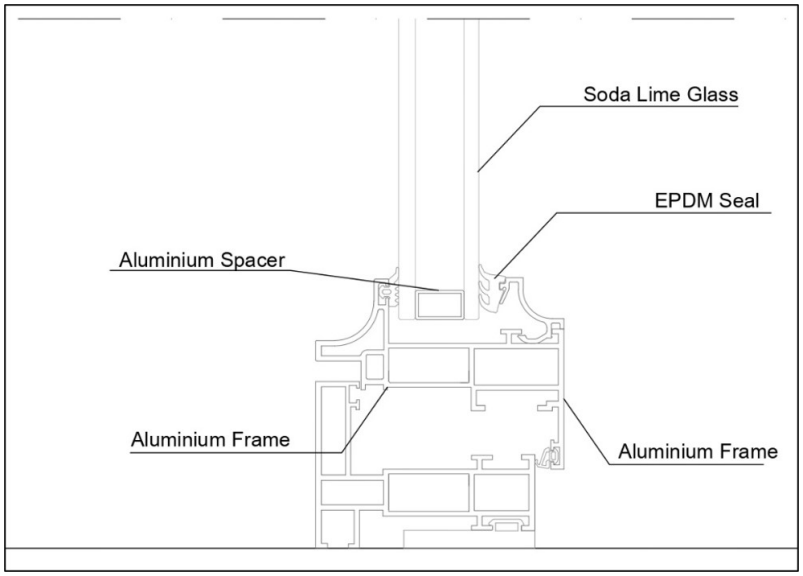

Fig. 5.23 Aluminium window section

5.5.2 Timber Windows

Another type of material widespread in the Campi Flegrei and Vesuvian area for the construction of windows and doors is wood (Figure 5.24). The choice of this material depends mainly on the good thermal insulation characteristics compared to UPVC and

aluminium windows and doors. In fact, this choice is economically disadvantageous because wood is certainly a more delicate material compared to PVC and aluminium, as it requires regular maintenance, and because the price of wooden windows and doors is still higher than that of aluminium and PVC. There are several species of wood, belonging to the broadleaf and conifer families, used for the construction of windows and doors:

- chestnut,
- fir,
- pine

Besides a first hypothesis was to consider the material as a homogeneous and isotropic, whose behaviour has been hypothesized linear elastic until breakage. Therefore, the characteristics of the two wood species (Table 5.9, Table 5.10).

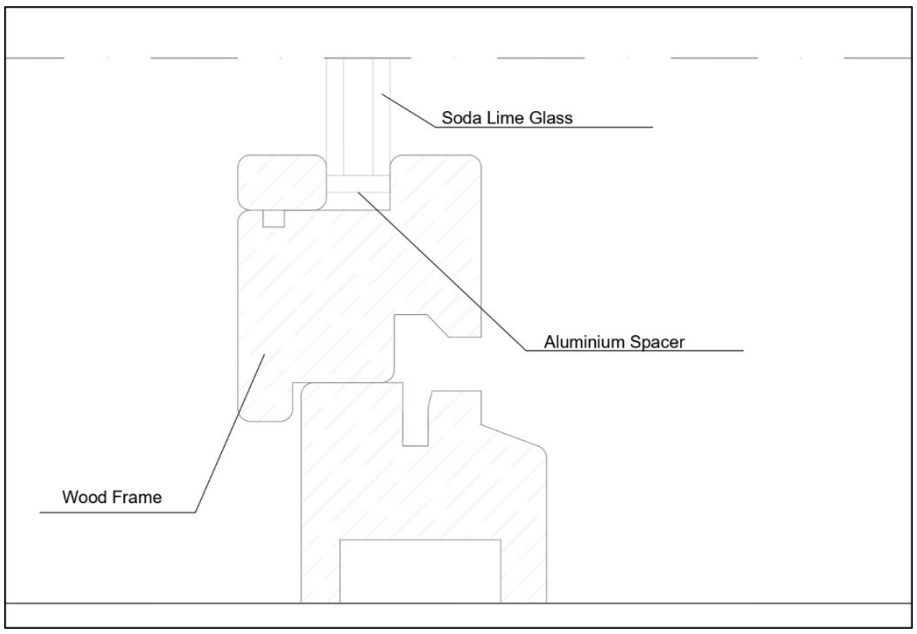

Fig. 5.24 Wood window section

Table 5.9 Physical and mechanical properties of Pine

Density	532 [kg/m^3]
Elastic Modulus	13700 [MPa]
Tensile Strength	85 [MPa]
Compressive Strength	45 [MPa]
Poisson's ratio	0.33
Specific Heat Capacity	800 [J/kgK]
Thermal Conductivity	1 [W/mK]

Table 5.10 Physical and mechanical properties of Chesnut

Density	630[kg/m^3]
Elastic Modulus	114000 [MPa]
Tensile Strength	95 [MPa]
Compressive Strength	51 [MPa]
Poisson's ratio	0.30
Specific Heat Capacity	800 [J/kgK]
Thermal Conductivity	1 [W/mK]

5.5.3 UPVC windows

Another common material to produce windows and doors is UPVC. UPVC is a plastic material composed of macromolecules which are in turn formed by hydrogen, carbon and chlorine atoms. A UPVC window and door frame have very similar characteristics to those of wood. UPVC has a low mechanical resistance; to overcome this, multi-chamber profiles are extruded and reinforced with the help of metal elements (Figure 5.25). These windows and doors have the main characteristic of resisting very well to the aggressions of atmospheric agents, are very light and offer good thermal insulation (Mottura and Pennisi, 2014)[25]. UPVC is a thermoplastic, so its mechanical characteristics (Table 5.11) are highly dependent on the glass transition temperature (T_g); that is the temperature, below which the physical properties of plastics change to those of a glassy or crystalline state. Above T_g, they behave like rubbery materials, below the T_g, plastic's molecules have relatively little mobility thus the material behaves rigidly and fragile (Ebnesajjad, 2016) [12]. UPVC has a glass transition temperature of 80°C. Hence, considering the temperatures expected in the red areas, PVC windows and doors will fail, and the building will be totally exposed to the impact of pyroclastic flows.

Table 5.11 Physical and mechanical properties of UPVC

Density	1400 [kg/m3]
Elastic Modulus	3700 [MPa]
Tensile Strength	47 [MPa]
Coefficient of thermal expansion	0,8e-4 [1/K]
Poisson's ratio	0.40
Specific Heat Capacity	800 [J/kgK]
Thermal Conductivity	1 [W/mK]

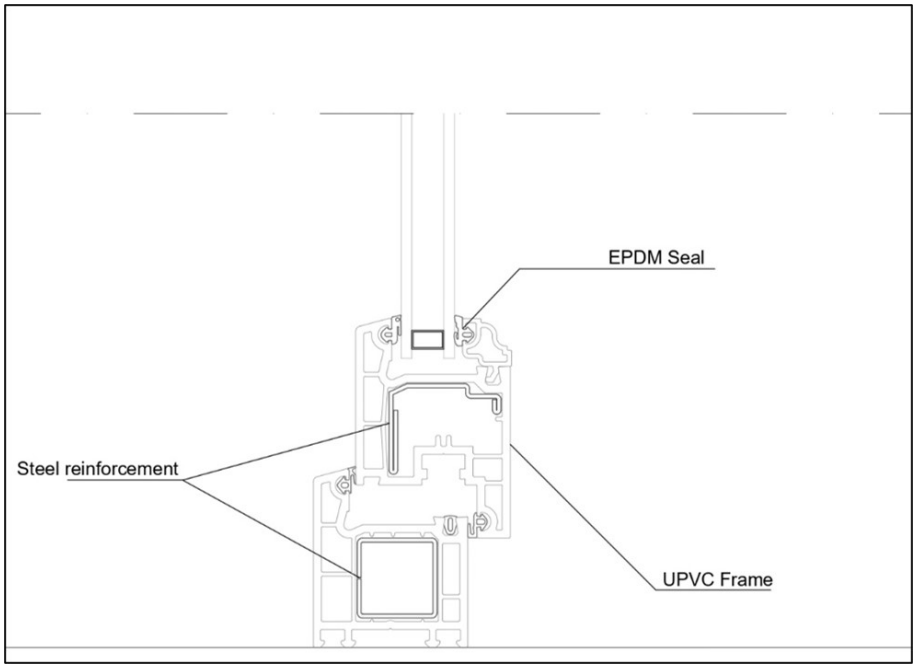

Fig. 5.25 Section of UPVC windows

5.6 Formulations

In order to define the vulnerability of the analysed elements, regarding the expected stresses, mechanical, thermal and fluid-dynamic analyses were carried out, whose equations used are explained in the following paragraphs.

5.6.1 Solid Mechanics

For the mechanical analysis, the stress generated by the application of flow pressure was analysed. The Cauchy model (5.4) was used to determine the value of the stress:

$$0 = \nabla \cdot (FS)^T + F_V \tag{5.4}$$

$$F = I + \nabla_u \tag{5.5}$$

5.6.2 Material Models

It was also necessary to define the model of material behaviour. For a linear elastic material, Hooke's law relates the stress tensor to the elastic strain tensor:

$$\sigma = F : \varepsilon_{el} \tag{5.6}$$

While a non-linear behaviour has been assumed for metal alloys. The nonlinear elastic materials present nonlinear stress-strain relationships even at infinitesimal strains. Here the model assumed is Ramberg-Osgood (5.7). As it is an elastic model, it can only represent plasticity during pure on-loading conditions. For uniaxial extension, the stress-strain curve is defined by the expression:

$$\varepsilon = \frac{\sigma}{E} + \varepsilon_{ref}(\frac{\sigma}{\sigma_{ref}})^n \tag{5.7}$$

Here, E means the initial Young's modulus, and ε_{ref} is the strain at a reference stress $sigma_{ref}$. The parameter n is the stress exponent. It is common to use ε_{ref} = 0.002, so σ_{ref} is the stress at 0.2% strain, typically denoted by the symbol σ 0.2. This parameter has several names depending on the literature: 0.2% offset yield strength, 0.2% proof stress, 0.2% proof strength, or 0.2% yield stress. The linear strain is given by:

$$\varepsilon_{el} = \frac{\sigma}{E} \tag{5.8}$$

and the nonlinear strain by:

$$\varepsilon_{nl} = \varepsilon_{ref}(\frac{\sigma}{\sigma_{ref}})^n \tag{5.9}$$

5.6.3 Heat Transfer

For thermal analyses, the first step was the analysis of heat transfer. The amount of heat transferred per unit time (heat transfer rate) depends on the underlying physical mechanisms that define the mode of transfer. The models assumed are:

- **Conduction**: Heat conduction (or diffusion) occurs as a consequence of different mechanisms in different media. In a continuous medium, Fourier's law of heat conduction states that the conductive heat flux, q, is proportional to the temperature gradient:

$$q = -K\nabla T \tag{5.10}$$

The coefficient of proportionality, k, is the thermal conductivity (SI unit: W/(m·K)) and takes a positive value meaning that heat flows from regions of high temperature to low temperature. Since heat diffusion has been assumed to be isotropic, therefore:

$$K = k\mathbf{I} \tag{5.11}$$

- **Convection**: Heat convection (sometimes called heat advection) takes place through the net displacement of a fluid that transports the heat content with its velocity. The term convection (especially convective cooling and convective heating) also refers to the heat dissipation from a solid surface to a fluid, typically described by a heat transfer coefficient.

The Heat Balance Equation

The first law of thermodynamics states that the variations of macroscopic kinetic energy, K_Ω, and internal energy, E_Ω, of a domain Ω are caused either by the mechanical power of forces applied to the system, P_ext, or by exchanged heat rate, Q_{exch} (5.12):

$$\frac{dE_\Omega}{dt} + \frac{dK_\Omega}{dt} = P_{ext} + Q_{exch} \tag{5.12}$$

Mass and momentum balance are needed to complete the description of the system. The mechanical laws, either for solids or fluids, generate the following balance equation between variation of kinetic energy, K_Ω, stress power, P_{str}, and power of applied forces, P_{ext}

$$\frac{dK_\Omega}{dt} + P_{str} = P_{ext} \tag{5.13}$$

Combining Equation 5.12 and Equation 5.13 yields the so-called heat balance equation

$$\frac{dE_\Omega}{dt} = P_{str} + P_{ext} \tag{5.14}$$

This time, the equation involves quantities of the microscopic level (exchanged heat rate, Q_{exch}, and internal energy, K_Ω) more concerned with the atomic vibrations and similar microscopic phenomena that are felt as heat. The presence of the stress power, P_{str}, in both Equation 5.13 and Equation 5.14 stands for the fact that such power is converted into heat by dissipation. The Heat Transfer interfaces, described in the next sections, simulate the heat exchanges described by Equation 5.12.

Localized Form

Variation of Internal Energy The equations given in the previous paragraph holds for a given macroscopic continuous domain Ω where the internal energy is defined using the specific internal energy (per unit mass), E, as:

$$E = \int_\Omega E dm \tag{5.15}$$

Note that by conservation of mass, the variation of internal energy in time is:

$$\frac{dE_\Omega}{dt} = \int_\Omega \frac{dE}{dt} dm = \int_\Omega \rho \frac{dE}{dt} dv \tag{5.16}$$

In these last relations, ρ is the density, and dv denotes an elementary volume of Ω. Contrary to the constant elementary mass, dm, the elementary volume changes by expansion or contraction of the domain. The stress power, derived from the Continuum Mechanics theory, is defined by:

$$P_{str} = \int_\Omega (\sigma : \mathbf{D}) dv \tag{5.17}$$

Finally, the exchanged heat rates, Qexch, account for thermal conduction:

$$Q_{exch} = -\int_{\delta_\Omega} (\mathbf{q} \cdot \mathbf{n}) ds - \int_{\delta_\Omega} (q_r \cdot \mathbf{n}) ds + \int_{\delta_\Omega} Q dV \tag{5.18}$$

Recall the following notations used above: q for the heat flux by conduction, qr for the heat flux by radiation, Q for additional heat sources, and n for the external normal vector to the boundary δ_ω With all these elements, the heat balance equation (Equation 5.12) becomes:

$$\int_\Omega \rho \frac{dE}{dt} dv + \int_{\delta_\Omega} (\mathbf{q} \cdot \mathbf{n}) ds + \int_{\delta_\Omega} (q_r \cdot \mathbf{n}) ds = \int_\Omega (\sigma : \mathbf{D}) dv + \int_{\delta_\Omega} Q dV \tag{5.19}$$

which leads to the following localized form in the spatial frame:

$$\rho \frac{\delta E}{\delta t} + \rho \mathbf{u} \cdot \nabla E + \nabla \cdot (\mathbf{q} + q_r) = \sigma : \mathbf{D} + Q \tag{5.20}$$

The heat transfer in solid derived from Equation 5.20:

$$\rho C_p (\frac{\delta T}{\delta t} + u_{trans} \cdot \nabla \mathbf{T} + \nabla \cdot (\mathbf{q} + q_r)) = -\alpha \mathbf{T} : \frac{dS}{dt} \mathbf{Q} \tag{5.21}$$

where:

- ρ is the density (kg/m^3),
- C_p is the specific heat (J/(kg*K)),
- T is the temperature (K),
- u is the speed vector of motion (m/s),
- Q is the heat source (W/m^3),
- dz is thickness of domain in the out-of-plane direction (m),

- q is the conduction heat flow (W/m^2).

Thermal Expansion

Another type of analysis needed for vulnerability assessment is thermal stress, so coupling the two models through thermal expansion. As the temperature changes, most materials react by a change of volume. For a constrained structure, the stresses that evolve even with moderate temperature changes can be considerable. The volume change can be is represented a thermal strain ε_{th}, which produces stress-free deformations.

$$\sigma = C : (\varepsilon - \varepsilon_{th}) \tag{5.22}$$

where:

$$\varepsilon_{th} = \alpha(\mathbf{T} - T_{ref}) \tag{5.23}$$

where α is the secant coefficient of thermal expansion.

Heat Transfer in Fluids

$$\rho C_p(\frac{\delta T}{\delta t} + u_{trans} \cdot \nabla \mathbf{T} + \nabla \cdot (\mathbf{q} + q_r)) = -\alpha \mathbf{T}(\frac{dp}{dt} + \mathbf{u} \cdot \nabla p + \tau : \nabla \mathbf{u} + Q \tag{5.24}$$

which is derived from Equation 5.20, considering that:

- the Cauchy stress tensor, *sigma*, is split into static and deviatoric parts as in:

$$\sigma = -p\mathbf{I} + \tau \tag{5.25}$$

- the dependent variables are the temperature, T, and pressure, p

The different quantities involved here are recalled below:

- ρ is the density (kg/m^3),
- C_p is the specific heat (J/(kg*K)),
- T is the temperature (K),
- u is the speed vector of motion (m/s),
- Q is the heat source (W/m^3),
- q is the heat flux by conduction (W/m^2),
- q_r is the heat flux by radiation (W/m^2),

- α_p is the coefficient of thermal expansion (SI unit: 1/K):

$$\alpha_p = -\frac{1}{\rho}\frac{\delta\rho}{\delta T} \tag{5.26}$$

- for ideal gases, the thermal expansion coefficient takes the simpler form $\alpha_p = 1/\mathrm{T}$
- p is the pressure (SI unit: Pa)
- τ is the viscous stress tensor (SI unit: Pa)
- Q contains heat sources other than viscous dissipation (SI unit: W/m^3)

For a steady-state problem the temperature does not change with time and the terms with time derivatives disappear. The first term of the right-hand side of Equation 5.24 is the work done by pressure changes and is the result of heating under adiabatic compression as well as some thermoacoustic effects. It is generally small for low Mach number flows.

$$Q_p = \alpha_p T(\frac{\delta p}{\delta t} + \mathbf{u}\cdot\nabla p) \tag{5.27}$$

The second term represents viscous dissipation in the fluid:

$$Q_{vd} = \tau : \nabla\mathbf{u} \tag{5.28}$$

5.6.4 Fluid Dynamics

The model used for pyroclastic flows is the Single-Phase model in a turbulent field (k-ε). The former is based on the Navier-Stokes equations:

$$\frac{\delta\rho}{\delta t} = \tau : \nabla\mathbf{u} \tag{5.29}$$

$$\rho\frac{\delta\mathbf{u}}{\delta t} + \rho(\mathbf{u}\cdot\nabla)\mathbf{u} = \nabla\cdot[-p\mathbf{I}+\tau] + \mathbf{F} \tag{5.30}$$

$$\rho C_p(\frac{\delta T}{\delta t} + (\mathbf{u}\cdot\nabla)T) = -(\nabla\cdot q) + \tau : \mathbf{S} - \frac{T}{\rho}\frac{\delta\rho}{\delta T}\bigg|_p(\frac{\delta p}{\delta t} + (\mathbf{u}\cdot\nabla)p) + Q \tag{5.31}$$

where:

- ρ is the density (kg/m^3),
- u is the speed vector of motion (m/s),

- p is the pressure (Pa),
- τ iis the viscous stress tensor (SI unit: Pa),
- F is the volume force vector (SI unit: N/m3),
- C_p is the specific heat at constant pressure (J/(kg*K)),
- T is the absolute temperature (K),
- q is the heat flux vector (W/m^2),
- Q contains the heat sources (SI unit: W/m^3),
- S is the strain-rate tensor: $S = \frac{1}{2}(\nabla \mathbf{u} + (\nabla \mathbf{u})^T)$

To close the equation system, Equation xxx through Equation xxx, constitutive relations are needed. For a Newtonian fluid, which has a linear relationship between stress and strain, Stoke deduced the following expression:

$$\tau = 2\mu \mathbf{S} - \frac{2}{3}\mu(\nabla \cdot \mathbf{u})\mathbf{I} \tag{5.32}$$

The dynamic viscosity, μ (SI unit: Pa·s), for a Newtonian fluid is allowed to depend on the thermodynamic state but not on the velocity field.

Turbulence Modeling

Turbulence is a property of the flow field and it is characterized by a wide range of flow scales: the largest occurring scales, which depend on the geometry, the smallest, quickly fluctuating scales, and all the scales in between. The propensity for an isothermal flow to become turbulent is measured by the Reynolds number

$$R_e = \frac{\rho U L}{\mu} \tag{5.33}$$

where μ is the dynamic viscosity, ρ the density, and U and L are velocity and length scales of the flow, respectively. Flows with high Reynolds numbers tend to become turbulent. Most engineering applications belong to this category of flows.

REYNOLDS-AVERAGED NAVIER-STOKES (RANS) EQUATIONS

The following assumes that the fluid is incompressible and Newtonian in which case the Navier-Stokes equations take the form:

$$\rho \frac{\delta \mathbf{u}}{\delta t} + \rho(\mathbf{u} \cdot \nabla)\mathbf{u} = \nabla \cdot [-p\mathbf{I} + \mu(\nabla \mathbf{u} + (\nabla \mathbf{u})^T)] + F \tag{5.34}$$

$$p\nabla \cdot \mathbf{u} = 0 \tag{5.35}$$

Once the flow has become turbulent, all quantities fluctuate in time and space. It is seldom worth the extreme computational cost to obtain detailed information about the fluctuations. An averaged representation often provides sufficient information about the flow. The Reynolds-averaged representation of turbulent flows divides the flow quantities into an averaged value and a fluctuating part,

$$\phi = \bar{\phi} + \phi\prime \tag{5.36}$$

where ϕ can represent any scalar quantity of the flow.

The k-ε Turbulence Model

The k-ε model is one of the most used turbulence models for industrial applications. This module includes the standard k-ε model. The model introduces two additional transport equations and two dependent variables: the turbulent kinetic energy, k, and the turbulent dissipation rate,ε. The turbulent viscosity is modeled as:

$$\mu_T = \rho C_\mu \frac{k^2}{\varepsilon} \tag{5.37}$$

where C_ν is a model constant. The transport equation for k reads:

$$\rho \frac{\delta k}{\delta t} + \rho \mathbf{u} \cdot \nabla k = \nabla \cdot ((\mu + \frac{\mu_T}{\sigma_k})\nabla k) \; + P_k \breve{} \rho \varepsilon \tag{5.38}$$

where the production term is:

$$P_k = \mu_T (\nabla u : (\nabla u \; + (\nabla u))^T \; - \; \frac{2}{3} \; (\nabla \cdot u^2) \; - \frac{2}{3} \rho k \nabla \; \cdot \mathbf{u} \tag{5.39}$$

The transport equation for ε reads:

$$\rho \frac{\delta \varepsilon}{\delta t} + \rho \mathbf{u} \; \cdot \nabla \varepsilon = \nabla \cdot ((\mu + \frac{\mu_T}{\sigma_\varepsilon})\nabla \varepsilon) \; + C_{\varepsilon 1} \frac{\varepsilon}{k} P_k \; - C_{\varepsilon 2} \rho \frac{\varepsilon^2}{k} \tag{5.40}$$

5.7 Openings' vulnerability assessment

To assess the vulnerability of both aluminium and wooden frames to the pressures expected in both areas, a Structural Mechanics static model 5.4 was used. Since the resistance of openings to dynamic pressure depends on several factors of which the most important are the size; therefore, three different heights have been considered for each group of windows, i.e. for the large openings a height of 2.4 m had been considered, for the Typical a height of 1.2 m and for the small a height of 0.8 m has been considered; and for each window size the different thicknesses of the glass have been considered. Additionally, it has been considered half section in order to reduce the computational time, assuming a condition of symmetry in the upper part of the window. Besides, the glass was modelled as a linear elastic material until failure according to equation (5.6). According to equation (5.7), the aluminium frame was modelled to consider both elastic and plastic behaviour fully. In addition, a uniformly distributed load applied (5.41) on the external front has been assumed, in favor of opening, which is linearly variable according to a parameter that has been imposed through a range function.

$$S \cdot n = F_A \tag{5.41}$$

$$F_A = \frac{F_L}{d} \tag{5.42}$$

For modelling better, the problem and overcoming the convergence problem, it has been necessary to insert a Stop Function in the Solver Configuration, imposing an if condition for the glass:

$$\text{comp1.StressMax} > 40[\text{MPa}]$$

Subsequently, from these first mechanical analyses, the glass of 4 mm of large dimensions, therefore with height equals to 2.4 m is the most vulnerable because the calculated breaking pressure is equal to 0.6 kPa (Table 5.12). This situation is not entirely similar for wooden frames, as the glass of this type is placed inside the frame without the aid of gaskets, so the glass is perfectly embedded in the frame itself (Table 5.13). Although the glass in the case of wooden frames may be suitable to withstand the expected pressures, the problem lies in the resistance of the glass to temperature variation.

5.7.1 Thermal Analysis

Thermal shock occurs when a thermal gradient (ΔT) causes different parts of an object to expand in different quantities. This differential expansion can also be understandable

Table 5.12 Glass breakage load aluminium windows

Frame	Glass								
Aluminium	SODA LIME GLASS								
	Large			Typical			Small		
	4mm	5mm	6mm	4mm	5mm	6mm	4mm	5mm	6mm
	0,6 kPa	1 kPa	1,3 kPa	2 kPa	3 kPa	4,3 kPa	5,3 kPa	8 kPa	10 kPa

Table 5.13 Glass breakage load timber windows

Frame	Glass								
Wood	SODA LIME GLASS								
	Large			Typical			Small		
	4mm	5mm	6mm	4mm	5mm	6mm	4mm	5mm	6mm
	2 kPa	2.3 kPa	3.3 kPa	4.6 kPa	6.6 kPa	9.6 kPa	8.6 kPa	14.6 kPa	22.6 kPa

in terms of stress or deformation (5.43). At some point, this stress may exceed the strength of the material, causing a crack to form. If nothing prevents this crack from propagating through the material, the glazing will lose its structural integrity. Glass objects are particularly vulnerable to failure due to thermal shock, due to their low strength and low thermal conductivity. If the glass is then suddenly exposed to extreme heat, the shock will cause the glass to break. The thermal analysis of the transparent elements was carried out, in particular the exposure time at three different temperatures (100/200/300)°C was calculated, until the critical temperature that causes the glass to break due to the thermal shock, considering both the three different thicknesses and the three different dimensions previously defined.

$$\Delta T = \frac{(\sigma_{TS} * (1 - \upsilon))}{E * \alpha} \tag{5.43}$$

where:

- $\sigma_T S$ is the yield strength of the material,
- ν Poisson's ratio,
- E Elastic modulus,
- α coefficient of thermal expansions.

In the case of soda lime glass, the critical temperature is 52 °C. Once the critical temperature is defined (5.43), it has been necessary to assess the time to reach it through the time-dependent heat transfer equation (5.20), and the set time interval is 60 seconds, which varies linearly with a one-second step. For this analysis, since it has been hypothesized to apply the temperature directly to the glass surface of the window, the temperature variation, besides depending on the intrinsic characteristics of the material such as density

(ρ), specific heat (C_p) and the thermal conductivity (k) will depend on the conductive contribution of the heat flow (5.10).

Moreover, to model the sudden temperature rise, a ramp function (Figure 5.26) was applied on the external face, using the following expression:

$$T = 20 + x * rm1(t) \tag{5.44}$$

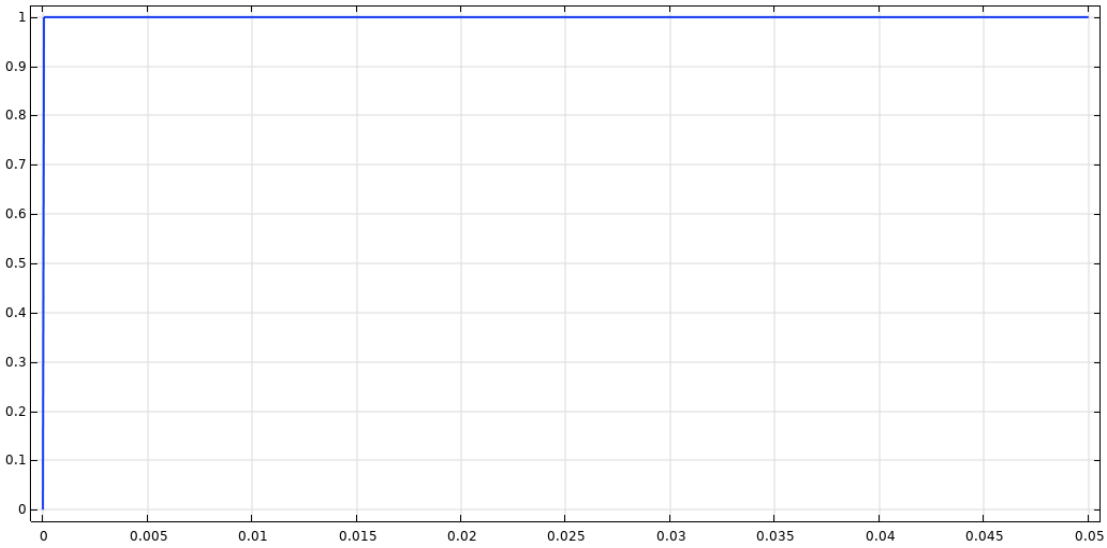

Fig. 5.26 Ramp Function

The results (Figure 5.27) highlight that the soda-lime glass reaches the critical temperature around 5 seconds. Hence, the ordinary glass of the windows is vulnerable to the temperatures expected in the red areas.

Aluminium resistance

The aluminium frame's resistance is assessed by computing thermal stress due to the different temperature that is assumed to be applied on the external front. The thermal stress evaluated by coupling the two physicists, the mechanical and the thermal, in particular with the formula (5.20) a deformation speed ($epsilon_{th}$) is calculated, which depends both on the temperature variation and the coefficient of thermal expansion (α) characteristic of the materials. The strain calculated in this way will vary the stress tensor S of the (5.4). In these analyses, the applied temperature is defined through three different functions:

- A ramp function (5.44) for four different temperatures from 100°C to 400°C, considering as time interval 1200 seconds, considering it as the maximum duration of the phenomenon.

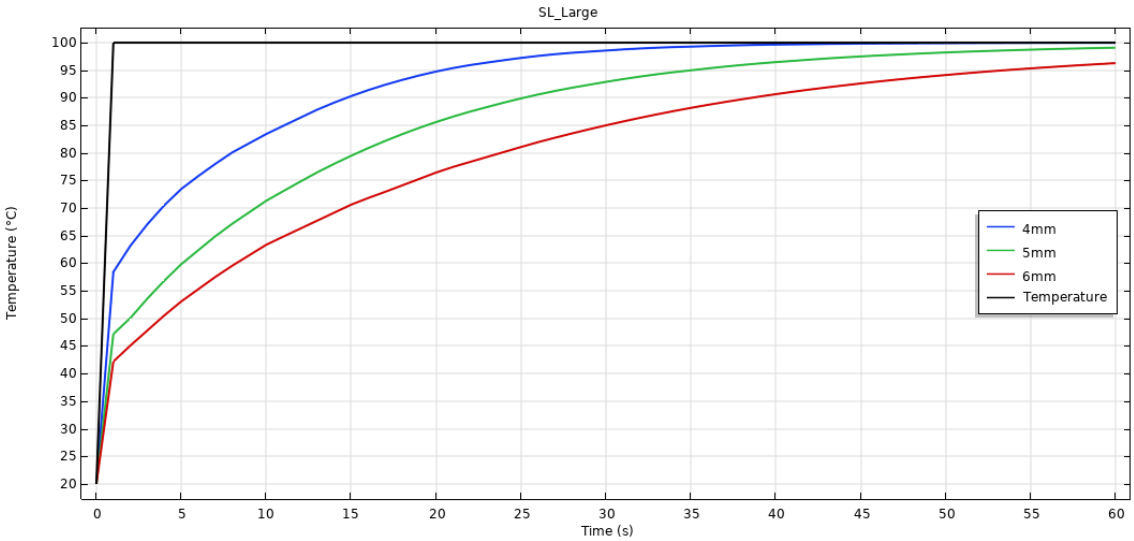

Fig. 5.27 Heat Transfer for large glass pane

- A piecewise function (5.45) whose time range is 400s and the temperature increases by 50 degrees every 50 seconds (Figure 5.28) until the maximum temperature of 400°C is reached.

$$T = T_i + 50 \tag{5.45}$$

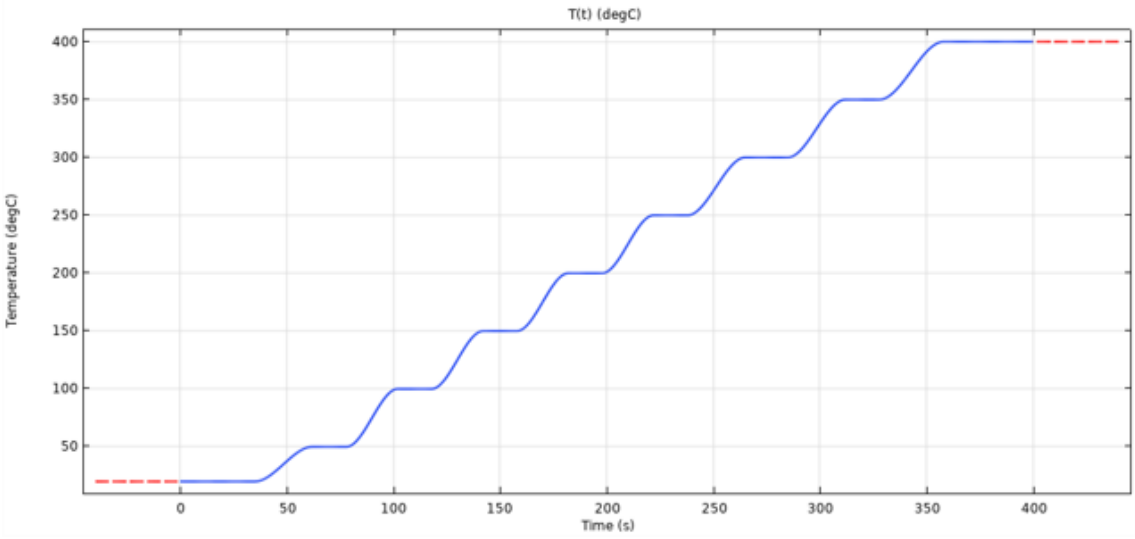

Fig. 5.28 Piecewise function

- An interpolated function (5.46) presents a sinusoidal variation of temperatures for 240 seconds that is the minimum interval of time (Figure 5.29). The peculiarity of this function lies in reaching different maximum temperatures by changing the

parameter P, indeed if the P is less than one, the maximum temperature is around 200°C, while if it is greater than 1, the temperature reaches the 500/600 °C. In the first analysis, the maximum temperature was 400°C.

$$T = T_i + sin(T) * t * P \tag{5.46}$$

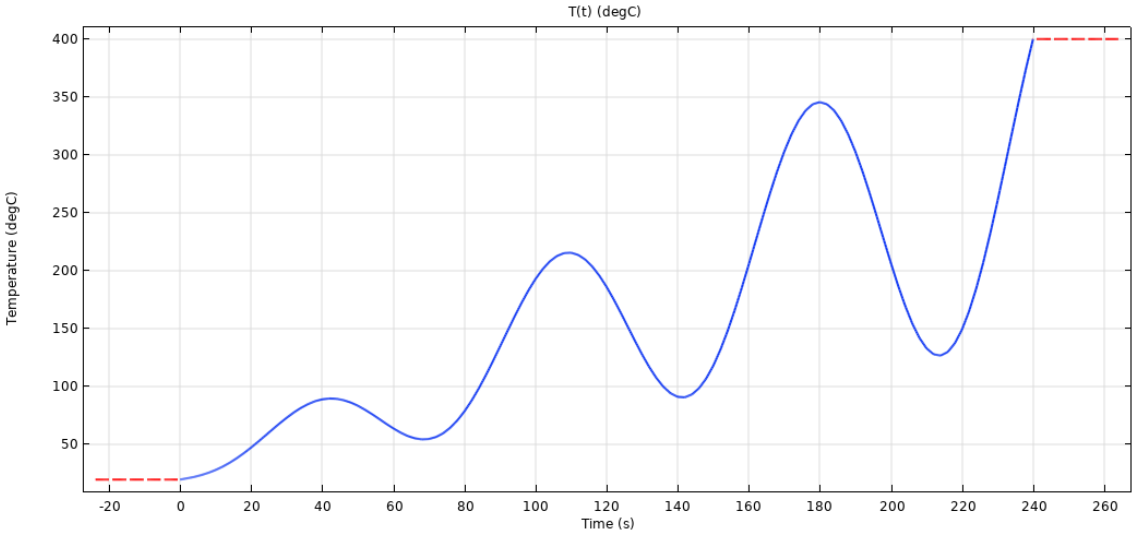

Fig. 5.29 Interpolated Function

These analyses show that the aluminium frame can resist the high temperatures, In fact, if the temperature variation is expressed by (5.44), the frame reaches a maximum tension of 120 MPa in the case of an acting temperature of 100°C or a maximum tension of 150 MPa in the case of a temperature of 400°C (Figure 5.30). Furthermore, in the second analysis, the frame reaches a maximum tension of 146 MPa (Figure 5.31); finally, through the third analysis, the aluminium frame can resist the temperature variation, reaching a maximum tension of 120 MPa (Figure 5.32). Therefore, the analyses show that the real issues are the plastic material of thermal break and sealing. Indeed, from the first analysis, the polyamide reaches its critical temperature in a range of 600s in the case of 100°C, while in the case of 200°C, 300°C and 400°C the time is reduced to 50s, 20s and 14s respectively (Figure 5.33). Besides the EPDM, considering the temperature higher than 100°C, it reaches the critical temperature around the 30 seconds and lower (Figure 5.34).

Also, the results of piecewise function (5.45 show that the plastic elements are the most vulnerable elements of the windows; indeed, both the polyamide and the EPDM reach their temperature of glass transition in 175 seconds (Figure 5.35 and Figure 5.36).

Moreover, if the temperature is described by the interpolated function 5.46, the results show that the polyamide reaches its T_g about 100s (Figure 5.37); at the same time, the EPDM reaches its T_g around 95 s (Figure 5.38).

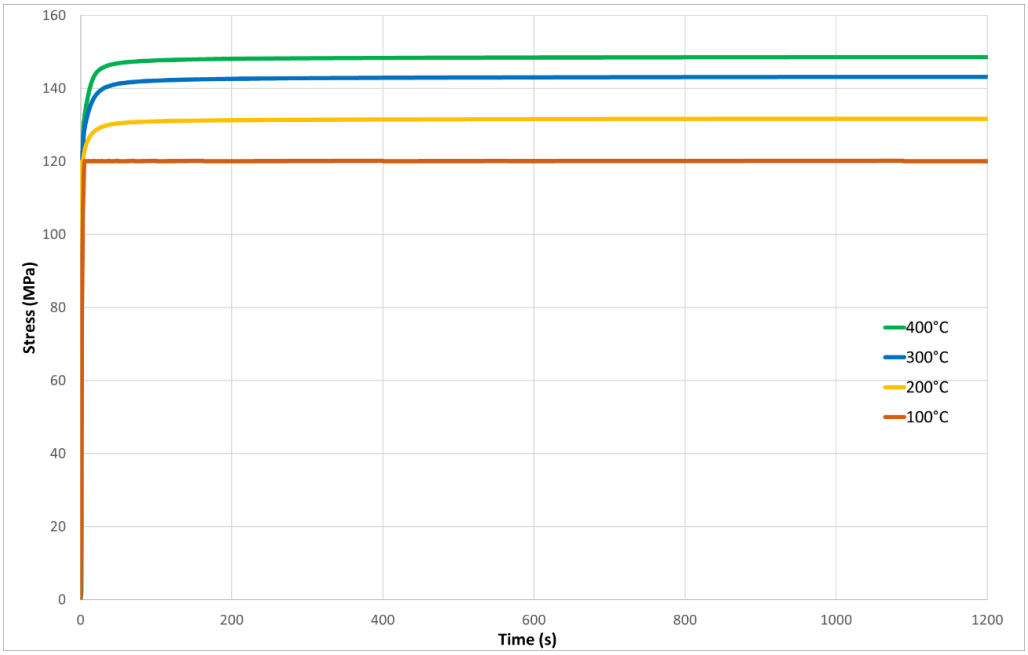

Fig. 5.30 Von Mises stress of aluminium frame due to the temperature expressed by ramp function (5.44)

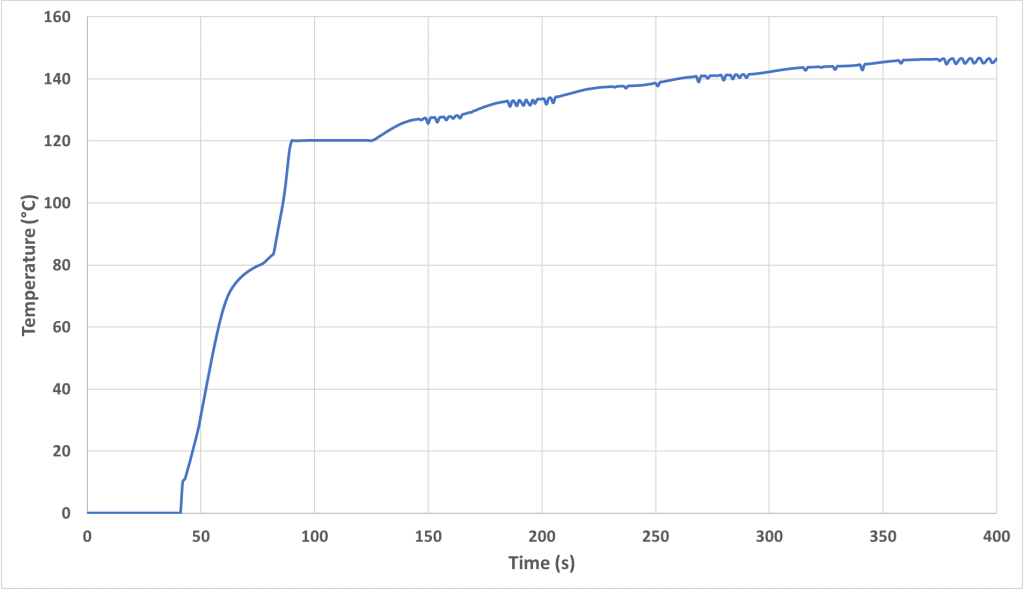

Fig. 5.31 Von Mises stress of aluminium frame due to the temperature expressed by piecewise function (5.45

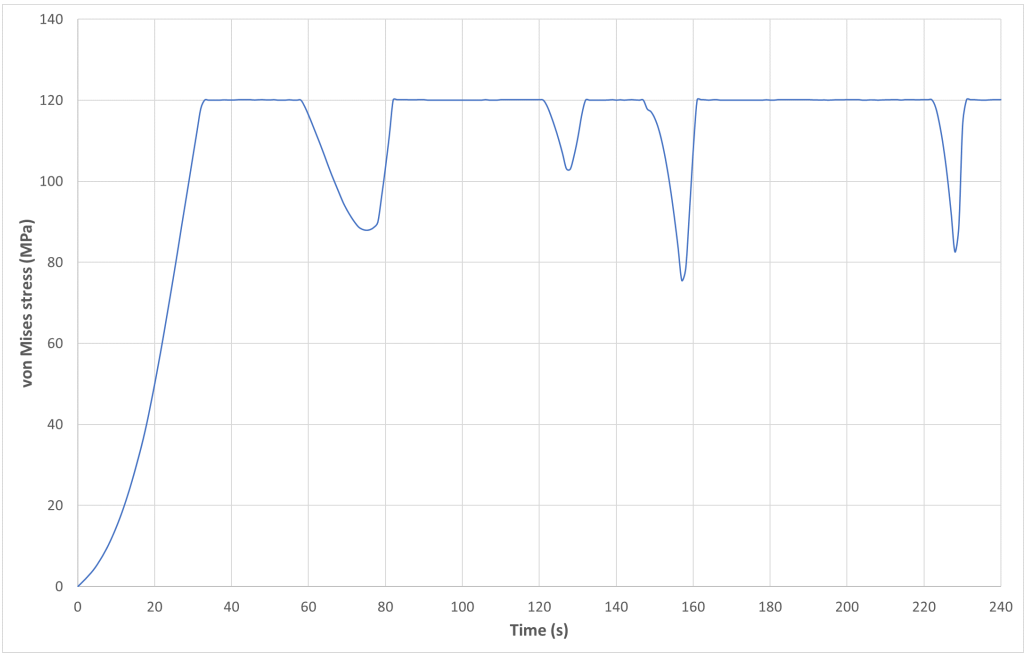

Fig. 5.32 Von Mises stress of aluminium frame due to the temperature expressed by interpolation function (5.46)

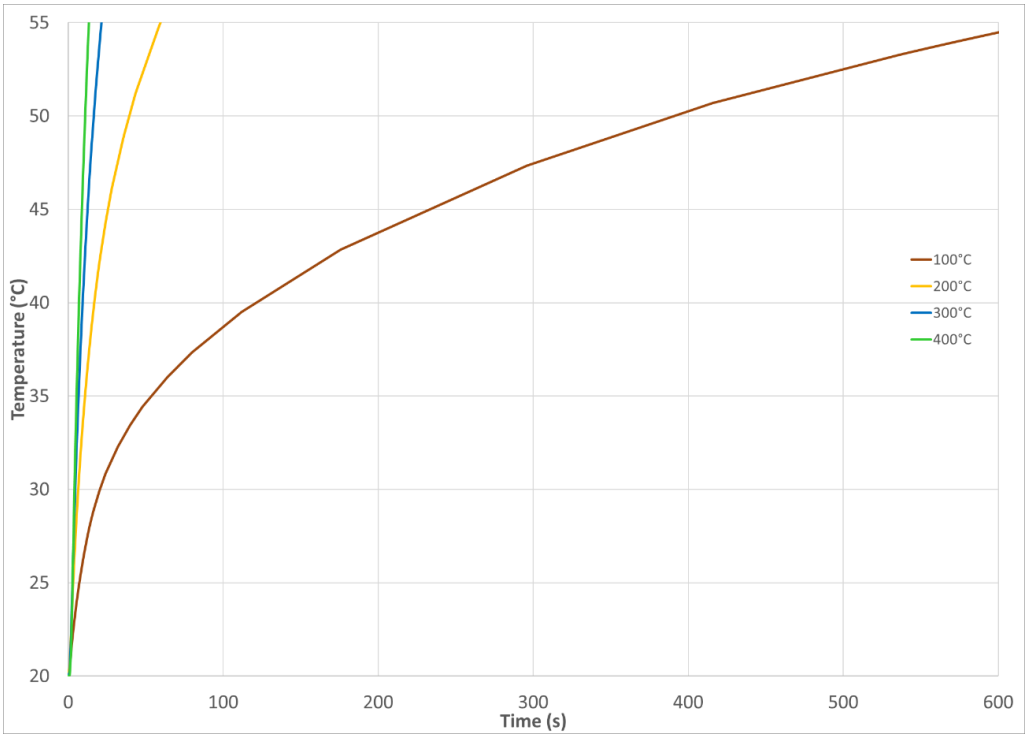

Fig. 5.33 Von Mises stress of aluminium frame due to the temperature expressed by ramp function (5.44)

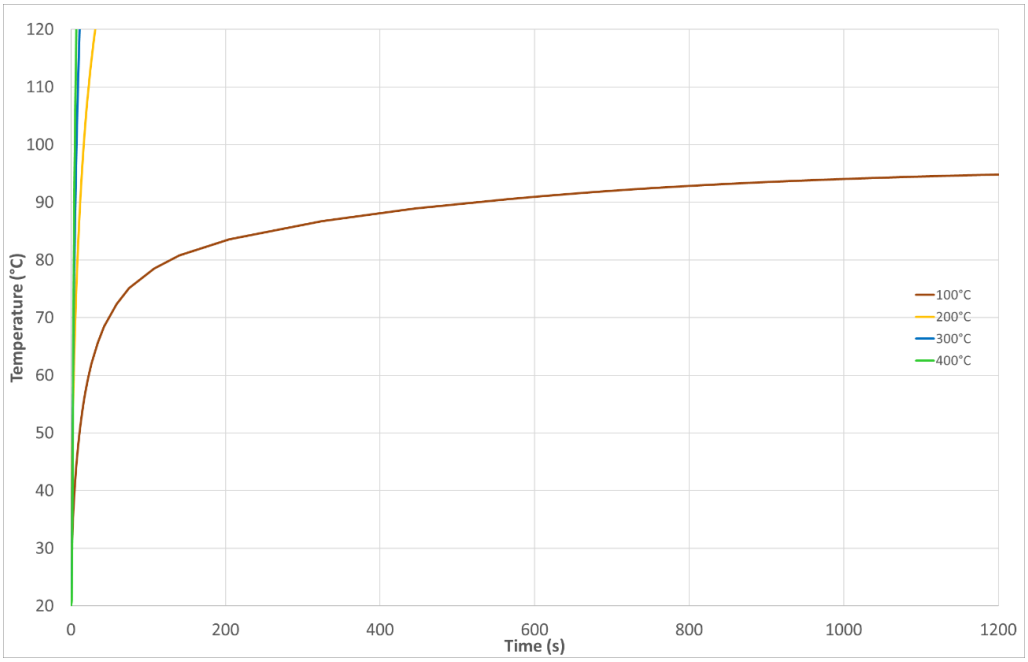

Fig. 5.34 Temperature reached by EPDM due to the temperature expressed by ramp function (5.44)

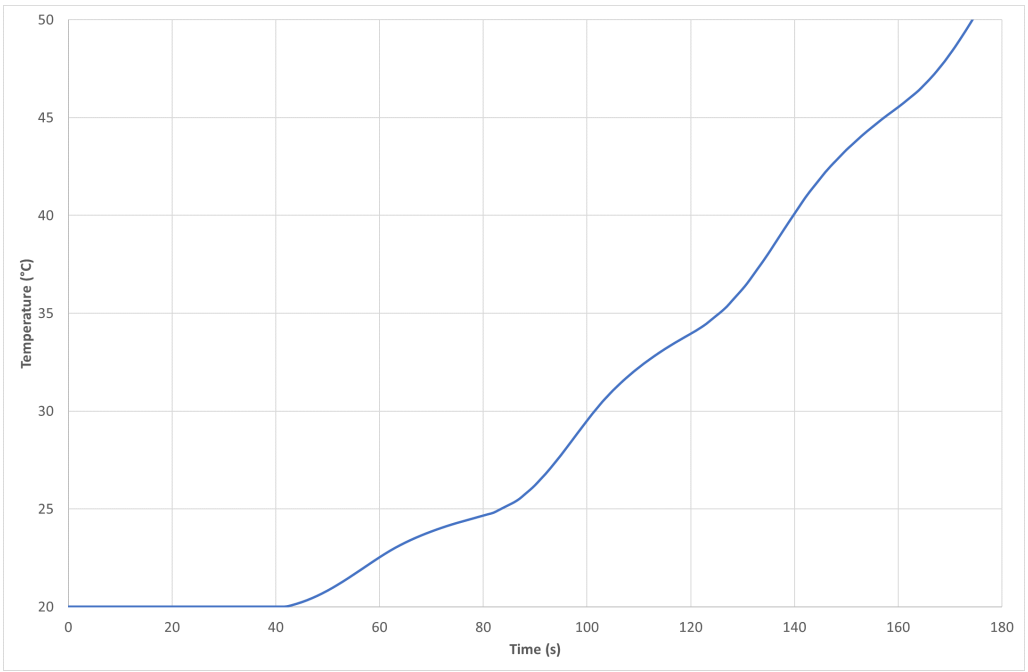

Fig. 5.35 Temperature reached by polyamide due to the temperature expressed by piecewise function(5.45)

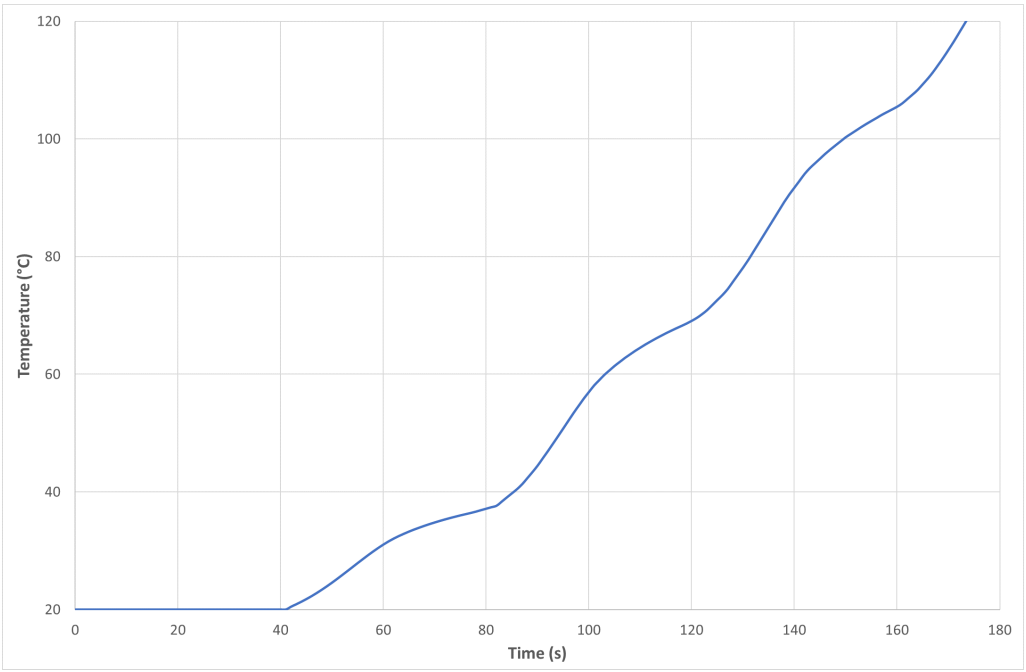

Fig. 5.36 Temperature reached by EPDM due to the temperature expressed by piecewise function (5.45)

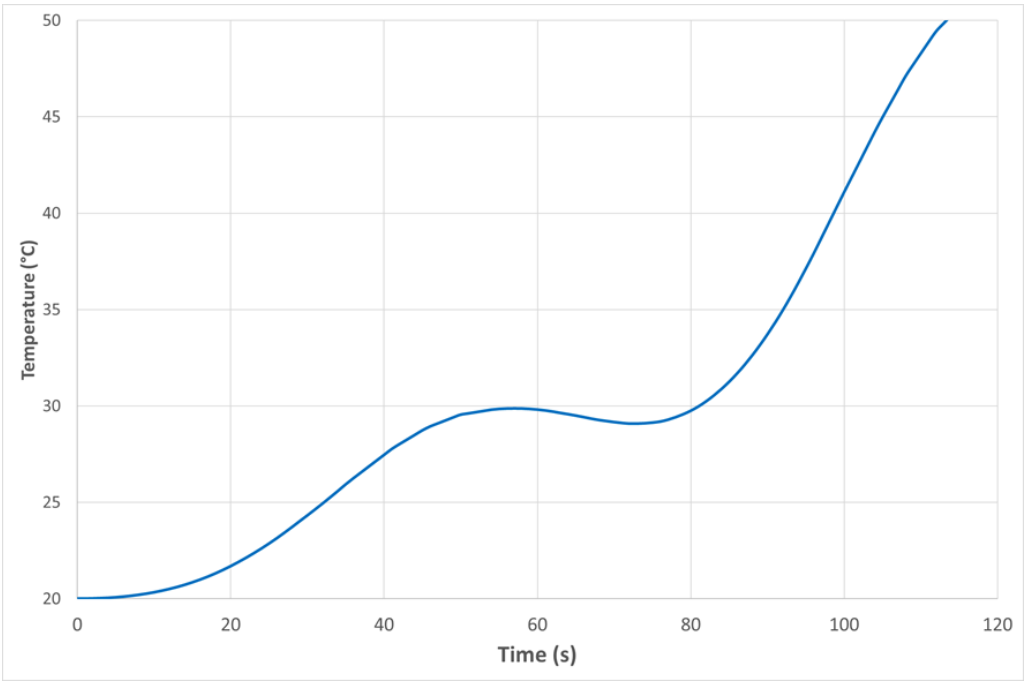

Fig. 5.37 Temperature reached by polyamide due to the temperature expressed by interpolation function(5.46)

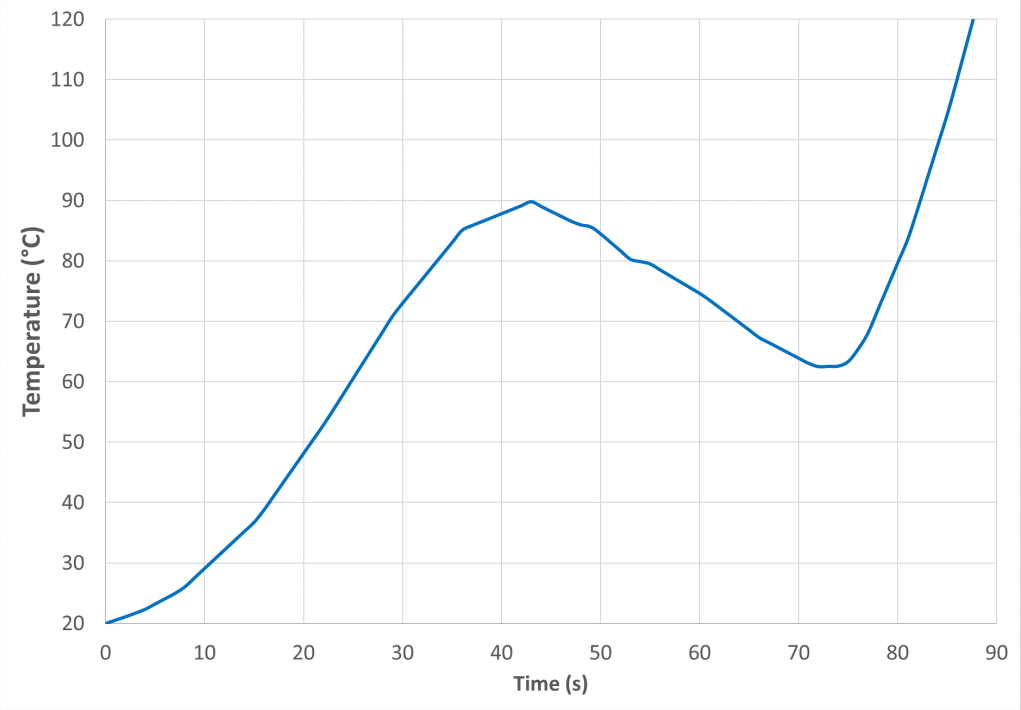

Fig. 5.38 Temperature reached by EPDM due to the temperature expressed by interpolation function (5.46)

From the results of the thermal analysis, regardless of the model used to describe the flow temperature, the plastic elements, together with the glass, are the most vulnerable elements of the frame. Although the aluminium frame can withstand temperature variation, once the polyamide reaches the glass transition temperature, the continuity function between the frame elements is lost and therefore the window is failed. This situation is also valid for seals; indeed, if they reach the critical temperature, the glass loses the only element that constraint it with the frame. Although it is difficult in the in situ investigations to identify which aluminium frame technology was used, it is necessary to analyse thermally also the frame without thermal break as its diffusion within the Campania area is detectable for economic reasons. In fact, the windows without thermal break costs around 300 €/m against 400 €/m of the windows with thermal break. The window has been evaluated considering as temperature variation the function (5.46). The results show that this technology shows a resistance to temperature variation. Indeed the frame does not reach the breaking tension (Figure 5.39), and the only vulnerable plastic element is the glass seal. Although this technology is valid for the maximum expected temperature, it does not represent a valid option for improving the building's energy efficiency. In fact, Ministerial Decree 06/08/2020 on energy requalification for existing buildings has defined energy transmittance limits based on the area in which the requalification is being carried out; in particular, for the province of Naples, which has been classified as climate zone C,

the transmittance limit for windows and doors has been set at 2.1 $\frac{W}{m^2K}$; and a non-thermal break window frame, according to EN 10077-01:2007, has a linear thermal transmittance varying between 7 and 5 $\frac{W}{m^2K}$, which is much higher than the imposed limit.

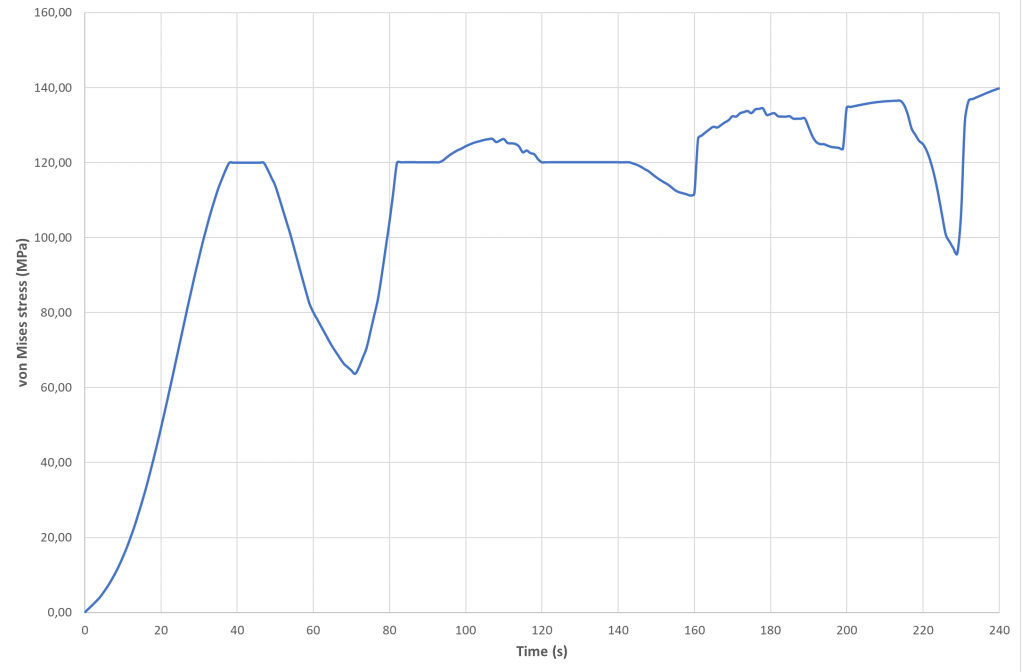

Fig. 5.39 von Mises stress of aluminium frame without thermal break due to the temperature expressed by interpolation function(5.46)

Shutters

Once the windows system's criticalities had been defined, it was also necessary to assess the vulnerability of the shutters to the phenomenon of PDCs and highlight any positive aspects that could constitute the starting point for the definition of a mitigation strategy. First of all, a typological and material evaluation was carried out. Shuttering is classified according to the position of the screen to the window frame, and its morphology; hence we have the following types:

- **sunshade**: a screen fixed to the outside of the wall, formed by several horizontal and/or vertical elements, with the main function of controlling the radiant energy of the sun;
- **external shutter**: a screen placed on the outside of the window frame, made up of a fixed frame if any, and one or more sashes, with rotation movement on a vertical, lateral axis or with lateral or vertical running movement;
- **roller shutter**:a screen placed outside the window frame, made up of a curtain sliding on two lateral guides, an upper horizontal roller, on which the curtain is wound, and the operating accessories.
- **external Venetian blind** :a screen made up of several movable horizontal elements, which with one manoeuvre are gathered at the top or arranged equidistantly, and with another manoeuvre are inclined to the horizontal plane to regulate the radiating energy.
- **external blind**: a screen made of flexible material, regulates radiant energy and/or visibility.
- **intermidiate Venetian blind**: a screen placed inside a double glazing unit, in the interspace of double glazing units, made up of several mobile horizontal elements, which, with one manoeuvre, gather at the top or are arranged equidistant from each other, and with another manoeuvre, incline for the horizontal plane to regulate radiant energy.
- **internal shutter**: a screen placed inside the window frame, allows shading; it is made up of several opaque wings, with a rotating movement on a vertical, lateral axis, connected to the sash frame or the fixed frame of the window.

The arrangement of the data from the PLINIVS database stresses that in both two study areas the most commonly used material for shading systems is UPVC, followed by aluminium and iron (Figure 5.40, Figure 5.41). For the reasons already expressed above for

UPVC window frames, shutters made of the same material are also considered unsuitable for flow protection. Therefore, vulnerability analyses have been carried out for the other two materials; particularly for aluminium, the EN-AW 6060 alloy has been considered, whose characteristics are reported in Table 5.14. While for the iron shutter, the S235 type was considered, whose characteristics are shown in Table 5.15 since this type of screen is generally burglar-proof.

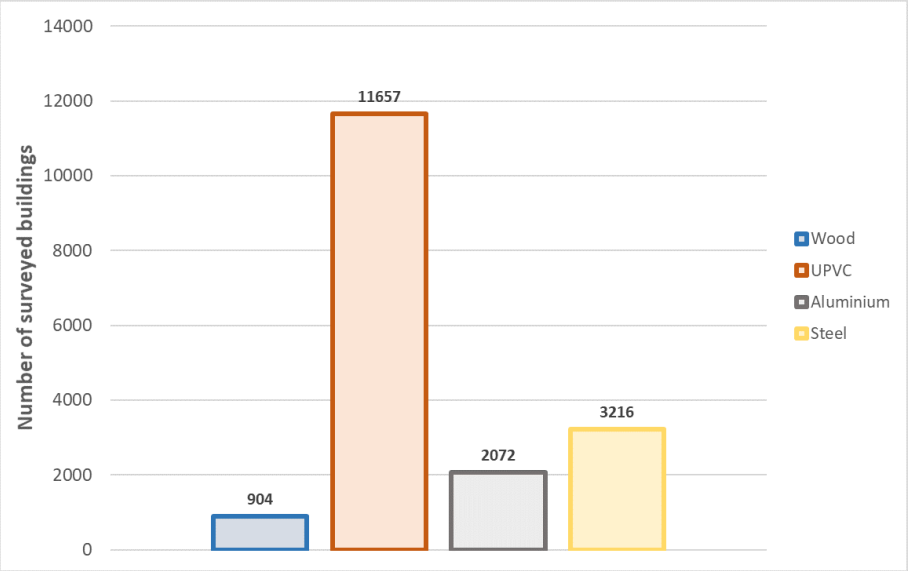

Fig. 5.40 Breakdown of surveyed buildings in the Campi Flegrei area by shutters

Table 5.14 Physical and mechanical properties of aluminium EN-AW 6060

Density	2700 [kg/m3]
Elastic modulus	70000 [MPa]
Ultimate Tensile Strength	160 [MPa]
Poisson Coefficient	0.33
Specific heat capacity	900 [J/kgK]
Thermal conductivity	238 [W/mK]
Thermal expansion	3,7 e-7 [1/K]

In the Vesuvius and Campi Flegrei area, the most common types are the UPVC rolling shutter and the external shutter; since UPVC has a critical temperature of 80°C, the system is not suitable for the eventual task of protecting the window frame. Therefore, the model analysed is the external shutter in aluminium and iron; in particular, the single slat that makes up the shading system was considered (Figure 5.42), with a simplified elliptical section with a thickness of 1 mm.

The first analysis carried out was of the mechanical type (5.4) in a stationary field, to evaluate the stress caused by the application of the pressure exerted on the external face by

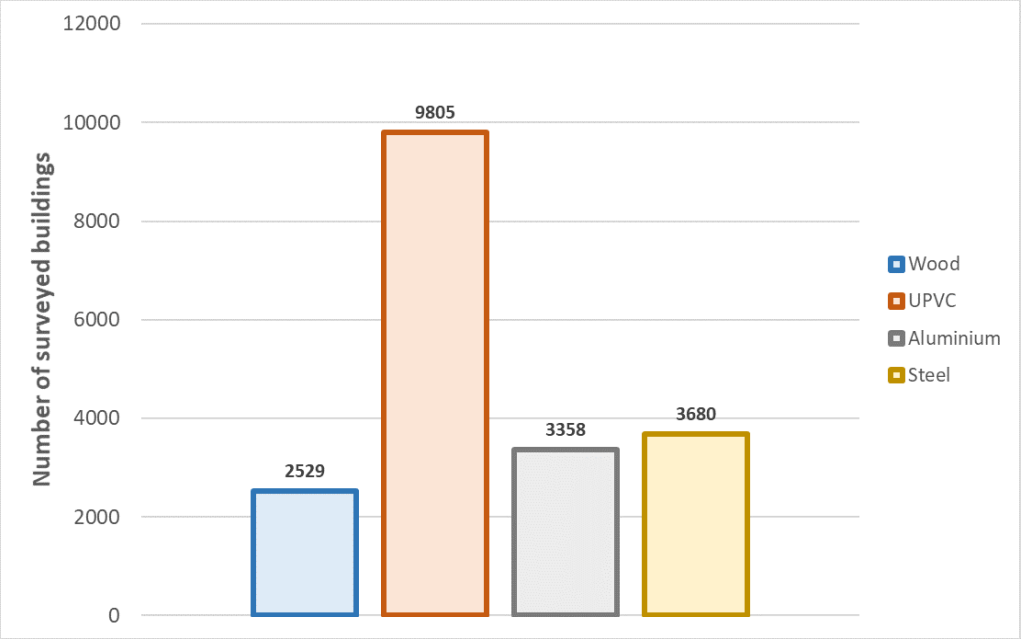

Fig. 5.41 Breakdown of surveyed buildings in the Vesuvio area by shutters

Table 5.15 Physical and mechanical properties of steel S235

Density	7500 [kg/m3]
Elastic modulus	210000 [MPa]
Ultimate Tensile Strength	360 [MPa]
Poisson Coefficient	0.3
Specific heat capacity	475 [J/kgK]
Thermal conductivity	44,5 [W/mK]
Thermal expansion	12,3 e-6 [1/K]

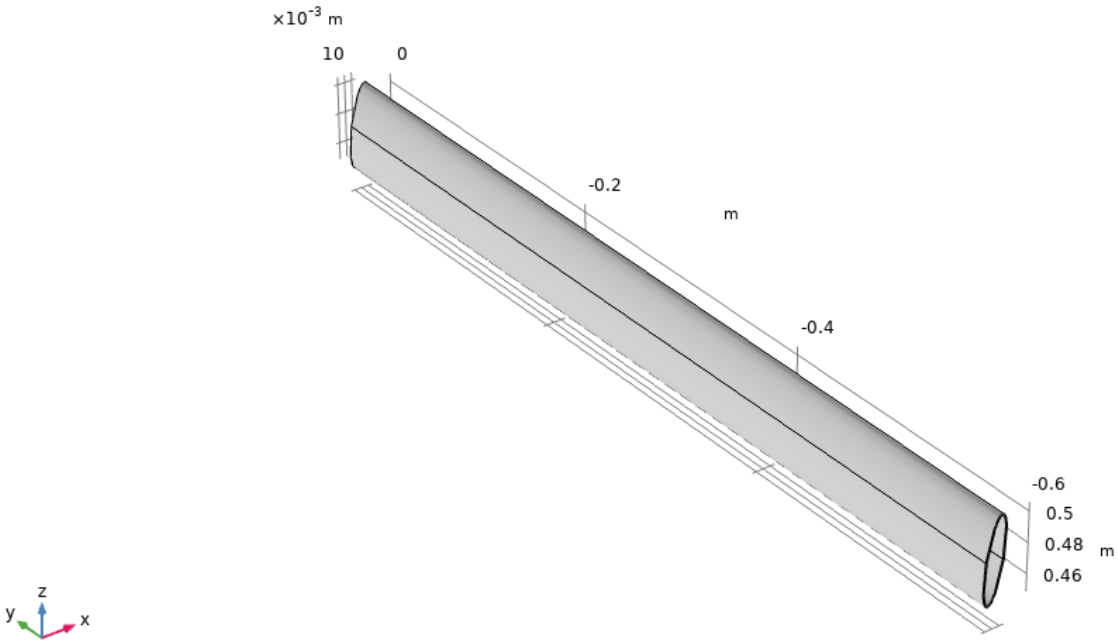

Fig. 5.42 Geometric model of slat composing the shutter

the flow, which was schematised as a uniformly distributed load (5.47) with linear growth up to the maximum pressure of 7 kPa, on the external face (Figure 5.43).

$$\mathbf{F} = -p\mathbf{n} \tag{5.47}$$

where :

- p is the pressure [kPa],
- n is the normal vector

Also, to reduce the computational load, half of the section was considered (Figure 5.44), setting a symmetry condition in the mechanical field (5.48), and the condition means that the model is free in the plane and fixed in the out-of-plane direction.

$$\mathbf{u} \cdot \mathbf{n} = 0 \tag{5.48}$$

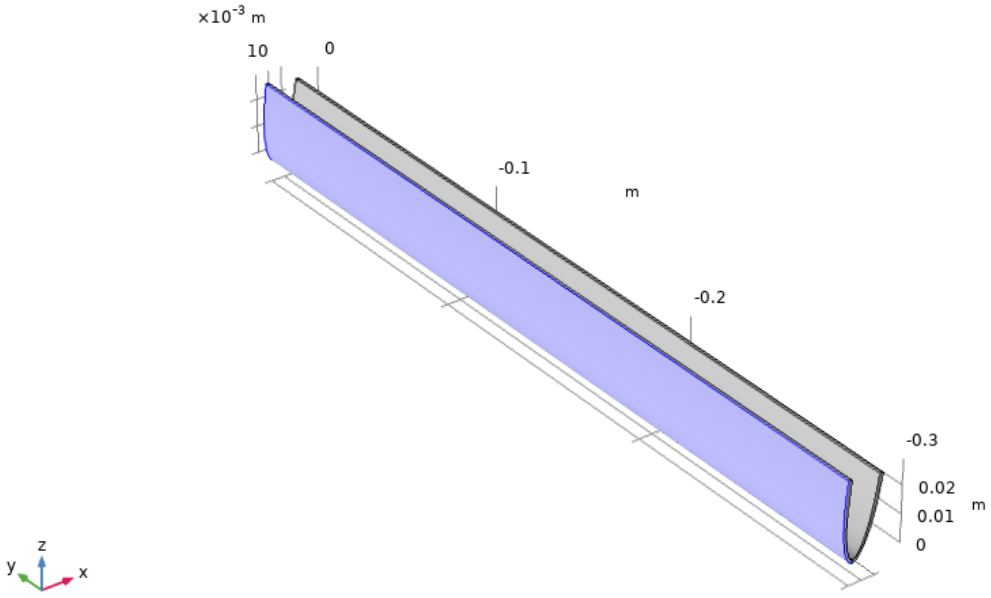

Fig. 5.43 Pressure and temperature application surface

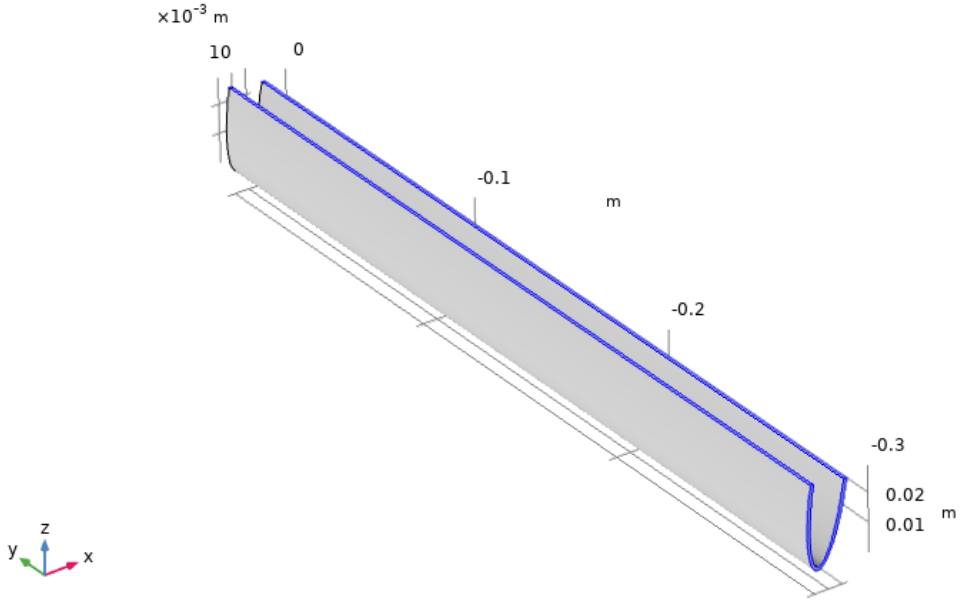

Fig. 5.44 Symmetry surfaces

The results show that both the aluminium and the steel element can withstand the different pressures exerted since the maximum tension that the aluminium element reaches is 100 MPa, while the steel element reaches 80 MPa (Figure 5.45).

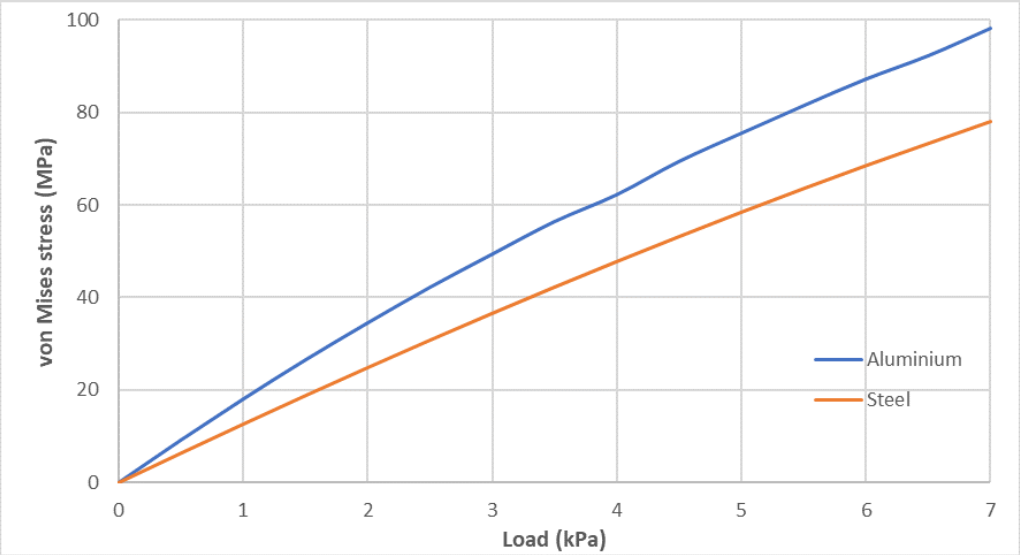

Fig. 5.45 von Mises stress owing to the application of the pressure

Subsequently, the thermal stress (5.20) was evaluated, resulting from the application on the external front of the temperature expressed by the function (5.46), which in the time span of 240 seconds reaches the maximum temperature of 400°C. Also, in this type of analysis, a symmetry condition (5.49) was considered, which means no heat flux across the boundary.

$$-\mathbf{n}\cdot\mathbf{q}=0 \tag{5.49}$$

where :

- q is the temperature gradient [W/m],
- n is the normal vector

This analysis shows that both the aluminium and the steel shutter resist the temperature variation effectively. In fact, the aluminium shutter reaches a maximum tension of 156 MPa; while the steel shutter has a maximum tension of 240 MPa (Figure 5.46).

Although the elements analysed resist both mechanical and thermal stress, it is necessary to evaluate the shutter's shielding effect to the infiltration of the flow to avoid the most vulnerable elements, such as glass and seal, can reach their critical temperatures. For this reason, a fluid-dynamic and heat-transfer assessment was carried out in a turbulent field and, also, to study the shielding effect of the shutter, two different slots inclinations were

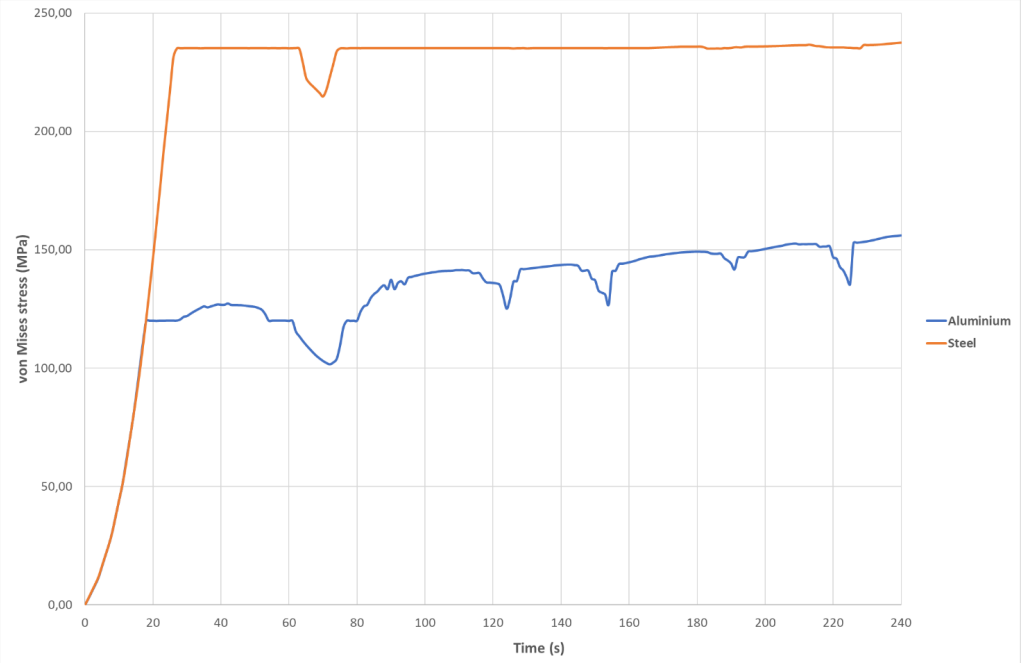

Fig. 5.46 von Mises stress due to the temperature expressed through the interpolation function (5.46)

evaluated. The pyroclastic flow, the characteristics of which are defined in Table 5.16, was analysed using a turbulent model (5.31) that solves the Reynolds-averaged Navier-Stokes (RANS) equations for conservation of momentum and conservation of mass, which allow calculation of the fluid velocity along the path and the pressures exerted.

Table 5.16 Physical characteristics of pyroclastic flow

Density	2265 [kg/m^3]
Dynamic viscosity	0.001 [Pa * s]
Thermal conductivity	2.2 [W/m * K]
Heat capacity at constant pressure	1255 [J/kg * K]
Ratio of specific heats	1
Velocity	25 [m/s]

The hypotheses are:

- Incompressible fluid,
- Turbulent movement,
- Homogeneous density and speed profile.

The fluid-flow geometry (Figure 5.47), is defined as a rectangle where the fluid enters to the right side with a speed of 25 m/s, besides in the centre of the domain there is a piece

of wall with two windows, covered by louvre shutters. Moreover, two types of louvre have been considered, one with an angle of 45° and another one of 60°. Finally, the outlet is on the left side, where the hypothesized pressure is equal to 0 Pa.

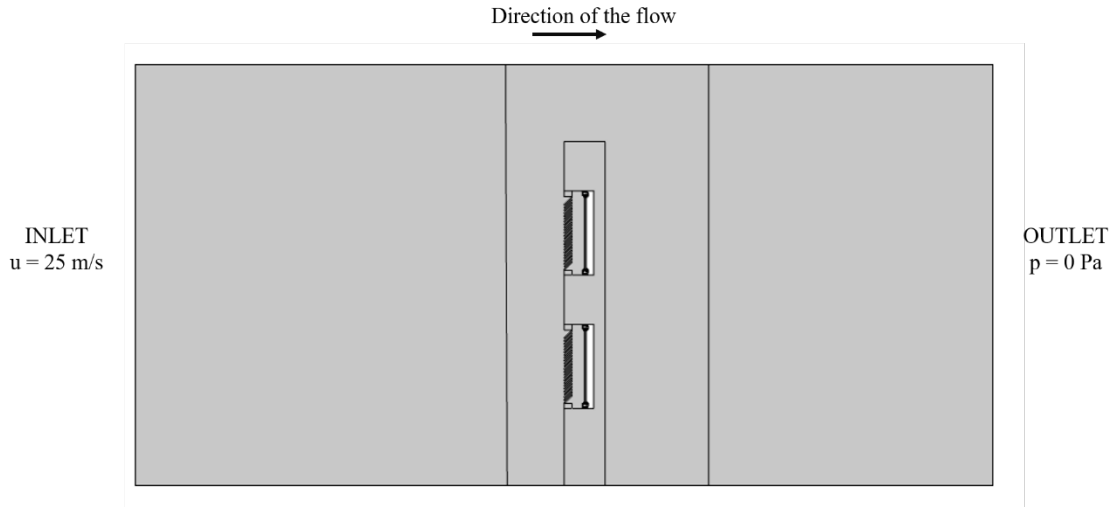

Fig. 5.47 Geometric model for CFD

The pyroclastic flow enters the computational domain at a speed of u = 25 m/s normal to the inlet surface. The floor and the ceiling of the flow domain and surface of the wall are described by wall functions. The geometric model has been divided into three domains in order to diversify the meshes used. In fact, for flow only domains a mapped mesh of about 2800 elements was used, while in the domain where there is the wall an extra-fine triangular mesh was used, in which there are 92740 elements (Figure 5.48).

Once the velocity range has been defined (Figure 5.50), in order to analyse the heat transfer between the fluid and the considered solids, the equation (5.8) has been considered, considering the temperature expressed by (5.13) in the time interval of 240 seconds, in particular, the heat flow is obtained considering the conductive flow rate expressed by the following equation:

$$\mathbf{q} = -(\mathbf{k} + k_T)\nabla T \tag{5.50}$$

where:

- k is the thermal conductivity of the solids (W/mK),
- k_T is the turbulent thermal conductivity which depends on the fluid and solids characteristics (W/mK),
- T is the temperature (K).

The results show that shutters, commonly used, are not suitable for window protection against the flow. The EPDM, in both cases considered, reaches the critical temperature after

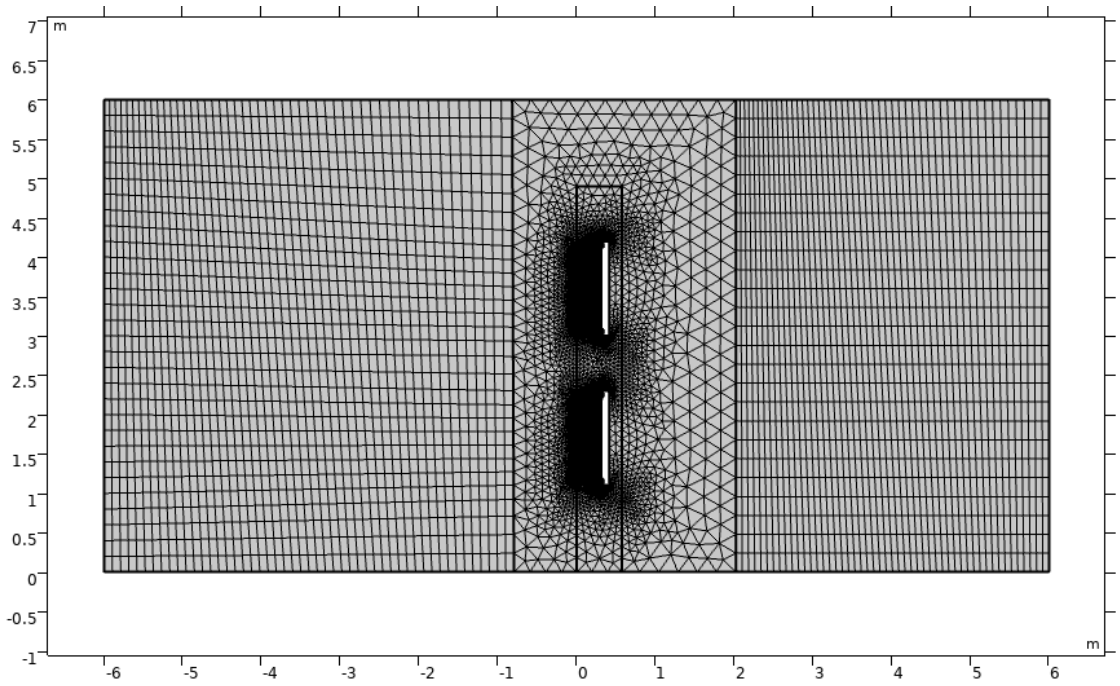

Fig. 5.48 Geometric model mesh

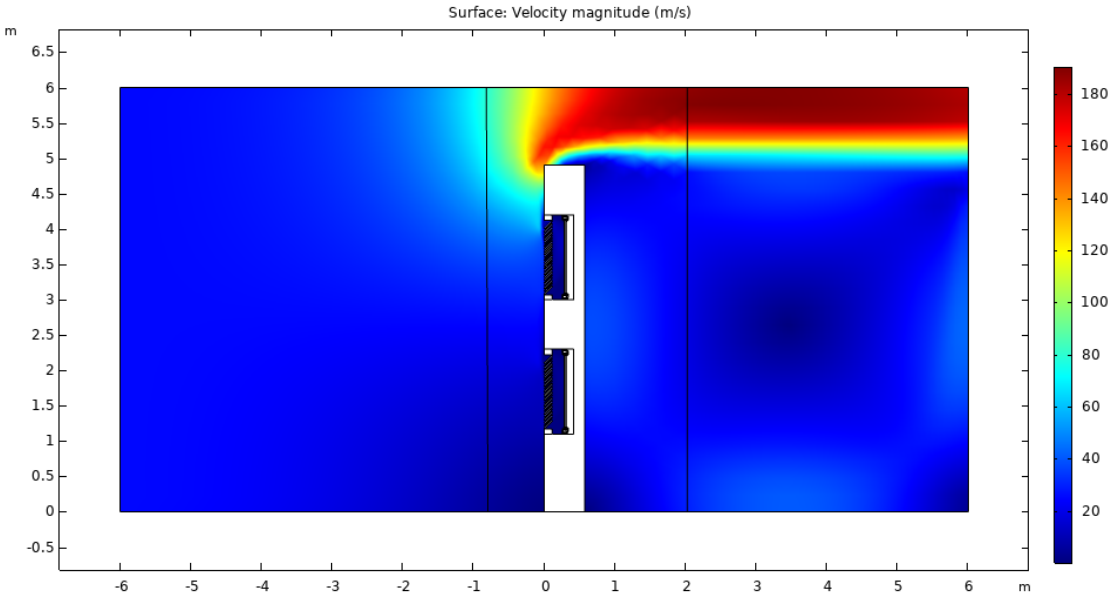

Fig. 5.49 Velocity field (m/s)

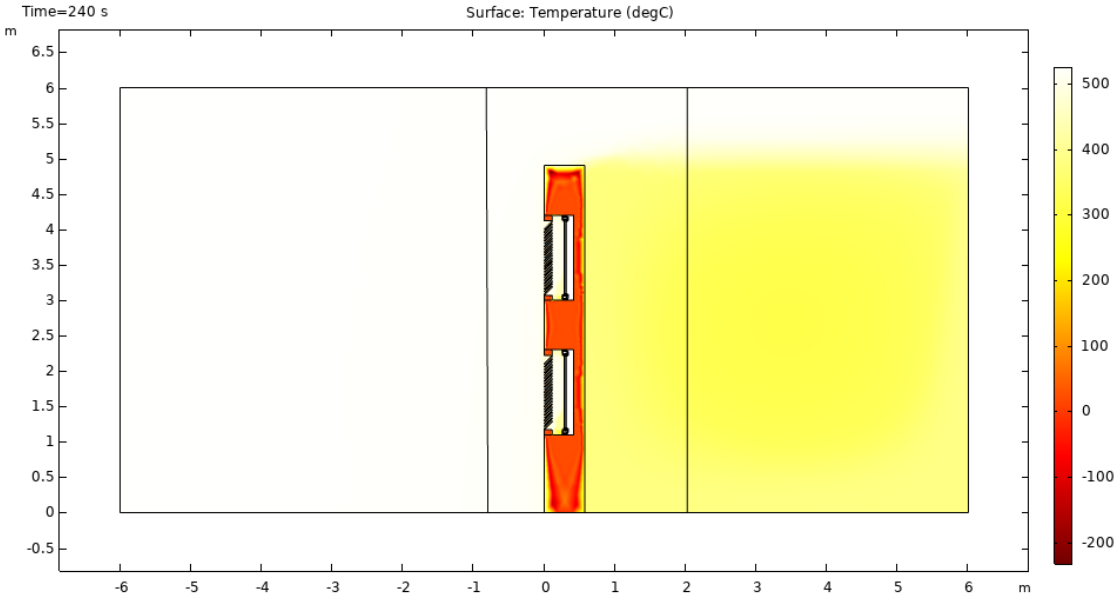

Fig. 5.50 Temperature field (°C)

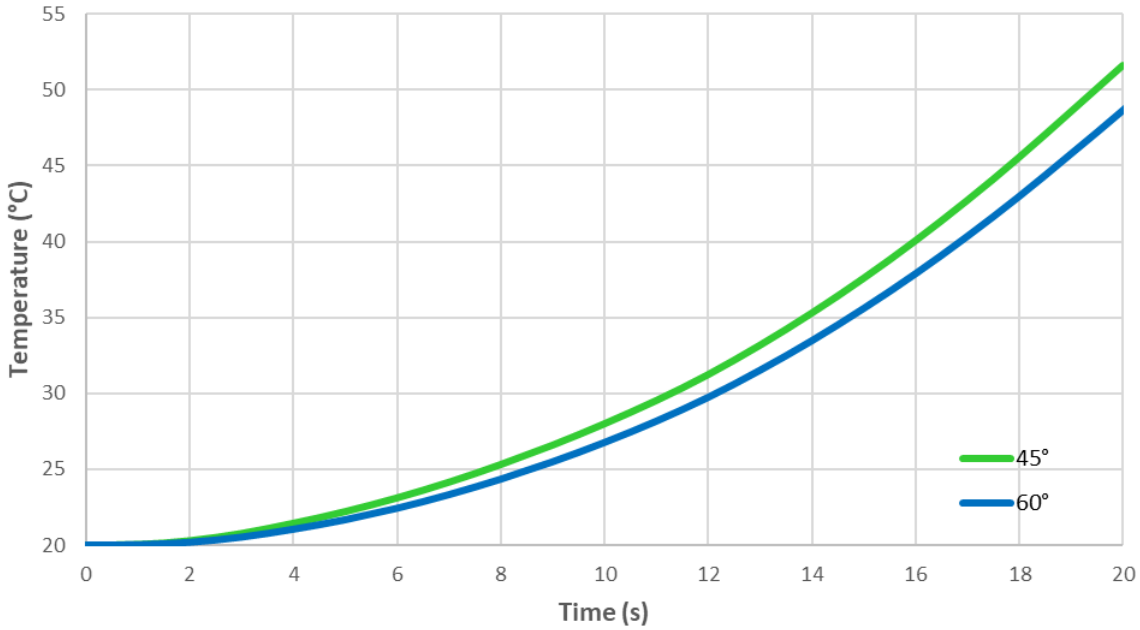

Fig. 5.51 Reached temperature by glass changing the angle of the slots

about 100 seconds. At the same time, polyamide reaches its glass transition temperature after about 120 seconds (Figure 5.52). Also, the glass is exposed to the effects of pyroclastic flow, indeed it breaks due to thermal shock after 20 seconds (Figure 5.51). Since, the shutters does not fulfil the task so the idea would be to replace the shutters with solid laminated panels that resist both thermal and mechanical stress.

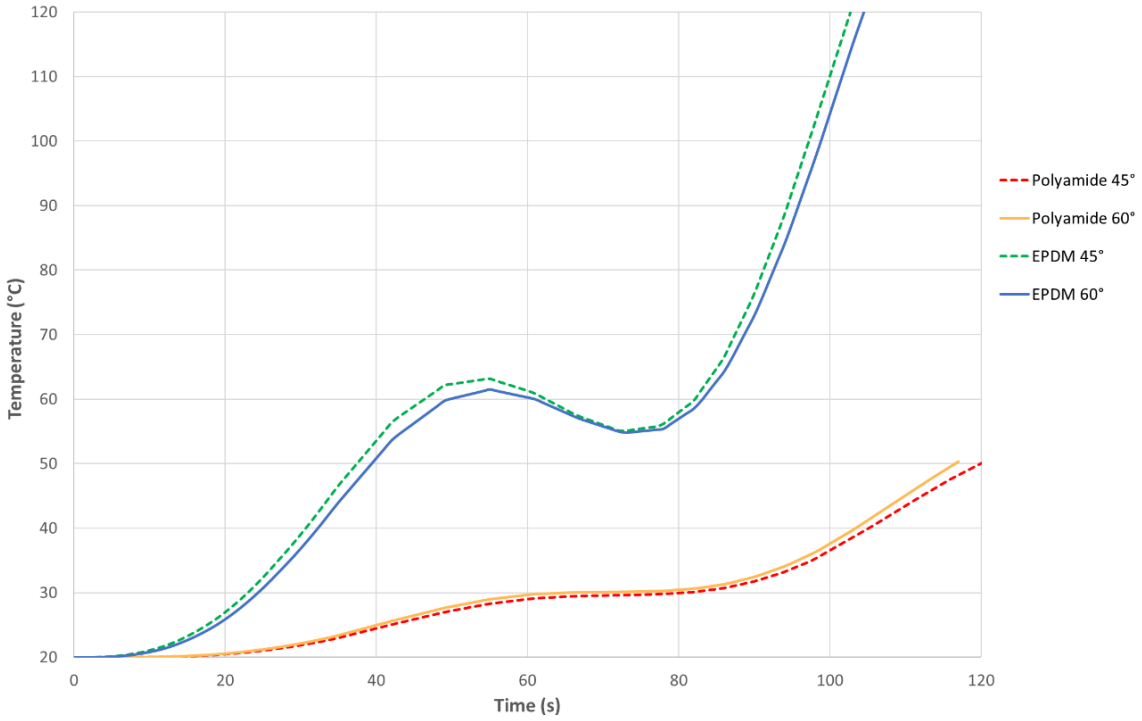

Fig. 5.52 Reached temperature by polyamide and EPDM

Chapter 6

Design and prototypes of mitigation device to PDCs and ash fall actions

Once the vulnerabilities of each previously studied technological unit were defined, the logic of incremental innovation was followed to define a valid mitigation strategy to the different mechanical and thermal stresses. Incremental innovation is an improvement (or adaptation) of something that already exists. So, interventions in a punctual way on the different components of the element considered. This choice stems from the need to contain the production costs of the prototypes and facilitate marketing within the Campania region. To promote the marketing of the analysed products, the ministerial decree (06/08/2020), which provides for state subsidies for any energy requalification work, was taken into account. Therefore, the elements analysed must resist the stresses exerted by volcanic phenomena and meet the thermo-hygrometric limits imposed to obtain state funding

6.1 Façade

To protect a building façade as a mitigation strategy, which was both easy to market and valid for energy saving, a ventilated façade model was analysed. Ventilated façades are a special type of lightweight façade in which the cavity separating the cladding layer from the load-bearing structure is open to the outside environment at the top and bottom with appropriately sized perforations. Recently, installation techniques have been proposed that are typical of "dry" stratified constructions; these techniques allow the materials making up the cladding layers to be aggregated using various types of mechanical fixings, without resorting to traditional cement mortars ("wet" installation). Physical-technical considerations and architectural-constructive considerations can determine the thickness of the air space. This thickness may vary according to the choice of materials used to make the external covering layer, the anchoring systems adopted, and the environmental

and operating conditions considered. It is generally between 5 and 15 centimetres. We speak of a micro-ventilation layer for cavity thicknesses of just a few centimetres (< 5 cm). The external cladding layer and the anchoring system are of considerable interest in the ventilated wall's stratigraphy. The cladding layer has the function of delimiting the cavity towards the outside and protecting the building's structure from atmospheric agents and obviously representing the most appropriate aesthetic-formal choice. Among the cladding systems, a distinction can be made between those realised with "traditional" materials (e.g. wood and stone) and those realised with the use of "innovative" materials (e.g. metal alloys and plastic materials) (Ciampi et al., 2002 [7]). In particular, the Suspended Tray Panels model of the Alucobond company was analysed. This system consists of a U-shaped steel substructure (Figure 6.1) fixed to the wall face, with a distance between centres of 1.20 from the wall face. It also envisages applying a layer of insulation on the masonry with a variable thickness that depends on the whole system's temperature-hygrometric characteristics. A further upright is inserted into the upright intrados to act as a bracket, with a U-shaped section (65/55/2.5), fixed through stainless steel bolts with a diameter of 10mm (M10). The panel is 1.20 m long by 1.20 m high, with a thickness varying from a minimum of 4 to a maximum of 6 mm and is attached to the steel bolts. Although the panel is made with the interposition of mineral insulation, for the analyses carried out it has been assumed to consider the solid aluminium panel.

The geometric model considered is the single aluminium panel alloy EN-AW 5005 (Figure 6.2), whose mechanical characteristics are shown in Table 6.1; also for this type of alloy, the mechanical behaviour has been described through the Ramberg-Osgood (5.7) model.

Table 6.1 Physical and mechanical properties of EN-AW 5005 alloy

Density	2400 [kg/m3]
Elastic Modulus	70000 [MPa]
Tensile Strength	130 [MPa]
Coefficient of thermal expansion	2.4 e-6 [1/K]
Poisson's ratio	0.23

The first study concerned the static mechanical analysis (5.4) of the panel, which in this analysis was also considered as a half section (Figure 6.3), in order to evaluate the stress derived from the application of pressure alone (5.47), applied to the external face of the façade (Figure 6.4), which again is expressed by a linear function with a maximum value of 8kPa.

Since the model considered is half, a symmetry condition (5.48) has been set with respect to the two directions (Figures 6.5).

Finally, the steel bolt hole was considered as a fixed constraint (5.48).

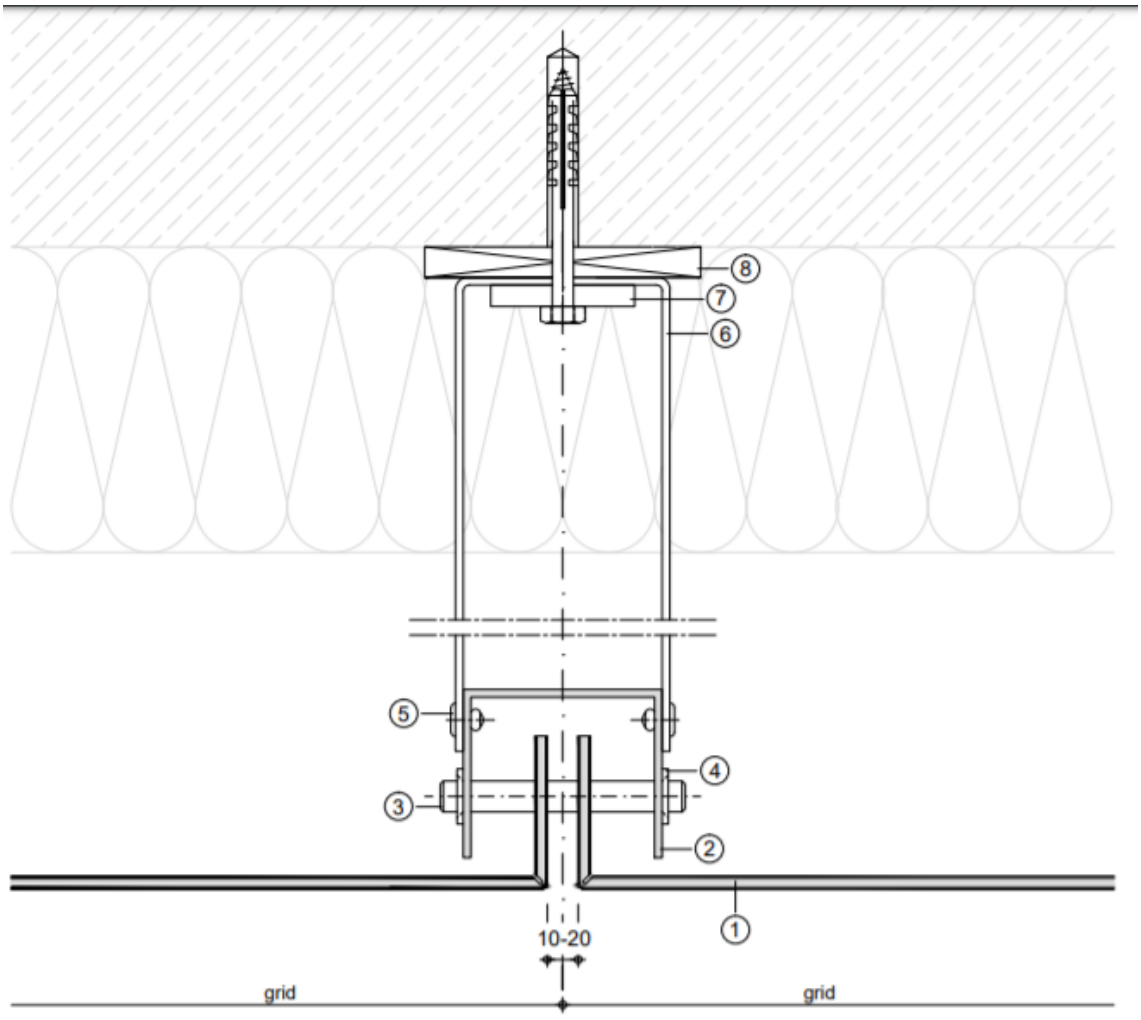

① ALUCOBOND
② U-Section 65/55/2,5
③ Stainless steel bolt, 10 mm dia.
④ STARLOCK quick fastener
⑤ Aluminium-blind rivet
⑥ Wall bracket
⑦ Extruded Al-liner
⑧ Plastic board (thermal separation)

Fig. 6.1 Façade construction detail

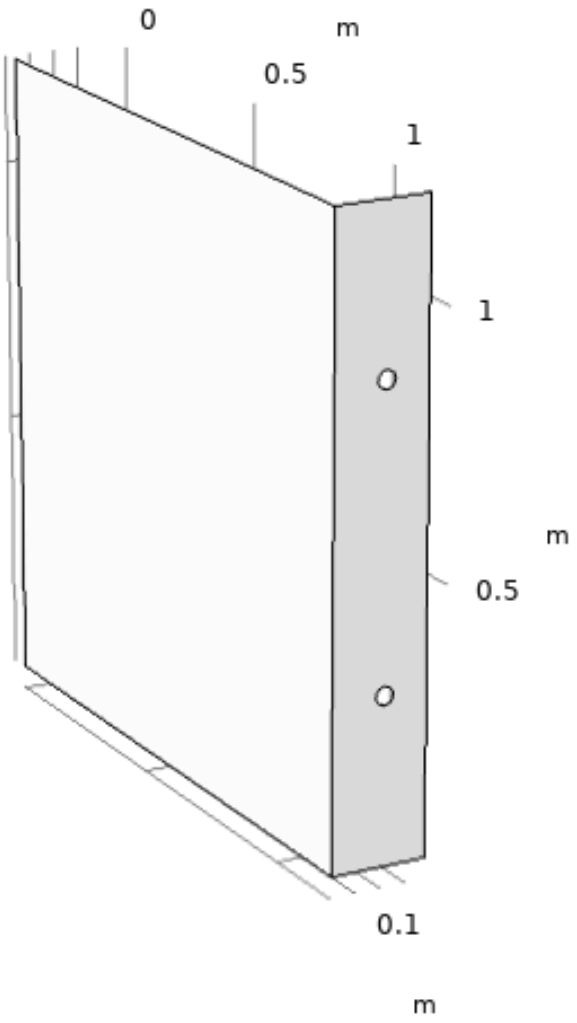

Fig. 6.2 3D model of the panel

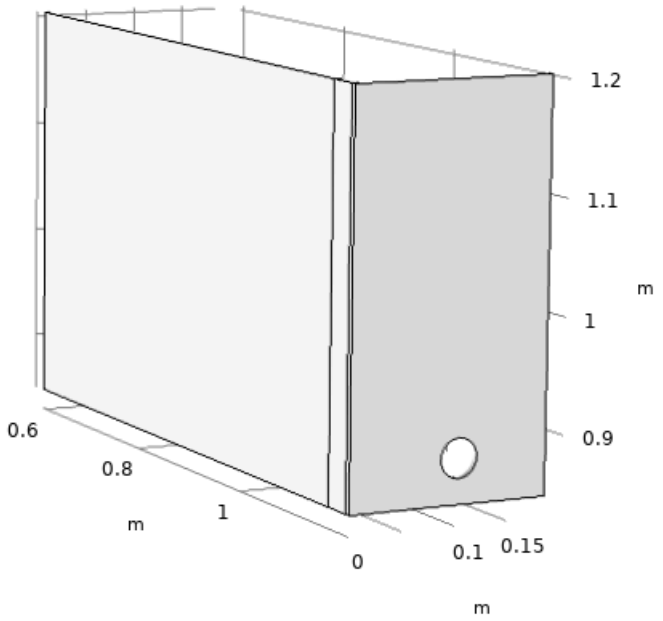

Fig. 6.3 Half section of the panel

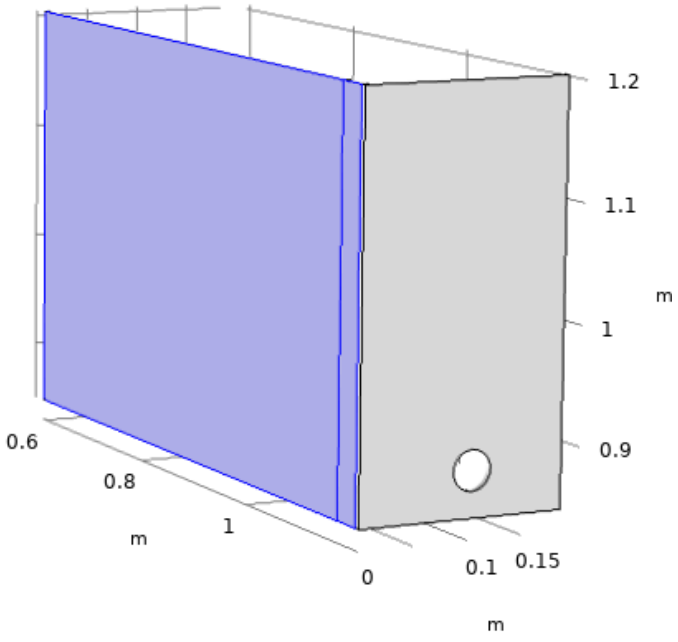

Fig. 6.4 Surface of application of mechanical and thermal loads

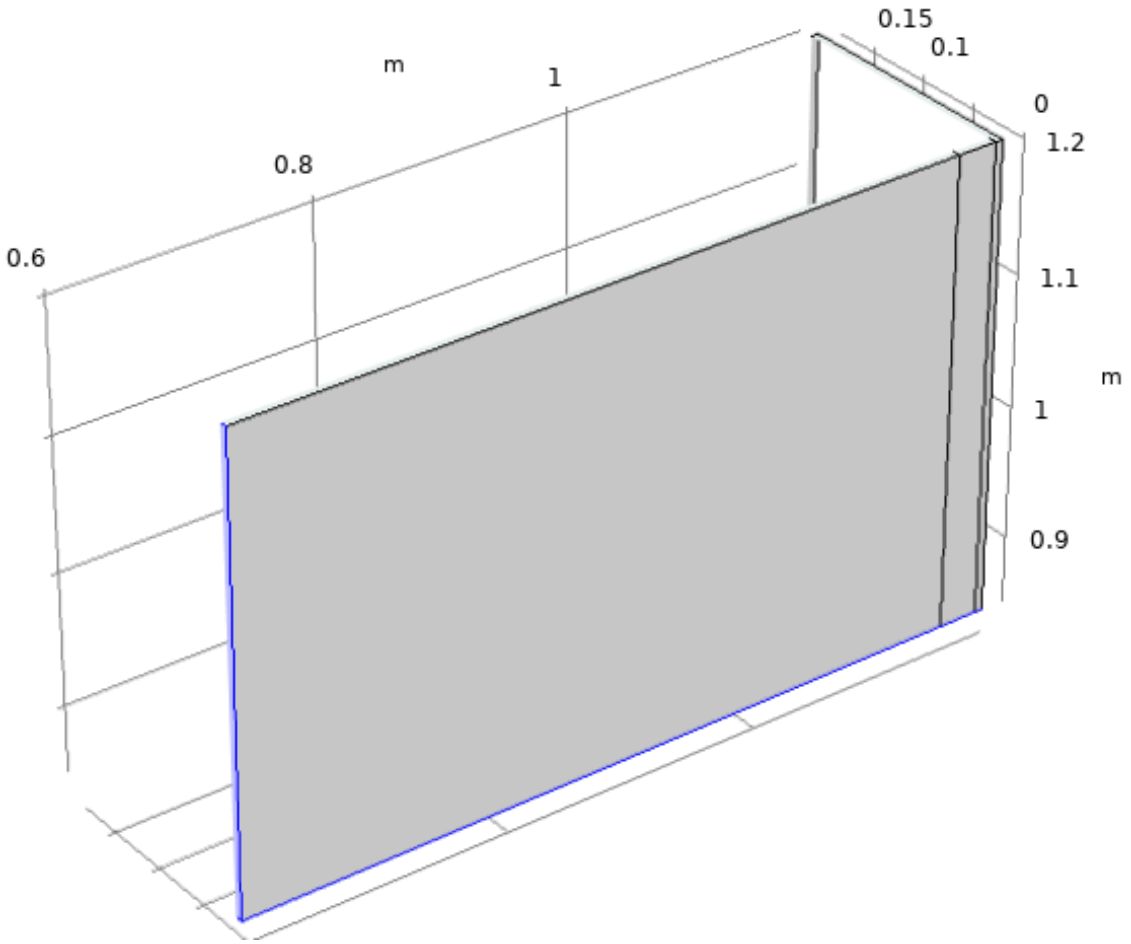

Fig. 6.5 Symmetry surfaces

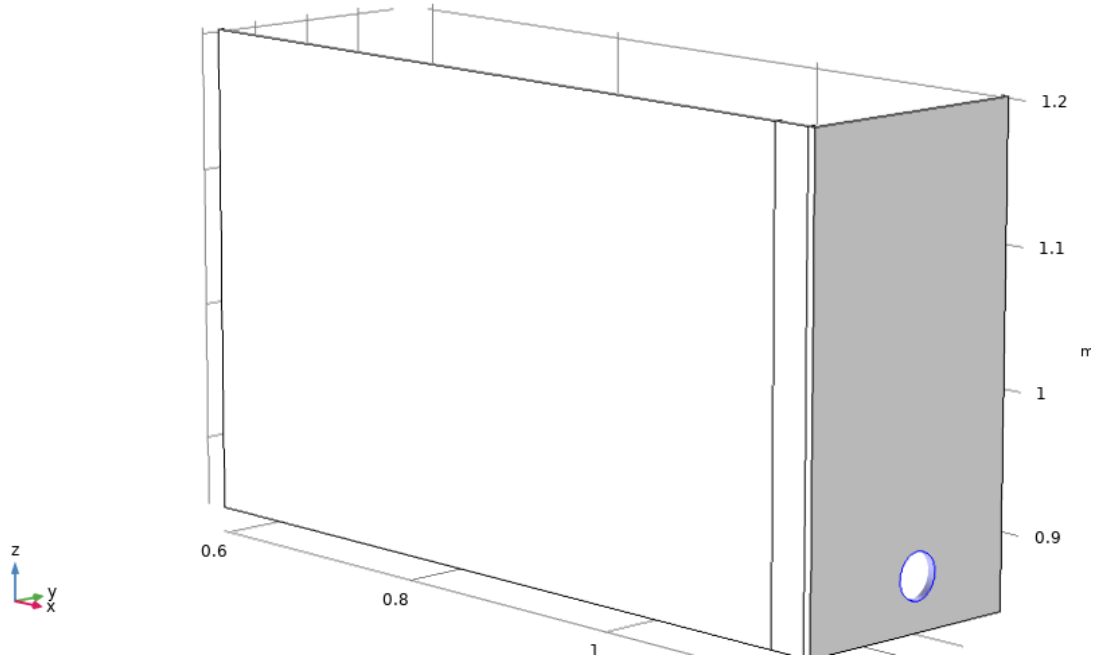

Fig. 6.6 Fixed constraint

The result highlights that the panel is able to withstand the assumed pressures, in fact a tension of 92 MPa is recorded for a pressure of 8 kPa (Figure 6.7).

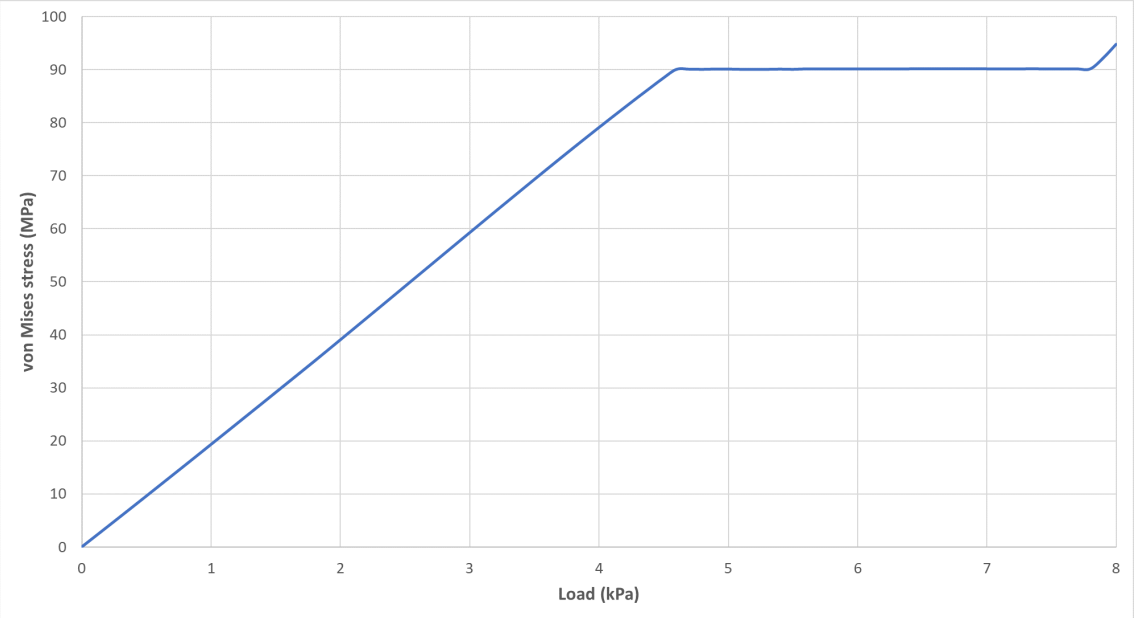

Fig. 6.7 von Mises stress of the panel due to the pressure

The curtain wall model was also analysed in the thermal field utilising the time-dependent study (5.21) to assess the stress due to temperature (5.46). The results show that the panel reaches a maximum tension of 80 MPa and is therefore still intact since the breaking tension is 130 MPa (Figure 6.8). Subsequently, the study's solution in the thermal field was used as a starting point for the mechanical analysis, to assess the panel's capacity, which has already undergone thermal stress, to resist the flow's pressures. Therefore, the panel is subjected to an increasing pressure up to the maximum value of 8 kPa (5.22). The results show that the panel, despite the stress due to temperature application, can resist the maximum pressure of 8 kPa reaching a tension of 100 MPa (Figure 6.9. Therefore, from the information of these combined analyses, it is possible to state that the panel considered, which is already a well-established solution on the market for the building's requalification, can also perform the dual task of protecting the structure of the building from PDCs.

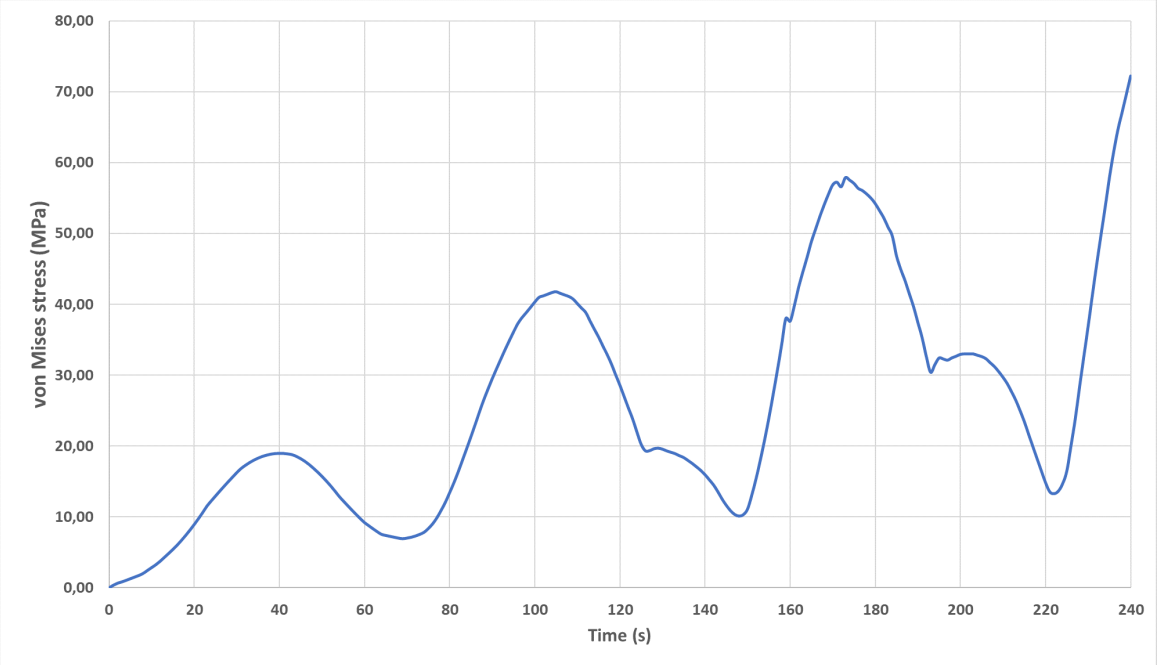

Fig. 6.8 von Mises stress of the panel owing to the temperature expressed by the interpolation function (5.46)

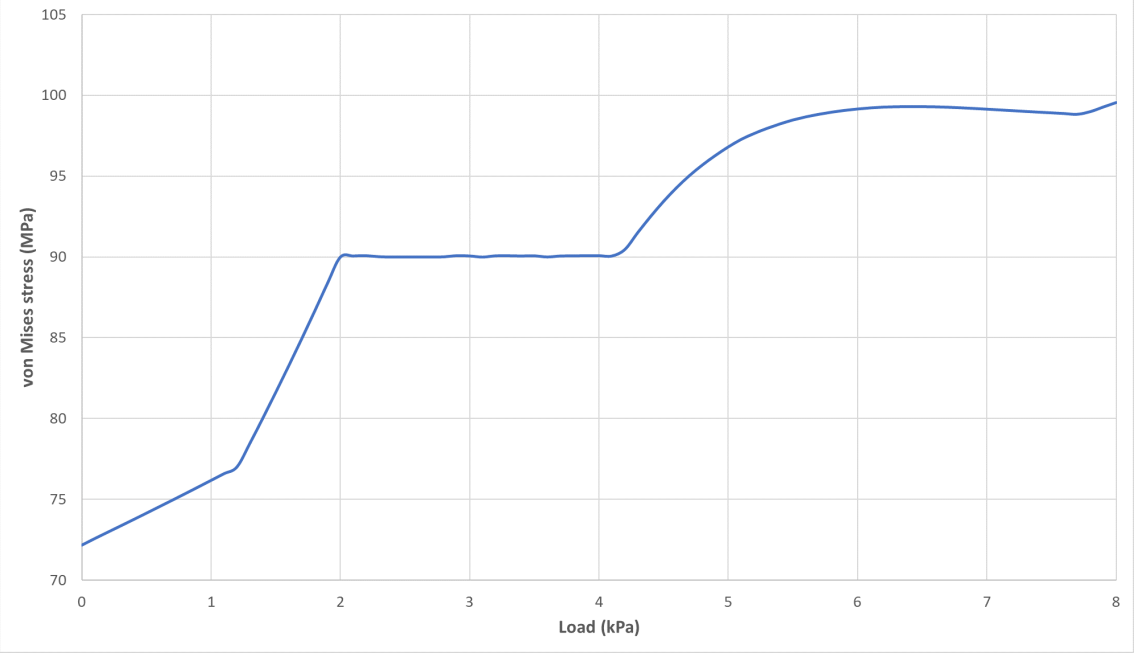

Fig. 6.9 von Mises stress of the panel applying both pressure and temperature

Finally, in order to assess whether the element in question can obtain state funding as an element of energy requalification, it is necessary to determine the thermal transmittance of the façade package and check that it is lower than the limit imposed by the law decree 06/08/2020, which sets a limit value of 0.30 for the province of Naples, which belongs to climate zone C 0.30 $\frac{W}{m^{2K}}$. Thermal transmittance (denoted by U) is a physical quantity that indicates the thermal power that passes through the building envelope per unit of dispersing surface and per unit of temperature difference between inside and outside. Thermal transmittance U is measured in $\frac{W}{m^{2K}}$ and is, therefore, a value that indicates the capacity of a square metre of building envelope element to disperse heat at a temperature difference of 1 K between inside and outside. Two methodologies defined in UNI EN ISO 10077-1:2018 can be used for the determination. The first method consists of applying equation (6.1); in particular, the thermal transmittance is the inverse of each layer's thermal resistance that makes up the structure of the ventilated façade

$$U = \frac{1}{R_{int} + \sum R_i + R_{est}} \tag{6.1}$$

The thermal resistance (Ri) of each layer can be calculated using the following formula:

$$R_i = \frac{s_i}{\lambda_i} \tag{6.2}$$

the formula relates the thermal conductivity of the material (λ_i) and the thickness (s_i), which are defined in Table (6.2)

Table 6.2 Thermal and geometrical characteristics of the different layer of the ventilated façade

Material	Thermal Conductivity [W/mk]	Thickness [m]	Density [Kg/m^3]	Specific Heat [kJ/kgK]
Aluminium sheet	1.13	0.006	2690	950
Air cavity		0.1	1	
Rock wool insulation	0.035	0.15	70	0.67
Hollow brick	0.41	0.30	800	0.84
Interior plaster	0.700	0.01 m	1400	1.01

Furthermore, in the transmittance formula the Rint and Rest represent the resistance of internal and external environment, which are 0.13 $\frac{W}{m^2K}$ and 0.04 $\frac{W}{m^2K}$, respectively. While the second methodology involves the use of calculation programs, in this case, the Grasshopper programming environment and the LadyBug and Honeybee plugins were used (Figure 6.10). From both calculation methods, it is established that the package's transmittance considered is 0.19 $\frac{W}{m^2K}$, which is lower than the imposed limit, and therefore the solution represents a good solution for the energy improvement of the building and to obtain the state funding foreseen for the construction.

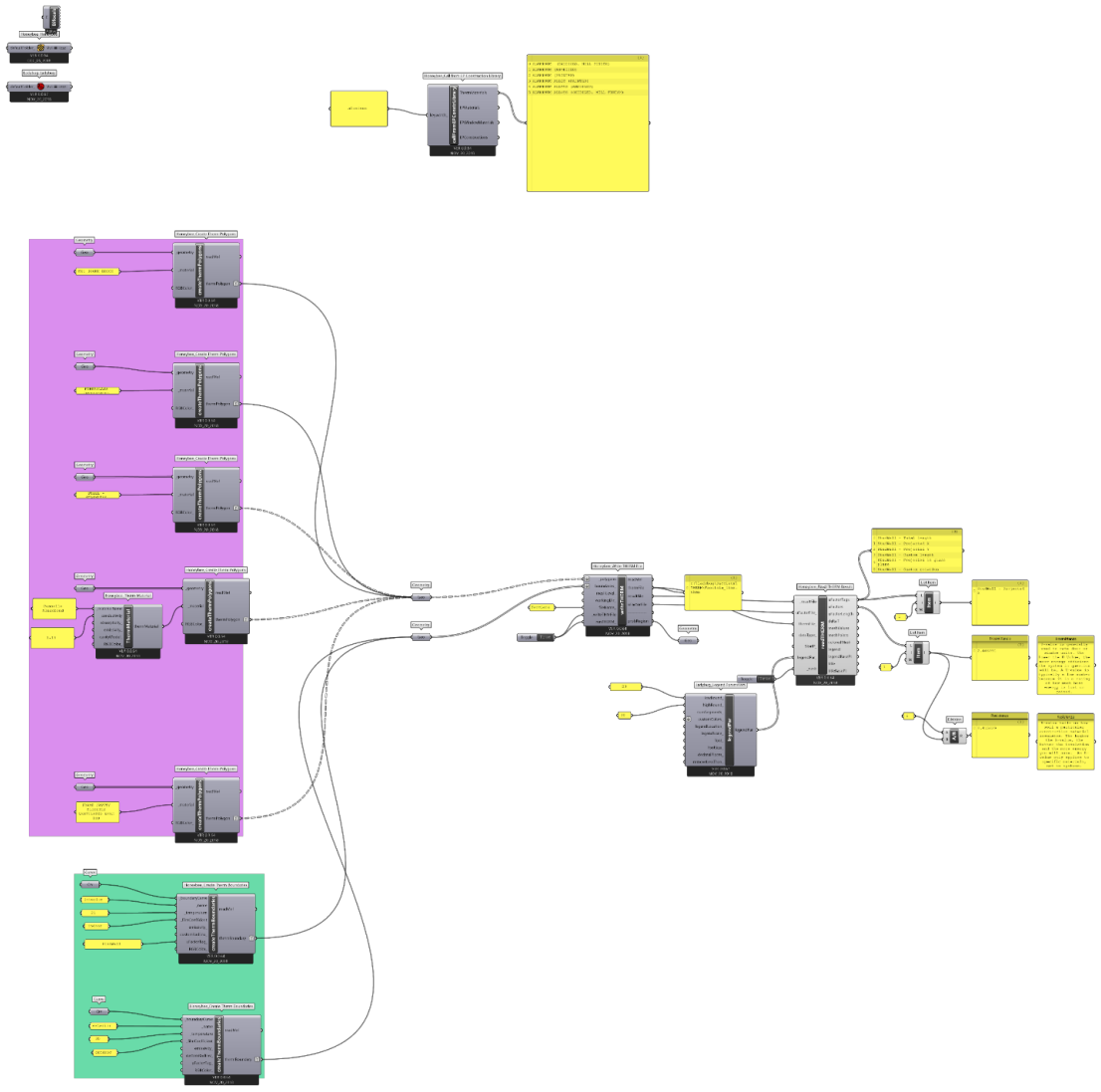

Fig. 6.10 Grasshopper scripts for thermal analysis

6.2 Openings

The mechanical analysis showed that the element most vulnerable to pressure alone, without considering temperature, is glass, regardless of the three thicknesses considered. Therefore, to make the glass resistant to the pressures foreseen in the Civil Protection reference scenarios, laminated glass technology was studied. Laminated glass for architectural glazing applications consists of two layers of glass bonded to a thin thermoplastic interlayer. The interlayer is responsible for keeping the glass fragments together after breaking, while increasing the residual strength of the material. There are different types of interlayer depending on the material used, the most used is Polyvinyl butyral (PVB) even though it has low mechanical qualities. Currently a new type of interlayer produced by Dupont® is also used, the Sentry Glass Plus (SGP) which, unlike the previous one, presents a resistance relatively high. This hypothesis of mitigation is not suitable for the pyroclastic flow, since these interlayers are thermoplastic, and their behaviour depends on the temperature of exposure. Indeed, above the 80°C the PVB film starts to separate from the glass (delamination); besides, the SGP structural interlayer is also characterized by a melting temperature of 94°C. Therefore, the proposed new mitigation strategy is the complete replacement of the glass with toughened glass. This type of safety glass is treated with controlled thermal or chemical processes to increase its resistance compared to normal glass; in fact, it has a higher resistance of between 180 and 200 MPa compared to 90 MPa for simple glass. The maximum working temperature of tempered glass was calculated to verify its application in the study areas and avoid breakage due to thermal shock. Therefore, considering the relative characteristics of the glass (Table 6.3) and using equation (5.43) the maximum temperature is 355 °C; therefore, this option could be suitable for urban settlements present at distances very far from the vent, e.g. in the Vesuvius area, where the foreseen temperatures are below the calculated limit.

Table 6.3 Physical and mechanical properties of Tempered Glass

Density	2400 [kg/m3]
Elastic Modulus	70000 [MPa]
Tensile Strength	180¸200 [MPa]
Coefficient of thermal expansion	9 e-6 [1/K]
Poisson's ratio	0.23
Thermal conductivity	1.1 [W/m2K]

While to resolve the polyamide issue, it has been hypothesized to apply the wood-aluminium frame technology in reverse. In fact, it has been placed on the external front of the fixed and mobile frame of the pinewood sections with a thickness of 2 cm with the function of shielding (Figure 6.12).

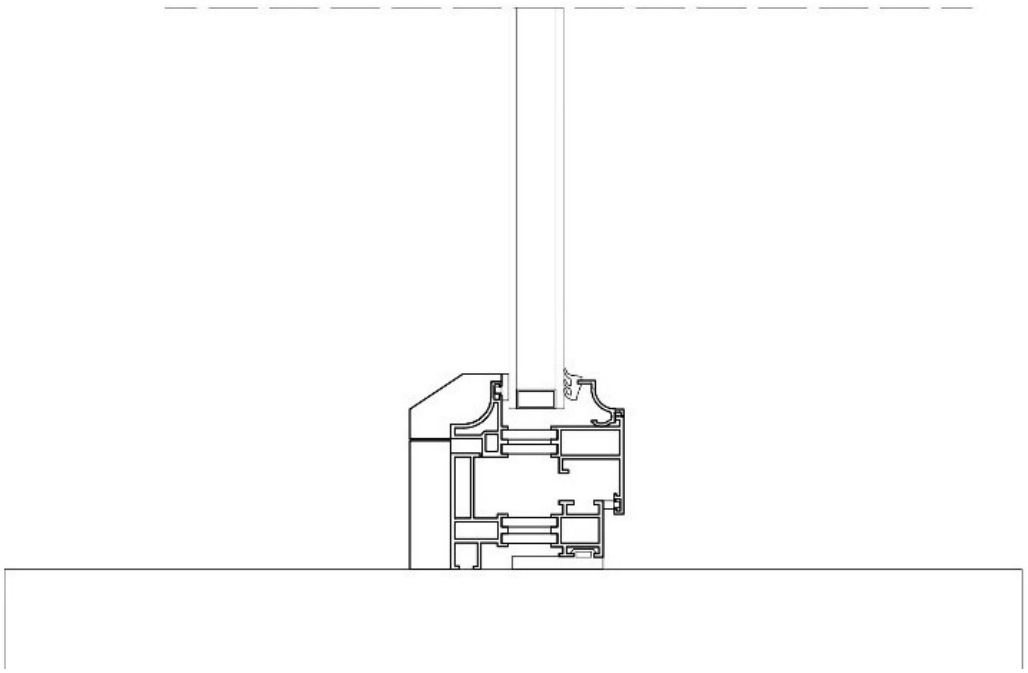

Fig. 6.11 Geometrical model of the proposed wood-aluminium window

This type of frame, considering tempered glass in the three different thicknesses, was analysed in the thermal field through a time-dependent study (5.21), in which the temperature, applied to the external face of the frame, is expressed by the function (5.46) which in the time interval of 240 seconds reaches the maximum temperature of 400°C. Thermal analysis shows that the polyamide is totally protected as the maximum temperature recorded is 25°C (Figure 6.12), so the aluminium sections' continuity is preserved. In contrast, EPDM is preserved for about 160 seconds before reaching its critical temperature (Figure 6.13). A possible solution could be the overlapping of an intumescent material which would perform a protective function for this material, which, following the increase in internal temperature, tend to increase their volume and therefore have a retarding effect on heat transmission.

Moreover, to a better model, the effects of the flow on the opening and better assess the tempered glass's vulnerability, a model combining both pressure and temperature effects were built. The geometric model considered is that of a large frame with 4mm toughened glass. The first study was carried out to assess both the stress (5.22) generated by the temperature and whether the glass has reached its critical temperature of 355°C, considering the temperature expressed by the function (5.46) applied to the external face of the frame. From the results of this first analysis, it should be noted that the tempered glass, at the end of the application (240 seconds) of the thermal stress, reaches a maximum temperature of 300°C (Figure 6.14) and therefore it is possible to state that the glass does

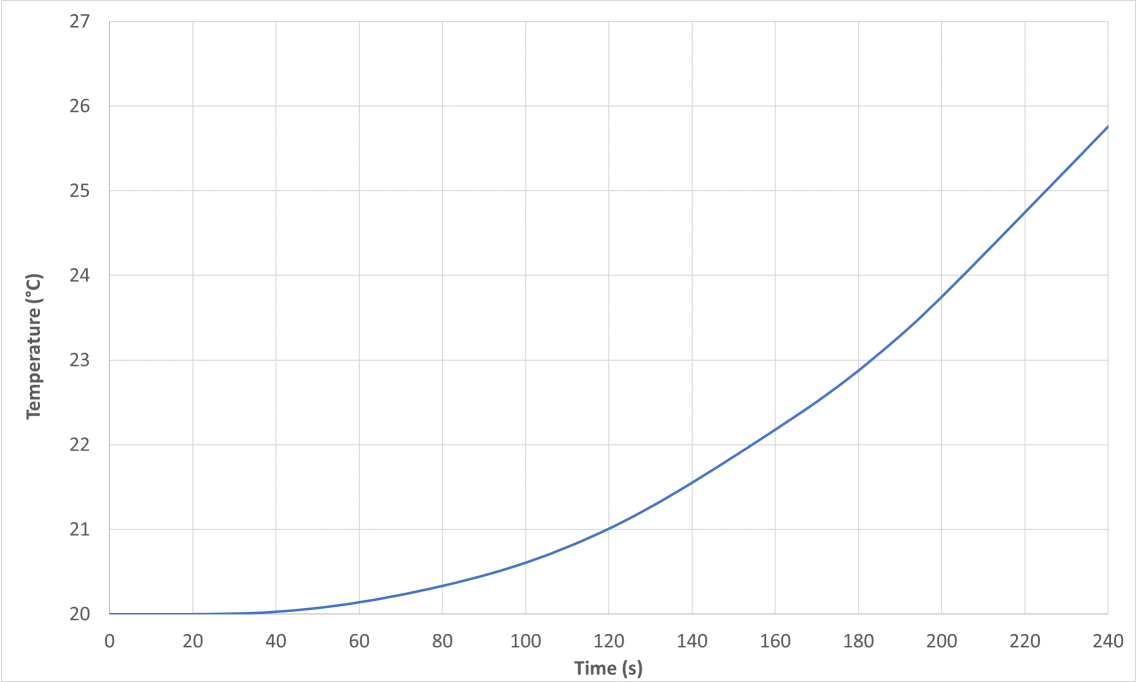

Fig. 6.12 Reached temperature by polyamide

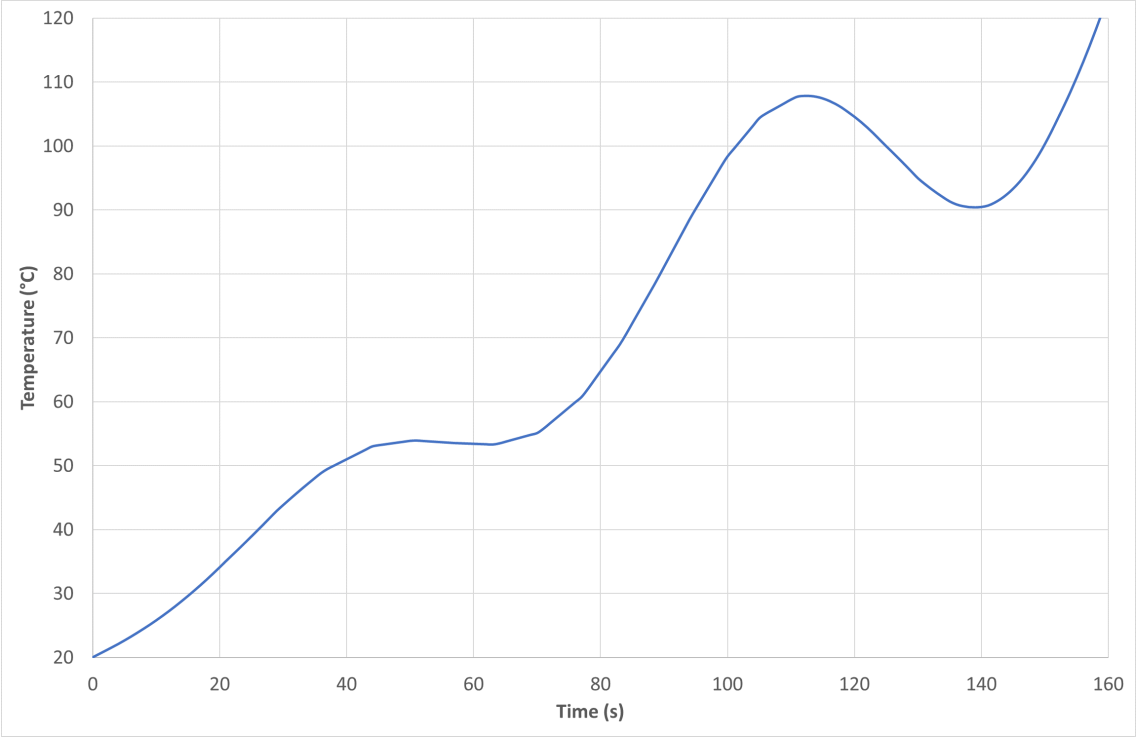

Fig. 6.13 Reached temperature by EPDM

not break due to thermal shock. The stress generated in the transparent element is 120 MPa (Figure 6.15); it was possible to evaluate the resistance to the pressures exerted.

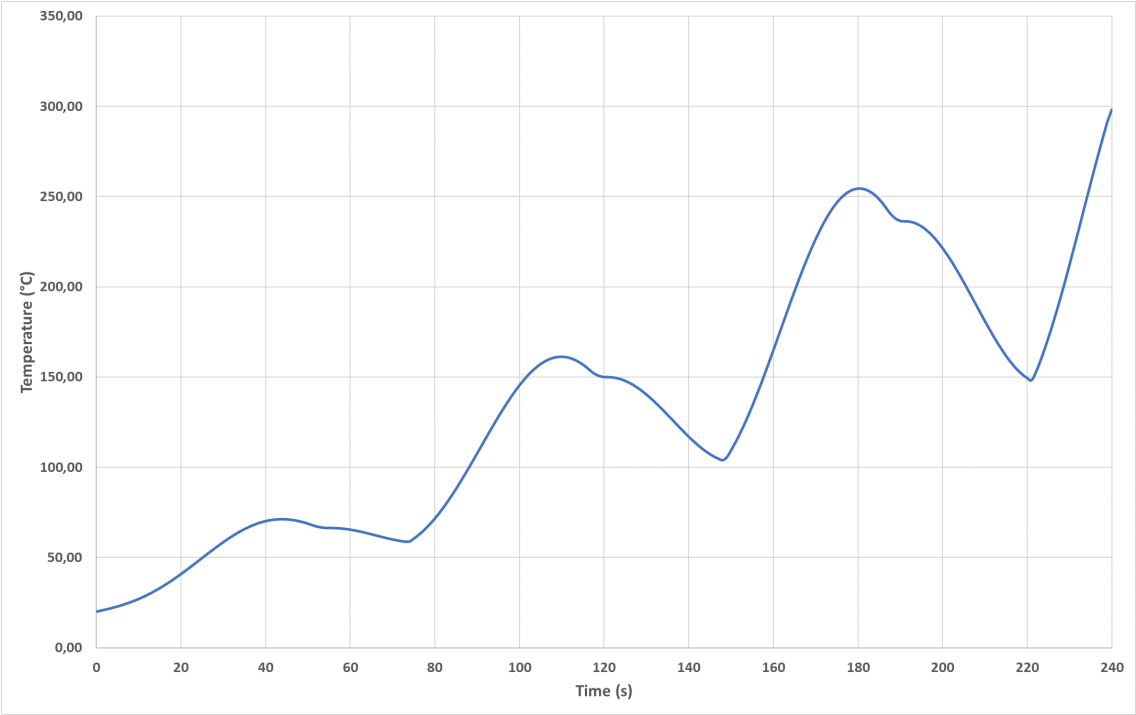

Fig. 6.14 Reached temperature by tempered glass

Starting from the thermal analysis solution, therefore with the heated window, we proceeded with applying the load (5.47) and evaluated the breaking tension reached by the glass. Again we assumed the window failed when the glass reached the breaking tension; therefore, we used a Stop Function, setting an if condition for the glass:

comp1.StressMax > 180[MPa]

The analysis shows that the 4 mm toughened glass reaches its breaking stress by applying a pressure of 5.5 kPa (Figure 6.16).

Finally, the last consideration is thermo-hygrometric to assess whether the prototype window can be included in the energy requalification works and obtain the state funding established by the ministerial decree 06/08/2020. This decree establishes, for climate zone C, a limit value of unitary transmittance UW of 2.1 $\frac{W}{m^2K}$. The following equation (6.3) was used to calculate the proposed window frame:

$$U_w = \frac{A_g * U_g + A_f * U_f + I_g * \psi_g}{A_g + A_f} \tag{6.3}$$

where:

- A_g is the area of the glass [m2],

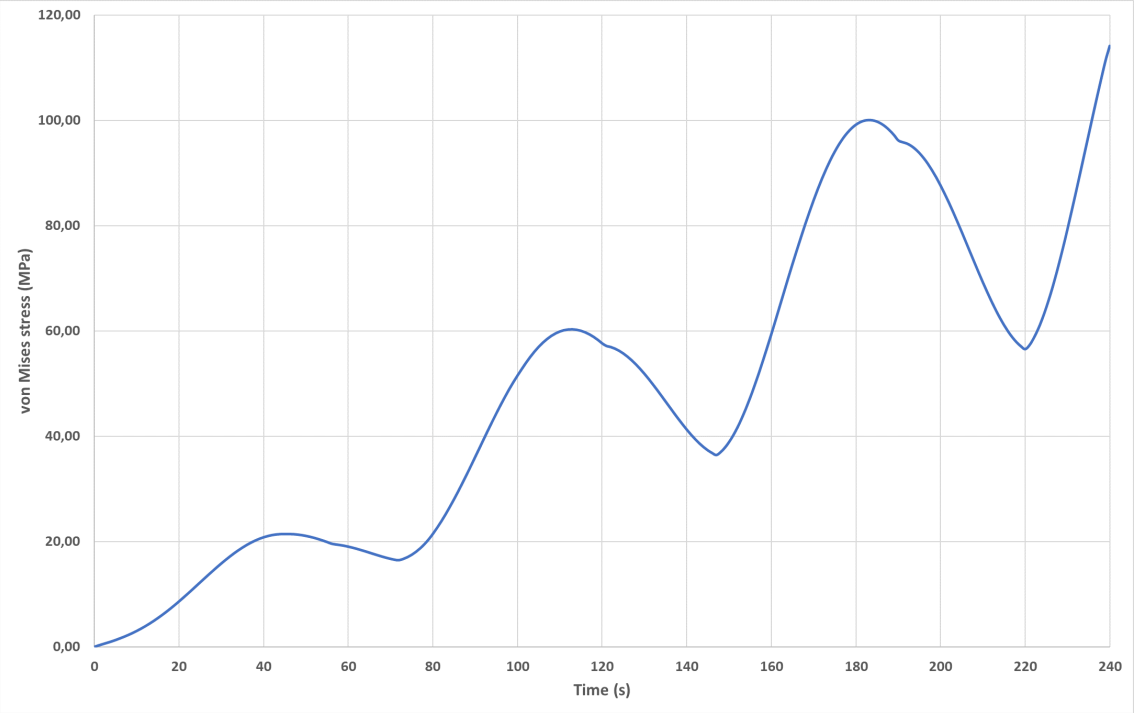

Fig. 6.15 von Mises stress of the tempered glass

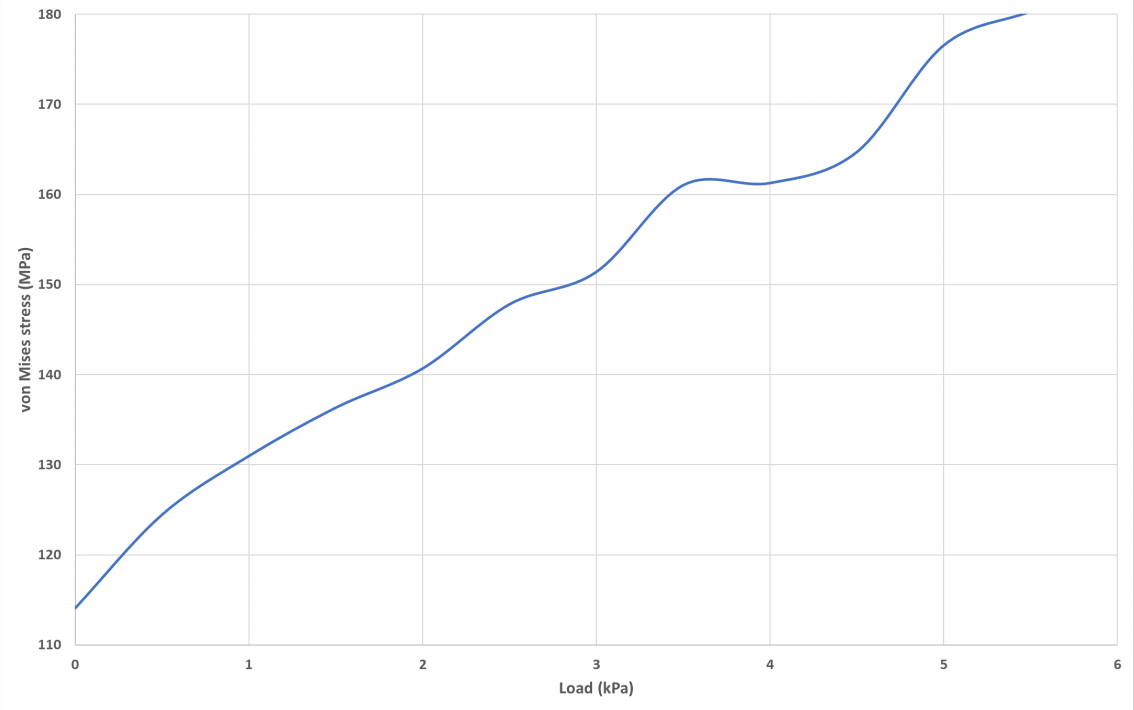

Fig. 6.16 von Mises stress of the tempered glass after the combined actions

- U_g is the thermal conductivity of glass [W/m2K],
- A_f is the are of the frame [m2],
- U_g is the thermal conductivity of frame [W/m2K],
- I_g is the perimeter of glass [m]
- ψ_g is the linear thermal transmittance due to combined thermal effects of glazing, spacer and frame.

The following equation was applied to calculate the thermal transmittance of the glass (U_g):

$$U_g = \frac{1}{R_{int} + \sum R_i + R_{est}} \tag{6.4}$$

Assuming double-glazing as the glass (4/6/4), the gas in the cavity must also be taken into account in the calculation of resistance; in this analysis, an air cavity of 6 mm has been assumed, with thermal conductivity (λ) of $2.58 \cdot 10^{-2}$ $\frac{W}{m^2K}$. Therefore, the thermal transmittance value of the insulating glass unit alone is 2.45 $\frac{W}{m^2K}$. Furthermore, in this type of analysis, it was not possible to consider the protective wooden layer, so the thermal transmittance of the frame (U_f) was set at 2.2 $\frac{W}{m^2K}$. Furthermore, the linear thermal transmittance value due to combined thermal effects is equal to 0.06 as defined in the prospectus E.2 of the ISO 10077-2 standard, since a thermal break aluminium frame with double glazing without surface treatments is considered. Finally, to determine the surface of the various components and the glass perimeter, a single window of 60 cm width and 130 cm height has been considered (Figure 6.17). From the following premises and the calculations made, the window frame's linear thermal transmittance value is 2.2 $\frac{W}{m^2K}$; therefore, it would not be suitable for thermal upgrading. This problem can be solved by increasing the thickness of the cavity, indeed if the air thickness is 9 mm, the transmittance of the U_W glass will be 1.93 $\frac{W}{m^2K}$ and the transmittance of the whole window will be 2.08 $\frac{W}{m^2K}$.

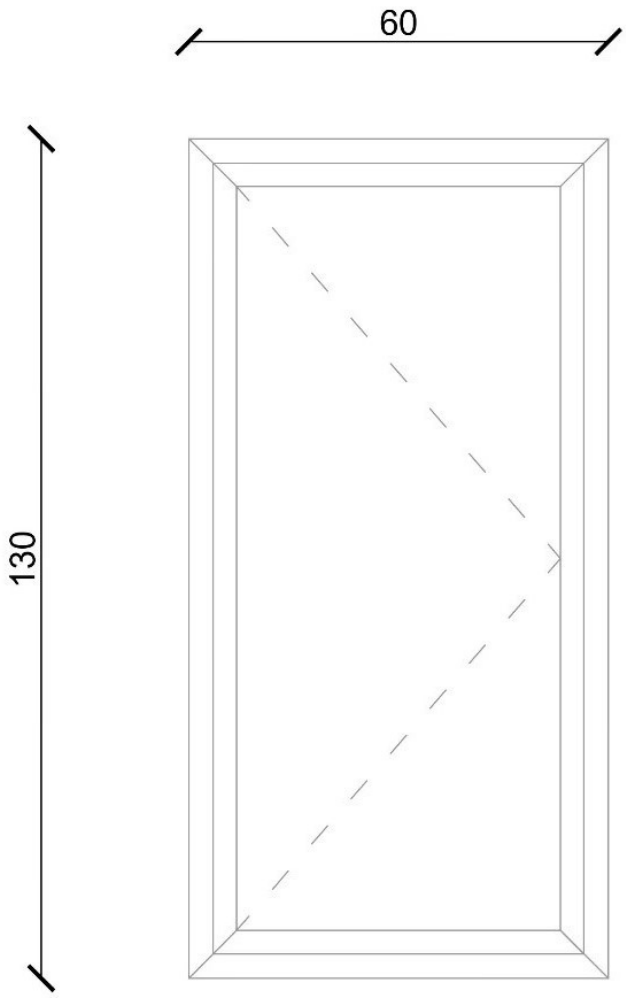

Fig. 6.17 Example of a window frame used for thermohygrometric calculation

6.3 Shutters

Although the aluminium and steel shutters are suitable for resisting the thermal and mechanical stresses exerted by the flow, fluid dynamic analyses showed that the shutters' common model could not perform a protective function, as it allows the flow to penetrate and cause damage to the existing frame. Therefore, it is necessary to replace these elements with a solid panel to avoid fluid infiltration and resist thermal and mechanical stress. In particular, a multilayer aluminium-wood panel has been hypothesised. The hypothesised model has dimensions of 1.30 x 0.60 m, i.e. typical dimensions of a shutter leaf, with a thickness of the whole panel varying between 4 and 10 cm (Figure 6.18).

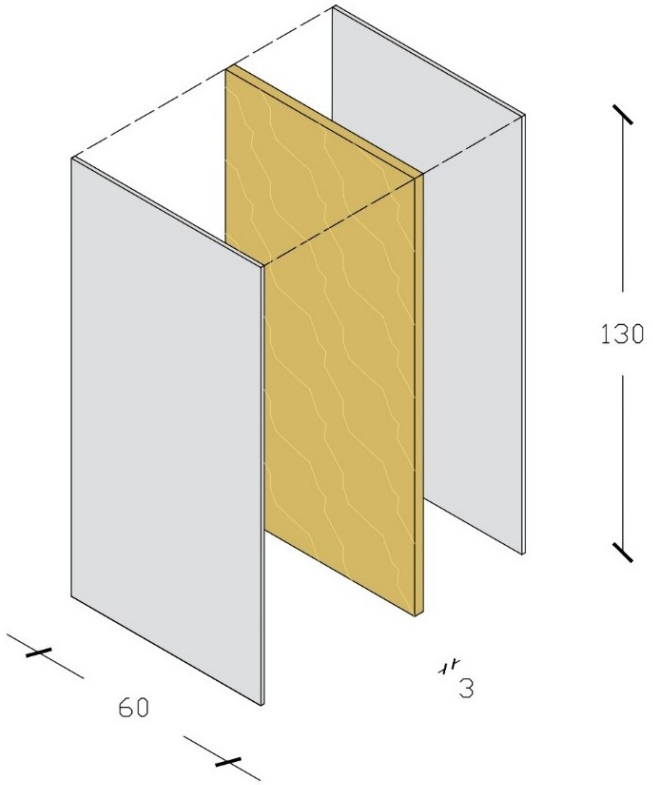

Fig. 6.18 Geometric model of shutter

This model was initially analysed to evaluate the stress caused by the temperature (5.19), defined by (5.46), which reaches a maximum temperature of 400°C in a time interval of 240 seconds. The results of the analysis show that the aluminium panel reaches the breaking tension (130 MPa) as the thickness increases, in fact for a thickness of 5 mm the maximum tension reached is 127 MPa, while for a thickness of 3 mm, the aluminium reaches the breaking tension after about 200 seconds (Figure 6.19). The insulating function

of the wood is greater as the thickness of the panel increases. A further consideration was made for the temperature reached by the external wood surface; in particular, Jenkins et al. (2014) [17] establish the lower boundary condition for wood ignition as around 280-300 °C, above which ignition is considered unlikely on any time scale, and the upper boundary is defined at around 350-400 °C, above which ignition is considered likely to occur within three minutes. Jenkins et al. (2014) [17] establish the lower boundary condition for wood ignition as around 280-300 °C, above which ignition is considered unlikely on any time scale, and the upper boundary is defined at around 350-400 °C, above which ignition is considered likely to occur within three minutes. Therefore, the boundary temperature for the wood panel's external surface was considered 350°C. For this type of panel assumed, it is stressed that the wood reaches the critical temperature towards the end of the phenomenon, i.e. after about 240 seconds, while the panel with the thicker foil does not reach the limit temperature of 350°C (Figure 6.20).

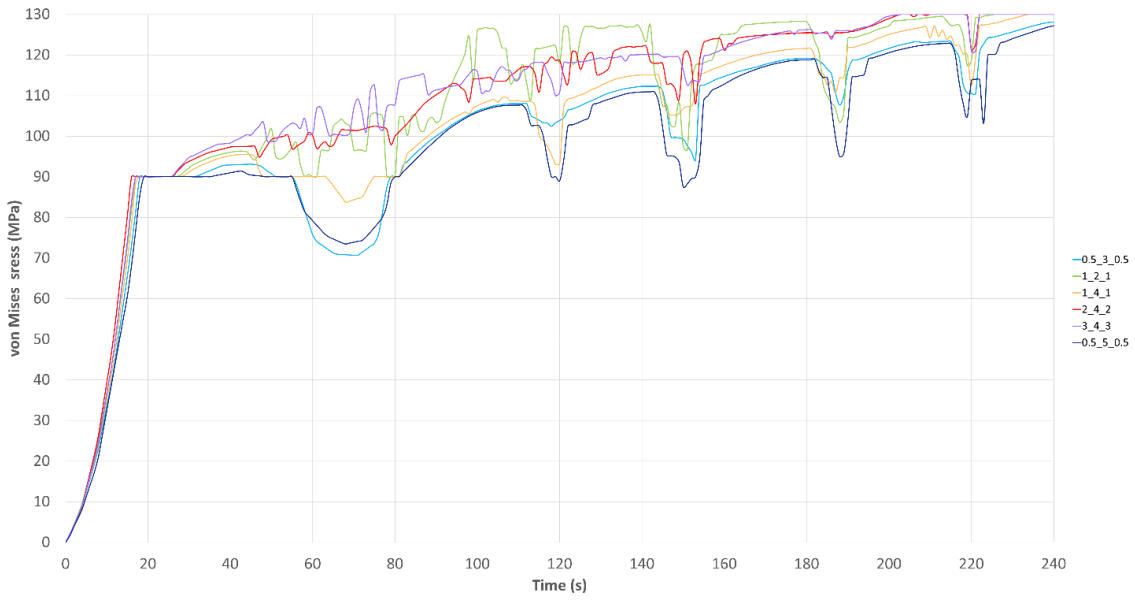

Fig. 6.19 von Mises stress of different configurations of panel

The right compromise would be a panel made from an aluminium panel with a minimum thickness and a wooden panel with a greater thickness from these analyses. As far as the aluminium panel is concerned, the minimum thickness that can be foreseen is 1 mm, since greater thicknesses are difficult to find and therefore the cost of constructing the panel would be very high. The hypothesised panel is a stratified panel consisting of a 3 cm pine wood core placed between two 1 mm thick sheets of EN-AW 5005A aluminium alloy, whose characteristics are shown in Table 6.4, so the panel has a total thickness of 4 cm.

This model was also evaluated to estimate the thermal stress in the time interval of 240 seconds by applying the function's temperature (5.46) to the external surface. The first

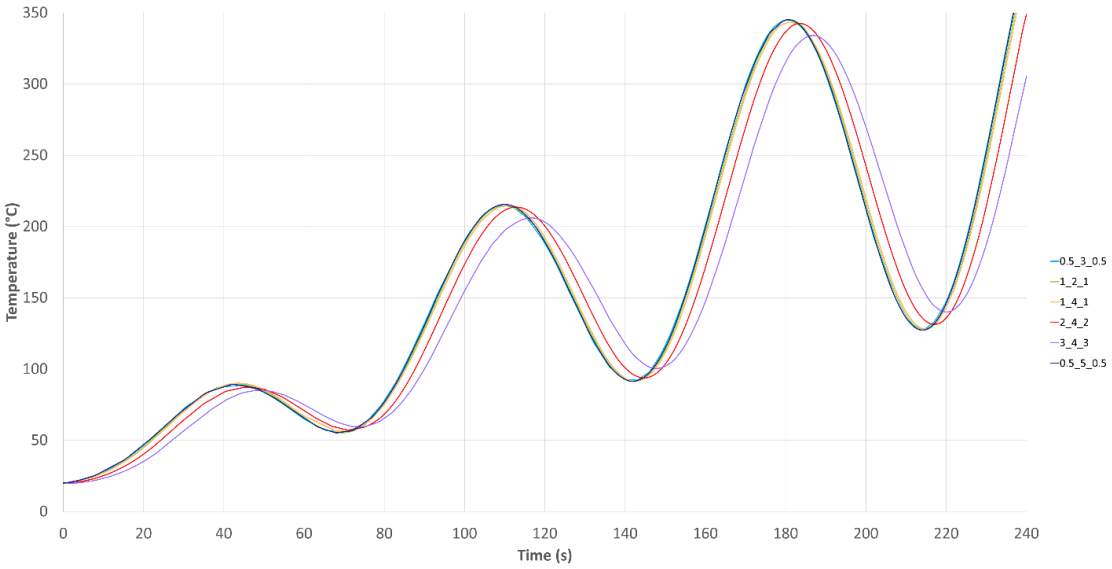

Fig. 6.20 Temperature reached by the wood panel of different configurations of panel

Table 6.4 Physical and mechanical properties of Aluminium EN-AW 5005A

Density	2700 [kg/m3]
Elastic Modulus	70000 [MPa]
Ultimate Tensile Strength	130 [MPa]
Poisson's ratio	0.33
Specific heat capacity	900 [J/kgK]
Thermal conductivity	238 [W/mK]
Thermal expansion	3,7 e-7 [1/K]

results highlight that the external aluminium sheet is resistant to temperature, reaching a maximum of 128 MPa (Figure 6.21). Although at the same time the external wooden surface reaches a temperature of 350 °C (Figure 6.22) and according to Jenkins et al. (2014) [17] when the wood reaches a temperature of 350 - 400 °C then it is possible to assume that the ignition probably takes place. However, in this case, it is possible to state that the probability of ignition is lower than that identified by Jenkins et al. (2009) [17] (Table 6.5) since the exposure time is minimal indeed the critical temperature on the external surface is reached at the end of the phenomenon.

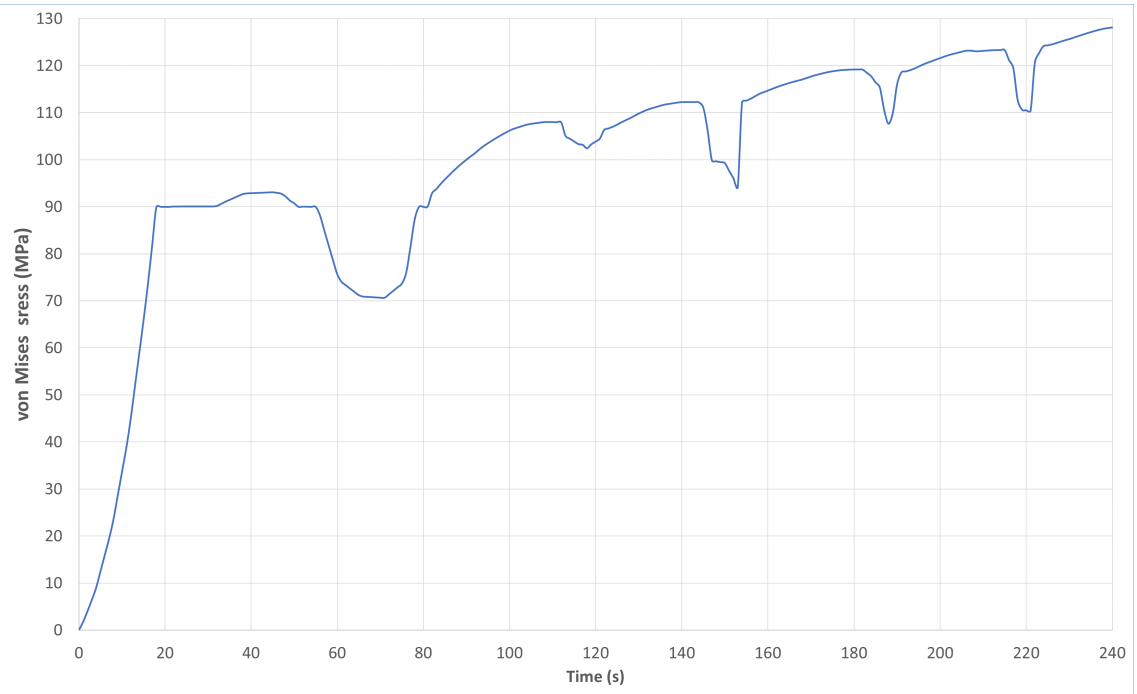

Fig. 6.21 von Mises stress of aluminium

Although the panel's exposure time at a temperature of 350 °C is shorter, to avoid possible ignition of the internal wooden panel, it has been assumed that fireproof rock wool panels will be placed in front. The new panel's stratigraphy includes a 1 mm thick aluminium panel on the outside, then 20 cm wide panels of solid pine with a thickness of 2 cm. Besides improving the hypothesized panel's mechanical characteristics, a series of wooden pillars (2x2 cm) with a 20 cm spacing were placed between the previously defined stratigraphy (Figure 6.23).

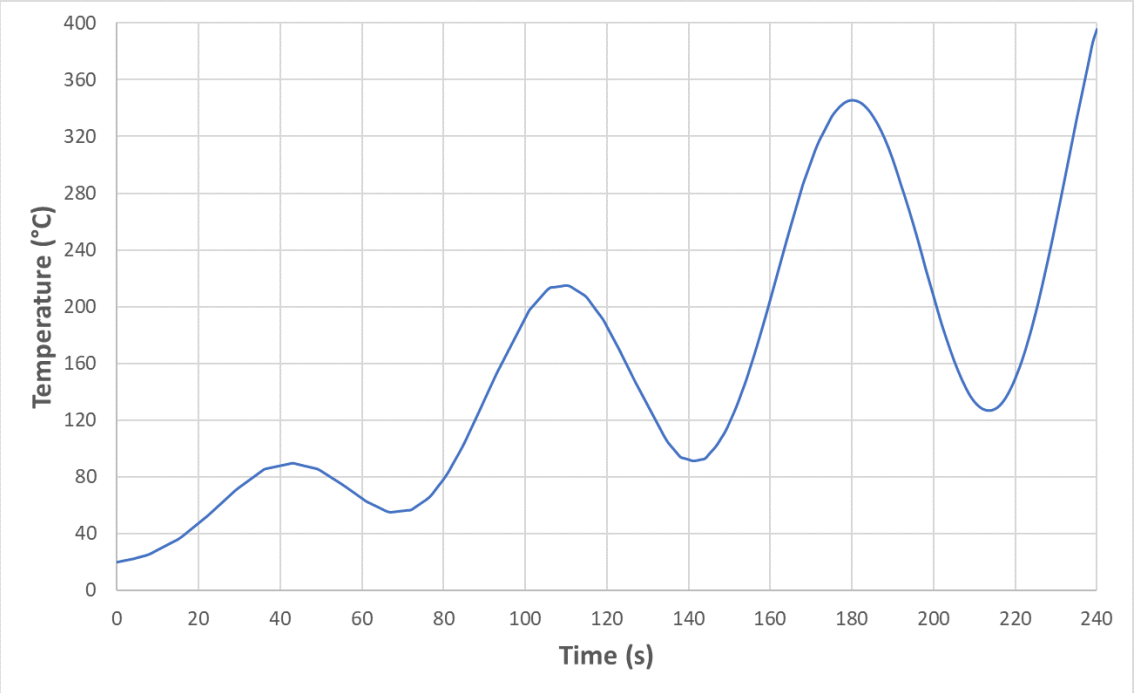

Fig. 6.22 Temperature reached by the external wood panel

Table 6.5 The incident heat flux for a range of PDC temperatures and the associated time to ignition for wood (Jenkins et al., 2009) [17].

PDC temperature (°C)	**Heat flux (kW/m^2)**	**Time to ignition of wood**	
		(seconds)	**(minutes)**
50	2,34	**No piloted ignition**	
150	10,4		
250	18,52	523,02	8,72
350	26,74	96,92	1,62
450	35,09	40,48	0,67
550	43,61	22,24	0,37
650	52,37	14,02	0,23
750	61,42	9,6	0,16
850	70,82	6,93	0,12

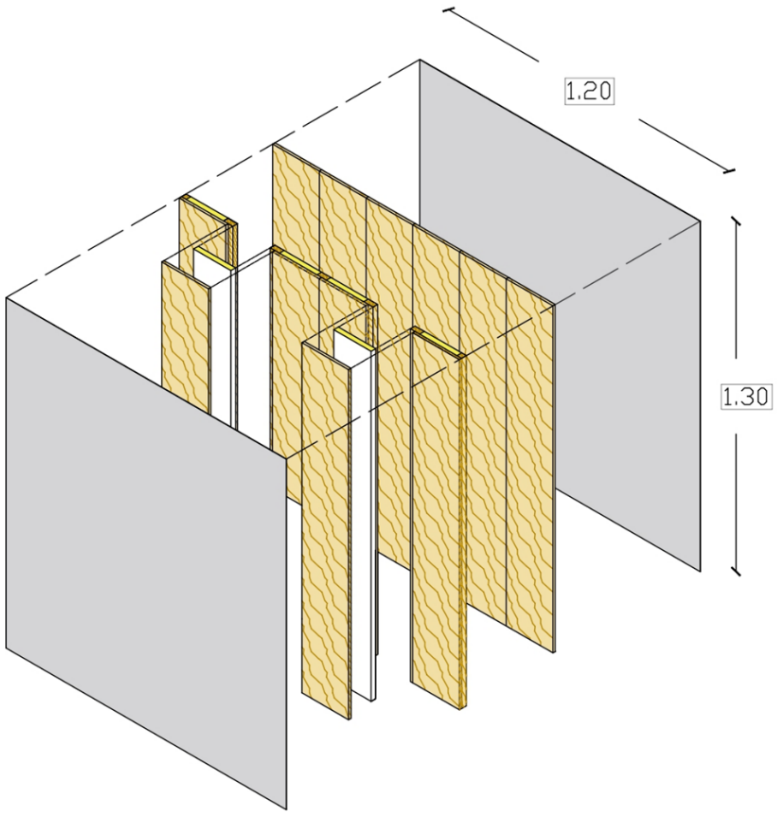

Fig. 6.23 Model of shutters

The final panel, with a total thickness of 6 cm, was first thermally analysed and then its stress due to the application of flow pressure was assessed. The geometric model studied was the portion of the panel between two wooden pillars and the analyses were carried out in the two-dimensional field (Figures 6.24), and half of the panel was considered by imposing the relevant symmetry conditions (5.48) (5.49) (Figures 6.25).

The panel was analysed considering the temperature function (5.46), which reaches three different maximum temperatures: 200, 300 and 400°C in the time interval of 240 seconds. The external aluminium panel does not reach the breaking stress in any of the three analyses considered (Figure 6.26).

Also, the maximum temperature recorded on the external surface of the wood panel has been assessed. It can be seen that the external wood panel reaches the critical temperature of 350°C at about 237 seconds for a maximum exposure time of 3 seconds (Figure 6.27). In this case, the exposure time is short, in any case, both the window frame and the last layers of the panel will be protected from the possible spread of fire by the fireproof rock wool insulation, also given the high melting point of 1000°C.

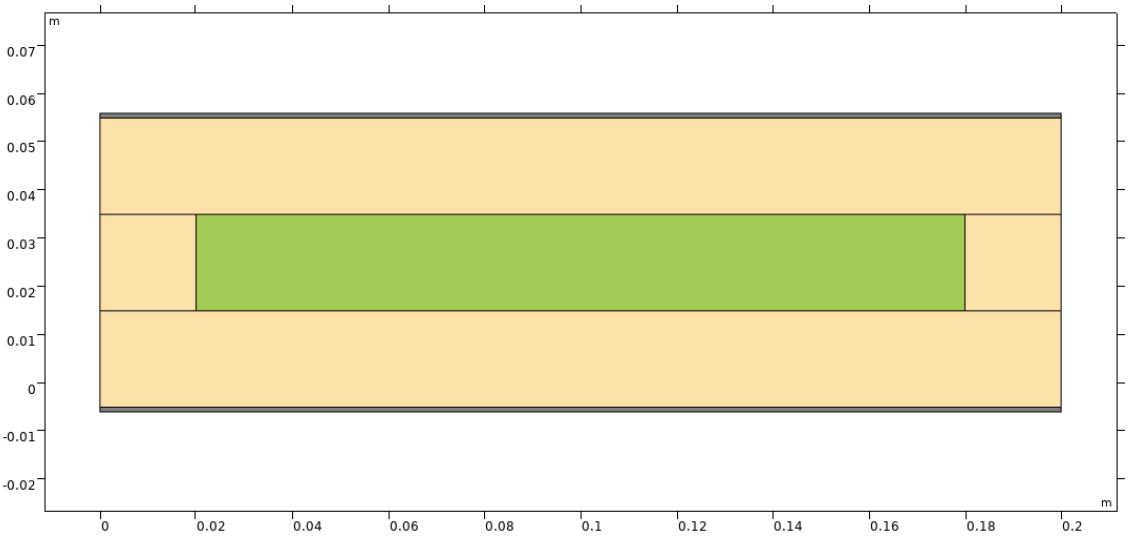

Fig. 6.24 2D Geometrical model of the proposed shutters

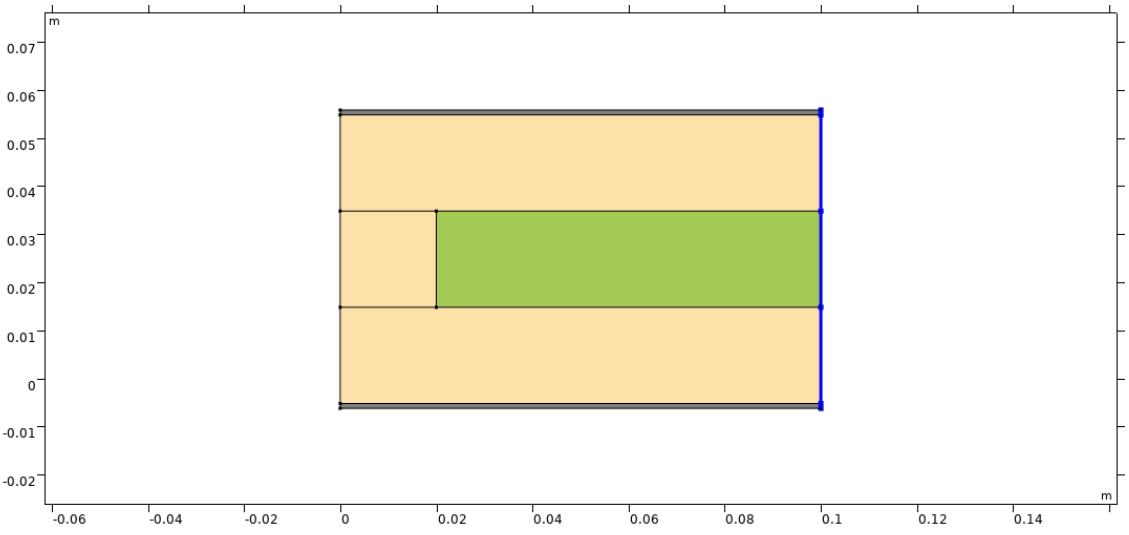

Fig. 6.25 Simmetry plane condition

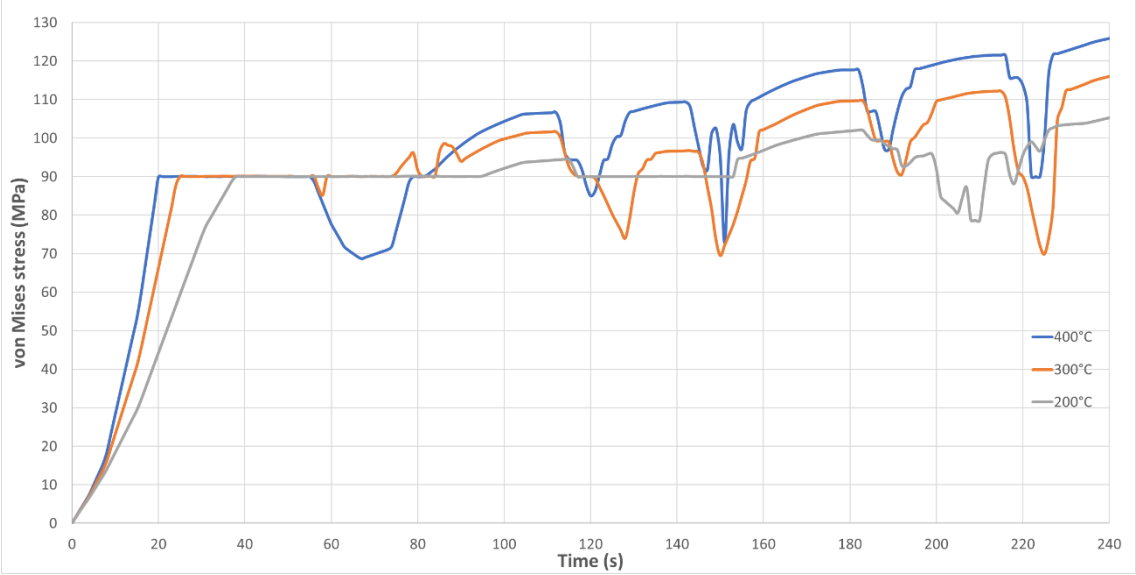

Fig. 6.26 von Mises stress of aluminium owing to the temperature considering different maximum temperature

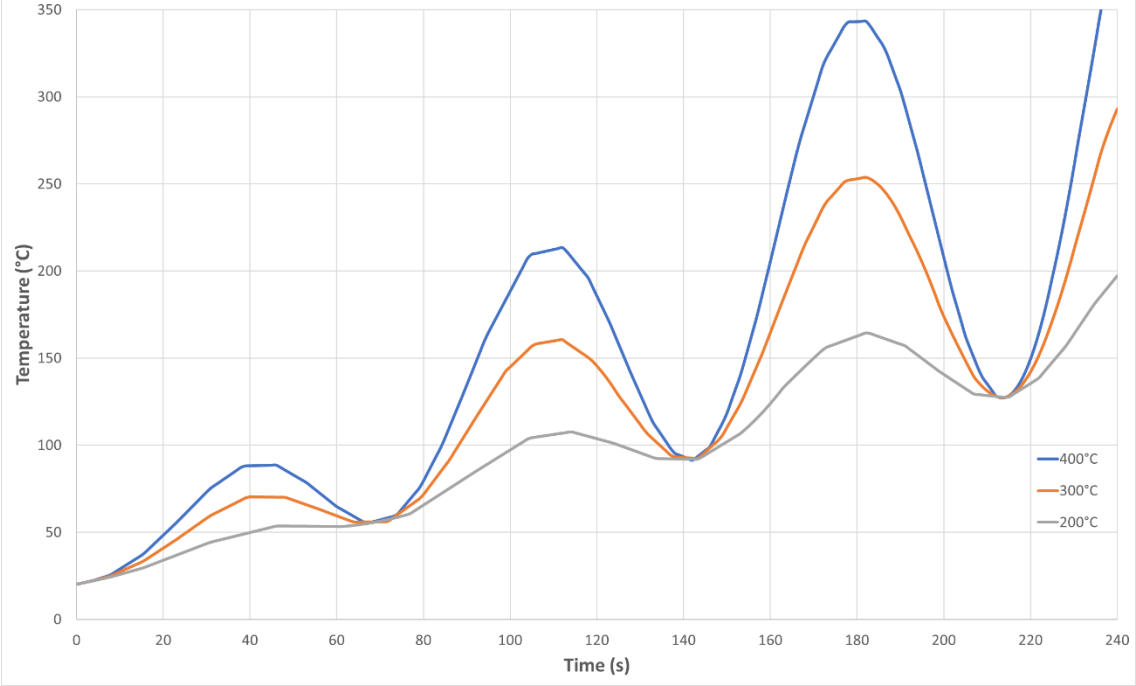

Fig. 6.27 Temperature reached by the wood core owing to the temperature considering different maximum temperature

Furthermore, the panel was also analysed mechanically (5.4), applying a linear function pressure until a maximum pressure of 8 kPa was reached (5.47). The aluminium panel has a very low von Mises stress; in fact, for a pressure of 8 kPa, there is a stress of 0.45 MPa (Figure 6.28). Therefore, the panel turns out to be a suitable solution for the pressures exerted by the flow only.

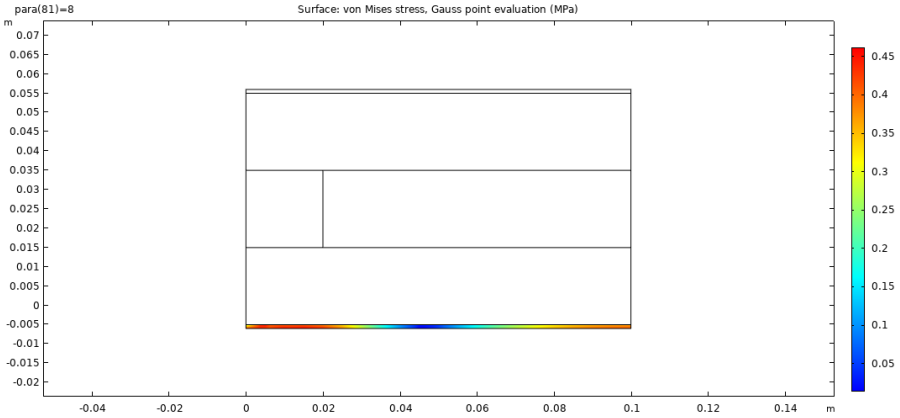

Fig. 6.28 von Mises stress of the aluminium panel due to the application of pressure

Finally, the panel has also been analysed, considering the combined action (5.23). Therefore, the thermal analysis solution has been used as a starting point for the application of the pressure. From the analysis carried out, it is noted that in the aluminium panel, there is no increase in stress at the subsequent application of pressure (Figure 6.29). This result is due to the stress generated by the thermal action which is much greater than that due to the mechanical pressure alone.

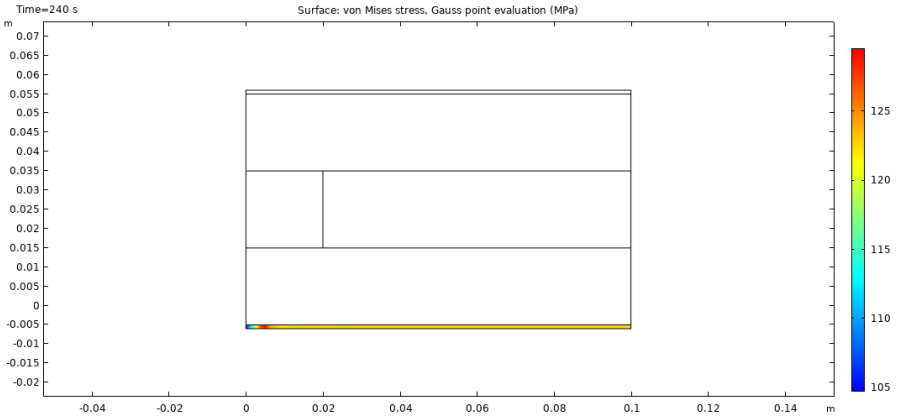

Fig. 6.29 von Mises stress of the aluminium panel due to the application of the temperature and pressure

Although the results obtained were advantageous for mechanical and thermal stresses, the panel was discarded due to its excessive weight. Therefore, a further panel hypothesis

involves constructing a sandwich panel with a substructure made of wood and aluminium panels (Figure 6.30).

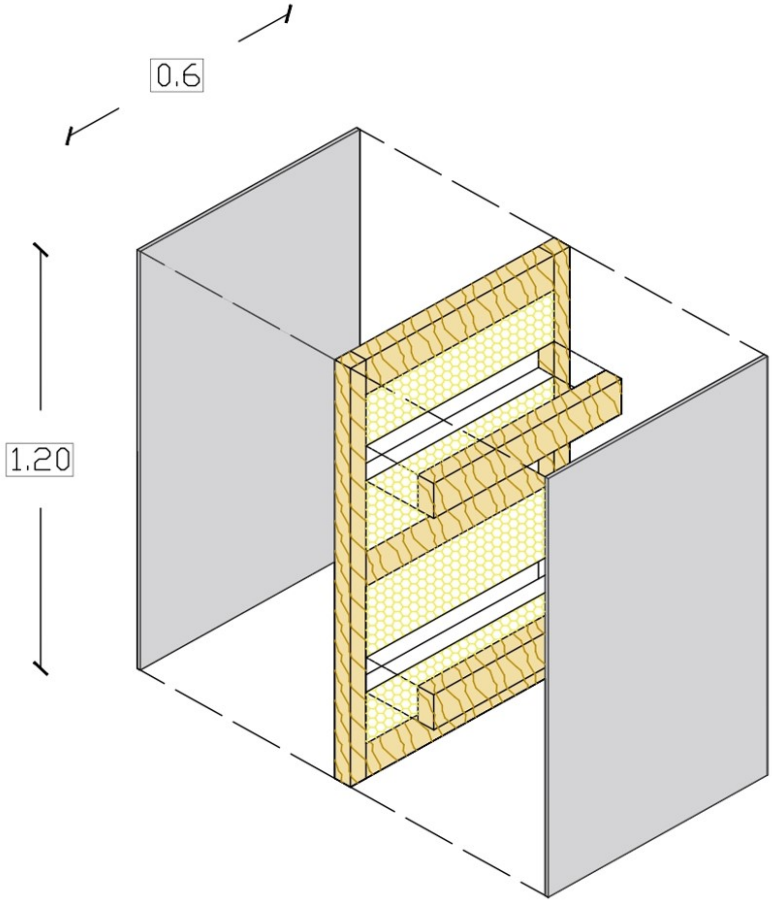

Fig. 6.30 Model of a third idea of shutter

This model was also evaluated in the mechanical field (5.4) and in the thermal area (5.21). The mechanical results (Figures 6.31) show that the panel can withstand the expected stresses without drawing the failure stress.

The thermal results (Figure 6.32) also show that both aluminium panels do not reach the breaking tension and that the temperature recorded on the internal board is about 100°C (Figure 6.33); therefore, the window is effectively protected.

Finally, owing to its strength and size (1.20 x 0.60) m can also be used as a panel for a ventilated façade.

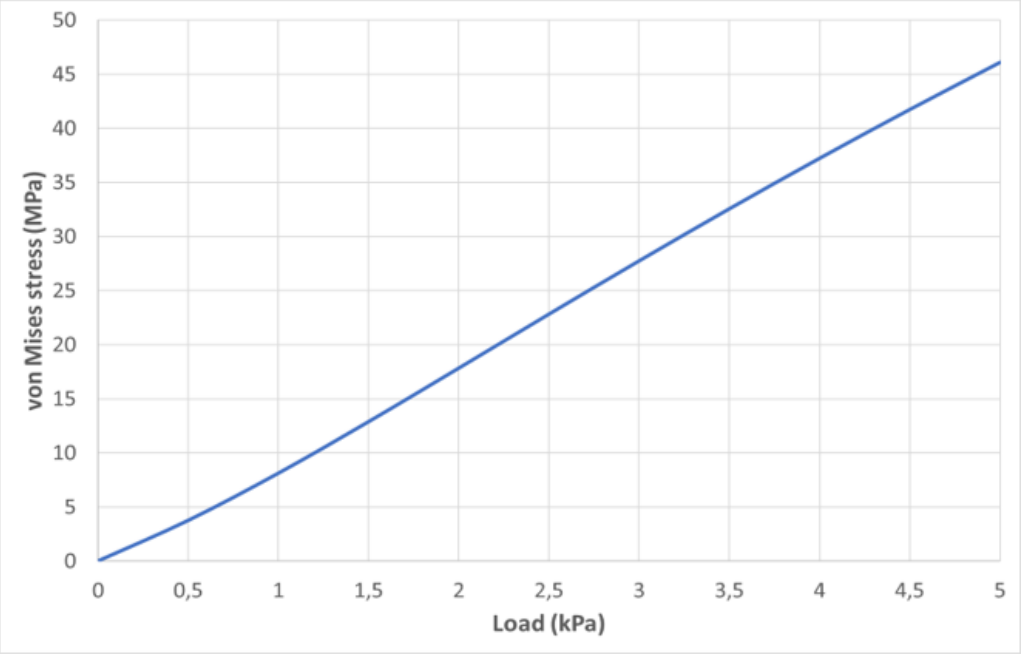

Fig. 6.31 von Mises stress of aluminium panel due to the application of the pressure

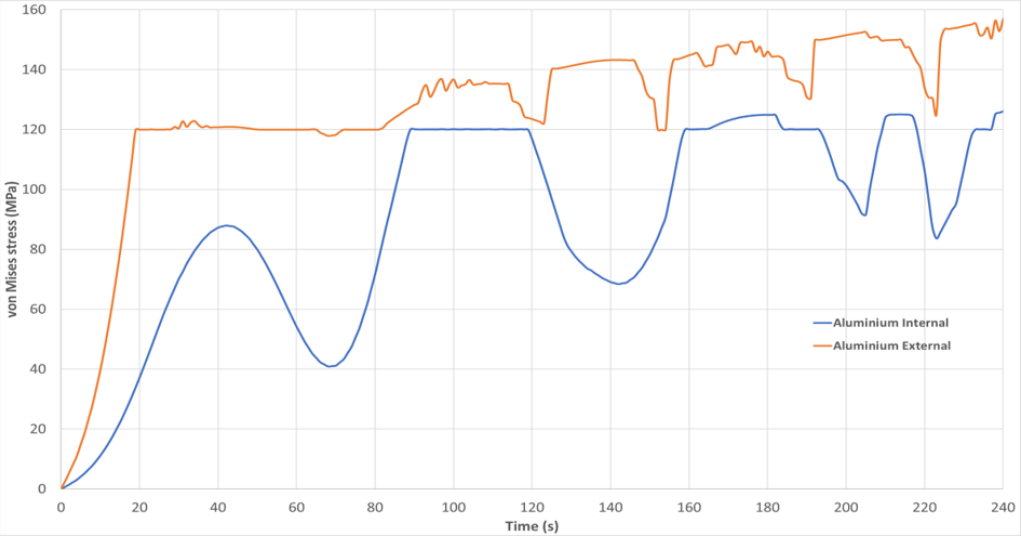

Fig. 6.32 von Mises stress of the aluminium panels due to the application of the temperature

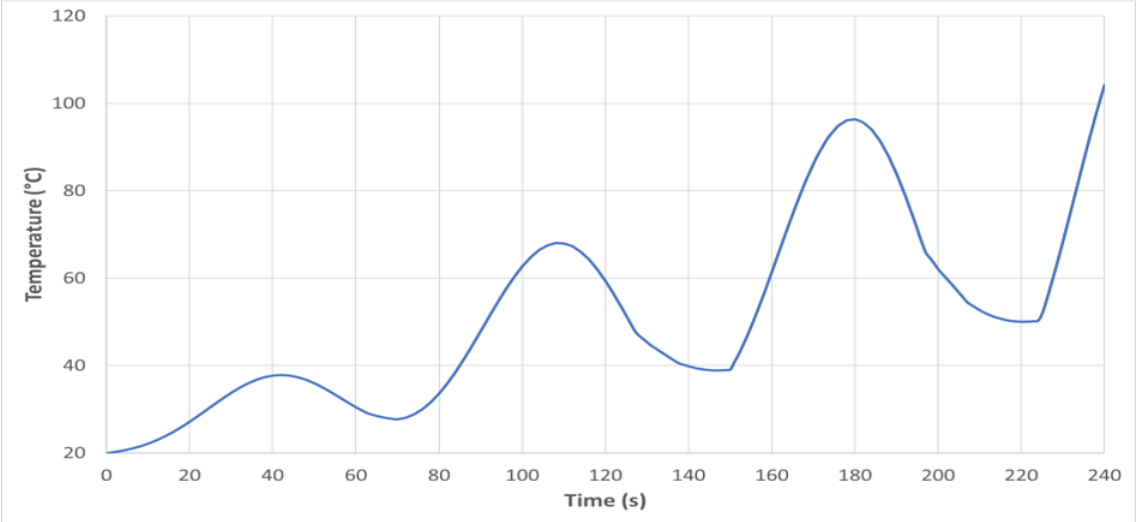

Fig. 6.33 Temperature measured on the inner surface of the inner aluminium panel.

6.4 Roofs

The elements of greatest vulnerability to falling deposits are roofs, and therefore the main mitigation measures must address these sub-structures. In particular, as analysed by De Gregorio (2010) [11], the thermal degradation of the materials, due to the high temperature of the clasts (150-400°C) can be mitigated through the use of thermal insulation, which is characterised by a thermal conductivity equal to 0.04 W/mK, can triple the collapse time of wood, steel and concrete roofs (Table 5.5). Although the insulation assumed in the analysis is a 3cm layer of rock wool, this material needs to be tested at high temperatures before any use in volcanic areas. While for the modification of the angle of inclination of the roof, two advantages can be obtained:

- the removal of part of the deposits,
- increasing the ultimate residual load on the structure.

Therefore, in volcanic risk areas, it would be necessary to define a minimum angle of inclination of the roofs, and for flat roofs, this inclination can be achieved by superimposing a superstructure in cold-formed steel (Figure 6.34). The advantages of using CFS elements are:

- Lightness: CFS elements are lighter than traditional structural elements, so the existing structure is not overloaded.
- Structural performance: CFS profiles provide a higher strength-to-weight ratio.
- Reduction of construction costs generated both by saving the basic material and reduced construction time thanks to the level of prefabrication achieved.
- Flexibility: cold forming offers a wide choice in terms of shape and size of the sections which, where necessary, can be defined by the designer according to project requirements.
- Durability: the profiles are generally cold-formed from hot-dip galvanised steel sheets, providing the necessary protection against corrosion.
- Eco-Efficiency: reversibility, recyclability, reduction of environmental impact.

Zuccaro and Leone (2012)[47] carried out a cost-benefit analysis in the municipalities falling within the yellow area, considering two trusses, one of 10 m and the other of 15 m, consisting of:

- Upper and lower beams with a C 180 section with a thickness of 3mm,

- Rods of type profiles arranged at an interest of 1 m,
- 8 mm thick corrugated sheet metal,
- Pitch angle of 15°

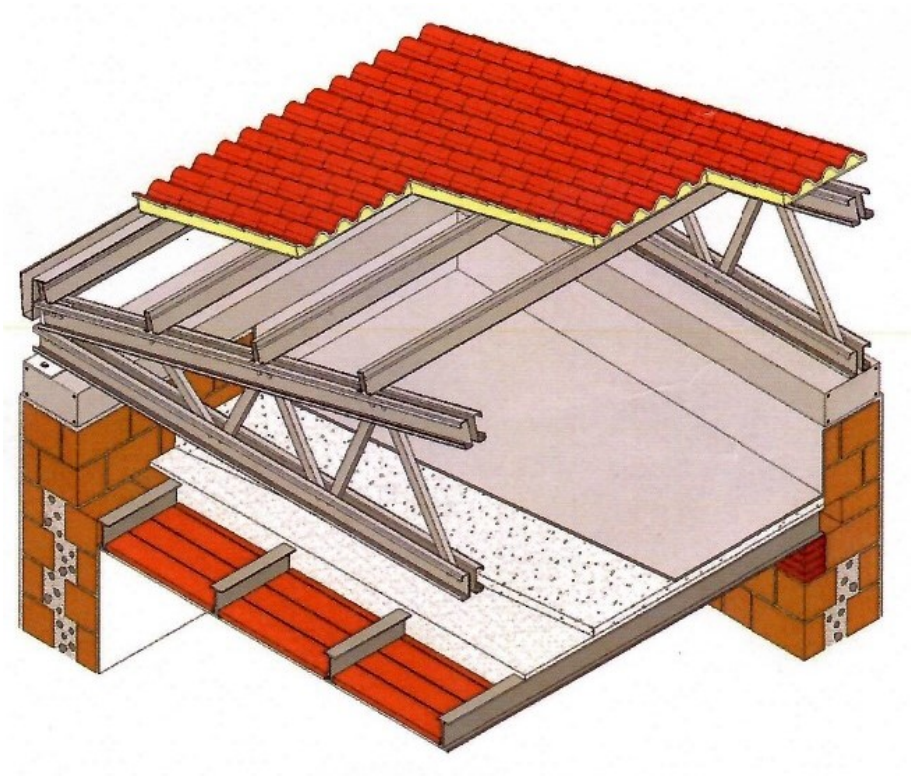

Fig. 6.34 Example of application of CFS roofing on existing roof with steel beams and bricks (Zuccaro and Leone, 2012) [47]

In addition, for both trusses, the construction costs per m2 were evaluated according to the expected overload (Table 6.6 and Table 6.7)

Table 6.6 Cost of CFS roofing with a spacing of ten meters per square metre to expected overload in the municipality (Zuccaro and Leone, 2012) [47]

10m Truss	
Load (kg/m^2)	**Intervention cost (€/m^2)**
2000	176
1500	136
1000	116
800	104
500	86

Table 6.7 Cost of CFS roofing with a spacing of fifteen meters per square metre to expected overload in the municipality (Zuccaro and Leone, 2012) [47]

15m Truss	
Load (kg/m^2)	**Intervention cost (€/m^2)**
2000	190
1500	145
1000	122
800	109
500	89

The reference scenario considered (Figure 6.35) shows that 59 municipalities are affected. The proposed intervention is foreseen for the municipalities in which the surface of vulnerable roofs exceeds 50% and the surface of collapsed roofs exceeds 5%; and of the 59 municipalities falling in the yellow zone, only in 11 is it necessary to intervene. In addition, Zuccaro and Leone (2012) [47] assumed a parametric cost of 86 €/m^2 because the assumed ash fall load is 400 kg/m^2.

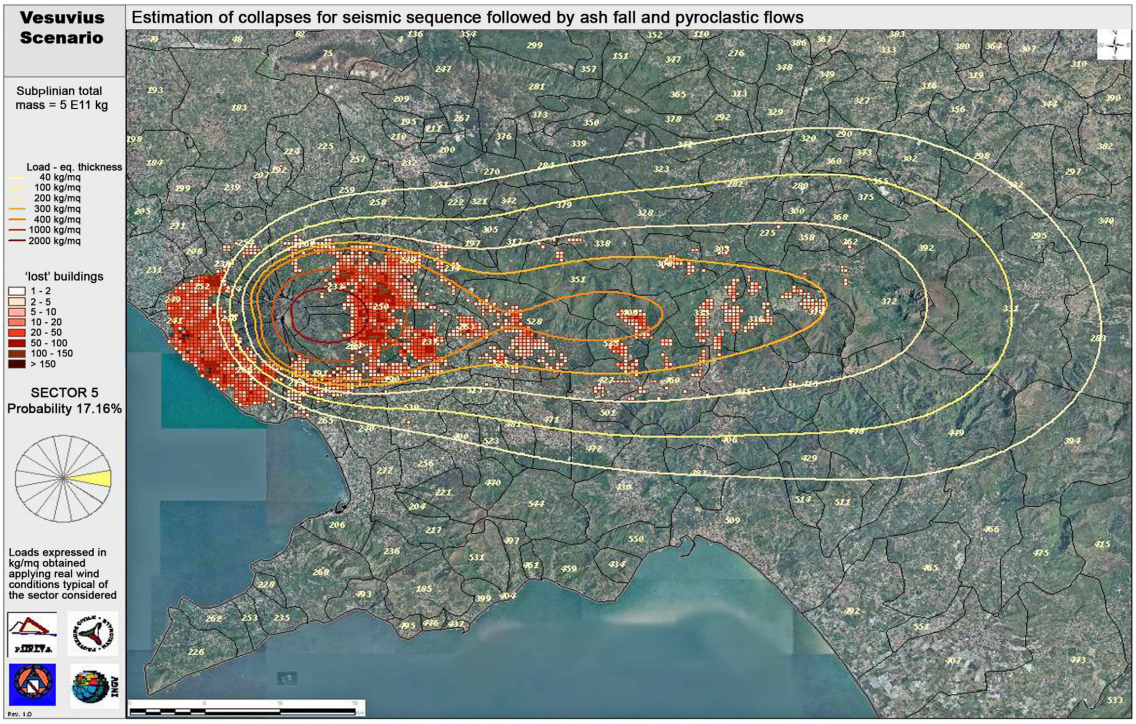

Fig. 6.35 Possible final impact scenario at Vesuvius developed through PLINIVS, used as reference scenario for ash-fall-mitigation case study (Zuccaro and Leone, 2012) [47]

6.5 Application

Once the mitigation strategy for shutters and façades have been defined, their applicability in red areas was analysed in detail. For Vesuvius, the municipalities of Ercolano and Torre del Greco were considered. For the municipality of Torre del Greco, the area (Figure 6.36) was considered, whose technological data regarding openings and shutters were obtained from the aggregated results of the survey (Figure 6.37); in particular, a high percentage of wooden windows with steel shutters (17%) and aluminium windows with steel shutters (33%) was found. Regarding the information on windows and doors, it would be necessary to carry out a more detailed analysis on-site, to understand whether aluminium windows and doors have a thermal break or not or check whether the glass used is single or double glazed. Whilst for shutters, it was possible to carry out further analysis on the outside, as the verification included the type used, in fact in Torre del Greco, there are two types (Figure 6.38) (Figure 6.39), which are unsuitable as first protection for the frames since they would allow the passage of the fluid that causes the glass breaking. Therefore, to preserve the building and reduce reconstruction costs, it is necessary to provide for the building's complete replacement. (Iacuaniello et al., 2020) [16]

Fig. 6.36 Analysed area of the municipality of Torre del Greco

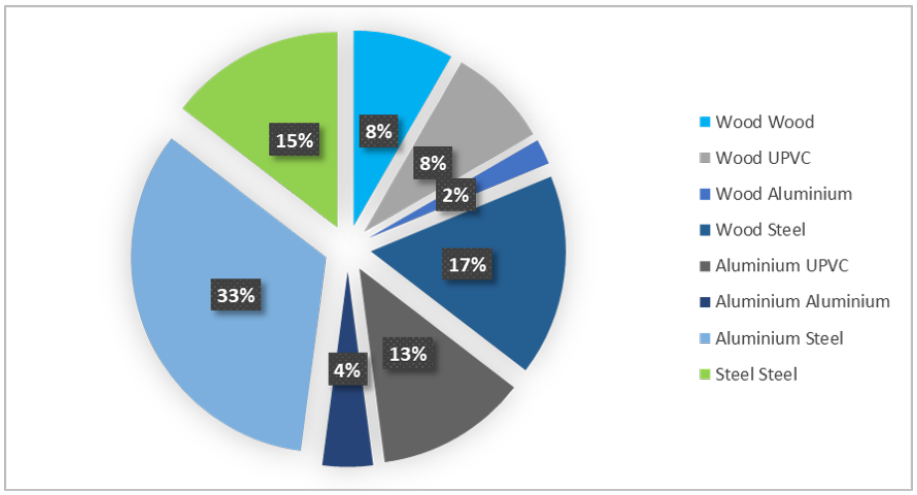

Fig. 6.37 Distribution of window-shutters classes in the municipality of Torre del Greco

Fig. 6.38 Examples of steel shutters in the municipality of Torre del Greco (Google Earth Pro)

Fig. 6.39 Examples of steel shutters in the municipality of Torre del Greco (Google Earth Pro)

While for the municipality of Ercolano, in the area considered (Figure 6.40) a diffusion of wooden windows with steel shutters (44%) and UPVC windows with steel shutters (17%) was considered (figure 6.41). In this case, the first strategy to be adopted is the total removal of UPVC windows, which have a critical temperature of 80°C and are therefore unsuitable; In contrast, for aluminium windows, also, in this case, it is necessary to carry out a detailed analysis to verify which type of section has been used. Finally, the recurring types of shutters (Figure 6.42) (Figure 6.43) are not suitable because they would allow the flow to pass through.

Fig. 6.40 Analysed area of the municipality of Ercolano

The thermal (Figure 6.44) and mechanical (Figure 6.45) stresses considered in both areas have been evaluated by the PLINIVS research centre for the EXPLORIS research

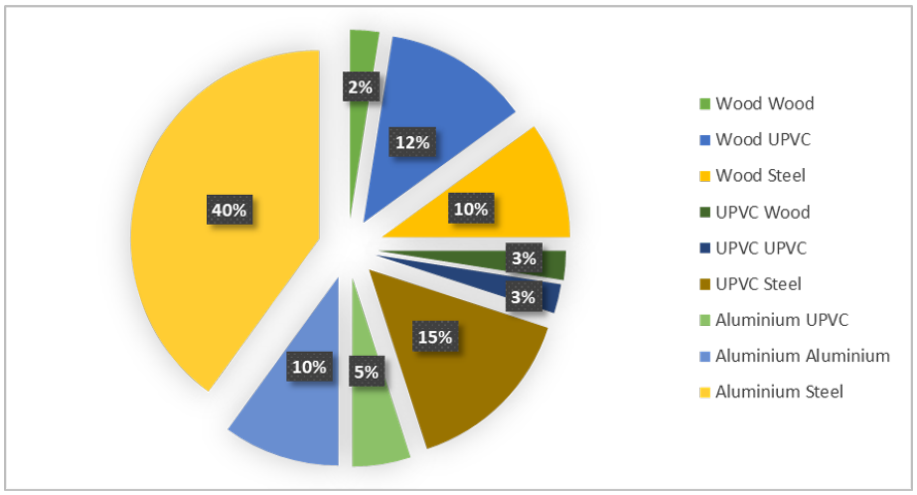

Fig. 6.41 Distribution of window-shutters classes in the municipality of Ercolano

Fig. 6.42 Examples of steel shutters in the municipality of Ercolano (Google Earth Pro)

Fig. 6.43 Examples of steel shutters in the municipality of Ercolano (Google Earth Pro)

project; considering as reference scenario the one defined by the Civil Protection for the drafting of the evacuation plan, i.e. a sub-Plinian eruption of the type occurred in 1631. The reference scenario envisages that a series of explosions may occur first in conjunction with the vent's reopening, preceded by seismicity, ground deformation, increased gaseous emissions, the activation of new fumaroles and the opening of fractures. An eruptive column composed of steam, gas, magma fragments (pumice and ash) and rock fragments (lithics) will then rise from the volcano, which can reach a height of tens of kilometres.

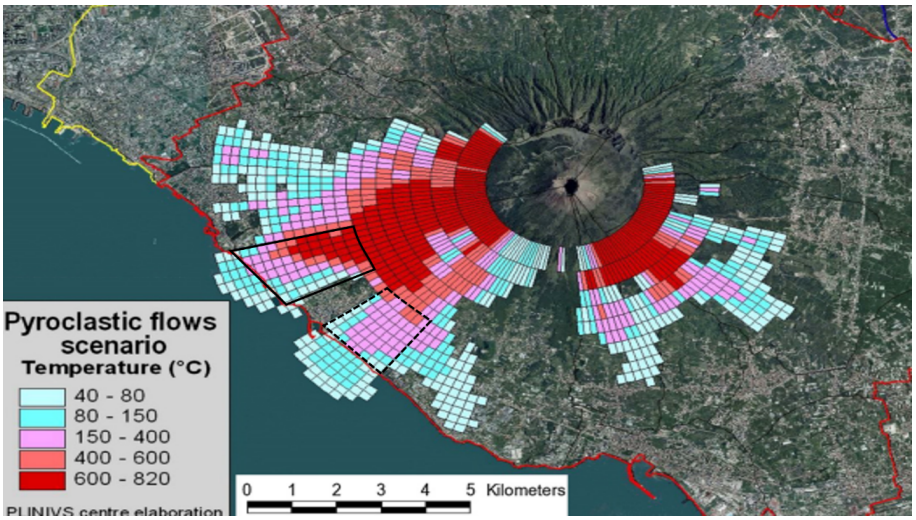

Fig. 6.44 PDCs scenario, Temperature, Exploris project (Zuccaro, 2006). The municipality of Ercolano is marked with a black continuous line, the municipality of Torre del Greco is marked with black dotted line.

For Torre del Greco, a temperature range between 150 °C and 400 °C is assumed, while for pressures a range between 0.1 kPa and 0.5 kPa is considered. Furthermore, the temperatures predicted for the Ercolano area (Figure 6.44) are similar to those of the Torre del Greco area, for which a temperature range between 150 °C and 400 °C is assumed, while pressures are higher; indeed pressures between 0.5 kPa and 1.5 kPa are assumed (Figure 6.45). From the evaluations carried out it is possible to define, for the types of window and door classes present in the two territories considered, a series of mitigation actions (Table 6.8), ordered according to an order of vulnerability of the elements, in fact in the case of the pair of UPVC window and door frames and steel shutters, the first action to be undertaken is the removal and replacement of the frame and then, the replacement of the glass with tempered glass and finally the replacement of the shutters. Also, these mitigation strategies cannot be applied in areas closer to the slopes of Vesuvius, as temperatures can reach a maximum of 820°C. Finally, for the two test areas of the Vesuvius area, the application of the ventilated façade technology is not necessary since

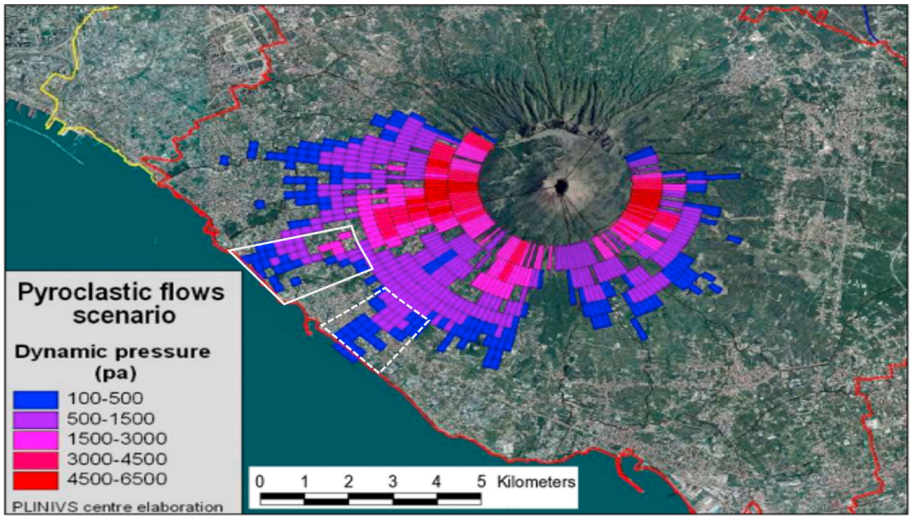

Fig. 6.45 PDCs scenario, Temperature, Exploris project (Zuccaro, 2006). The municipality of Ercolano is marked with a black continuous line, the municipality of Torre del Greco is marked with black dotted line.

Table 6.8 Proposal for mitigation measures for the window system for the municipalities of Ercolano and Torre del Greco

Municipality	Frame	Shutters	Glass	Intervention
Torre del Greco	Aluminium	Steel	Soda Lime Glass	• 1. Replacing the shutters, • 2. Replacing the glass with tempered glass, • 3. Replacing the window frame if it is a thermal break window.
	Wood	UPVC		• 1. Replacing the shutters, • 2. Replacing the glass • 3. Assessment of the state of preservation of the frame.
Ercolano	Wood	UPVC	Soda Lime Glass	• 1. Replacing the shutters, • 2. Replacing the glass with tempered glass • 3. Assessment of the state of preservation of the frame.
	UPVC	Steel		• 1.Frame replacement, • 2. Shutters replacement, • 3.Glass replacement with tempered glass
	Aluminium	Steel		• 1. Replacing the shutters, • 2.Replacing the glass with tempered glass, • 3.Replacing the window frame if it is a thermal break window.

the pressures assumed are lower than the resistance of the vertical reinforced concrete and masonry structures.

A detailed analysis of the analysed strategies' applicability in the Campi Flegrei area was also carried out. In the whole Phlegraean area, the municipality of Pozzuoli was considered. In particular, two heterogeneous areas were analysed (Figure 6.46) from a structural point of view. A majority of reinforced concrete structures characterises the area located in the upper part. In contrast, in the second area, there is a majority of masonry structures in the tuff.

Fig. 6.46 Analysed areas of the municipality of Pozzuoli (Google Earth Pro)

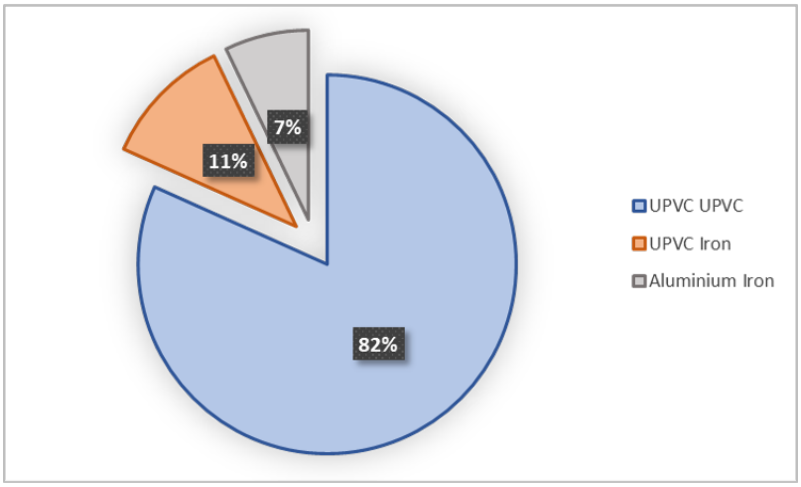

Fig. 6.47 Distribution of window-shutters classes in the municipality of Pozzuoli

Besides, the window and door frames in the municipality of Pozzuoli mostly belong to the group of UPVC frames and shutters, whose critical temperature is 80°C; it is

necessary to replace the frame and the shuttles completely. Then there is a small diffusion of aluminium, which need a more detailed evaluation to define if the frame has a thermal break with iron shutters (Figure 6.47). Since the most common types of shutters in the area are roller shutters and louvre shutters (Figures 6.48) (Figure 6.49), which cannot protect the window frame from possible infiltration is necessary to replace them.

Fig. 6.48 Examples of UPVC roller shutters in the municipality of Pozzuoli (Google Earth Pro)

Regarding stresses, the spatial distribution maps of hazard in terms of pressure and temperature due to pyroclastic flows at varying positions of the eruptive vent produced by the PLINIVS research centre for the ARES convention (2014) DPC (Department of Civil Protection) were considered. The National Institute of Geophysics and Volcanology (INGV), which produced the data, assumed a Sub-Plinian eruption for the Campi Flegrei caldera, and the eruptive vent was considered to be inside, in the middle and on the edge of the Agnano caldera. For evaluating the proposed strategies, the scenario with the vent located in the centre of the caldera was considered and the hazard data considered are those

Fig. 6.49 Examples of aluminium shutters in the municipality of Pozzuoli (Google Earth Pro)

calculated 500 seconds after the beginning of the collapse phase of the eruptive column (Figure 6.50).

Therefore, the expected temperatures are higher than in the Vesuvian areas, in fact, in the two areas studied, a temperature range between 126 °C and 500 ° is assumed (Figure 6.51), while the expected pressures are between 2 kPa and 4 kPa (Figure 6.52). The high expected temperatures represent the main problem since the distance between the vent and the houses are minimal. Therefore the shutter model is not suitable, in fact when analysing its resistance at 500°C, it underlined that it breaks after about 225 seconds; a different solution is to consider another aluminium alloy, in particular, EN-AW 6060, the one also used for window frames, which has a maximum resistance of 160 MPa and when analysed at a temperature of 500°C does not reach the crisis tension (Figure 6.53). Finally, for the municipality of Pozzuoli, the interventions to be carried out are defined according to an order of vulnerability of the characteristic technological elements (Table 6.9). Furthermore, for the area with a majority of reinforced concrete structures, it is advisable to foresee applying the ventilated façade system since the pressures recorded are more significant than the established resistance of the infill panels.

Conclusively, the strategies proposed for both areas, before being applied on the buildings, whether they are of reinforced concrete or masonry, it is advisable to carry out surveys of the building to assess the state of conservation of the materials. For example, before proceeding with the replacement of windows and doors, it is necessary to assess the shaft's state into which they will be inserted to define the best solution for fixing them. A

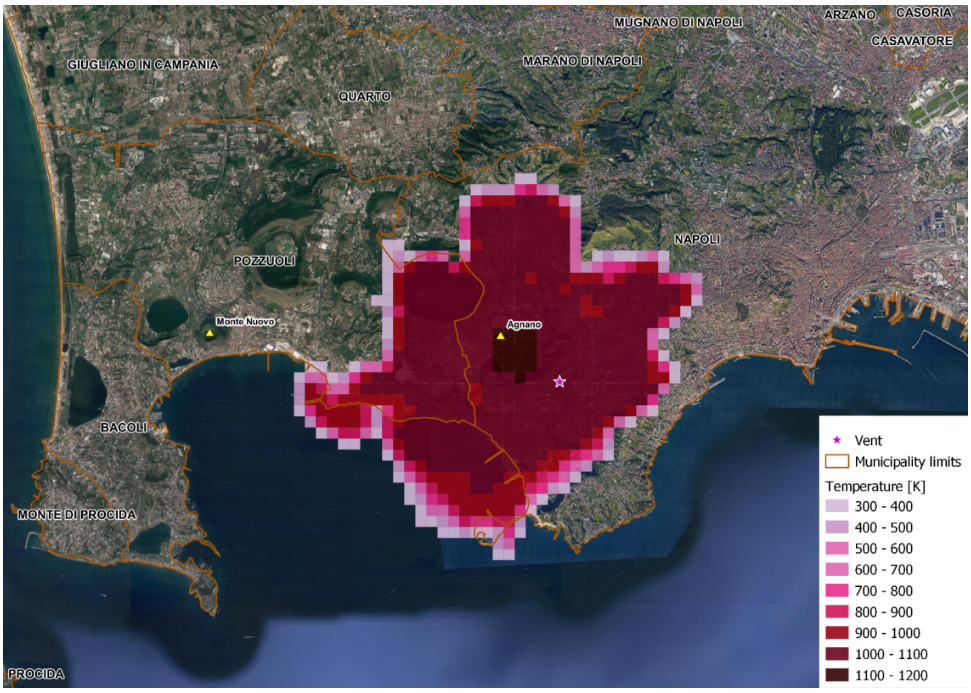

Fig. 6.50 Pyroclastic flows temperature, Pressure, Ares Convention (2012).

Fig. 6.51 Pyroclastic flows temperature, Pressure, Ares Convention (2012).

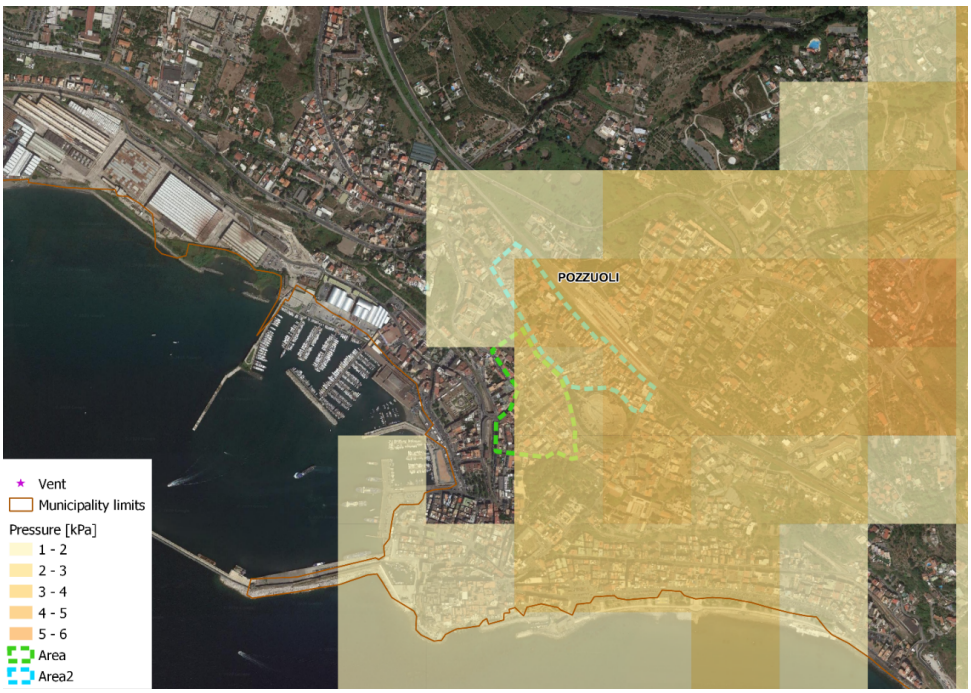

Fig. 6.52 Pyroclastic flows pressure, Pressure, Ares Convention (2012).

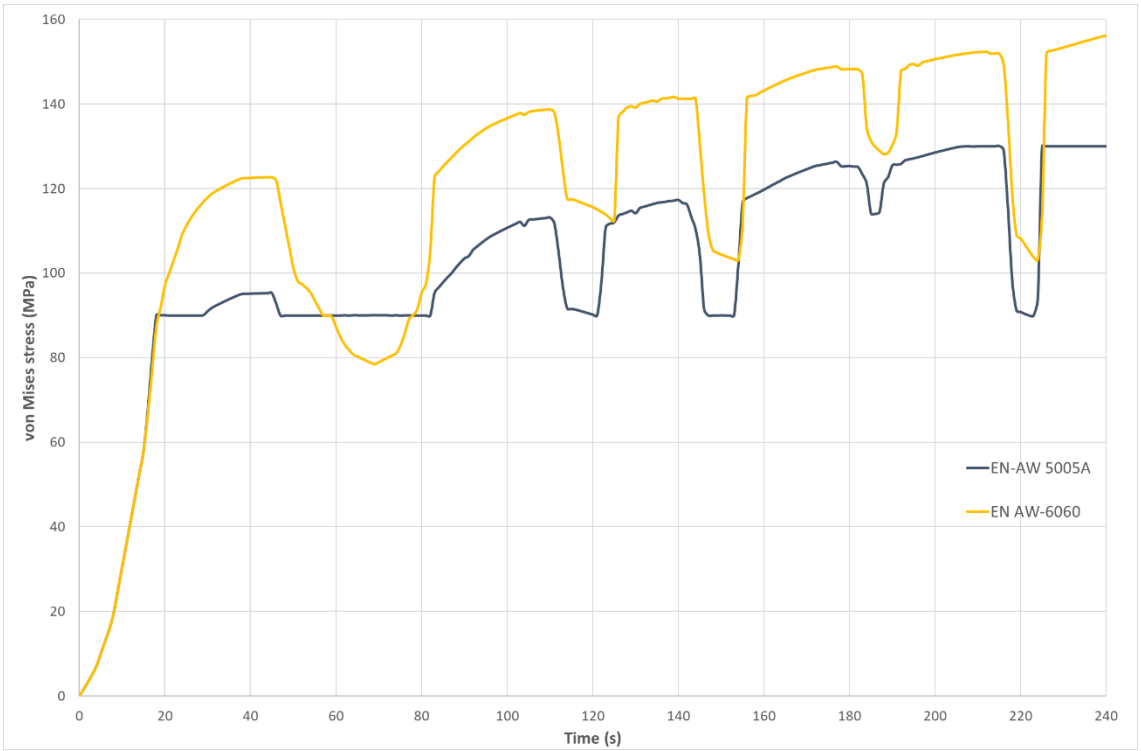

Fig. 6.53 Comparison of von Mises stresses, for the aluminium alloys used for the panel, considering a maximum temperature of 500°C

Table 6.9 Proposal for mitigation measures for the window system for the municipalities of Pozzuoli

Municipality	Frame	Shutters	Glass	Intervention
Pozzuoli	UPVC	Steel	Soda Lime Glass	• 1.Frame replacement, • 2. Shutters replacement, • 3.Glass replacement with tempered glass
	UPVC	UPVC		• 1.Frame replacement, • 2. Shutters replacement, • 3.Glass replacement with tempered glass
	Aluminium	UPVC		• 1. Replacing the shutters, • 2.Replacing the glass with tempered glass, • 3.Replacing the window frame if it is a thermal break window.

similar procedure should be carried out to define the fixing system of the ventilated façade. These assessments will be carried out well in advance, as the proposed strategies are also valid as energy-saving strategies and can therefore be applied even if the alert level should remain low.

Chapter 7

International Volcanoes

A final objective was to evaluate whether the volcanic mitigation strategies designed for the two areas of Campania could be used in different territorial contexts. In particular, the island areas of the Philippines, the Azores, the French Antilles and Tenerife were evaluated since the reference scenarios studied assume an explosive type eruption, the expected phenomena being the same as those considered in the Italian areas. Firstly, a detailed exposure analysis was carried out, with particular attention to the vertical structure, roofs, windows and shutters, of each area.

7.1 Kanlaon Volcano (Philippines)

Kanlaon volcano, along with three other volcanoes, forms part of the Negros volcanic arc in the Central Philippines, resulting from eastward subduction to the west of Negros Island. Kanlaon volcano is located on Negros Island and rises to 2435m above sea level (Figure 7.1).

Six major rivers run from the slopes of Kanlaon to the west coast of Negros, creating an efficient drainage system that carries fertile volcanic deposits and deposits them on the lower slopes. This makes Negros Island very suitable for agriculture, supporting much of the population through subsistence farming, small-scale trade and large commercial ventures such as fruit farms, rice and sugar mills. Future eruptions are expected to either continue producing the small magnitude ash emissions recorded since 1866 or return to the large magnitude explosive or effusive eruptive behaviour indicated by geological history. Five volcanic hazards have been identified at Kanlaon: 1) ballistic projectiles, 2) pyroclastic density currents, 3) ash fall, 4) lahars and 5) lava flows. The Philippine Institute of Volcanology and Seismology defined the hazard zones at Kanlaon based on the volcano's historical activity, the type and extent of geological deposits, the present

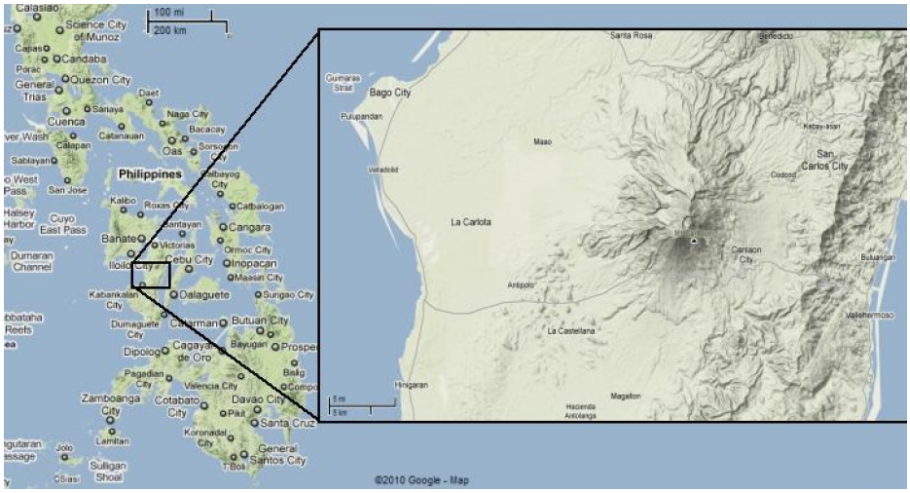

Fig. 7.1 Location of Negros Island in the Philippines, with inset: Kanlaon volcano and local communities on Negros Island. (Jenkins et al., 2011)

topography and assumed next eruptive vent (PHIVOLCS, 2003b). Besides, based upon the current topography and distance reached by geological pyroclastic flow units, the areas to the south and west of the volcano are likely to be exposed to pyroclastic density currents (PDC) and lahar (Figure 7.2).

The data of the building stock of the areas surrounding Kanlaon are extracted from the survey conducted by Jenkins et al [17]. In total, 174 buildings were surveyed in detail, with additional less structured and detailed investigations for other communities carried out. From a structural point of view, there are four main typologies:

1. Nipa dwellings: timber frame with bamboo weave or timber infill, one or two storey basic rural dwellings with nipa (palm frond) roof (Figure 7.3 a).

2. Timber frame dwellings: timber frame with bamboo weave, timber or metal infill, one or two storey buildings with corrugated steel roof (Figure 7.3 b).

3. Reinforced concrete frame: generally one or two storey, but possibly up to four in more built up areas, with masonry infill walls and corrugated steel roofs (Figure 7.3 c).

4. Mixed construction buildings: one to two storey buildings generally comprising a reinforced concrete lower half and a timber frame, timber infill upper half with a corrugated steel roof (Figure 7.3 d).

Detailed building typology classifications were needed to determine the likely resistance of buildings in the Kanlaon area to different volcanic hazards. Separate typology classes are consequently established for each volcanic process. Regarding the 174 buildings

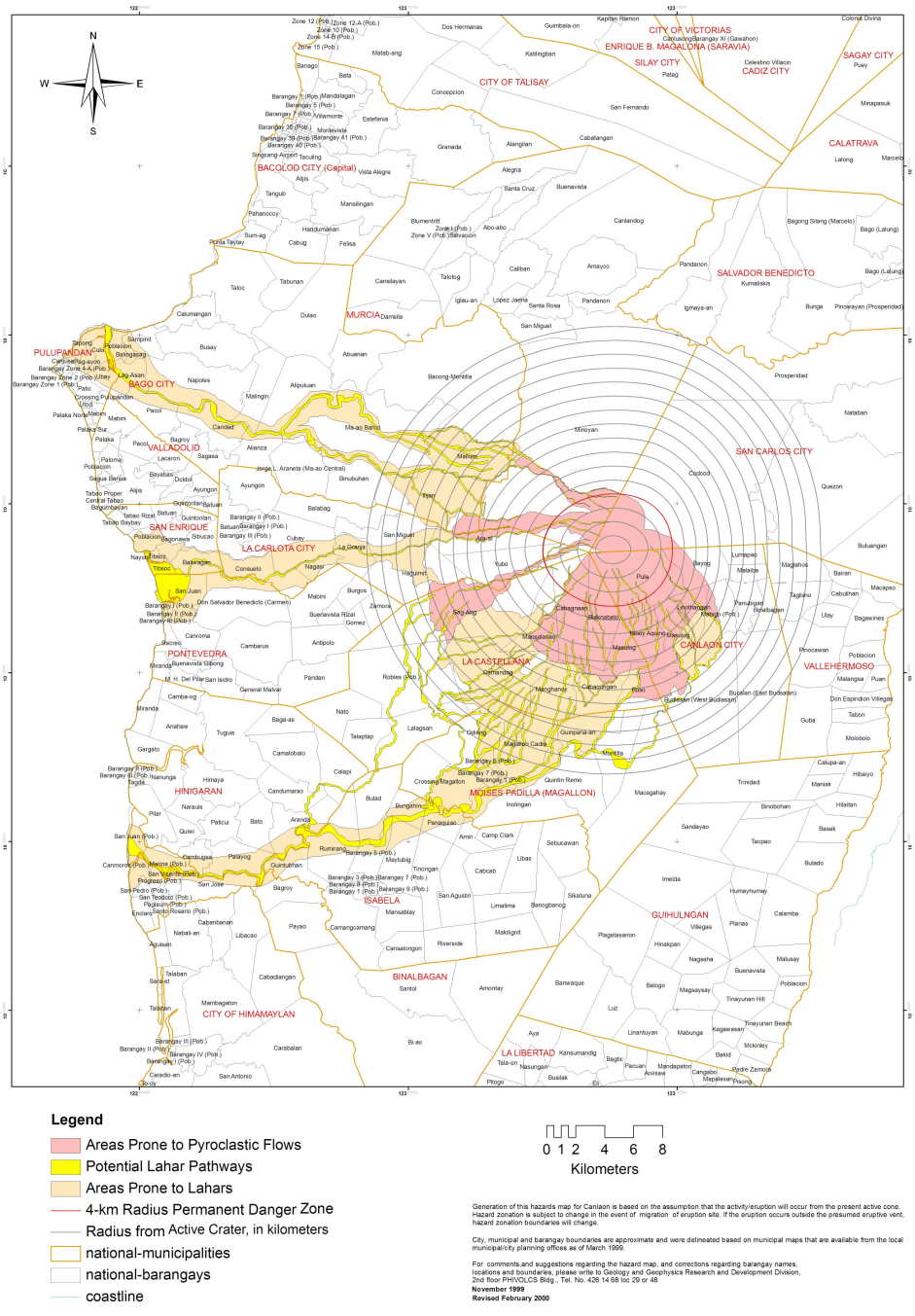

Fig. 7.2 Kanlaon volcano pyroclastic flow and lahar hazards map. (Jenkins et al., 2014)

Fig. 7.3 a) typical nipa hut with thatched roof, b) typical timber frame dwelling with metal sheet roof, c) typical reinforced concrete frame building with metal sheet roof, d) typical mixed construction building with a lower reinforced concrete frame and upper timber frame with timber boards. (Jenkins et al., 2014)

surveyed by Jenkins et al., 91% of roofs comprised corrugated steel sheet roofs in good, average or poor condition supported by timber battens and rafters and generally pitched at angles approximately 20 to 30° (Figure 7.4 b, Figure 7.4 c). The Kanlaon area roofs are pitched, which may allow ash fall to slide off or be washed off by rain. Nipa thatch roofs are used for 8% (n=13) of the buildings and only one building comprised a timber board roof, one was built under a large reinforced concrete bridge, and one made with a combination of nipa thatch and corrugated steel sheets. Given this breakdown (Figure 7.6), the following roof types likely within the Kanlaon area, assigned roof codes and ordered from most vulnerable to least vulnerable, have been considered:

- Kanlaon A_T: Nipa thatch on timber supports.
- Kanlaon B_T: Corrugated steel sheets in poor condition ($>$ 75 % visible corrosion) on timber supports.
- Kanlaon C_T: Corrugated steel sheets in average condition (between 25 and 75 % visible corrosion) on timber supports.
- Kanlaon D_T: Corrugated steel sheets in good condition ($<$ 25 % visible corrosion) on timber supports.

Nipa thatch roofs include woven leaves of nipa palms on timber (generally bamboo) battens and represent a common and economical construction material in the Kanlaon area. When such covers are newly built, they are relatively strong, though they deteriorate over time and become more brittle and, hence, more vulnerable as they age. Since to establish the condition of the timber supports, it would be necessary to enter each building and analyse the timber supports from inside, but it was not possible, so the condition was assumed as average.

There is no clear pattern of the typology distribution, but it is clear that the less vulnerable classes, C_T and D_T, are more frequent (70%). In Kanlaon 3 types of panels have been identified, divided by their vulnerability to lateral pressure, ordered from most (APDC) to least (CPDC) vulnerable:

- $Kanlaon_{APDC}$: Timber panels,
- $Kanlaon_{BPDC}$: Unreinforced regular (cut stone/concrete) block masonry; reinforced concrete frame buildings without earthquake resistant design (non-aseismic)
- $Kanlaon_{CPDC}$: Reinforced concrete frame buildings with earthquake resistant design (aseismic).

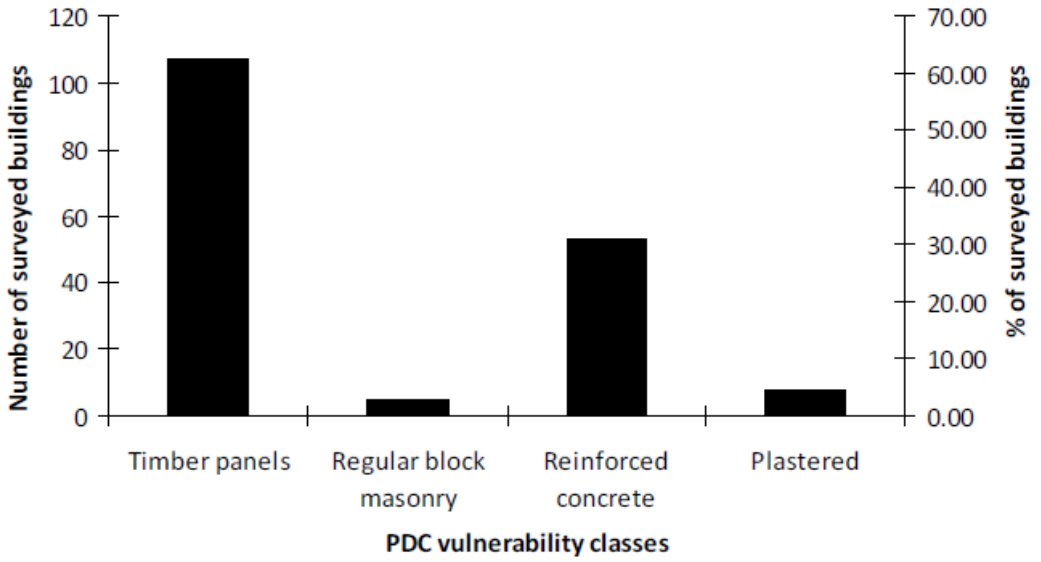

Fig. 7.4 Breakdown of the wall and panel types identified through field surveys in the Kanlaon area. (Jenkins et al., 2011)

The exposure and vulnerability analyses carried out by Jenkins et al. (2009) show that it is impossible to intervene with the same solutions as in Italy because the buildings' technological characteristics are entirely different, making it difficult to spread the protected areas widely. Thus, it is necessary to identify new mitigation strategies that must, at the same time, respect the technological and construction characteristics of the island.

7.2 Furnas Volcano (Azores)

Furnas in the island of Sao Miguel, Portugal, is one of the active volcanoes of Europe. The island contains three active volcanoes that have been documented to have explosively erupted at least 30 times in the past 5000 years (Booth et al., 1983). Furnas is characterised by explosive volcanism with a history of 10 explosive eruptions, some classified as sub-Plinian and Plinian, during the past 5000 years (Guest et al., 1999). The last eruption occurred in 1630 and caused the loss of more than 190 lives (Cole et al., 1995). In the event of a Furnas eruption, similar to or stronger than the 1630 sub-Plinian eruption, there will be a need for immediate evacuation of all the people in the high-risk zone and contingency measures will have to be taken across the whole of the island. Pre-eruption earthquake activity will probably be the main precursor and is currently monitored throughout the island. The town of Furnas situated inside the caldera and the coastal settlements of Ponta Garca and Ribeira Quente are nearest to the volcano. Volcanic hazards with potential to destroy many buildings in these settlements are volcanic earthquakes, lapilli impact and

most of all, dense PDCs. In the case of an eruption in any of the three volcanoes, the role of the buildings will be crucial as the main shelter for the affected population. In this context, it is important to assess the condition and strength of the building stock, so that adequate risk assessment can be made and where necessary, remedies and preparedness techniques be proposed. The surveys, conducted by Pomonis et al.(1999)[34], of all the residential buildings were carried out in two towns (Figure 7.8): Furnas (Figure 7.9), Ribeira Quente. Residential buildings in the centre of Povoaçao (Figure 7.10), which is the main town in the study area, were also surveyed. Ponta Garça, on the southern coast of the island, stretches for 4.5 km and a survey of its eastern part was made. The surveys took place in May 1994.

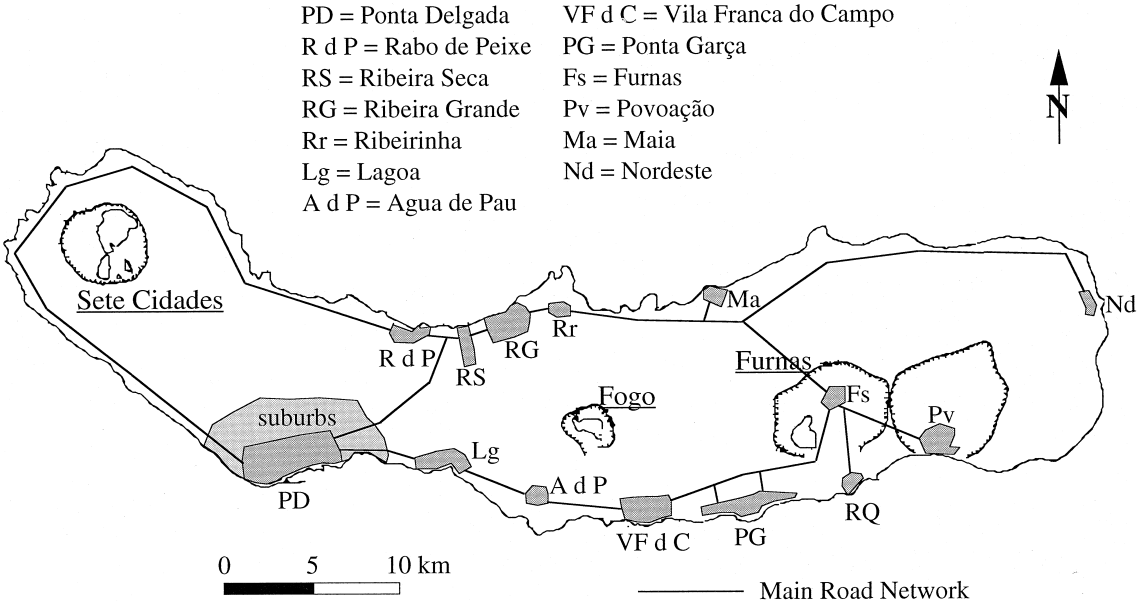

Fig. 7.5 Sketch map of Sao Miguel island with location of the main towns, main road network and the three active volcanoes (Pomonis et al., 1999)

The survey investigated the condition of residential buildings with a view to their volcanic and seismic vulnerability. The aim was to identify their features, assess the present-day condition, and group them in vulnerability classes to assist in the creation of a simulation model that would assess the impact of a possible eruption in Furnas. The surveys were external from street level. In addition, 15 representative buildings in Furnas were also surveyed in more detail, including old houses, new houses, and houses under repair or upgrading. The classes found in the Azores survey are:

- Old rubble stone masonry of 50–60 cm thick, with large regularly hewn dark-coloured basalt stones used in corners and sometimes around openings. Other large but irregularly cut basalt stones are placed randomly, reducing towards the top. The rest of the masonry is filled with lapilli, pebbles and other small rubble stones of

Fig. 7.6 A view of Furnas town (Pomonis et al., 2010)

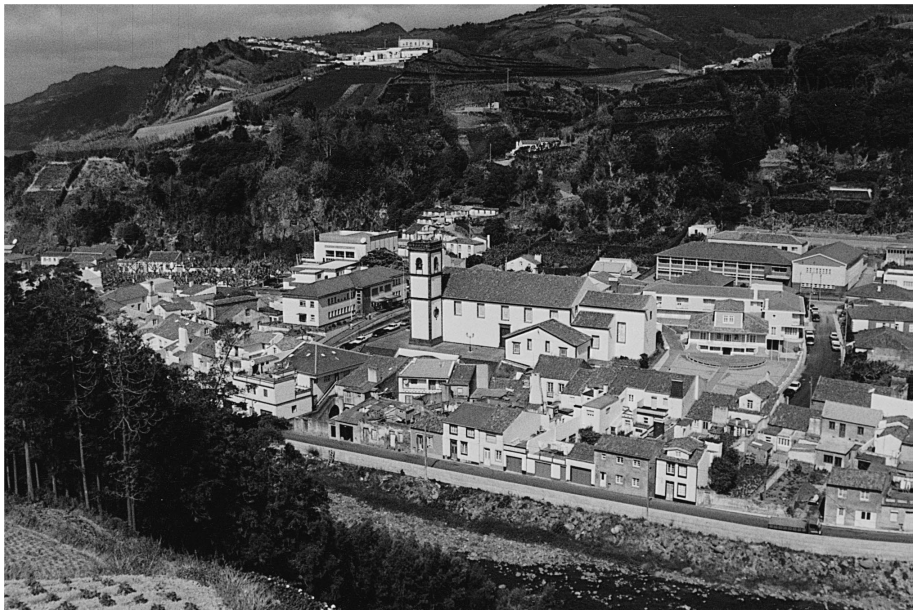

Fig. 7.7 A view of Povoação town.

volcanic origin and set in loose mortar, without cement. The walls are often covered with cement plaster on both sides and are whitewashed on the outside, besides floors made from timber joists covered underneath with boarded ceiling and on the top with wooden planks or boards. Finally, the most used roofs are gable roofs with 30 degrees sloping, covered with clay tiles in the shape of a half-moon interlocking half-moon above the landing stage. The roof is usually supported by wooden truss spaced every 3 or 4 m, with beams and purlins.

- Unreinforced concrete block masonry of blocks 200 mm thick with perforations and set in cement mortar. The floors made from timber joists or 100–150 mm reinforced concrete cast-in-situ slab. Finally, most commonly gable roofs with 30° pitch, covered with crescent shaped (half-round) interlocking clay tiles placed above the boarding or with new pressed clay pantiles. Roof support on purlins and rafters. The boarding is nailed on the rafters that are placed above the purlins without joinery. Trusses are less common; instead, masonry walls are carried up into the roof space.

- Reinforced concrete frames, generally two-storey cast-in-situ reinforced concrete frame consisting of columns and beams. Columns are quite slender (usually 200 mmx200 mm). Moreover, the walls are made of perforated bricks of burnt clay or, more commonly, concrete blocks 200-300 mm thick, not reinforced. At the same time, the horizontal structures are most commonly in situ filler-block floors and cast in situ reinforced concrete slabs and beams also in use, but less common. Finally, timber-framed, but flat or pitched RC slabs also used in some cases.

Another element necessary for the vulnerability assessment, besides the structural type, wall condition and roof type, are the windows and shutters. To enlarge the data regarding the technological and typological characteristics of the openings collected by Pomonis et al., a further survey was carried out using the Google Earth Pro programme. The area analysed is the residential neighbourhood of Furnas's city between R. Formosa Street and Av Vitor Manuel Rodrigues (Figure 7.11). Most of the buildings are made of reinforced concrete whose openings are made of either aluminium or UPVC, and it was assumed that they are single-pane glass due to the island's thermal characteristics (Figure 7.12). Furthermore, it is highlighted that not all the analysed windows have shutters, and the only examples present are the UPVC roller and louvre shutters (Figure 7.13). The condition of windows and shutters is of crucial importance in protecting from the PDCs and ballistics. In this study, a generally adequate condition was assumed. Finally, from the data collected by Pomonies et al. (1999) and the area analysed in the Portuguese island, it is possible to hypothesise to apply the mitigation strategies, and also the intervention procedures in the case of fixtures, foreseen for the areas of the Campania region since the characteristics of the buildings are the same as in Italy.

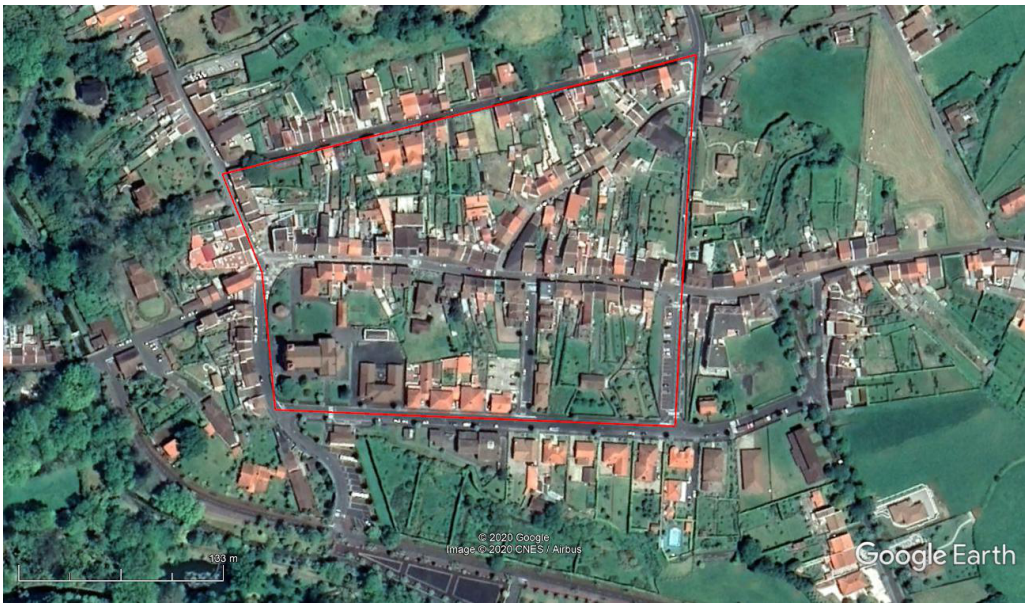

Fig. 7.8 Analysed area of the town of Furnas (Google Earth Pro)

Fig. 7.9 Example of UPVC roller shutters in the analysed area of Furnas (Google Earth Pro)

Fig. 7.10 Example of UPVC louvre shutters in the analysed area of Furnas (Google Earth Pro)

7.3 Mount Pelée (Martinique) and Soufriere Hills (Guadeloupe)

The islands of Martinique and Guadeloupe belong to the West Indies archipelago in Central America and are an overseas department of the French administration, but an integral part of the French Republic. Like most of the Antilles islands, both islands are characterised by the presence of an active volcano. In the island of Martinique, there is the Mount Pelèe (1397 m) whose last eruption dates back to 1902 that destroyed the arrondissement of Saint Pierre causing the death of about 30000 people; while in the island of Guadeloupe, there is the Soufriere Hills (1467 m) whose last eruption dates back to about 40 years ago (1976-1977). Hence significant building typologies on Guadeloupe and Martinique, defined according to their vulnerability to volcanic hazards, have been analysed through remote and ground surveys. Hence significant building typologies on Guadeloupe and Martinique, defined according to their vulnerability to volcanic hazards, have been analysed through remote and ground surveys. The data regarding the technological, structural and typological characteristics of the buildings on the island of Martinique were obtained from the study by Jenkins et al. for the CASAVA project (2009) while for the island of Guadeloupe the data were collected from the CAR study for the EXPLORIS project (2008). For Martinique, the areas studied are Saint-Pierre Le Prechuer and Le Morne Rouge (Figure 7.14); while for the island of Guadeloupe the area of Saint Claude was analysed (Figure 7.15).

Fig. 7.11 Island of Martinique (Google Earth Pro)

From the aggregated data for the island of Martinique (Table 7.1), it can be seen that the most frequent type of roofing in the three areas is metal roofing which comprises 65% of the sample analysed; the remaining part comprises reinforced concrete roofing, which in

Fig. 7.12 Island of Guadeloupe (Google Earth Pro)

some cases may be covered with a pitched metal sheet roof to promote ventilation and rain runoff, and this choice tends to make it difficult to identify the type of roofing accurately. The data concerning the vertical structure show a variation of the type in the three areas. In fact, in Saint Pierre and Le Precheur, there is a greater diffusion of rubble stone masonry (RSM) buildings, which is rare or absent in the town of Le Morne Rouge; the thickness of the post-eruption 1902 buildings varies between 20 and 40 cm, while the buildings constructed before the 1902 eruption are approximately 1 m thick; while Le Morne Rouge before the eruption was characterised by a high number of wooden buildings that were razed to the ground following the eruption.

Table 7.1 Major vertical and roof typology field classifications and the percentage of the total surveyed buildings they comprise. (Jenkins et al., 2011)

Vertical structural type	**Field code**	**Description**	**%**
Reinforced concrete frame	RCF	Reinforced concrete beams and columns from a frame which is infilled with cut block masonry	21
Reinforced concrete infilled frame	RCiF	The RC frame is built first and then infilled with a cut block masonry wall	30
Confined masonry	CM	The cut block masonry wall is constructed first and then the RC frame built around it	10
Cut block masonry	CBM	Square blocks, including perforated and solid concrete, terracotta or locally sourced blocks, that do not sit within a frame	16
Rubble stone masonry	RSM	Building blocks are not squared, generally arise from locally sourced material and do not sit within a frame	23
Roof Type	**Field code**	**Description**	**%**
Metal sheet	MG, MR, MP	Metal sheeting in good, reasonable or poor condition, nailed on to timber supports	66
Reinforced concrete	RC	Flat or pitched RC slab roof that covers the entire floor area of a building , usually with some overhang, resting upon the walls or as part of the frame	31
Tiles	Ti	Terracotta tiles nailed onto, or resting upon, timber supports	2

Furthermore, in the areas of Le Morne Rouge and Le Precheur, there is uncertainty in the definition of the RCF (Reinforced Concrete Frame) typology, as this typology should be characterised by an RC frame, with beams and piers, and infilled with cut block masonry; but it could be characterised as the infilled frame and therefore belong to the RCiF (Reinforced concrete infilled frame) class or as CM (Confined masonry); the distinction between the two classes lies in the order in which the frame has been filled. In fact, confined masonry has the frame built after the infilled masonry wall has been built, and a filled frame has the frame built before and the infilled masonry wall after. In terms of their respective vulnerability to dynamic lateral pressures associated with PDC, a confined masonry building is generally less vulnerable than a filled masonry frame due to a greater degree of continuity between the frame and the masonry. However, due to the plastering, it was not possible to define the detail of this typology in detail, and therefore only the RCF class was marked; furthermore, the low categorisation of RCF buildings in St Pierre indicates that many buildings were not plastered, potentially due to the older building stock or for economic reasons. The three test areas attest that RC frames are used over confined masonry. Concrete-filled frame buildings (RCiF) are a more regular construction method than confined masonry; therefore, it can be adopted preferentially over confined construction for multi-storey or complex-shaped buildings. Finally, in Martinique, many single-storey rectangular buildings were frame-filled, and RC frame buildings (RCiF and CM) were more prevalent than frameless cut-block masonry (CBM) buildings, most likely due to seismic regulations. Five main vertical structures have been identified for the island of Guadeloupe (Figure 7.13):

- RC infilled frame: Reinforced concrete slabs, beams and columns make up the frame, which is then infilled with squared masonry.
- RC shear wall: Sit within a reinforced concrete frame of slabs, beams and columns and are essentially vertically oriented wide beams that carry earthquake loads downwards to the foundation. The RC frame and walls are generally poured in situ.
- Rubble masonry: Building blocks are not squared and generally arise from locally sourced material, e.g. scoria blocks. These buildings do not always have mortar between the blocks and can be distinguished from squared masonry because of the wall thickness, generally around double (40cm thick) that of squared masonry (20cm thick).
- Squared masonry: This may include perforated concrete blocks, solid concrete blocks, terracotta blocks, or squared locally sourced material blocks and they do not sit within a frame. The regularity of blocks is especially important in terms

of earthquake shaking, with regular blocks less vulnerable than irregular or rubble blocks.

- Timber frame with lightweight cladding: Lightweight cladding includes timber boards or metal sheeting.

In addition, 5 types of roof have been identified:

- Pitched tiles: Tiles are generally terracotta and may either be nailed on to, or rest on, timber support battens.
- Pitched bitumen shakes: Bituminous tiles, or shingles, nailed on to timber supports.
- Pitched sheeting: Metal sheets nailed on to timber supports.
- Flat concrete: Reinforced concrete slab roofs that cover the entire floor area of a building, usually with some overhang, resting upon the building's walls or as part of the frame. A small number of reinforced concrete roofs in Guadeloupe are pitched and these should be considered to offer the same vulnerability as flat concrete roofs.
- Flat roofing felt: Roofs covered in roofing felt inhibit accurate assessment of the roof type, in the same way a plastered building inhibits assessment of the vertical structure. In Guadeloupe, such roofing felt may cover concrete or timber boards: the thickness of the roof may help in identifying the likely type.

A survey of the openings and shutters' typological characteristics was also carried out for the two French islands. Although different areas were analysed, even on the same island, Saint Pierre and Le Morne Rouge in Martinique, the same technologies and construction techniques were used. In fact, there is an absence of window frames (7.14 a) and the exclusive presence of full height shutters in UPVC (7.14 b) or solid wood shutters, and some buildings, those of recent construction, have louvre shutters (7.14 c). Finally, the only types of window and door frames found in the test areas are single-pane UPVC (7.14 d).

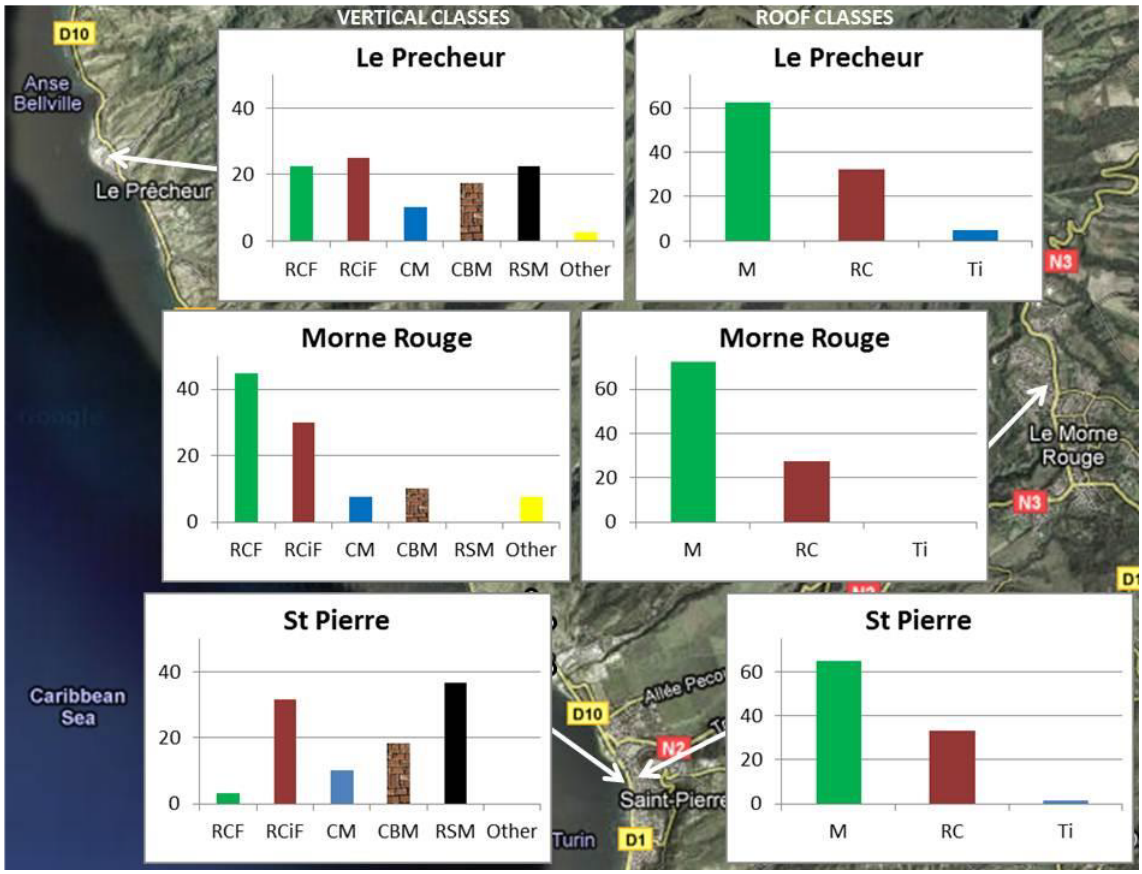

Fig. 7.13 Building vertical and roof typology distributions (as %) for three test areas in Martinique (Jenkins et al., 2011)

Fig. 7.14 a) example of absence of window's frame, b) typical UPVC louvre shutters, c) Example of uPVC roller shutters in new buildings, d) typical mixed UPVC windows and doors frame. (Google Earth Pro)

7.4 Teide (Tenerife)

Tenerife consists of a complex of overlapping Miocene-to- Quaternary stratovolcanoes that have remained active into historical time. Teide, the volcano in question for this study, is situated inside the Cañadas caldera, a 9 by 16 km volcanic depression at an altitude around 2000 m, formed after a long explosive period of volcanism. Teide, the volcano that dominates the centre of the island has an altitude at its summit of 3718 m, the highest point in Spain and indeed the Atlantic Ocean. Its height from the surrounding seabed is N 7000 m. It is the world's third-largest volcano after Mauna Loa and Mauna Kea in Hawaii. Currently dormant, it last erupted in 1798 with the mafic eruption of Narices del Teide, at the western flank of the twin volcano Pico Viejo. Teide has been very active during the last 5000 years with at least eight phonolitic eruptions from its central vents and flanks, including the subplinian eruption of Montaña Blanca at about 2000 years ago (Ablay et al., 1995 [1]; Carracedo et al., 2003 [6], 2007 [5]). The history of eruptive activity in the area includes both effusive and explosive eruption typologies (Marti et al., 2008) [22]. Tenerife's island was also the subject of the EXPLORIS project, particularly Icod de Los Vinos for which the hazards considered are earthquakes, pyroclastic density currents, and the ashfall. Each of these hazards affects the building differently. Therefore it was necessary to study the building heritage; in fact, Icod de Los Vinos has been divided into six zones (Figure 7.15), different for construction morphology. So zone 6 is characterised as the rural zone that was closest to Teide. Zones 2 and 5 are also rural zones or similar building density and morphology to Zone 6, but both further away from Teide and near the central transport infrastructure. Zone 1 is the coastal zone with similar if slightly higher density to Zones 2, 5 and 6. Zones 3 and 4 are urban zones, Zone 3 including the historical and commercial centre of Icod de Los Vinos, whereas Zone 4 represents the more recent city's more recent suburban spread (Marti et al, 2008) [23].

For each zone, data collected, such as vertical structure, age of construction, height, roof. The characteristics of the vertical structure (Table 7.2) and the height of the buildings (Table 7.3) greatly influence the resistance to earthquakes and PDCs. The data collected shows that vertical structures are classified into four groups:

Table 7.2 Classes of construction material for the vertical load-bearing frame and their identifiers (Marti et al., 2008)[23]

Field name	Type
CF	Reinforced concrete, in infilled frame
MB	Masonry in block/ squared/ cut stone
MR	Masonry, rubble
TI	Timber

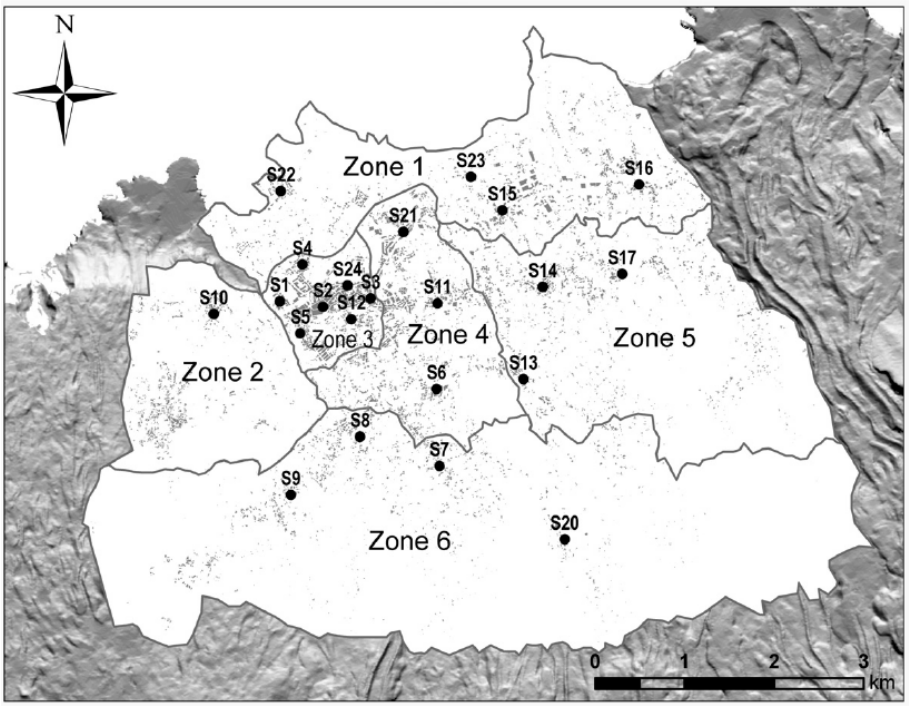

Fig. 7.15 Location of Survey Zones in Icod de los Vinos (Marti et al., 2008)[23]

While four groups were used for the height classification:

Table 7.3 Classes of building height and their identifiers (Marti et al., 2008)

Field name	Number of storeys
S	1 (single-storey)
L	2 (low-rise)
M	3/4/5 (medium-rise)
H	6+ (high-rise)

The types of roofing present are defined in Table 7.4

From the analysis of the building stock (394 buildings surveyed), the 54% of them had a concrete frame, 31% were constructed out of rubble masonry, 15% were constructed out of squared masonry 0.5% were built in timber (Table 7.4). Considering each zone of the valley, the proportion of the vertical structure change slightly; indeed in the zones 2 and 6 there are some examples of timber structures, besides the Zone 3, the historic centre has the highest proportion of rubble masonry buildings (Marti et al., 2008) [23]. The number of stories most diffuse is 2 or 3 with 56%, then the single storey with 36%, the 5% has 4 or 5 stories, and only the 2% has 6 or more stories. Few zones included any 6 stories or more, the exception remaining Zones 1, 3 and 4. These represent the central, urban/suburban and coastal zones, respectively. The centre of Icod de Los Vinos municipality (Zones 3 and 4) comprises high-rise residential and office buildings, and the coastal zone (Zone 1)

contains a few high-rise hotels and apartment blocks. The rate of old buildings was zero or negligible in Zones 2, 4 and 5, very low in Zone 1 and higher than average in Zone 3, which is the zone that represents the historic centre of Icod de Los Vinos. Surprisingly, Zone 6 also had many old buildings. The overall trend from this data shows that the outer zones of the Icod de Los Vinos area (Zones 1,2,5 and 6) have a greater homogeneity of building classes than the central urban and historic areas of Icod de Los Vinos (Zones 3 and 4) that show a wider variety of vertical structural typologies, building heights and ages. Tenerife's island was also surveyed using the Google Earth Pro programme to evaluate the openings' specific characteristics, such as the most common material used and the possible presence of shutters. In particular, the area of the built-up area of zone 2 was analysed (Figure 7.16), in which it can be seen that the most common windows are those with a wooden frame and it can also be assumed that a single pane of glass characterises them (Figure 7.18), followed by UPVC (Figure 7.17) and aluminium. Furthermore, the majority of the windows analysed in area 2 are without shutters (Figure 7.18). From the data collected by Marti et al.(2008) [23] and from the analysis of area 2 through Google Earth Pro, it underlines that for the island of Tenerife it is possible to intervene on the whole territory as the typological and structural characteristics are European and therefore with some similarities to the buildings in Campania.

From the exposure analysis carried out on the different islands, it is possible to state that only in some islands such as Tenerife and Azores it is possible to apply the strategies foreseen for the Campania region since they are European islands the structural and technological characteristics are similar to the Neapolitan reality. On the other hand, in the French Antilles and Philippines' islands, the building stock is different from the European one in terms of load-bearing structure and the fixture technologies used. Therefore, in order to define suitable volcanic mitigation strategies that at the same time could bring additional benefits, in the case of the islands of the Antilles and the Philippines the starting point was to start from mitigation strategies for cyclones and make them also volcanic. Hurricane Hugo hit the island of Guadeloupe in 1989 (Figure 7.19); the hurricane when it arrived in the Caribbean was a category 4 hurricane with speed between 209 and 251 km/h. Damage to buildings ranged from superficial to total devastation (Emanuel et al., 2006) [13]. Many roofs were damaged or destroyed, and nonstructural elements such as doors, windows, and cladding also suffered extensive damage. Single-story concrete buildings weathered the storm well, with minimal damage (Li et al., 2006) [21].

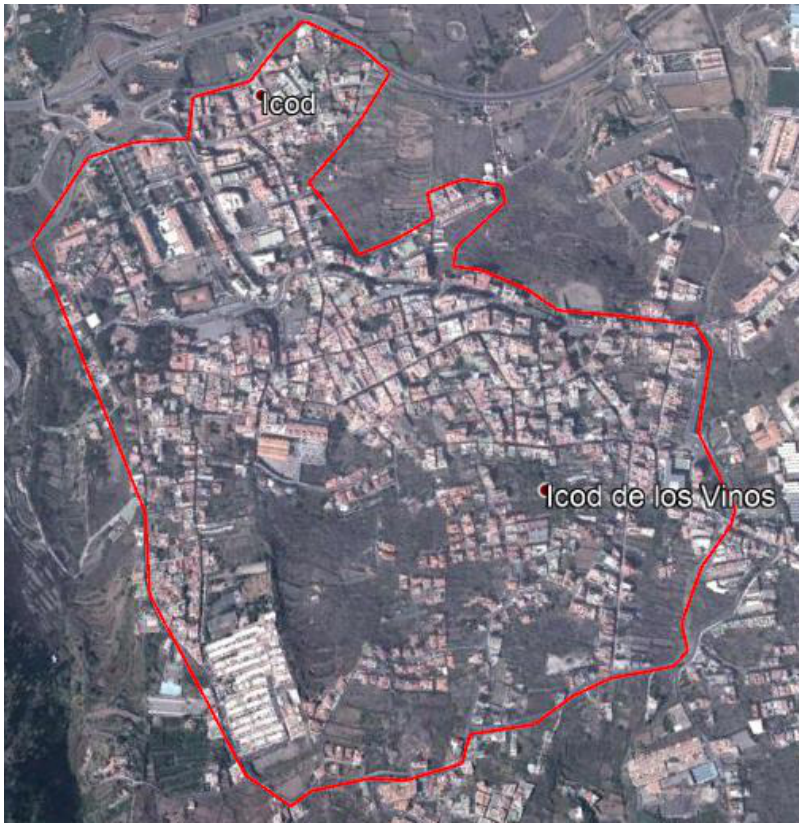

Fig. 7.16 Analysed area of the zone 2 of Icod de los Vinos. (Google Earth Pro)

Fig. 7.17 Example of UPVC windows (Google Earth Pro)

Table 7.4 Roof classes, their resistances, and the equivalent roof structures found in the Icod de los Vinos survey (Marti et al., 2008) [23]

Roof Class	Description	Roof structure classes found in Icod de los Vinos survey	Typical design load range
WE (weak)	Sheet roofs, old or in poor condition. Tiled roof, old or in poor condition. Masonry vaulted roof.	Old pitched tile or sheet metal	Pre-design code, or no design code.
MW (medium weak)	Sheet roof on timber; average quality; average or good quality tiled roof on timber rafters or trusses. Steel or precast rc joists and flat terrace roof.	Modern pitched tile or sheet metal, old flat or pitched concrete	1–2 kPa
MS (medium strong)	Flat RC roof not all above characteristics; sloping rc roof. Sheet roof on timber rafters or trusses, good quality and condition, designed for cyclone areas	Recent pitched tile or sheet roofs, modern flat or pitched concrete	2–3 kPa
ST (strong)	Flat RC roof designed for access; recent, good quality construction, younger than 20 years.	Recent flat or pitched Concrete	>3 kPa

Fig. 7.18 Example of wooden windows (Google Earth Pro)

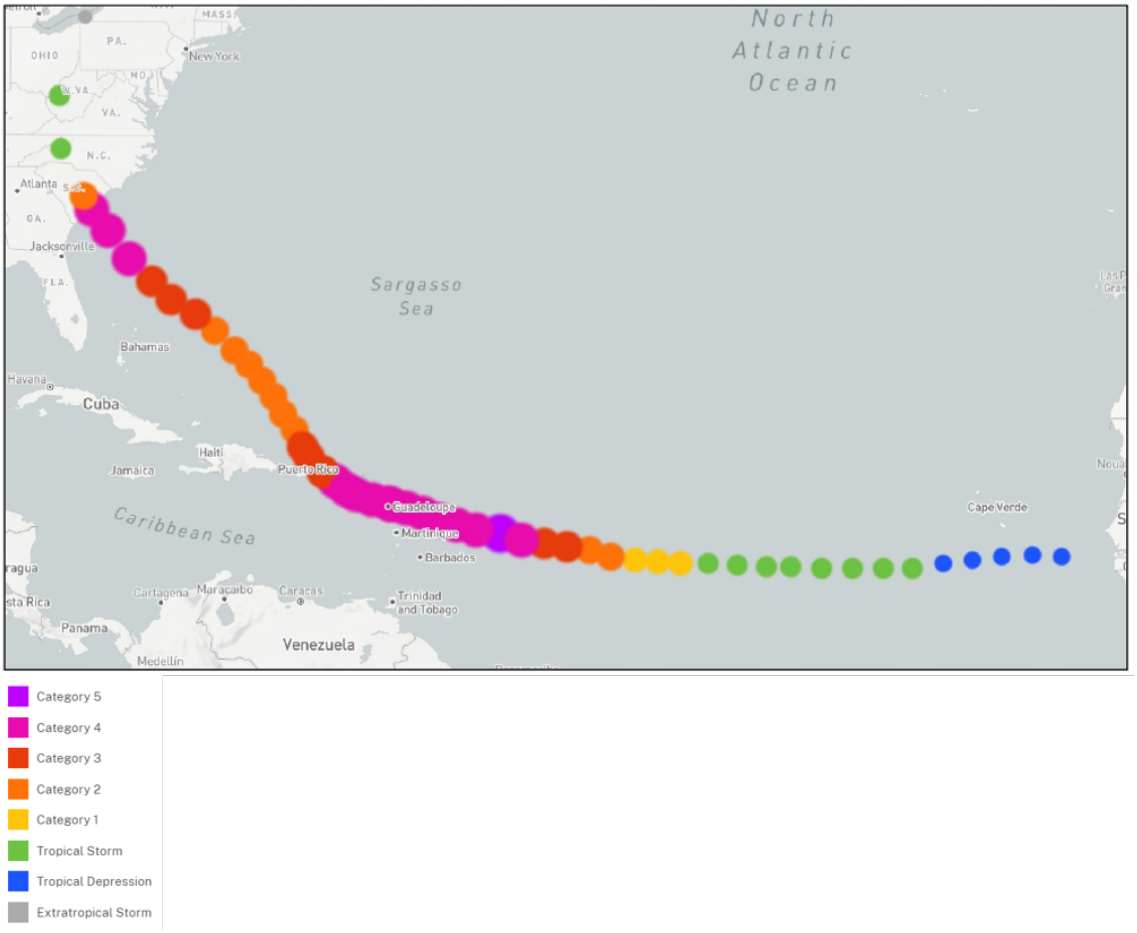

Fig. 7.19 Path map and intensity of Hurricane Ugo

Chapter 8

Synergy Volcanic and Hurricane mitigation

The Soufriere Hills volcano (Montserrat) experience showed how simple measures could enable the building to withstand the impact of pyroclastic flows. The strategy used was to place a minimum thickness wood panel over the openings, a frequently used intervention due to its economy and application speed. Therefore, for the areas of the French Antilles and the Philippines, where both volcanic and storm risk coexist, additional cyclonic mitigation was studied that may also represent a useful strategy for volcanic risk. The starting point was to analyse the documentation provided by both FEMA (Federal Emergency Management Agency) and the Guide de construction parasismique et paracyclonique de maisons individuelles a structure en bois aux Antilles (The Parasismic and Paracyclonic construction guide for individual homes with wooden structure), a kind of technical manual for the construction of new houses that can withstand cyclonic and volcanic stress.

8.1 FEMA

FEMA specifies different levels of mitigation strategies and their costs for roofs, windows and walls. There are three mitigation packages described in the guide - Basic, Intermediate, and Advanced - providing improved resistance to wind damage; each protection level can only be achieved if the retrofit projects included in the lower levels have been performed. The level of protection provided by the Advanced Mitigation Package can only be achieved if the projects included in both the Basic and Intermediate Mitigation Packages have been implemented. The Basic Mitigation Package is the most straightforward initial package for a residential retrofit project. It focuses on securing the roof system and improving the

Fig. 8.1 Example of building which withstood the pyroclastic pressure (Baxter,)

water infiltration resistance of the existing house. The Basic Mitigation Package is the initial, most basic package for a residential wind retrofit project. It focuses on securing the roof system and improving the water intrusion resistance of the existing home.

1. Improving the roof system through one of two options:
    - Option 1 – Improve roof with roof covering replacement
    - Option 2 – Improve roof without a roof covering replacement
2. Strengthening vents and soffits
3. Strengthening overhangs at gable end walls (if gable end walls exist on the home)
4. Protecting openings (if located within the windborne debris region).

The intermediate mitigation package is the second level of high wind mitigation. For this package to be useful, the basic mitigation package's mitigation measures must first be properly executed. The intermediate mitigation package includes retrofits to preserve openings, further increase the strength of gable ends that are over 1.20 metres high (if applicable) and improve the anchorage of attached structures such as porches and carports. Building openings include windows, skylights, doors and garage doors. If these components fail in either scenario, fluid could enter and cause extensive damage. Indeed, wind pressure and pyroclastic flows are likely to increase the possibility of structural and non-structural failure. Besides, the temperature of the hot ash could ignite a fire that could spread throughout the building. The tornado opening protections, described in the guide, belonging to the Intermediate Mitigation Package are:

- An approved impact-resistant covering capable of resisting windblown debris impacts can be installed over an existing unprotected opening (such as a window or door). Types of impact-resistant coverings include shutter systems and fabric and screen products.

- An approved impact-resistant product (such as a new window or door assembly) can be installed in place of a product that is not designed to resist such forces or as an alternative to impact-resistant shutters or screens.

Shutters are a common and cost-effective technique for mitigating windblown debris, especially when the glass is not suitable. Shutters can be divided into two macro-groups: temporary and permanent. The former is cheaper but needs specific interventions for fixing and require special attention for conservation, such as the wood panel, which is the cheapest strategy but has a shorter life, and it is necessary to identify an area for conservation that does not allow possible rotting. On the other hand, Permanent shutters are more expensive and are always in place and ready for immediate closure (Table 8.2).

There are different types of shutters; the most common ones are:

- colonial,

- the Bahamas,

- roll-up,

- accordion.

FEMA recognises these shutters as possible hurricane mitigation strategies. Considering the volcanic hazards, they are unsuitable because they are made of plastic material, generally PVC with a glass transition point of 80°C. However, a first starting point can be identified in some types such as colonial and accordion because the two opening systems are suitable even if solid panels are placed.

A further mitigation system proposed by FEMA is the impact-resistant window, which is made of laminated glass in the case of tornadoes. This strategy requires replacing the existing window with the new assembled one that meets the hurricane-prone areas resistance criteria. Generally, laminated glass is made by interposing a PVB film which increases the mechanical characteristics. This proposal cannot effectively respond to volcanic hazards, as the film is a plastic material whose mechanical behaviour is strongly influenced by temperature variations. Therefore, in this case, it could always be proposed to replace the existing window with a new one that is made with tempered glass on the outside and laminated glass on the inside. Finally, FEMA's final strategy is the overlapping of light and transparent polycarbonate panels with high impact resistance qualities. The

Fig. 8.2 Shutter styles (FEMA 2010, Technical Sheet No.6.2)

sheets' resistance is much higher than that of non-laminated glass (i.e. more than 200 times stronger) or acrylic sheets or panels (i.e. more than 30 times stronger). Since it is a plastic material, this mitigation proposal does not respond appropriately to a possible volcanic event.

Fig. 8.3 Example of Polycarbonate system

Table 8.1 Shutter Type Cost Advantages

Shutters Type	Cost	Advantages	Disadvantages
Wood Structural panel	Low	Inexpensive	Must be installed and take down every time they are needed; must be adequately anchored; difficult to install on upper levels; storage space is needed
Metal or polycarbonate panels	Low/Medium	Easily installed on lower levels	Must be installed and take down every time they are needed; must be adequately anchored; difficult to install on upper levels; storage space is needed
Accordion, manual closing	Medium/High	Always in place; ready to be closed	Always in place; ready to be closed. Must be closed manually from the outside; difficult to access on upper levels
Permanent, motor driven	High	Easily opened and closed from the inside	Expensive It is important to find a motorized shutter that allows the shutter to be manually raised in order to allow the interior to vent following the storm and prior to electrical power restoration

Another critical issue is the water intrusion around window and door openings, which can cause dry rot and fastener corrosion that weaken the window or door frame or the wall itself, and lead to water damage to interior finishes, mould growth, and preventable building damage during coastal storms. Proper flashing sequence must be coordinated across responsibilities, sometimes divided between two or more trade activities (e.g., weather barrier, window, and siding installation). Window and door frames must be

adequately attached to walls, and they must be adequately integrated with the wall's moisture barrier system to avoid wind-driven rain penetration and high wind pressures, For installations that require an exposed sealant joint, installing a removable stop (see Figure 2) is recommended to protect the sealant from direct exposure to the weather and reduce the wind-driven rain demand on the sealant.

- **Frame anchoring** : Window and door frames should be anchored to the wall with the type and number of fasteners specified by the designer.
- **Shutters** : If shutters are installed, they should be anchored to the wall rather than the window or door frame.
- **Weatherstripping** : E 2112 does not address door weatherstripping. However, weatherstripping is necessary to avoid wind-driven rain penetration. A variety of weatherstripping products are available (Figures 8.4 a and 8.4 b).

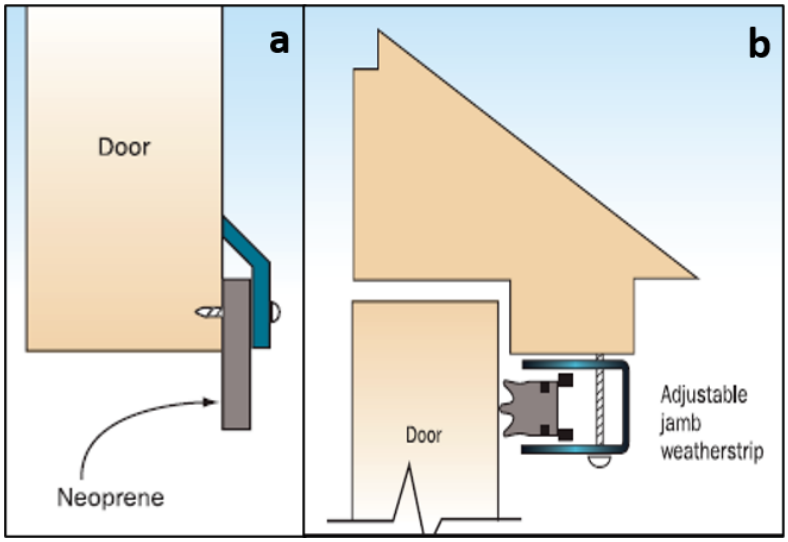

Fig. 8.4 a) Neoprene door bottom sweep. (FEMA 2010, Technical Fact Sheet No. 6.1) b) Adjustable jamb/head weatherstripping. (FEMA 2010, Technical Fact Sheet No. 6.1)

As far as roofs are concerned, the FEMA guide foresees the Basic package two options, as described above, total replacement of the roof or improvement without replacement (Figure 8.5). The first option can be studied in detail for ashfall verification, in particular, to define material ignition temperatures and exposure time. The objective is to identify flame-retardant materials and have a low heat transfer coefficient to perform the insulation function correctly. For the second option, the aim is to perform load analysis and design a shaped roof to validate the ash flow.

The guide mentions that the most common exterior wall coverings (Figure 8.6) include vinyl veneer, brick veneer, concrete fibre coatings, wood coatings and hardboard. All types

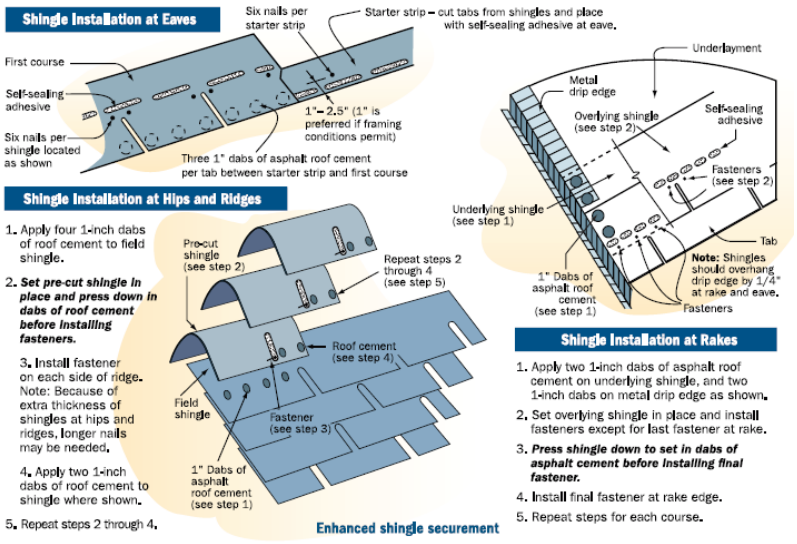

Fig. 8.5 shingle installation procedures (FEMA (2010) Technical Sheet No.7.3)

of wall coverings can work well in strong winds if installed correctly for strong winds. The focus may be on analysing such systems' technical data to understand what pressures they can withstand and verify their resistance to high temperatures. Besides, it is necessary to define a stratification of the wall in order to take into account the energy saving problem.

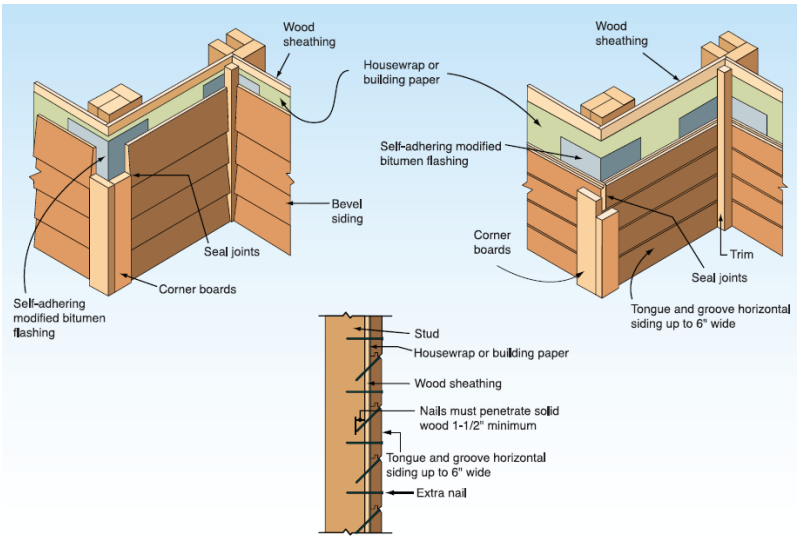

Fig. 8.6 Wood siding installation details (FEMA 2010, Technical Sheet No. 5.3)

8.2 Parasismique and Paracyclonic construction guide

The Parasismique and Paracyclonic construction guide for individual homes with wooden structure" by AFPS designates two types of braces.

- VT "work sails" bracing: the bracing panels are prefabricated plywood elements or OSB/3 or OSB/4 plates nailed to a wooden frame with reinforced end studs.
- Bracing with "triangular stability brackets" PST: the bracing panels consist of a wooden frame with wooden diagonals, called slings, which work essentially in compression. The uprights framing the braces are reinforced

. The following general conditions must be observed for the location of the upwind panels:

- Bracing panels must be installed in load-bearing walls (facades or partitions).
- The minimum number of bracing panels to be placed on the façade is at least half the total number of bracing panels resulting from the sizing for the appropriate scenario;
- Minimum required for façades $\leq$ 10m in length: 2 bracing panels per façade (one at each end of each façade);
- Minimum required for façades > 10 m long: 3 bracing panels per façade (one at each end and one in the middle third of each façade).
- In the case of a simple facade step (rectangular terrace), each of the recessed facade lengths, ending in one of the corners must include at least one bracing panel.
- In the case of a double step on the façade (L-shaped terrace), each of the recessed sections of the façade, ending in one of the corners, must include at least one bracing panel; in addition, the external corner of the building must have a bracing panel in each direction. (See schematic diagram in article 3.6.).
- In the wind bracing panels for working walls, the total length of the façade panels is at least 4.8 m per wall.
- The distance between two parallel load-bearing walls, facades, and cracks, including bracing panels, is less than 5 m.

8.2.1 VT System

This bracing type is only allowed for the bracing of houses in a single ground floor or ground floor with the partial attic floor. The framework wood must be softwood (exotic wood D40 is excluded). The working sails are panels prefabricated in the factory or the workshop. They are made by nailing plywood or OSB panels (or plates) to a reinforced wood frame. They are inserted in the reservations of the current framework, in the places required by Article 3.3. No opening, drilling or other types of weakening is tolerated in the panels of the working sails. Each working sail is made up of one or two sheets, laid at full

height, following the specifications of EN 13986. These plates are nailed, preferably with a pneumatic hammer, on all the uprights (peripherals, walls, and intermediate) and on the crosspieces of the supporting framework which they cover. (Figure 8.7) If the working veil is made up of 2 plates, at the right of the vertical joint of 2 to 3 mm must be left between the plates to ensure a good seal take into account dimensional variations due to humidity

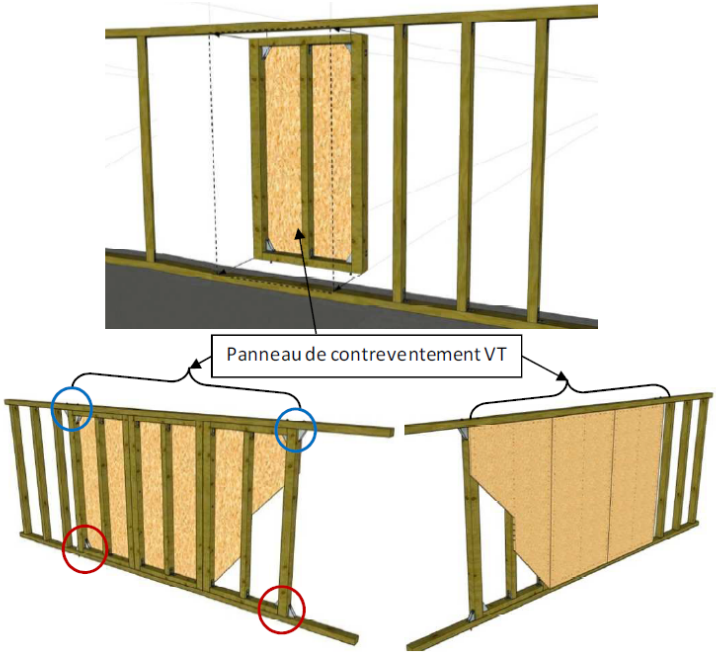

Fig. 8.7 Perspective view of the VT system

The OSB, Oriented Strand Board, consists of orientated spruce and pine chips held together by a synthetic resin and then pressed together to form several layers with a smooth surface.

- Good resistance to horizontal wind and seismic stress: due to its structure, it is widely used as a bracing element for external building constructions.
- Excellent quality/price ratio: for this reason, it is one of the most popular woods, offering very high quality (in terms of performance and versatility) and at the same time a low price.
- It has a uniform surface: composed of small elements (the lamellas) glued and pressed, it is free from deformation under stress, knots, cracks, cavities and weak points.
- Sturdy and non-deformable: Due to the previous characteristic, OSB offers high mechanical resistance to stress, remaining non-deformable (at least from a macroscopic perspective).

There are four types of OSB:

- OSB 1 are panels for general use, non-structural, and interior design (including furniture) are used in a moisture-free environment.
- OSB 2 more resistant than OSB 1, therefore load-bearing panels, but always suitable for a dry environment (usually used for packaging, platforms, exhibition displays).
- OSB 3 used to make the roofs of small sheds; these panels are therefore suitable for structural use in humid environments thanks to a unique adhesive.
- OSB 4 are load-bearing panels for structural use, resistant and suitable for humid environments.

Wood-based panels used for wall cladding other than working walls VT (bracing) should preferably be made of a less resistant material than that of the working walls (CTBX plywood panels in thickness < 12 mm, CTBH chipboard panels or OSB panels in thickness < 12 mm and density < 650 kg / m3). The nailing density of the panels not participating in the bracing must be halved so that these elements remain less stiff than the bracing panels. Once the constituent elements of the system have been defined, it is necessary to evaluate with particular attention the thermal resistance as the types presented by AFPS are designed for high-speed winds and seismic actions. The thermal analysis must start from studying the fire reaction, that is, the predisposition of material to participate in a fire's development. During the tests, indicators such as temperature, smoke development, drops, or debris falling to the ground, are measured. The European Standard EN 135011 provides the reaction to fire classification procedure for all products and building elements. According to it, reaction to fire is the response of a product in contributing by its decomposition to a fire to which it is exposed, under specified conditions. Besides, the additional designations are:

Smoke:

- S_1 = little or no smoke generation,
- S_2 = medium smoke generation,
- S_3 = heavy smoke generation

Burning droplets:

- d_0 = no droplets within 600 seconds
- d_1 = droplet form within 600 seconds but do not burn for more than 10 seconds
- d_2 = not as d0 or d1

Eurocode 5 provides a formula to calculate the combustion speed of a wood-based panel according to the panel's density and thickness. The calculations are the same whether the panel is fireproof or not.

$$\beta_0 = 0.9 \cdot \sqrt{\frac{450}{\rho_k}} \cdot \sqrt{\frac{20}{h_p}} \text{if } h_p < 20 \text{ mm} \tag{8.1}$$

$$\beta_0 = 0.9 \cdot \sqrt{\frac{450}{\rho_k}} \tag{8.2}$$

The breakage time of the panel protection if directly exposed to fire can be calculated (keeping 4 mm of safety for the panel fixing) with the formula:

$$t_f = (h_p - 4)/\beta_0 \tag{8.3}$$

Further consideration must be given to the presence of formaldehyde, a substance contained in glues that is carcinogenic, therefore as specified in appendix B of UNI EN 13986, the panels used must be classified with class E1 with low emission. Consulting various technical data sheets of OSB panels, some characteristics have been reported in Table 8.2:

Table 8.2 Mechanical and thermal characteristics of an OSB panel

Characteristics	Unit of measure	Value
Density	[kg/m^3]	550
Longitudinal modulus of elasticity	[N/mm^2]	4800
Transverse modulus of elasticity	[N/mm^2]	1900
Thermal conductivity	[W/mK]	0,1
Poisson's ratio	-	0.23
Reaction to fire	-	D-s2, d0

8.2.2 Bracing System

Triangulated stability bents are wall elements that provide bracing by the presence, in particular, of diagonals made up of wooden bars, later called "slings", fixed to a locally reinforced wooden framework (Figure 10.8). A triangulated stability brace is a panel consisting of two continuous diagonals working essentially in compression, crossing the intermediate uprights and fixed on reinforced end uprights. Depending on whether the triangulated beam is fixed on a foundation or directly on the floor, its height h is between 1.90m and 2.50m. The nomenclature of the different types of triangulated bents (PST1,

Table 8.3 Geometrical characteristics of bracing system

Type	Height [m]	Length (b) [m]	Number of intermediate montants	Features
PST1	2,70	1,20	2	Brace with diagonals in 2intermediate uprights spaced 0.40 m apart.
PST2	2,70	1	2	Brace with diagonals in 2 intermediate uprights spaced 0.33 m apart.
PST3	2,70	1,80	4	Brace with diagonals in 2 intermediate uprights spaced 0.36 m apart.
PST4	2,70	1,40	2	Bearing with two interrupted intermediate uprights and an uninterrupted continuous diagonal.

PST2, PST3, PST1sol and PST2sol, PST4), their characteristic lengths and requirements are defined as follows (Table 8.3).

Besides, the following provisions and conditions must be complied with:

- In multi-storey houses, only stability beams of type PST1, PST2 or PST3 are used.
- Additional beams can be placed in the inner load-bearing walls perpendicular to the facades to reduce the lifting forces at the foot of the bents and reduce the horizontal diaphragm (roof or floor).

As a result of this examination of seismic and cyclone mitigation techniques defined by AFPS, the second solution (PTS) is suitable for some considerations for volcanic mitigation, as the resistance of the building depends on the position and the bracing (Figure 10.9 and 10.10) itself and this allows to hypothesize the use of stratified panels able to withstand the expected pressures and temperatures.

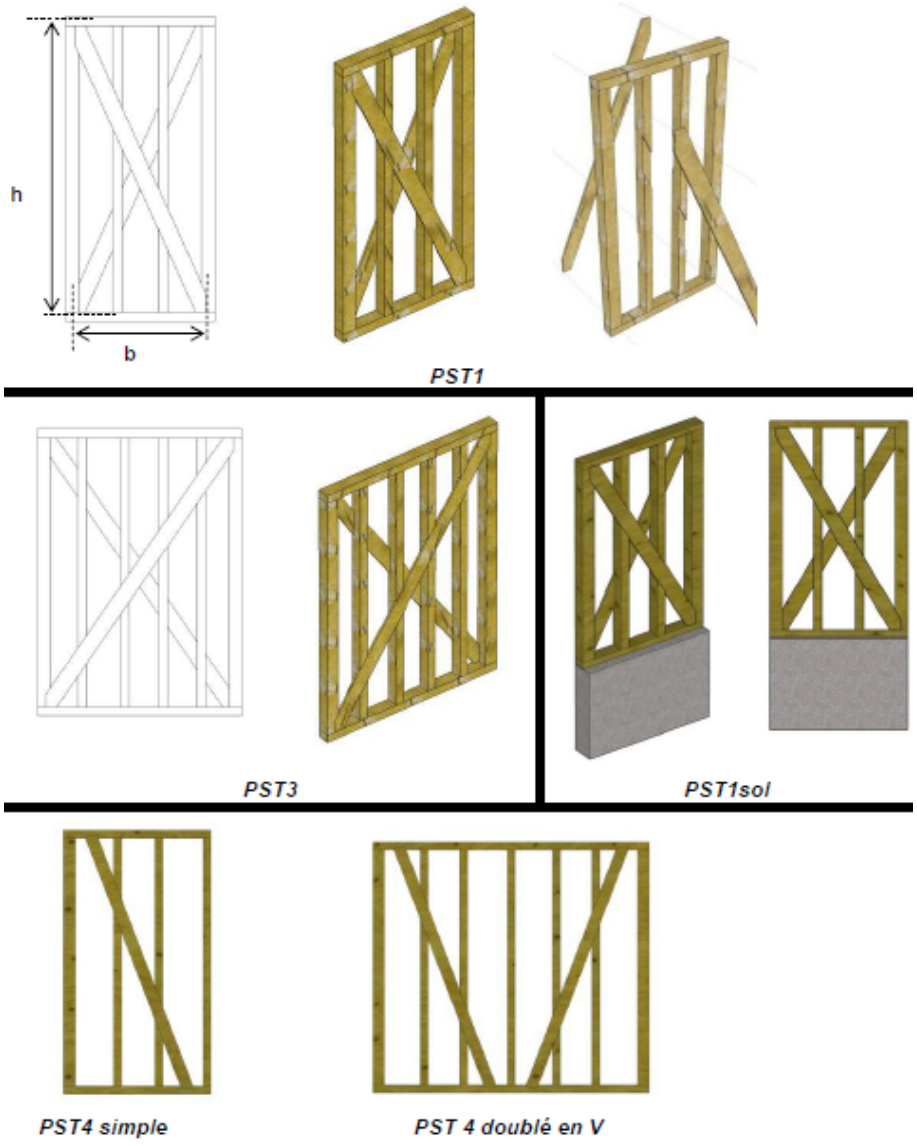

Fig. 8.8 Types of bracing system

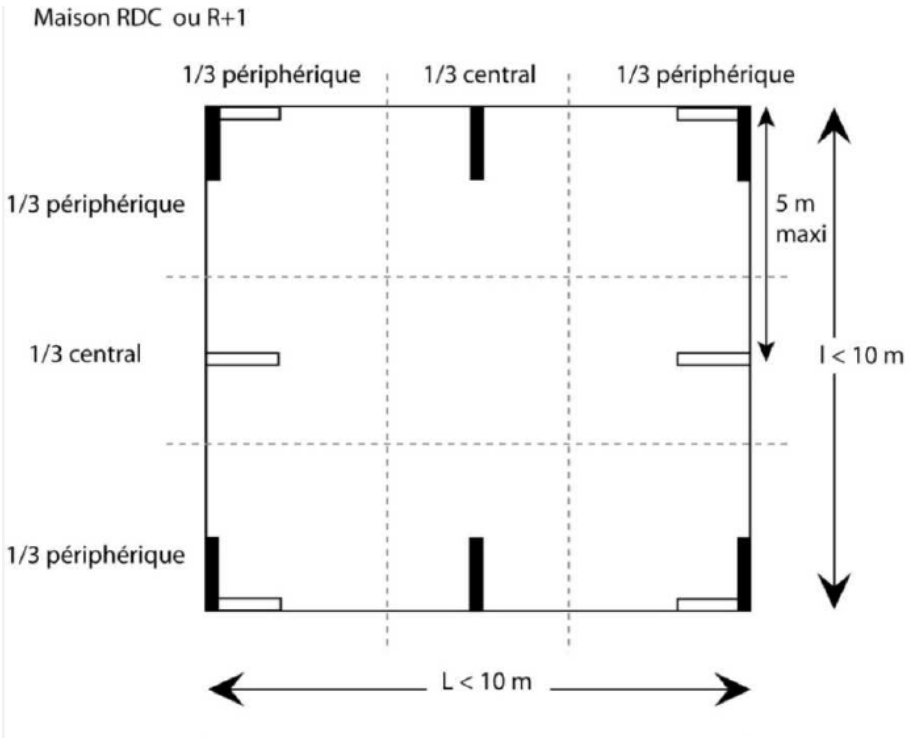

Fig. 8.9 Plan view of the bracing arrangement

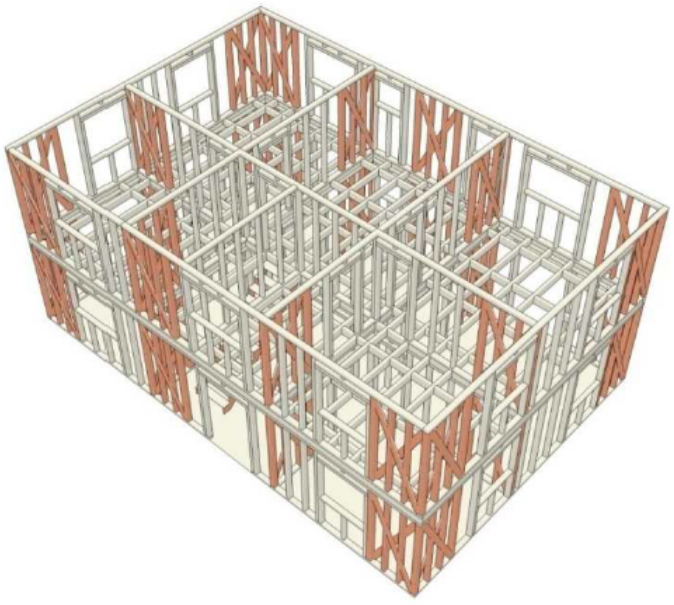

Fig. 8.10 Perspective view of the bracing arrangement

8.3 Assessment of bracing system

The model considered was evaluated at both temperatures and pressures predicted in Guadeloupe by Esposti Ongaro et al.(2020) [29]. Esposti Ongaro et al.(2020) [29] assumed that the 1530 CE eruption is a typical sub-Plinian (VEI 3) magmatic explosive eruption. The 1530 CE eruption began with phreatic explosions followed by partial collapse of the edifice that emplaced a debris avalanche (Komorowski et al. 2002 [19], Komorowski et al. 2005 [18] ; Boudon et al. 2008 [4]) which travelled at least 9 km in the South-West direction and reached the sea at Basse-Terre (Figure xxx). It then evolved into a short (ca. 1 h long) subplinian phase (with an intensity of between 5×106 and 2×10^7 kg/s; Komorowski et al. 2008, [20]). Also, four scenarios were considered, named SP1 through SP4, differentiated not only by the physical characteristics of the solid particles but also by the vent's size, which was positioned at [642985; 1774280] in UTM 20N WGS84 Cartesian projection. In particular, scenario SP4 represents the final summit crater collapse stage during a subplinian event and should be considered as an extreme but credible scenario for the culminating phase of the eruption. Due to the high mass flow rate, this scenario is characterised by high-speed pyroclastic flows that have a much longer run out. Esposti Ongaro et al. (2020) analysed the pyroclastic density currents initially branch and follow two main directions (one mainstream in the Rivière Noire valley and a second, minor stream through the Bains-Jaunes area; (Figure 8.11), but they eventually merge after about 2 km. About 300 s after the beginning of the collapse phase, PDCs have reached the inhabited region of St. Claude and become branched along the central valleys. Simultaneously, a large part of the collapsed mass is conveyed along the Rivière du Galion valley to the South into a narrow valley section (the Chute du Galion; Figure 8.11) and branches into two main flows. The first eventually merge South of the town of Saint-Claude (Rivière Dugommier valley) with the South-West branch, while the second form a channelised PDC propagating 6–7 km South from the vent, overtopping the Palmiste ridge to flow down towards the town of Trois- Rivières, along the Rivière du Petit-Carbet valley (Figure 8.11). To the East, the main branch is directed along the Rivière du Carbet (Grand Carbet) valley, towards the headland of Pointe-du-Carbet (Figure 8.11), where it is able to reach the sea (about 10 km from the vent). Figure 8.12 for the SP4 scenario shows that pyroclastic flows reach inhabited areas over the entire South-West sector and towards the East e the PDCs can maintain their initial high temperature (above 427 °C). While Figure 8.13 stresses the West, St. Claude and Matouba would be subject to PDCs with dynamic pressures exceeding 10 kPa at the edge of the town closest to the vent and > 5 kPa over most of the town (Figure 8.13). Pyroclastic density currents with dynamic pressures of >1 kPa would extend as far as the town of Basse-Terre, and to the South, dynamic pressures of > 1 kPa are predicted at distances out to about 6 km. To the

East, both the Rivière du Carbet and Rivière du Perou valleys would be affected, with the inhabited region of the town of Capesterre-Belle-Eau impacted heavily by dynamic pressures of > 3 kPa. The region affected by dynamic pressures of > 1 kPa extends almost to the coast down the Rivière du Carbet valley (Figure 8.13).

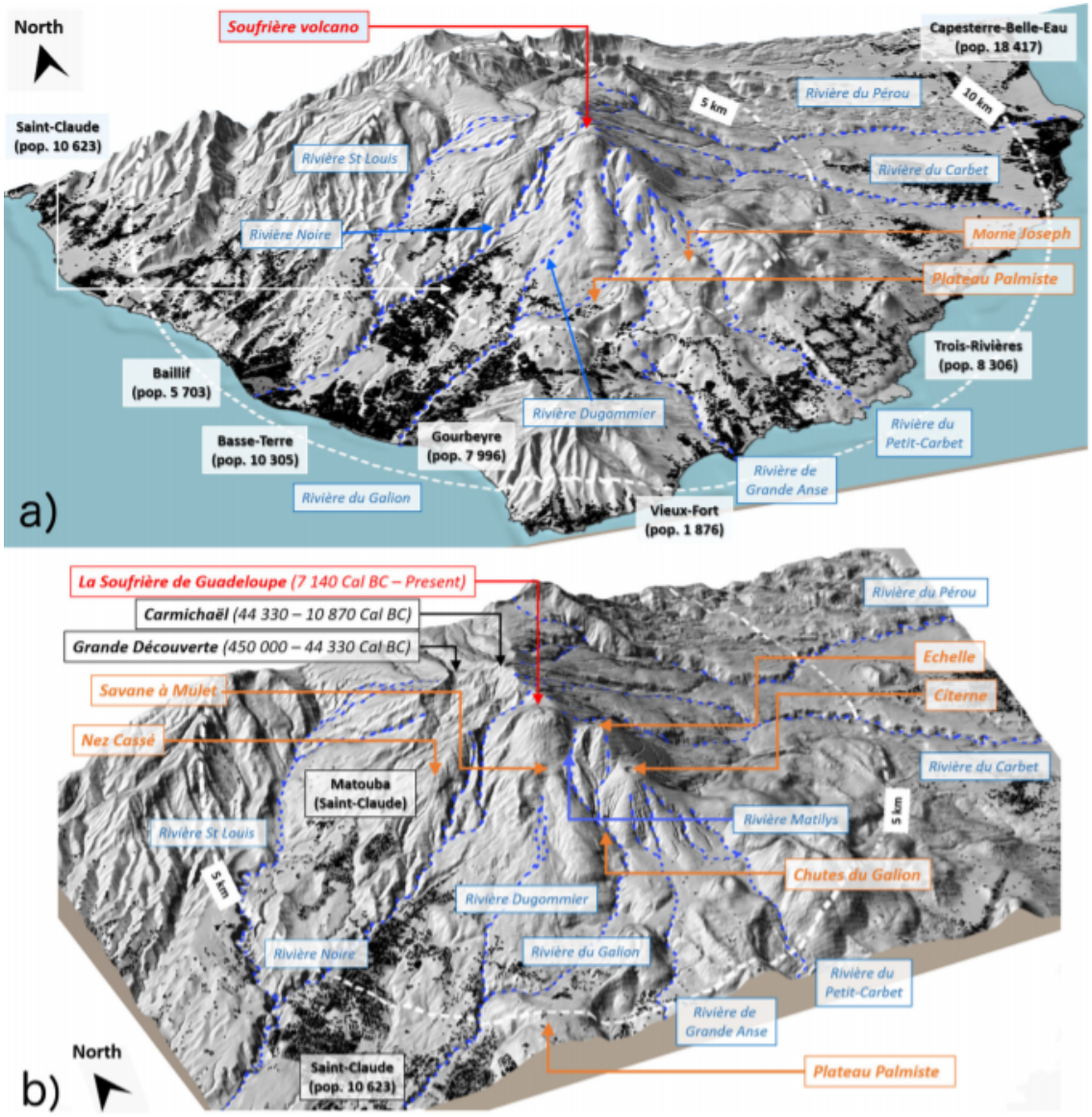

Fig. 8.11 Main topographic elements and locations mentioned in the paper: a) Southern Basse-Terre area (study zone), b) zoom on the SDG most proximal area

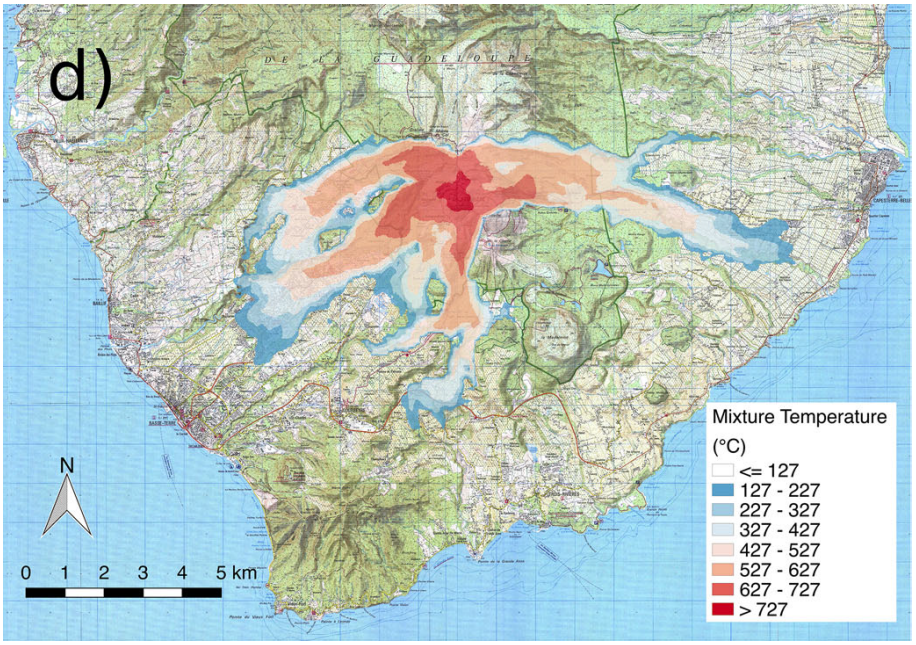

Fig. 8.12 Map of maximum dynamic pressure estimated for each point in the domain for scenarios SP4 (Esposti et al., 2020)[29]

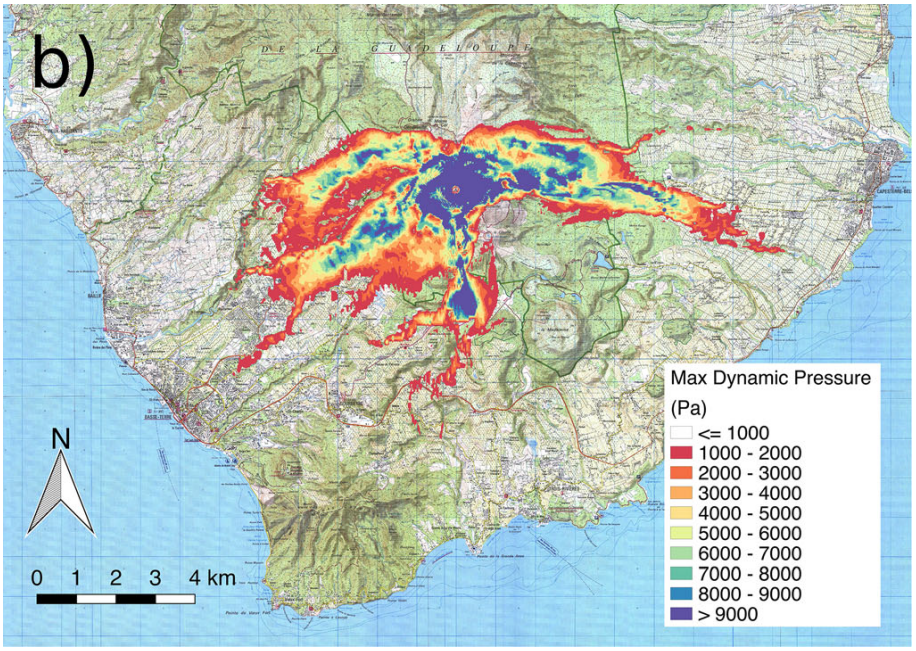

Fig. 8.13 Map of maximum dynamic pressure estimated for each point in the domain for scenarios SP4 (Esposti et al., 2020)[29]

Furthermore, applying the idea of incremental innovation, in order to make this panel capable of resisting the expected stresses, fireproof rock wool panels of 5 cm were added and to cover the whole, solid wood panels of 2 cm thickness were placed, connected to the upper and lower beams by mechanical connection, in addition, the dimensions of the panel were assumed to be 3 x 2.2 m (Figure 8.14).

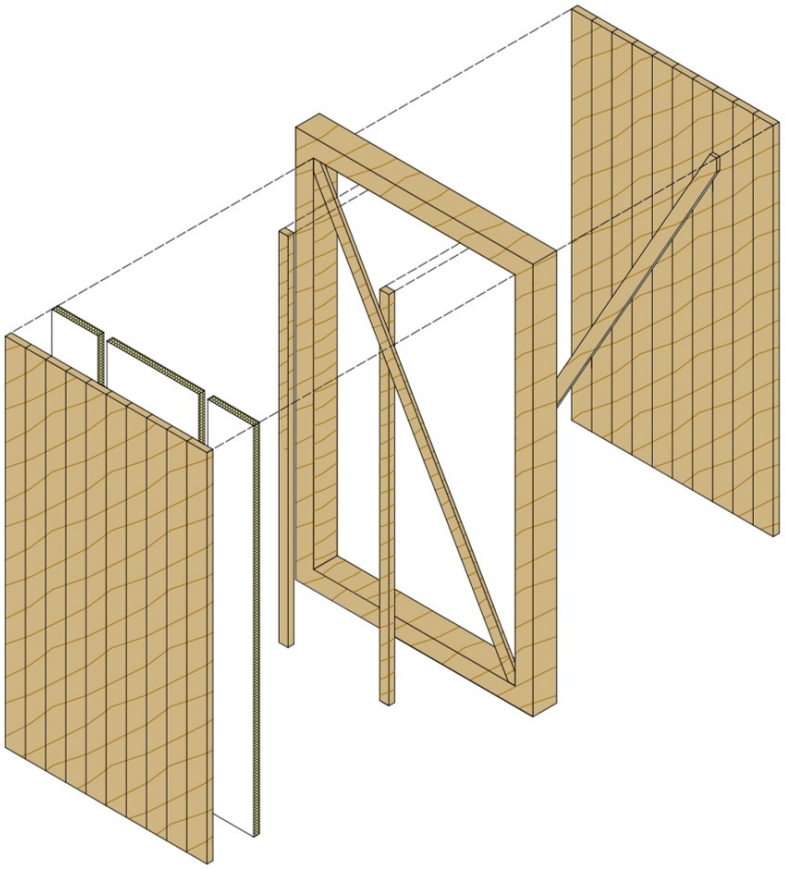

Fig. 8.14 Axonometric exploded view of the assumed panel

The first analysis is in the thermal field (5.21) to determine the wood's critical temperature that can trigger a fire. The model considered is half panel to reduce the computational time by imposing a symmetry condition (5.49) in the other direction.

The temperature, defined by the function (5.46), was applied to the external panel, which reaches the maximum temperature of 400°C in 240 seconds. The results show that the outer panels reach the critical temperature of 350°C for about 20 seconds in total (Figure 8.15). Thus, as defined by Jenkins et al. (2014) [17], the ignition probability is very low. In contrast, the interior panels record a constant temperature of 20 °C (Figures 8.15).

Subsequently, the panel was also analysed at the pressures (xxx) predicted by the scenario of Esposti Ongaro et al. (2020). In particular, the stresses generated in the external

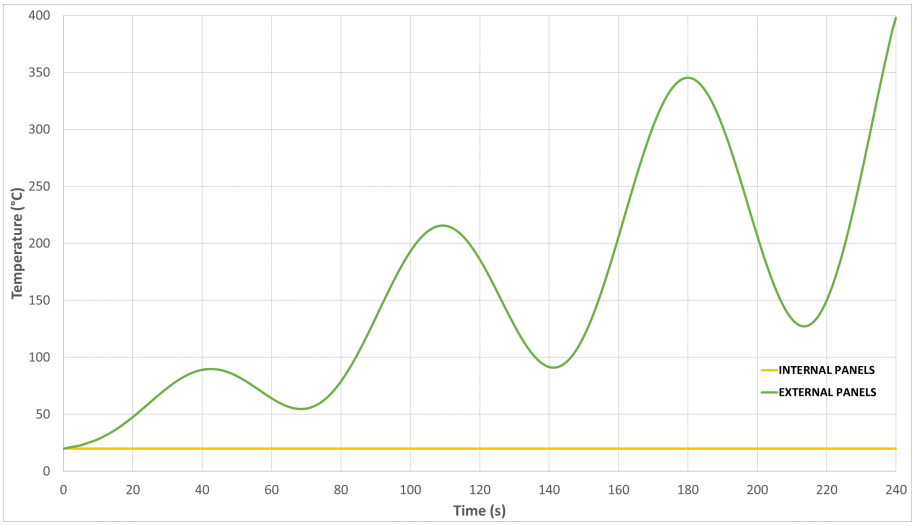

Fig. 8.15 Temperature reached by the outer wood panel (green curve) and the inner wood panel (yellow curve)

panels and the diagonals inside the frame were evaluated. The model has been assumed embedded, imposing along the external frame surfaces, the fixed constraint condition (5.42).

A symmetry condition (5.48) was also imposed in the static analysis. In addition, in order to model the system in the best possible way, a contact condition was defined both between the surfaces of the two diagonals and between the diagonal and the external panels. Finally, the material assumed for the whole structure is pine wood, assuming a linear elastic behaviour (5.6); furthermore, possible interactions of the insulation panels were excluded. The mechanical analysis shows that the external panels can withstand a pressure of 10 kPa, while the internal diagonals can withstand 5 kPa (Figure 8.16).

Finally, although the actions were considered separately from the results obtained, it is possible to state that the model considered is a valuable strategy for areas that are subject to volcanic and hurricane risk, where it would not be possible to intervene with the same strategies identified for Campania.

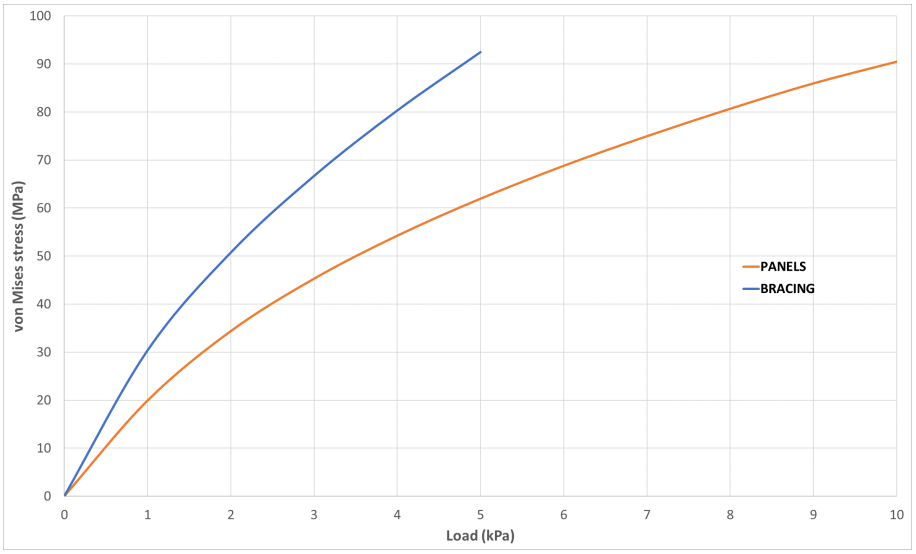

Fig. 8.16 von Mises stresses recorded in the outer panels (orange curve) and in the bracing (blue curve)

Conclusion

This thesis presents a new model of analysis of building elements' vulnerability to PDCs hazards and ash fall following an explosive eruption expected in the Neapolitan areas. In the case of PDCs, the vulnerability analysis was presented in detail by explaining the governing equations, and the analytical procedure was described for mechanical and thermal stresses. Moreover, the various types of window frames and their components were analysed in detail, assessing the relative vulnerabilities to stress exerted by the flows. These first analyses have shown that the PDCs represent a risk, especially for the temperatures that characterise them; in fact, not only glass fails due to thermal stress, but also the other constituent elements such as seals and thermal break are vulnerable as thermoplastics. In order to fully illustrate the extension of the temperature vulnerability analysis method, two functions are described. One expresses the temperature variation through a ramp function that allows schematising the rapid temperature increase, while the other, expressed through an interpolated function, allows representing the continuous temperature variation of the flows during a time interval. Moreover, the first results obtained from the simulations in the thermal field show that the frames are vulnerable to high temperatures, regardless of which function is used to define them since the plastic elements reach critical temperatures in a short time. Therefore, the first mitigation strategy proposed, which has both a low economic impact and does not modify the window system, is the overlapping of a 2 cm wooden section placed on the external frame, which protects the plastic elements. Furthermore, fluid-dynamic analyses have shown that shutters, which had been hypothesised as a possible filter/protection element against flows, are unsuitable for this purpose. So the proposed panel is an aluminium/wood sandwich panel, which has excellent pressure resistance and to mitigate the effect of temperatures, a layer of fireproof rock wool has been interposed to preserve the internal aluminium panel in case the wood reaches the ignition temperature. The last proposed mitigation strategy concerns the roofs, which are the most vulnerable elements concerning pyroclastic deposits. The behaviour of roofs concerning pyroclastic deposits is substantially influenced by two factors: the thermal degradation of materials and the roof's pitch. The thermal degradation of the materials is due to the high temperature of the clasts (150-400°C) and can be mitigated by the use of thermal insulation, which, is characterised by low thermal conductivity

(λ), is able to triple the collapse time of timber, steel and concrete roofs. Therefore, in volcanic risk areas, it would be advisable to set a minimum pitch angle. For flat roofs, this can be achieved (Zuccaro and Leone, 2012) [47]: through a superstructure made of a light material, such as Cold-Formed Steel, CFS, which does not overload the underlying structure. Local governments and residents need to be fully aware of the likely damage from an eruption and possible mitigation measures' cost-effectiveness. Regarding the economic, political and social weight' of volcanic risk in densely populated areas, a valid method of assessing the effectiveness of mitigation solutions can contribute objectively to strategic choices and contingency plans. Although it concerns the area of Vesuvius and Campi Flegrei in the specific parameters analysed (hazard characterisation, building types, construction technologies), the approach discussed in this thesis represents a methodology that could also be adopted in other contexts. Other territories have been studied in Europe and overseas, where an attempt has been made to export the analysed prototypes. The applied methodology has foreseen first of all the analysis of the building stock of each area, in particular, the islands of Tenerife (Spain) and Azores (Portugal) are characterised by buildings very similar to the Neapolitan ones, both for the vertical structure and for the type of window frames; and in these two areas, it is possible to intervene with the same analysed strategies. While in Negros island (Philippines) and Martinique and Guadeloupe's islands (French Antilles), the building stock is different. Therefore, it is necessary to intervene with different strategies; mainly, these areas are characterised by periods in which hurricanes occur. Therefore, the different strategies proposed to safeguard the building during a windstorm were analysed, and an attempt was made to improve this device to make it valid for a possible volcanic eruption. enddocument

References

[1] Ablay, G., Ernst, G., Marti, J., and Sparks, R. (1995). The 2 ka subplinian eruption of montaña blanca, tenerife. *Bulletin of Volcanology*, 57(5):337–355.

[2] Baxter, P. J., Boyle, R., Cole, P., Neri, A., Spence, R., and Zuccaro, G. (2005). The impacts of pyroclastic surges on buildings at the eruption of the soufrière hills volcano, montserrat. *Bulletin of volcanology*, 67(4):292–313.

[3] Blong, R. J. (2013). *Volcanic hazards: a sourcebook on the effects of eruptions*. Elsevier.

[4] Boudon, G., Komorowski, J.-C., Villemant, B., and Semet, M. P. (2008). A new scenario for the last magmatic eruption of la soufrière of guadeloupe (lesser antilles) in 1530 a.d. evidence from stratigraphy radiocarbon dating and magmatic evolution of erupted products. *Journal of Volcanology and Geothermal Research*, 178(3):474–490. Evaluating Explosive Eruption Risk at European Volcanoes.

[5] Carracedo, J. C., Badiola, E. R., Guillou, H., Paterne, M., Scaillet, S., Torrado, F. P., Paris, R., Fra-Paleo, U., and Hansen, A. (2007). Eruptive and structural history of teide volcano and rift zones of tenerife, canary islands. *Geological Society of America Bulletin*, 119(9-10):1027–1051.

[6] Carracedo, J. C., Paterne, M., Guillou, H. 'e., Perez-Torrado, F.-J., Paris, R. M., Rodriguez-Badiola, E., and Hansen Mach ´ i n, A. R. (2003). Radiometric dating 'e tricas (14c and k / ar) of teide and the northwest rift, tenerife, canary islands. *Geol Studies 'o gicos*.

[7] Ciampi, M., Leccese, F., and Tuoni, G. (2001). Pareti ventilate e normativa tecnica.

[8] Cioni, R., Longo, A., Macedonio, G., Santacroce, R., Sbrana, A., Sulpizio, R., and Andronico, D. (2003). Assessing pyroclastic fall hazard through field data and numerical simulations: example from vesuvius. *Journal of Geophysical Research: Solid Earth*, 108(B2).

[9] Costa, A., Dell'Erba, F., Di Vito, M., Isaia, R., Macedonio, G., Orsi, G., and Pfeiffer, T. (2009). Tephra fallout hazard assessment at the campi flegrei caldera (italy). *Bulletin of Volcanology*, 71(3):259–273.

[10] Dato, F. (2017). An iterative model for vulnerability curves (pga) generation of masonry buildings.

[11] De Gregorio, D., Faggiano, B., Formisano, A., and Mazzolani, F. (2010). Air fall deposits due to explosive eruptions: action model and robustness assessment of the vesuvian roofs. In *Proceeding of the International Conference COST Action C*, volume 26, pages 507–512.

References

[12] Ebnesajjad, S. (2016). Effect of chemicals on plastics.

[13] Emanuel, K., Ravela, S., Vivant, E., and Risi, C. (2006). A statistical deterministic approach to hurricane risk assessment. *Bulletin of the American Meteorological Society*, 87(3):299–314.

[14] Esposti, O. T., Neri, A., Todesco, M., and Macedonio, G. (2002). Pyroclastic flow hazard assessment at vesuvius (italy) by using numerical modeling. ii. analysis of flow variables. *Bulletin of volcanology*, 64(3-4):178–191.

[15] Hampton, S., Cole, J., Wilson, G., Wilson, T., and Broom, S. (2015). Volcanic ashfall accumulation and loading on gutters and pitched roofs from laboratory empirical experiments: Implications for risk assessment. *Journal of Volcanology and Geothermal Research*, 304:237–252.

[16] Iacuaniello, M., Montanino, A., De Gregorio, D., and Zuccaro, G. (2020). Pyroclastic flow mitigation strategies: a new perspective for the red area. *Natural Hazards and Earth System Sciences Discussions*, pages 1–28.

[17] Jenkins, S., Spence, R., Fonseca, J., Solidum, R., and Wilson, T. (2014). Volcanic risk assessment: Quantifying physical vulnerability in the built environment. *Journal of Volcanology and Geothermal Research*, 276:105–120.

[18] Komorowski, J., Boudon, G., Semet, M., Beauducel, F., Anténor-Habazac, C., Bazin, S., Hammouya, G., Lindsay, J., Robertson, R., Shepherd, J., et al. (2005). Volcanic hazard atlas of the lesser antilles: Guadeloupe. *Volcanic Hazard Atlas of the Lesser Antilles*, pages 65–102.

[19] Komorowski, J., Boudon, G., Semet, M., Villemant, B., and Hammouya, G. (2002). Recurrent flank-collapses at soufrière of guadeloupe volcano: implications of acid hydrothermal fluids on edifice stability mount pelée 1902–2002; explosive volcanism in subduction zones. In *IPGP-INSU-IAVCEI International Congress, Martinique*, page 69.

[20] Komorowski, J.-C., Legendre, Y., Caron, B., and Boudon, G. (2008). Reconstruction and analysis of sub-plinian tephra dispersal during the 1530 ad soufrière (guadeloupe) eruption: Implications for scenario definition and hazards assessment. *Journal of Volcanology and Geothermal Research*, 178(3):491–515.

[21] Li, Y. and Ellingwood, B. R. (2006). Hurricane damage to residential construction in the us: Importance of uncertainty modeling in risk assessment. *Engineering structures*, 28(7):1009–1018.

[22] Martí, J., Geyer, A., Andujar, J., Teixidó, F., and Costa, F. (2008). Assessing the potential for future explosive activity from teide–pico viejo stratovolcanoes (tenerife, canary islands). *Journal of Volcanology and Geothermal Research*, 178(3):529–542.

[23] Marti, J., Spence, R., Calogero, E., Ordoñez, A., Felpeto, A., and Baxter, P. (2008). Estimating building exposure and impact to volcanic hazards in icod de los vinos, tenerife (canary islands). *Journal of Volcanology and Geothermal Research*, 178(3):553–561.

[24] Marzocchi, W. and Woo, G. (2009). Principles of volcanic risk metrics: Theory and the case study of mount vesuvius and campi flegrei, italy. *Journal of Geophysical Research: Solid Earth*, 114(B3).

[25] Mottura, G. and Pennisi, A. (2014). *Serramenti e schermature solari*. Maggioli Editore.

[26] Neri, A., Aspinall, W. P., Cioni, R., Bertagnini, A., Baxter, P. J., Zuccaro, G., Andronico, D., Barsotti, S., Cole, P. D., Ongaro, T. E., et al. (2008). Developing an event tree for probabilistic hazard and risk assessment at vesuvius. *Journal of volcanology and geothermal research*, 178(3):397–415.

[27] Newhall, C., Self, S., and Robock, A. (2018). Anticipating future Volcanic Explosivity Index (VEI) 7 eruptions and their chilling impacts. *Geosphere*, 14(2):572–603.

[28] Newhall, C. G. and Self, S. (1982). The volcanic explosivity index (vei) an estimate of explosive magnitude for historical volcanism. *Journal of Geophysical Research: Oceans*, 87(C2):1231–1238.

[29] Ongaro, T. E., Komorowski, J.-C., Legendre, Y., and Neri, A. (2020). Modelling pyroclastic density currents from a subplinian eruption at la soufrière de guadeloupe (west indies, france). *Bulletin of Volcanology*, 82(12):1–26.

[30] Ongaro, T. E., Neri, A., Menconi, G., Vitturi, M. d., Marianelli, P., Cavazzoni, C., Erbacci, G., and Baxter, P. (2008). Transient 3d numerical simulations of column collapse and pyroclastic density current scenarios at vesuvius. *Journal of Volcanology and Geothermal Research*, 178(3):378–396.

[31] Oppenheimer, C. (2011). *Eruptions that shook the world*. Cambridge University Press.

[32] Orsi, G., Cuna, L., De Astis, G., de Vita, S., Di Vito, M., Isaia, R., Nave, R., Pappalardo, L., Piochi, M., Postiglione, C., et al. (2001). *I vulcani napoletani: pericolosità e rischio*. Dolgetta.

[33] Orsi, G., Di Vito, M. A., Selva, J., and Marzocchi, W. (2009). Long-term forecast of eruption style and size at campi flegrei caldera (italy). *Earth and Planetary Science Letters*, 287(1-2):265–276.

[34] Pomonis, A., Spence, R., and Baxter, P. (1999). Risk assessment of residential buildings for an eruption of furnas volcano, sao miguel, the azores. *Journal of volcanology and geothermal research*, 92(1-2):107–131.

[35] Pyle, D. M. (1995). Mass and energy budgets of explosive volcanic eruptions. *Geophysical Research Letters*, 22(5):563–566.

[36] Pyle, D. M. (2015). Sizes of volcanic eruptions. In *The encyclopedia of volcanoes*, pages 257–264. Elsevier.

[37] Spence, R., Kelman, I., Baxter, P., Zuccaro, G., and Petrazzuoli, S. (2005). Residential building and occupant vulnerability to tephra fall. *Natural Hazards and Earth System Sciences*, 5(4):477–494.

[38] Spence, R. J., Baxter, P. J., and Zuccaro, G. (2004a). Building vulnerability and human casualty estimation for a pyroclastic flow: a model and its application to vesuvius. *Journal of Volcanology and Geothermal Research*, 133(1-4):321–343.

[39] Spence, R. J., Zuccaro, G., Petrazzuoli, S., and Baxter, P. J. (2004b). Resistance of buildings to pyroclastic flows: analytical and experimental studies and their application to vesuvius. *Natural Hazards Review*, 5(1):48–59.

[40] Todesco, M., Neri, A., Ongaro, T. E., Papale, P., Macedonio, G., Santacroce, R., and Longo, A. (2002). Pyroclastic flow hazard assessment at vesuvius (italy) by using numerical modeling. i. large-scale dynamics. *Bulletin of Volcanology*, 64(3):155–177.

[41] Walker, G. P. (1973). Explosive volcanic eruptions—a new classification scheme. *Geologische Rundschau*, 62(2):431–446.

[42] Wright, J. and Cas, R. (1988). *Volcanic successions, modern and ancient: a geological approach to processes, products, and successions*. London; Boston: Allen & Unwin/Chapman & Hall.

[43] Zuccaro, G., Cacace, F., Spence, R., and Baxter, P. (2008). Impact of explosive eruption scenarios at vesuvius. *Journal of Volcanology and Geothermal Research*, 178(3):416–453.

[44] Zuccaro, G. and De Gregorio, D. (2013). Time and space dependency in impact damage evaluation of a sub-plinian eruption at mount vesuvius. *Natural hazards*, 68(3):1399–1423.

[45] Zuccaro, G. and Ianniello, D. (2004). Interaction of pyroclastic flows with building structures in an urban settlement: a fluid-dynamic simulation impact model. *Journal of volcanology and geothermal research*, 133(1-4):345–352.

[46] Zuccaro, G. and Leone, M. (2010). Building technologies for the mitigation of volcanic risk. In *Proceedings of COST Action C26 Final International Conference*.

[47] Zuccaro, G. and Leone, M. F. (2012). Building technologies for the mitigation of volcanic risk: Vesuvius and campi flegrei. *Natural hazards review*, 13(3):221–232.

[48] Zuccaro, G., Leone, M. F., Del Cogliano, D., and Sgroi, A. (2013). Economic impact of explosive volcanic eruptions: A simulation-based assessment model applied to campania region volcanoes. *Journal of volcanology and geothermal research*, 266:1–15.